Gesellschaft für Anlagen-
und Reaktorsicherheit
(GRS) mbH

# Evaluation of Fire Models for Nuclear Power Plant Applications

## Benchmark Exercise No. 5: Flame Spread in Cable Tray Fires

International Panel Report

GRS - 214

**Gesellschaft für Anlagen- und Reaktorsicherheit (GRS) mbH**

# Evaluation of Fire Models for Nuclear Power Plant Application

## Benchmark Exercise No. 5: Flame Spread in Cable Tray Fires

International Panel Report

Compiled by:
Olaf Riese (iBMB)
Dietmar Hosser (iBMB)
Marina Roewekamp (GRS)

November 2006

**Remark:**

This report was prepared under contract No. SR 2491 "Übergreifende Bewertung des Brandschutzes bei Kernkraftwerken - Auswertung von spezifischen Brandereignissen, Mitarbeit in internationalen Gremien, Entscheidungshilfe bei der Verwendung von Brandsimulationsprogrammen" with the German Bundesministerium für Umwelt, Naturschutz und Reaktorsicherheit (BMU) durchgeführt.

The work was conducted by the Gesellschaft für Anlagen- und Reaktorsicherheit (GRS) mbH together with the Institut für Baustoffe, Massivbau und Brandschutz (iBMB).

The authors are responsible for the content of this report.

**GRS - 214**
**ISBN 978-3-931995-81-2**

**Deskriptoren:**
Ausbreitung, Auswirkung, Brand, Brandgefährdung, Brandschutz, Brandverhalten, Druck, Gas, Kabel, Kohlendioxid, Reaktor, Rechenverfahren, Sauerstroff, Simulation, Temperatur, Verbrennung

## Abstract

As a part of the Nuclear Regulatory Investigation Program, the German iBMB (Institut für Baustoffe, Massivbau und Brandschutz) of Braunschweig University of Technology and GRS (Gesellschaft für Anlagen- und Reaktorsicherheit mbH) participate in the ‘International Collaborative Project to Evaluate Fire Models for Nuclear Power Plant Applications” (ICFMP) for assessing and validating fire simulation codes for nuclear power plant applications. This assessment is being performed through benchmarking and validation exercises. The tests of Benchmark Exercise No. 5 simulate cable fire scenarios in a single compartment.

A major objective of the actual cable fire experimental series is the investigation of the effects of a naturally ventilated fire on vertically routed cables (worst case) with different cable insulation materials (PVC (*p*oly*v*inyl *c*hloride) and FRNC (*f*ire *r*etardant *n*on-*c*orrosive)). Another important aspect of cable fires in nuclear power plants is the risk of functional failures. Therefore within these test series short circuits as well as loss of conductivity of the cables have been measured.

This panel report includes a description of the specification and the experimental results for the Tests 1 to 4 of the ICFMP Benchmark Exercise No. 5 performed in December 2003 at the iBMB in Germany. The experimental data have been reported on the ICFMP platform and have been discussed at several ICFMP meetings. The measured data are the basis for fire simulations by the institutions from different countries participating in the ICFMP.

Four organizations from France, Germany and the USA applied in total five different fire models of different types in this international Benchmark Exercise. A major question was to which extent the models are appropriate to predict pyrolysis and flame spread on a cable tray. In a first step, so-called "blind" calculations have been performed without knowledge of the experimental data, but with a detailed specification. In a second step, "open" calculations with given experimental results have been carried out.

A major limitation of most of the codes applied within this benchmark Exercise is that they do not contain a special pyrolysis model for complex objects such as cables. The different approaches in the codes to model the pyrolysis of a cable tray as well as the comparison of the model predictions with the experimental results are both presented

in this panel report. The individual reports of the modelers' work are given in the appendices. One result is, that the used codes do not simulate realistically the behavior of the cables as observed in the experiments. Empirical approaches resulted in betters results than deterministic approaches at this time.

The tests show that the FRNC insulated cables have significantly better characteristics in case of fire. No substantial flame spread takes place, even in case of pre-heating up to 200 °C in the environment of the cables. PVC insulated cables could be ignited with a burner output of 50 kW, for FRNC cables a burner output of 150 kW was necessary. In Test 3 (PVC, no pre-heating) a continuous average flame spread rate from 40 cm/min over the length of the cable tray has been derived from the experimental data for I&C cables. It has been concluded that it is difficult to interpret the influence of pre-heating on ignition and flame spread. The test series indicate that the burning behavior of a pre-heated PVC cable is similar to that of an aged PVC cable. If a cable is pre-heated flammable plasticizers could leave the cable, a prozess which normally leads to better fire characteristics.

Short circuits occur first as 'conductor to conductor' shorts and later as 'conductor to tray" shorts (shorts to ground). The time period until short circuits occur strongly depends on the pre-heating of the cables. Without pre-heating, the short circuit times are by a factor of two higher then in case of pre-heating. In one case with pre-heating PVC insulated I&C cables failed already after 100 s. The average time to loss of function of PVC insulated I&C cables with pre-heating according to the experiments is approx. 220 s. The short circuit times of power cables are nearly two times higher then those of I&C cables and are independent of the cable insulation material. FRNC insulated cables show better characteristics in all tests and are ignited with a substantially higher burner output as mentioned above.

# Kurzfassung

In einem Vorhaben, welches im Rahmen eines Untersuchungsprogramms des BMU stattfindet, nehmen die GRS (Gesellschaft für Anlagen- und Reaktorsicherheit) mbH und in ihrem Unterauftrag das iBMB (Institut für Baustoffe, Massivbau und Brandschutz) der Technischen Universität Braunschweig an einem gemeinschaftlichen internationalen Projekt zur Bewertung von Brandmodellen hinsichtlich ihrer Anwendbarkeit für kernkraftwerksspezifische Szenarien, dem so genannten 'International Collaborative Project to Evaluate Fire Models for Nuclear Power Plant Applications' - ICFMP - teil.

Im Rahmen dieses internationalen Projektes werden die Erkenntnisse und Erfahrungen diverser Fachinstitutionen genutzt, um gemeinsam den internationalen Stand von Wissenschaft und Technik bei Brandsimulationsmethoden und Computerprogrammen hinsichtlich der Anwendungen auf die besondere Situation in kerntechnischen Anlagen zu bewerten und zu verbessern. Dabei hat die Zusammenarbeit im Rahmen der Arbeitsgruppe ICFMP vorrangig folgende Ziele:

- Erfassung des internationalen Kenntnisstandes zu Brandsimulationsrechnungen einschließlich Validierung für kernkraftwerksspezifische Brandszenarien anhand von Experimenten,
- Prüfung von Anwendungsmöglichkeiten und -grenzen derartiger Analysehilfsmittel für die Bewertung des Brandschutzes in kerntechnischen Einrichtungen und Einbezug derartiger Verfahren in kerntechnische Regelwerke,
- Erarbeitung von analytischen Hilfsmitteln für konkrete Anwendungen bei der Bewertung der Brandsicherheit von Kernkraftwerken,
- Beispielhafte Anwendung von Brandsimulationsrechnungen für ausgewählte Brandszenarien in Kernkraftwerken sowie Bewertung der Aussagesicherheit dieser Analysehilfsmittel für einen nationalen wie internationalen Einsatz.

Zur Umsetzung der unterschiedlichen Aufgabenstellungen des Projektes werden so genannte Benchmark-Aufgaben (Benchmark Exercises) und Validierungsuntersuchungen durchgeführt. Die Simulationsrechnungen werden hierbei von den teilnehmenden Institutionen aus verschiedenen Ländern mit unterschiedlichen Arten von Brandsimulationscodes zuerst 'blind', d.h. ohne Kenntnis der Versuchsergebnisse durchgeführt und später nochmals in Kenntnis der Versuchsergebnisse 'offen' nachgerechnet, um schließlich die Ergebnisse untereinander sowie mit den Versuchen zu vergleichen.

Elektrische Leitungen zur Versorgung und Ansteuerung elektrischer und elektronischer Komponenten und Systeme können eine erhebliche Brandgefahr innerhalb der Kraftwerksanlagen darstellen. Einerseits beteiligen sich brennbare Isolierungen der elektrischen Leitungen direkt am Brandgeschehen, andererseits kann eine Brandausbreitung durch die ungeschützte Kabelführung über große Abstände erfolgen. Die Möglichkeit der Brandrausbreitung entlang der Kabel besteht insbesondere bei einer erhöhten Belegungsdichte, wie sie in Großkraftwerksanlagen gegeben ist. Mit Kabelbränden sind unmittelbare Gefahren wie anhaltend hohe Temperaturen, hohe Rauchproduktion, Freisetzung von gefährlichen toxischen Verbrennungsprodukten, Funktionsausfälle von Komponenten und Systemen oder auch langfristige Beschädigungen von baulichen Strukturen und der Einrichtungen durch korrosive Gase verbunden. Versuche am iBMB haben gezeigt, dass die Vorwärmung von elektrischen Kabeln einen erheblich Einfluss auf das Entzündungsrisiko und die Brandausbreitung haben kann.

In Kernkraftwerken älterer Bauart sind überwiegend PVC-Kabel eingesetzt. Die Kabelindustrie stellt jedoch seit geraumer Zeit eine Vielzahl an Kabelisolationsmaterialien mit verbesserten Eigenschaften im Brandfall bereit, die verstärkt in Kernkraftwerken zum Einsatz kommen /HOS 03/. Eine Gruppe dieser Kabel mit solchen verbesserten Eigenschaften sind die so genannten FRNC (*f*ire *r*etardant *n*on *c*orrosive)-Kabel.

Im Rahmen der vorliegenden Studie wurden vier großmaßstäbliche Raumbrandversuche mit vertikal angeordneten Kabelpritschen in einem Brandversuchstand des iBMB durchgeführt. PVC- und FRNC-Kabel wurden dabei getrennt untersucht. Die Versuche wurden je Materialart einmal ohne und einmal mit Vorwärmung durchgeführt. Als Zündquelle wurde ein Propangasbrenner eingesetzt, für die Vorwärmung ein in der Brandkammer angeordneter Ethanol-Flüssigkeitspool. Um den Einfluss des jeweiligen Kabeltyps zu berücksichtigen, wurden die Kabeltrassen in zwei getrennten Bündeln mit Leistungs- und mit Steuerkabeln praxisgerecht belegt.

Im Unterschied zu den bisherigen ‘Benchmark Exercises’ des ICFMP-Projektes wurden die Kabeltrassen in dem hier beschriebenen Versuchsprogramm der Versuchsserie 5 (Benchmark Exercise No. 5 - Flame Spread In Cable Tray Fires) gezielt in Brand gesetzt, um das Entzündungsverhalten sowie das Brandausbreitungsverhalten zu untersuchen.

Vier Institutionen aus Frankreich, Deutschland und den USA haben vier verschiedene Modelle unterschiedlichen Typs (CFAST, COCOSYS, FDS, und CFX) eingesetzt und diese Benchmark-Aufgabe gerechnet. Die wesentliche Frage hierbei ist, ob bzw. auf welchem Level aktuelle Brandsimulationscodes die Brandausbreitung auf einer Kabeltrasse bei einem vergleichbaren Szenario, wie es hier vorgestellt wird, berechnen können.

Eine weitere Gefahr bei Kabelanlagen ist der Funktionsverlust der Kabel im Brandfall. Dieser wurde in den hier vorgestellten realmaßstäblichen Versuchen mit untersucht.

In dem vorliegenden Bericht werden die Spezifikation der Versuche, die Startbedingungen am Versuchstag sowie die Ergebnisse der Kabelbrandversuche (Test 1 – Test 4) und der parallel durchgeführten Funktionserhaltversuche dargestellt. Um für die Teilnehmer des ICFMP-Projektes den Vergleich der Daten zu vereinfachen, wurden abgeleitete Größen (z. B. Heiß- und Kaltgastemperaturen, Höhe der rauchgasarmen Schicht, Massen- und Wärmeströme) aus den Versuchsdaten berechnet und als Datenfile zur Verfügung gestellt. Die hierzu benutzten physikalischen Gleichungssysteme sind dokumentiert.

Eine Haupteinschränkung der Brandsimulationscodes, die innerhalb dieser Benchmark-Aufgabe eingesetzt wurden, ist, dass sie kein spezielles Pyrolysemodell für komplizierte Objekte wie Kabel enthalten. Die Vorausberechnung der Pyrolyse stellt nicht den Stand von Wissenschaft und Technik dar; zudem verfügt nur ein Programm (FDS) hierfür über ein Submodell. In den anderen Programmen werden Annahmen zur Pyrolyserate gemacht, die im Wesentlichen aus Ergebnissen anderer Versuche stammen. Die unterschiedlichen Ansätze in den Codes zur Modellierung der Pyrolyse einer Kabeltrasse sowie der Vergleich der (blinden und offenen) Simulationsrechnungen mit den experimentellen Resultaten werden in diesem Bericht zusammenfassend dargestellt. Die Ergebnisse der einzelnen Berechnungen der Teilnehmer sind in den Anhängen dokumentiert. Ein grundsätzliches Ergebnis ist, dass die verwendeten Modelle das in den Experimenten beobachtete Brandverhalten der Kabel nur unzureichend vorausberechnen können. Empirische Ansätze zur Berücksichtigung der Pyrolyse ergeben in dieser Studie insgesamt eine bessere Vergleichbarkeit mit den experimentellen Ergebnissen als deterministische Ansätze, jedoch ist ihre universelle Gültigkeit noch nicht bewiesen.

Die Versuche zeigen, dass FRNC-Kabel erheblich bessere Eigenschaften im Brandfall besitzen als PVC-Kabel. PVC-Kabel konnten mit einer Leistung des Brenners von 50 kW entzündet werden, FRNC erst bei Kabel 150 kW. Eine Brandausbreitung konnte auch bei einer Vorwärmung der FRNC-Kabel bis 200 °C in der direkten Umgebung der Kabel nicht festgestellt werden. In Test 3 (PVC, kein Vorwärmen) konnte für Steuerkabel eine mittlere Brandausbreitungsgeschwindigkeit von 40 cm/min über die Länge der Kabeltrasse abgeleitet werden. Die Versuche haben gezeigt, dass sich der Einfluss des Vorwärmens auf die Entzündung und das Brandverhalten der Kabel nicht eindeutig interpretieren lässt. Das Brandverhalten von vorgewärmten PVC-Kabeln scheint dem gealterter PVC-Kabel, bei denen brennbare Weichmacheranteile über eine längere Zeit entweichen konnten, ähnlich zu sein. Wenn ein Kabel vorgewärmt wird, findet ein vergleichbarer Prozess in wesentlich kürzerer Zeit statt und führt dazu, dass sich das Entzündungsverhalten der Kabel verbessert.

Funktionsversagen der Kabel tritt zuerst als “Leiter zu Leiter“-Kurzschluss und später als “Leiter zu Trasse“-Kurzschluss auf. Die Zeiten bis zum Funktionsversagen hängen erheblich vom Vorwärmen der Kabel ab. Ohne Vorwärmung sind die Kurzschlusszeiten um einen Faktor zwei höher als bei Vorwärmung. Im Test 4 mit Vorwärmen fiel ein PVC-Steuerkabel schon nach ca. 100 s aus. Als Mittelwert für den Funktionsverlust der PVC-Steuerkabel mit Vorwärmen ergibt sich aus den Experimenten 220 s. Die Kurzschlusszeiten der Leistungskabel sind fast zweimal höher als die der Steuerkabel und sind unabhängig von dem Material der Isolierung. Ein FRNC-Mantelmaterial führt in allen Versuchen zu längeren Zeiten bis zum Funktionsverlust, obwohl die FRNC-Kabel mit deutlich höherer Leistung des Brenners entzündet wurden.

## Table of Contents

# 1 Introduction

Different types of fire codes (zone models as well as lumped parameter codes or three-dimensional field models, so-called CFD (computational fluid dynamics) codes, have been used by expert institutions from different countries participating in the ICFMP to simulate the Benchmark Exercise No. 5.

This paper presents a complete report regarding the specification and the results of four real scale cable tray fire experiments carried out at iBMB of Braunschweig University of Technology /HOS 05/. It contains the entire work as well as the corresponding conclusions from the individual modelers of this Benchmark Exercise No. 5.

Other international fire tests and validation exercises within ICFMP include different fire scenarios like fires in large halls such as a turbine building, large pool fires in compartments, cable tray fires and special compartment fire experiments. The ICFMP Benchmark Exercises are listed below:

- Benchmark Exercise No. 1: Cable fire and thermal load on cables in a cable spreading room (theoretical) /DEY 02/,
- Benchmark Exercise No. 2: Heptane pool fire in a large hall (experiment) and large oil fire in a machine hall with 2 floor levels and horizontal openings (theoretical) /MIL 04/,
- Benchmark Exercise No. 3: Heptane spray fire in a cable room to investigate thermal loads on cables and cable trays /HAM 06/ and /MCG 06/,
- Benchmark Exercise No. 4: Relative large fuel pool fire with two variations of the door cross section area /KLE 06/,
- Benchmark Exercise No. 5: Fire spreading on vertical cable trays with variation of the pre-heating and cable material (this report).

The experimental results presented here can be used to assess and validate computational fire simulation models focusing mainly on cable flame spread. For studying pre-heating effects, an ethanol pool was used at the beginning of Test 2 and Test 4. This phase of the experiments is also useful to validate computational fire models focusing on liquid fuel combustion in a naturally ventilated fire compartment.

# 2 Specification of Benchmark Exercise No. 5

The cable fire experiments for this benchmark exercise have been performed considering the results of cable fire experiments with different types of cables carried out in the past as part of different projects for the German authorities as well as for nuclear industry /HOS 98/, /HOS 03/ and /RIE 03/. They take into account additional relevant aspects, such as mixed compositions of different cables on the tray and potential functional failures of electric/electronic equipment.

## 2.1 Review of Previous Related Work

Two test series dealing with cable fires have been conducted at the iBMB 1994 - 1997 /HOS 98/ and 1999 - 2002 /HOS 03 and RIE 03/.

The issues of the first test series were:

- Cable installations in existing nuclear power plants (NPP),
- investigation of arrangements typical for NPP and other nuclear installations,
- development of appropriate protection systems,
- basis for qualification of protection systems.

The goals of the second test series were:

- Investigation of cable fire scenarios with respect to different fire test methods,
- comparison of different protection and insulation systems for cables.

In both test series, large scale cable fire experiments have been conducted in the same compartment, which was used for the actual test series in the International Fire Modeling Project.

The primary fire and the operation mode of the ignition source was different from earlier tests. Instead of the oil burner used before, a liquid pool fire has been used for preheating of the compartment and of the cable surface. To be able to compare the results of the tests with former test results, all the other boundary conditions have been maintained the same as for those tests (e.g. fire compartment geometry, ventilation conditions, installation of a wall for separating the cables from the pool, ignition time).

## 2.2 Lessons Learned from Previous Work

The behavior of electric cables in case of a fire depends on different parameters. Two groups can be distinguished:

The group ‘construction’ includes:

– Technical type (instrumentation & control or power cable)

– age of cables,

– orientation of cable tray (horizontal/vertical),

– density of cable package (surface to mass relation),

– type of protection system (unprotected/coated).

The group ‘boundary conditions’ comprises:

– Pre-heating,

– ignition source,

– position of cable tray,

– ventilations conditions.

All the criteria significantly influence the fire behavior; however, in all cases, the vertical arrangement of a cable tray is the more hazardous scenario. The cable insulation material seems to be the key parameter, because the fire behavior of different cable insulation materials is extremely different /RIE 03/. The pre-heating of the cables has also been found to strongly influence the behavior under fire.

## 2.3 Experimental Design Process for ICFMP Benchmark Exercise No. 5

The first recommendation for a further Benchmark Exercise in the series of the international fire tests and validation exercises was presented at the 4$^{th}$ ICFMP meeting /HOS 02/. Eight cable tray fire tests were proposed, considering only PVC cable insulation material and vertically as well as horizontally oriented cable trays. Nearly the same proposal for the experiments was presented at the 5$^{th}$ meeting but with a reduction to 4 different tests /ROE 03/. At the 6$^{th}$ meeting, the test program was changed to consider different insulation materials. Two different materials are accounted for, namely PVC and FRNC insulation materials, which are often used in German NPPs. It has been consistently planned to investigate both I&C and power cables. The last specification of the Benchmark Exercise No. 5 was provided during the 7$^{th}$ ICFMP meeting in Worchester, USA.

## 2.4 Specification of Experiments

### 2.4.1 Fire Compartment

The cable fire experiments have been carried out in a special fire compartment (iBMB test facility) named ‘OSKAR’ with an inner floor area of 3.6 m $\times$ 3.6 m = 12.96 m$^2$. The inner room height is 5.6 m. **Tab. 2-1** gives an overview of the fire compartment data with respect to the thermo-physical data of the wall materials.

As the primary pilot fire for pre-heating of the cables, a pool fire of 0.5 m$^2$ pool area has been assumed. For measuring the burning rate of the liquid pool, the pan with the liquid is mounted on a weight scale. The cable tray is directly ignited / inflamed by means of a propane gas burner. The pre-fabricated trays filled with cables are mounted on a weight scale, which is located on top of the ceiling. Details on the pool fire are given in paragraph 2.4.2, details on the burner in paragraph 2.4.3.

There is an opening of 0.7 m width and 3.6 m height from the compartment, which was reduced by means of a 1.4 m wall to provide a 1.5 m$^2$ ventilation area to the outside. Smoke gases released are collected in a hood with an exhaust duct located over the opening and that leads to a smoke gas cleaning system. The measuring section for the gas analysis as well as the optical measurement equipment is located in the horizontal part of the exhaust channel. Details of the experimental setup can be found in Fig. 2-1 to Fig. 2-7.

**Tab. 2-1** Fire compartment data

| | **Fire compartment** |
|---|---|
| Floor area | 3.6 m x 3.6 m (inner area) |
| Height | 5.6 m (inner height) |
| Opening - Door | 0.7 m x 2.2 m, 1.4 m above the floor |
| Cable tray | 0.5 - 4.5 m above the floor |

| | Thickness [mm] | Material | Insulation [mm] |
|---|---|---|---|
| Walls | 250 | light concrete | 50 |
| Floor | 300 | concrete | - |
| Ceiling | 200 | light concrete | - |
| Walls, 1.4 m height | 200 | aerated concrete | - |
| **Material** | **Heat conductivity $\lambda$ [W/mK]** | **Heat capacity $c_p$ [J/kgK]** | **Density $\rho$ [kg/m$^3$]** |
| Concrete | 2.1 | 880 | 2400 |
| Light concrete | 0.75 | 840 | 1500 |
| Aerated concrete | 0.11 | 1350 | 420 |
| Insulation | 0.05 | 1500 | 100 |

The layout of the gas analysis measuring equipment meets the requirements of ISO 9705 /ISO 93/. In addition, a filter with lime-soda (carbon dioxide trapping) is located inside the duct leading to the oxygen analyzer, which has to be considered for determining the ‘oxygen depletion factor’. By this procedure, the off-gas volume flow, the amount of oxygen, carbon monoxide and carbon dioxide as well as the optical absorption inside the off-gas flow are measured. The rate of heat release can be estimated by means of the oxygen consumption method. The calibration (precision of the system and system response) is performed by pre-tests with a liquid fuel (ethanol) pool.

For measuring the smoke gas levels, four vertical measuring chains with seven thermocouples each, and one vertical measuring chain in the plume were used. The temperature in the vicinity of the cables is measured by a chain 40 cm in front of the vertical tray.

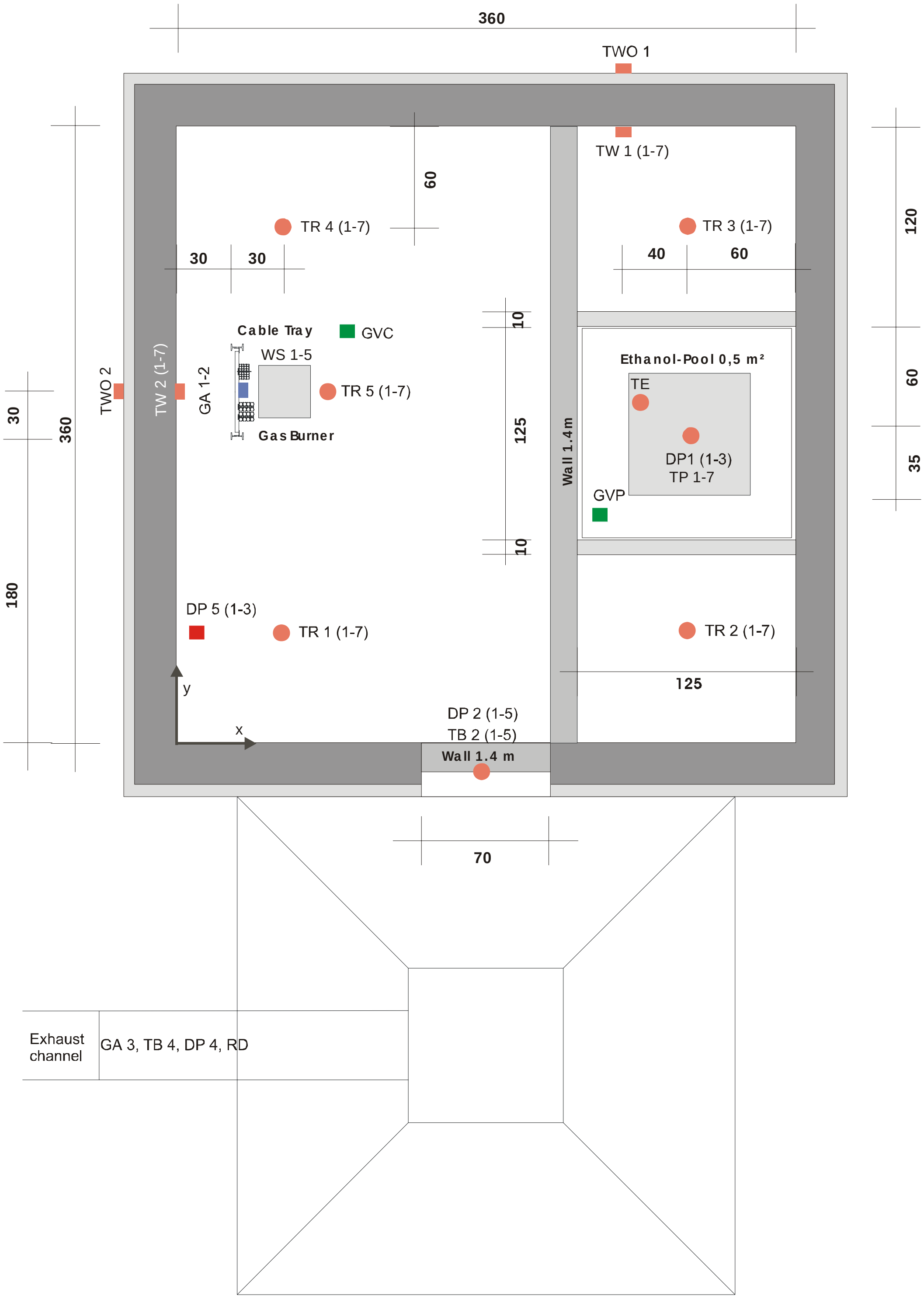


**Fig. 2-1** Top view of the fire compartment for the cable fire tests

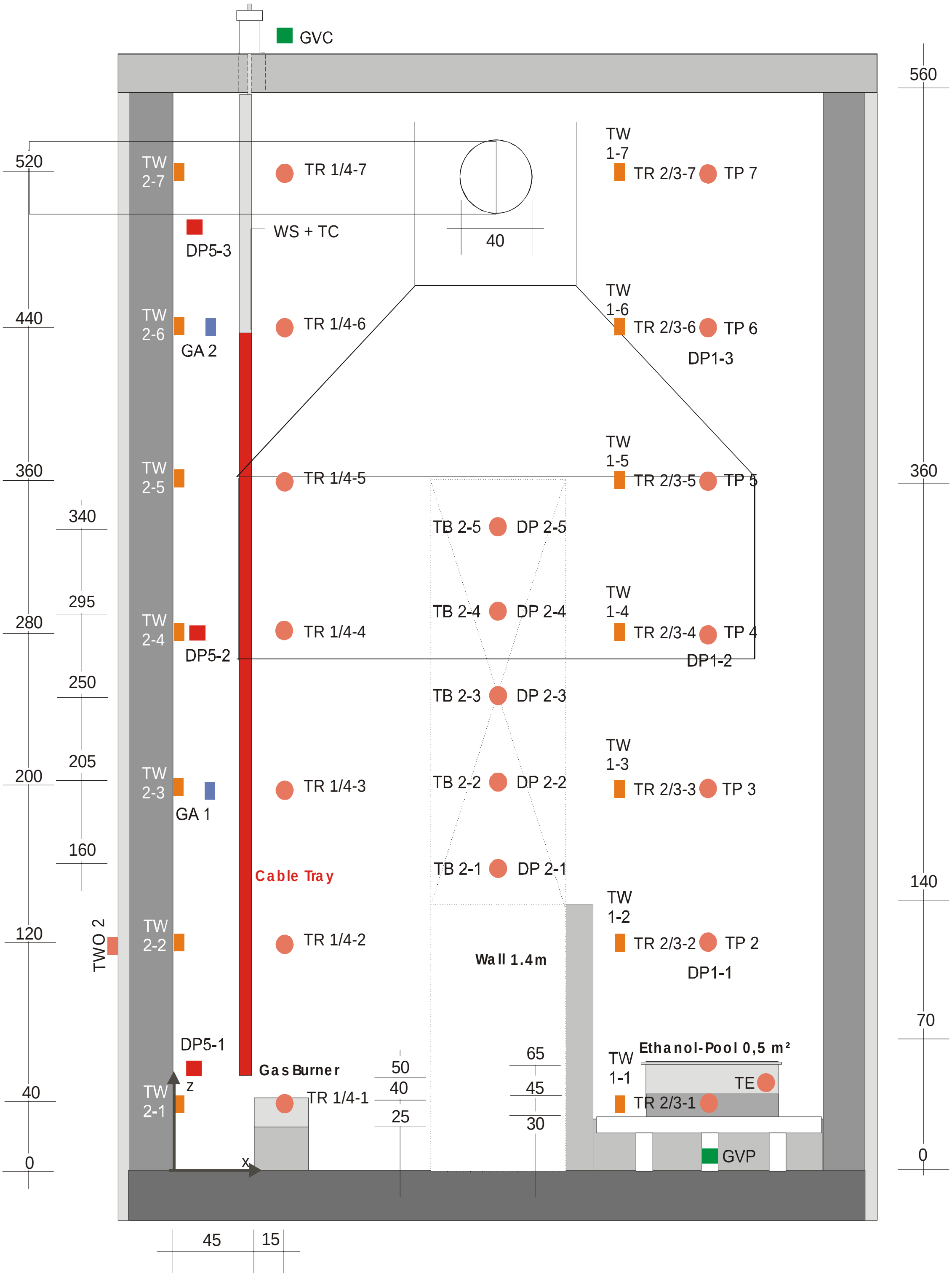


Fig. 2-2 Side view of the fire compartment (in +y direction)

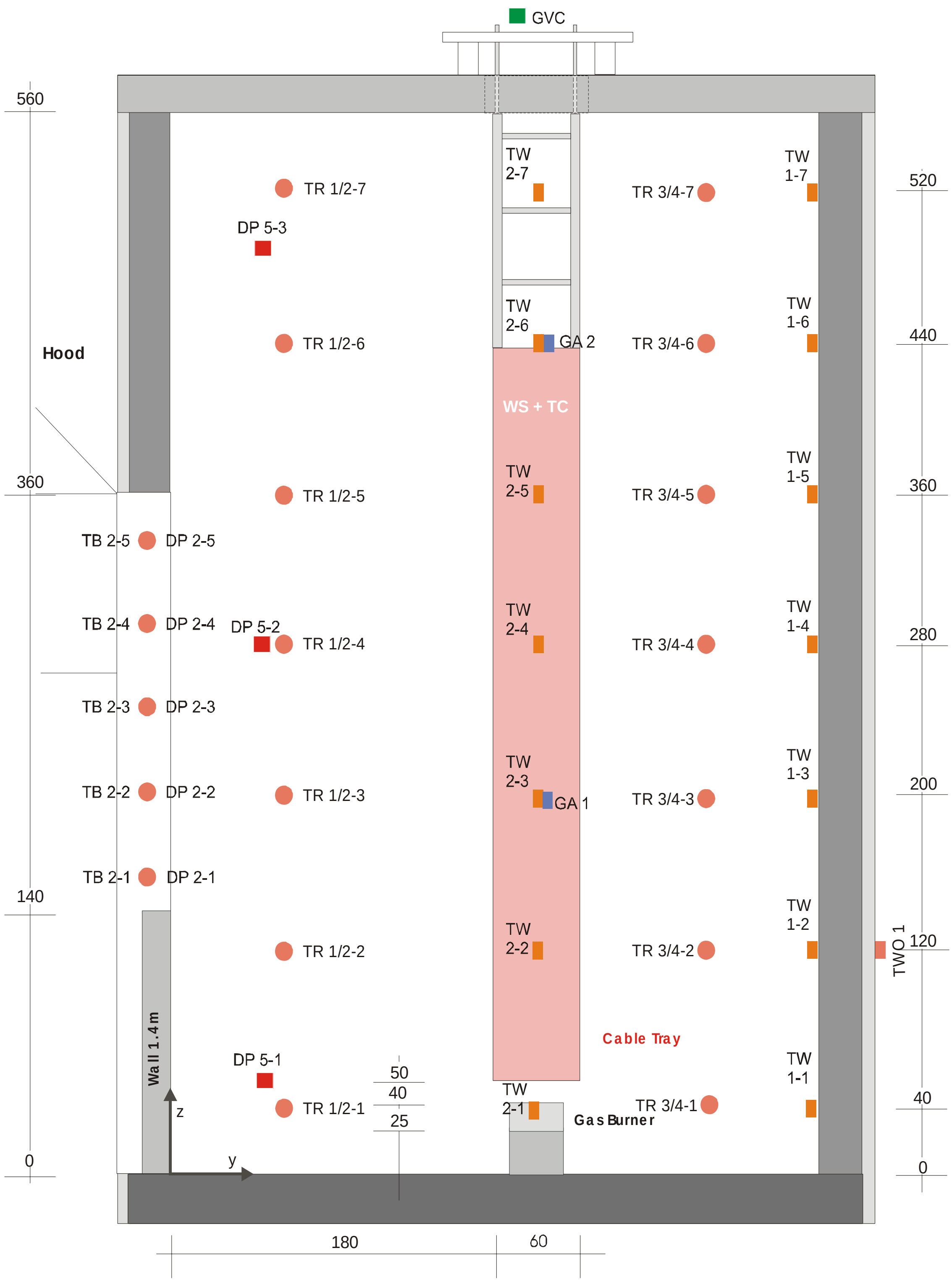


**Fig. 2-3** Side view of fire compartment (in -x direction)

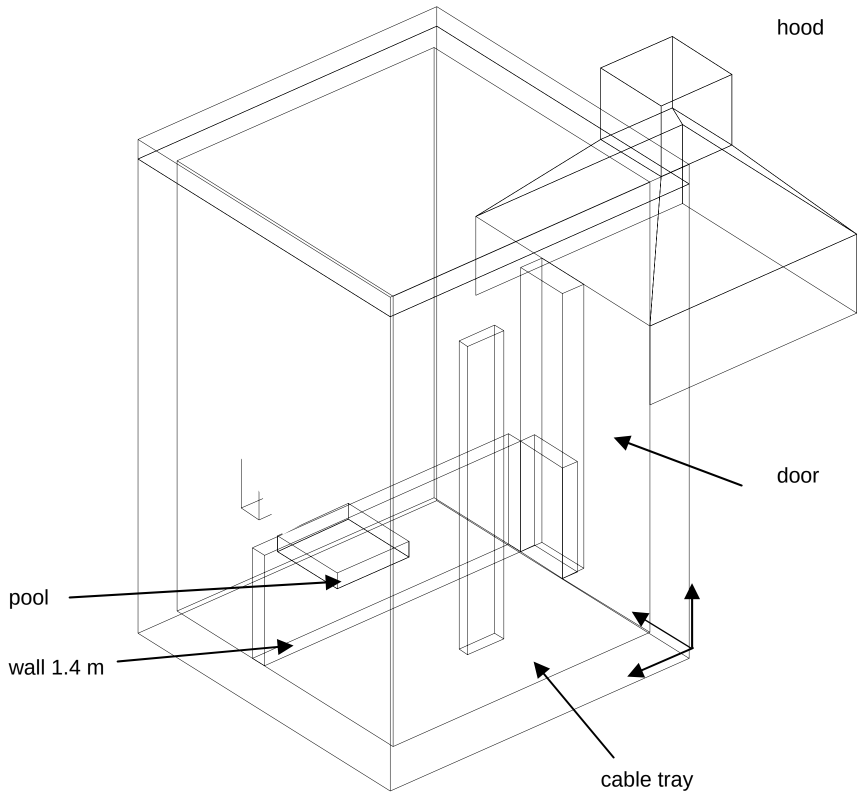


**Fig. 2-4** Three dimensional view of fire compartment

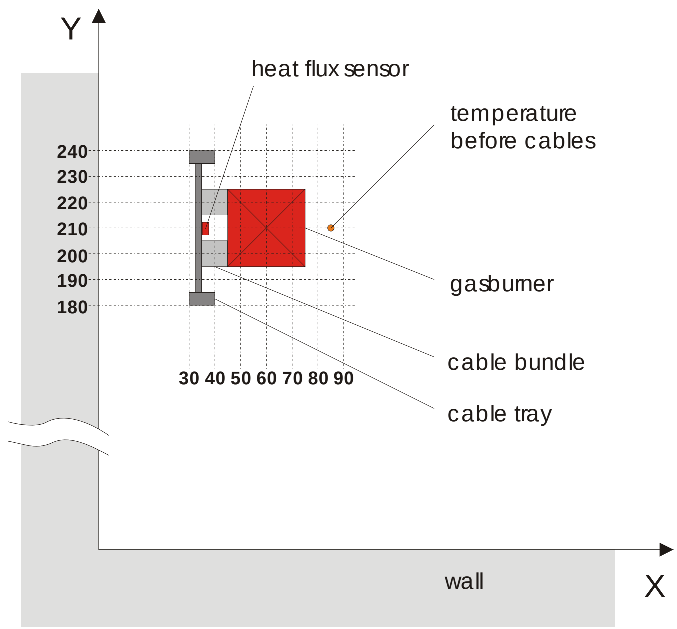


**Fig. 2-5** Layout scheme of the cable tray, bundles and burner

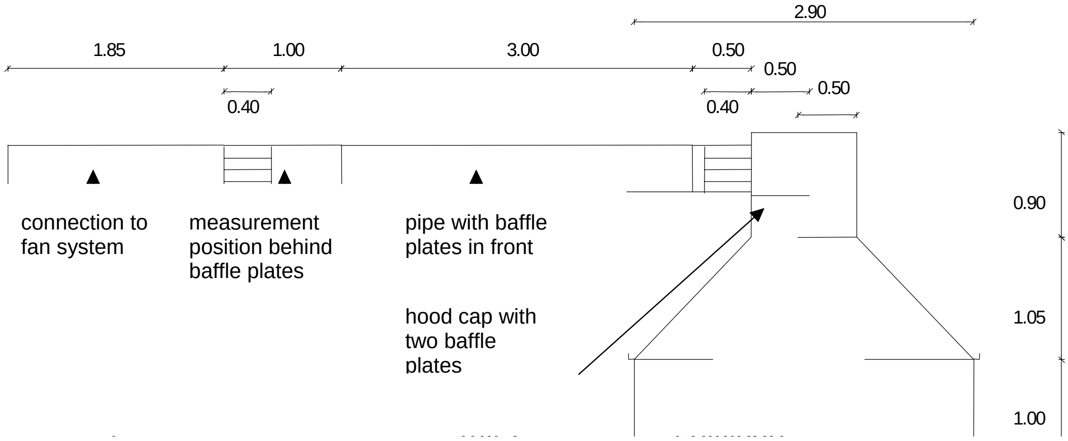


**Fig. 2-6** Scheme of the hood above the front door

**Fig. 2-7** View onto the hood above the front door

Tab. 2-2 gives an overview of the data for the fire compartment environment. The abbreviations of the measuring points and types of measurements are given in paragraph 2.5.2. Details of the cable tray itself and the corresponding measuring equipment on the cables are given in paragraph 2.4.4.

**Tab. 2-2** Environmental data

| | **Fire compartment environment** | |
|---|---|---|
| Hood with exhaust duct | 5 maximum, approx. 3.5 intended *) | $m^3/s$ |
| Temperature | 20 * | °C |
| Pressure | 101300 * | Pa |
| Height | 0 | m |
| Wind | 0 | m |

* depending on the day, see chapter 3.9.

### 2.4.2 Pre-heating

A pool of 0.5 m² floor area filled with ethanol (ethylene alcohol) has been used as a pre-heating source. For estimating the filling level, pre-tests and simulations have been carried out with the aim of pre-heating the cable surface to a maximum temperature level of 250 °C. In case of temperatures exceeding 250 °C to 300 °C, a flashover of the flame spread has to be assumed for PVC cables. The pool fire source has only been applied for tests with pre-heating of the fire compartment. Data on the pool fire are given in Tab. 2-3.

**Tab. 2-3** Pool fire data (see Fig. 2-2)

| | **Pool data** | |
|---|---|---|
| Pool size (quadratic) | 0.5 | $m^2$ |
| Pool pan height above ground (upper edge) | 0.65 | m |
| Pool pan height (thin metal plate) | 0.20 | m |
| Intended filling level | 0.125 | m |
| Construction under pool height | 0.15 | m |
| Ground plate (without weight loss cells) | 0.10 | m |

Information to the thermo-physical data of the liquid fuel ethanol used in the tests are given in. **Tab. 2-4**.

**Tab. 2-4** Liquid fuel data

| | **Ethanol properties (ethylene alcohol)** | |
|---|---|---|
| Formula | CH3CH2OH | (C2H6O) |
| Density | 793,7 | kg/m³ |
| Heat of combustion | 26.8 1 | MJ/kg |
| Heat of vaporization | 837 1 | kJ/kg |
| Ignition temperature | 91,9 2 | °C |
| Radiative fraction | 0.20 3 | - |
| Burning rate | 0.03 4 | kg/sm² |

[1] /KAN 03/, [2] /BAB 03/, [3] in Tewarson /TEW 03/ a radiative fraction from 0.15 is given for ethanol, but for BE 5 a little higher value is chosen, [4] Experimental data from pre-tests conducted at iBMB

### 2.4.3 Ignition Source

For igniting the cable tray a gas burner with propane gas has been used. The burner power can be varied between 0 and 300 kW. The gas consists of 95 % propane/propene mixture /DIN 85/ with a higher amount of propane as stated by the manufacturer. The other 5 % consists of ethane, ethene, and butane isomers.

For the actual test series it was intended to use the gas burner with 150 kW power output (Test 1 and Test 2) and with 50 kW power output (Test 3 and Test 4) until a temperature increase on the cable surface in level 2 (see paragraph 2.4.4) of more than 450 °C was measured. This is defined as an indicator for the burning of the cables themselves.

**Tab. 2-5** Gas burner for ignition

| Parameter | Gas burner | | |
|---|---|---|---|
| Area | 300 * 300 | | mm * mm |
| Height | 150 | | mm |
| Fuel | Propane | | DIN 51622 |
| Position | horizontal in front of and bottom of vertical cable tray | | |
| **Type of experiment** | **Propane gas burner operating mode** | | |
| | Time | | |
| | Start [min] | End criteria [1] | Power [kW] |
| Without pre-heating | 0 | cable fire 1.1 m above the lower tray level, both bundles | 50 / 150 |
| With pre-heating | 20 | | 50 / 150 |

[1] Temperature increase > 450 °C on the cable surface at the measuring point TCO 1/2-2 and TCO 3/4-2 (level 2)

### 2.4.4 Cable Routing and Installation, Temperature Measuring Points

The width of the cable trays is 50 cm. Both ladder type side racks have a width of 5 cm each. The cables are installed on the tray within two cable bundles with a width of 30 cm to ensure that the gas burner with an edge length of 30 cm will heat up all the cables as symmetrical as possible. The amount of cables per bundle depends on the diameter Ø [mm] of the individual cables. The amount can be roughly calculated to be the number of cables n = (230 mm / Ø) per bundle. The vertical ladder type cable trays are filled with cables with the corresponding measuring equipment as outlined in **Fig. 2-8**. The cables are mounted on the trays with cable clamps. The lowest series of thermocouples are installed approx. 70 cm above the lower side of the tray. The distance between the different measuring levels is 40 cm, the distance between highest series of measuring devices and upper edge of the tray is 10 cm.

The measuring devices of each row have numbers starting on the lowest level up to the highest one (last digit in the number).
The exact position of the thermocouples is given in **Fig. 2-9**.

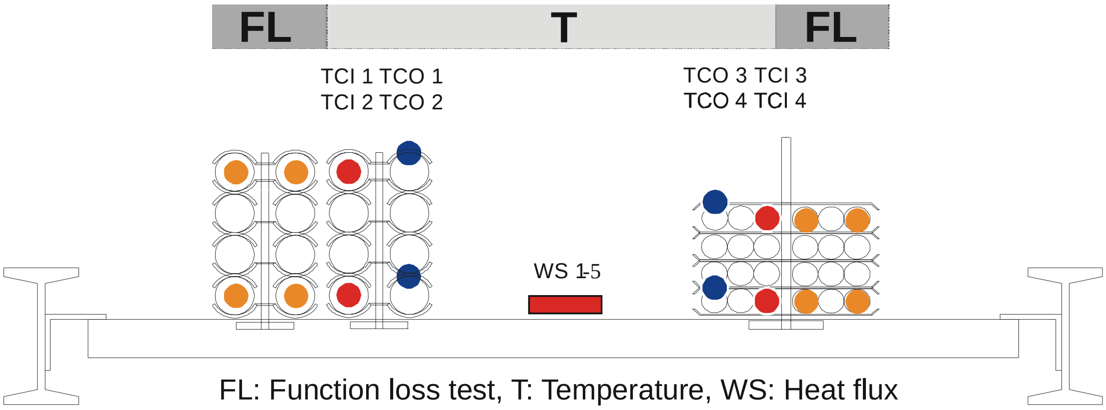


**Fig. 2-8** Vertical cable tray; two cable bundles; left: power cables, right: I&C cables

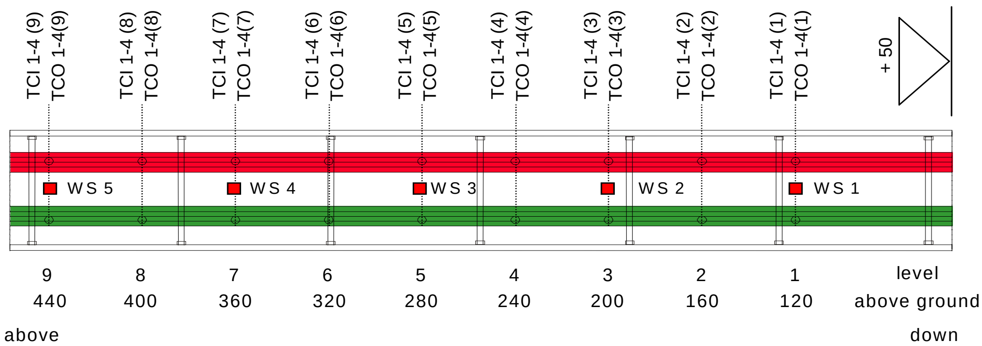


**Fig. 2-9** Temperature measurement positions on the cables tray, levels 1-9, and heat flux measurement positions at the cable tray

### 2.4.5 Cable Materials

PVC insulated cables as well as FRNC (fire retardant non-corrosive) cable materials have been used. Power cables as well as I&C cables have been installed in two different cable bundles of the tray. Tab. 2-6 gives an overview of the different types of cables and cable materials as intended for the experiments. The layout is outlined in paragraph 2.4.4. Further details on the cables can be found in the Appendix A.

**Tab. 2-6** Types of cable and cable insulation materials and bundle configuration

| Index | Material type - cable type | Name | Diameter Ø [mm] | n = (230 mm / Ø) per bundle | Total combustible material [kg]* |
|---|---|---|---|---|---|
| A | PVC - I&C cable | JE-Y-(St)Y 16×2×0.8 | 14.0 | 16 | 10.82 |
| B | PVC - power cable | NYM-J 5×25 | 30.0 | 8 | 23.94 |
| C | FRNC - I&C cable | JE-LIHCH (Bd) 16×2× 0.5 | 16.0 | 14 | 14.47 |
| D | FRNC - power cable | NHXMH-J 5×2.5 | 12.5 | 18 | 9.77 |

* For additional information see Appendix A

### 2.4.6 Functional Failure Tests

For measuring the current conduction and short circuits of electrical cables a measuring apparatus was developed in line with the German DIN 4102-12 standard /DIN 95/. This allowd the simultaneous measurement of current conduction and short circuits for up to 12 cable conductors. The equipment works with a voltage of 9 Volt. With this testing voltage the requirements of the German DIN 4102-12 /DIN 95/ are not met. However, it is crucial that this circuit permits a parallel installation of temperature probes on the cables without interfering in the recoding of the measurements in the case of short circuits. Therefore, the temperature development on the cables is possible to be measured without problems.

**Fig. 2-10** shows the electrical schematic diagram of the function loss test equipment. The principle is shown for two conductors from one cable. For each of the twelve pairs of conductors it is possible to measure the loss of the current conduction. Furthermore, the short circuit among each of the twelve cable wire pairs could be measured (conductor to conductor, e.g. K1). For getting meaningful measurement results it is necessary to have cable cores directly adjacent to each other. For one of every twelve pairs of conductors the short circuit was measured to the tray (conductor to tray, e.g. KR1). In the case of a functional failure, a light at the front panel of the test equipment indicates the loss of current conduction or a short circuit of the conductors. Fig. 2-11 shows a picture of the test equipment with the front panel.

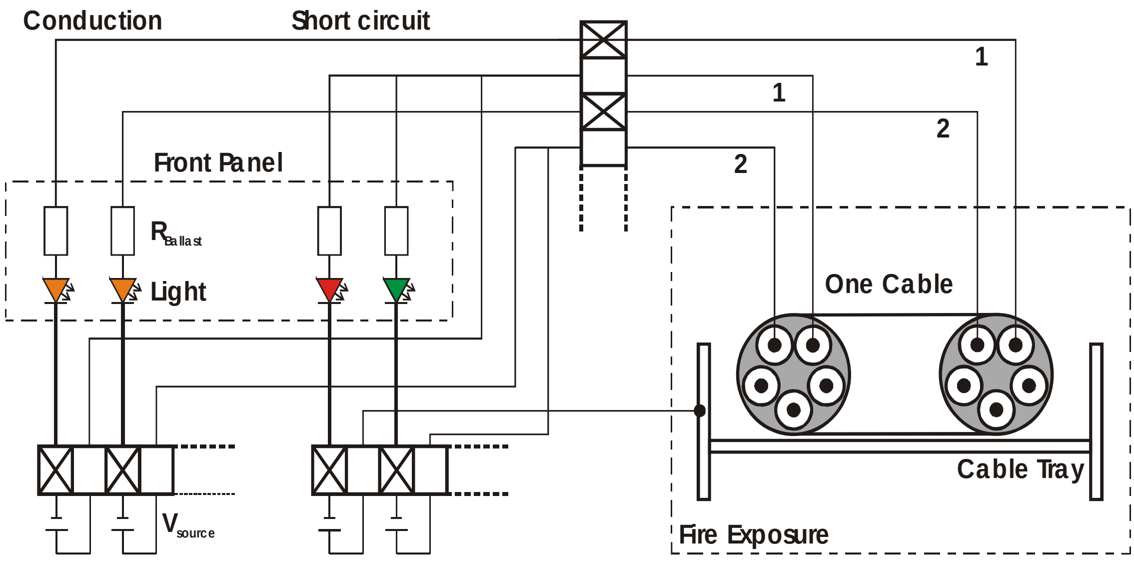


**Fig. 2-10** Electrical scheme of the functional failure tests; the principle is shown for two conductors (1 and 2) of one cable

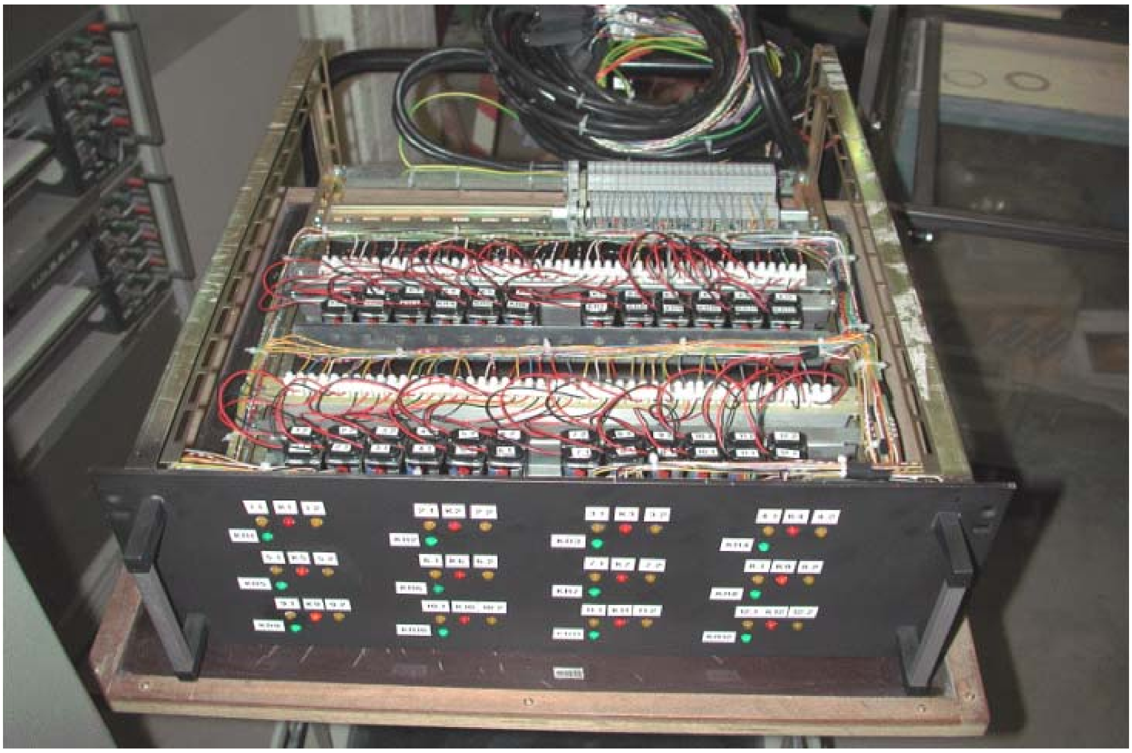

**Fig. 2-11** Functional failure test equipment of iBMB, test voltage 9 Volt

**Tab. 2-7** Functional failure abbreviations

| **Number**<br>USNRC Failure Mode | **Conduction**<br>Loss of conductor continuity | **Short circuit**<br>Conduction to conductor | **Short circuit to cable tray**<br>Conductor to external ground | **Cable type** | **Bundle side** |
|---|---|---|---|---|---|
| Failure indicator | light out | light on | light on | | |
| 1 | 1.1 und 1.2 | K 1 | KR 1 | power cable | right side |
| 2 | 2.1 und 2.2 | K 2 | KR 2 | | |
| 3 | 3.1 und 3.2 | K 3 | KR 3 | | |
| 4 | 4.1 und 4.2 | K 4 | KR 4 | | |
| 5 | 5.1 und 5.2 | K 5 | KR 5 | | not used |
| 6 | 6.1 und 6.2 | K 6 | KR 6 | | not used |
| 7 | 7.1 und 7.2 | K 7 | KR 7 | I&C cable | left side |
| 8 | 8.1 und 8.2 | K 8 | KR 8 | | |
| 9 | 9.1 und 9.2 | K 9 | KR 9 | | |
| 10 | 10.1 und 10.2 | K10 | KR 10 | | |
| 11 | 11.1 und 11.2 | K 11 | KR 11 | | |
| 12 | 12.1 und 12.2 | K 12 | KR 12 | | |

In the case of loss of electric function a light at the front panel of the test equipment indicates the loss of current conduction or short circuit of electrical cables. **Tab. 2-7** gives an overview on the abbreviations used in the context of the function loss equipment. A ‘K’ indicates a ‘conductor to conductor’ short circuit and a ‘KR’ indicates a short circuit between a cable conductor and the cable tray (‘K’ and ‘KR’ are used therefore as failure indicator indices).

Cable failure modes and effects of risk analysis perspectives are documented in /NOW 03/. The author pointed out, that the issue of fire induced cable failure modes and effects continues to be an area of both technical challenge and regulatory focus. For practical reasons, one cannot systematically consider the impact of all possible combinations. The cable failure modes reported in /NOW 03/ are given in **Tab. 2-8**. In the actual study, the most important failure modes according to **Tab. 2-8** are considered. These are failure mode number A.1 (conductor to conductor), C (conductor to external ground) and failure mode D (loss of conductor continuity) as mentioned above. Furthermore, cable failure influence factors have to be considered.

**Tab. 2-8** Cable failure modes as applied by Sandia National Laboratories (SNL) /NOW 03/

| Nr. | Failure mode | Special cases | Explanation |
|---|---|---|---|
| A | Intra-cable short circuits | | This failure mode involves circuits formed between the conductor of a given multi-conductor cable |
| A.1 | | General conductor to conductor short circuits | As the cable insulation breaks down, various conductors may short to each other. The circuit impact depends on the circuit function of the shorting conduc-tors |
| A.2 | | Hot short | A special case of the conductor-to-conductor short circuit where one of the shorting conductors is energized and, as a result of the short circuit, one or more other conductors become energized |
| A.3 | | Short to a grounded conductor | If one of the conductors in a shorting group is grounded b y design, then ef-fects of the short will be the same as the short to an external ground |
| A.4 | | Insulation resistan-ce degradation | This failure mode involves the formation of high-impedance short circuiting paths due to a breakdown in the insulation power of the conductor insulation |
| B | Inter-cable short circuit | | This failure mode involves short circuits formed between the conductors of sepa-rate cables. |
| C | Conductor to (external) ground short cir-cuit | | This failure mode involves a short circuit between one or more conductors and an external electrical ground such as a metallic cable raceway support system |
| D | Loss of conduc-tor continuity | | This failure mode involves a physical break in the conductor that will prevent electrical energy from reaching the in-tended circuit destination |

A list of cable failure mode influence factors is given in /WOO 02/. The list is based on a combination of SNL (Sandia National Laboratories) /NOW 03/ and USNRC (*United States Nuclear Regulatory Commission*) knowledge. The main factors are:

– Physical cable properties and configuration factors (e.g. insulation properties),

– routing factors (e.g. cable tray type),

– electric function factors (e.g. I&C or power cables),

– fire exposure condition factors (Exposure mode, intensity and duration).

All these factors are relevant for the tests in this study. Because of the limited number of tests it is not possible to provide an exact analysis of the effects, which have taken place and caused the functional failure of the cables. This report documents the functional failure times that occurs during the tests (see paragraph 3.10.4).

Some effects are discussed dealing with the thermo- physical properties of the cables representing a main factor because of the different insulation materials used. During the tests the failure mode C (loss of conductor continuity) did not occur. This indicates that the mounting and routing of the cables (routing factors having been chosen for the tests), could be neglected as a major functional failure influence in the present work.

## 2.5 Experimental Matrix and Instrumentation

**Tab. 2-9** gives an overview of the intended experiments. For each of the cable insulation materials, PVC and FRNC, two experiments have been carried out. One of these experiments with identical amount and type of cables has been performed without pre-heating, the other with pre-heating of the fire compartment. The operating mode of the ignition gas burner depends on the experiment and is explained in detail in paragraph 2.4.3.

**Tab. 2-9** Overview of the experiments

| Experimental parameters | Experiment 1 | Experiment 2 | Experiment 3 | Experiment 4 |
|---|---|---|---|---|
| Material | FRNC | | PVC | |
| Positioning | Vertical | | | |
| Cable type | power cable<br>I&C cable | power cable<br>I&C cable | power cable<br>I&C cable | power cable<br>I&C cable |
| Pre-heating | Liquid pool (Ethanol) | | | |
| | no | yes | No | yes |
| Ignition source | gas burner 50 - 150 kW | | | |
| Functional failure | Yes | | | |

### 2.5.1 Measured Values

The following parameters have been measured at the positions outlined in **Tab. 2-11**:

- Temperatures above the ethanol fire (plume) for 7 heights,
- temperatures in the fire compartment at 4 locations for 7 heights,
- temperatures 40 cm in front of the cable tray for 7 heights,
- temperatures at the wall surfaces,
- weight loss of the pool and of the cable tray,
- gas velocities and temperatures in the openings and in the plume,
- differential pressure distribution for 3 heights of the fire compartment,
- gas analysis (O2, CO2 und CO) for 2 heights in the fire compartment,
- heat flux densities in the level of the cable bundles for 5 heights,
- cable surface and inner cable temperatures for 9 heights,
- gas velocity and temperature in the exhaust channel,
- gas analysis (O2, CO2 und CO) and smoke gas density in the exhaust channel,
- functional failure tests for the cables,
- flame front height by video.

### 2.5.2 Measurement Overview

The different measurement locations are given in Fig. 2-1 to **Fig. 2-5** with the abbreviations explained in **Tab. 2-10**. **Tab. 2-11** gives an overview of the measuring devices and their respective locations. It further includes details of the thermocouples on the cable trays as given in paragraph 2.4.4. The environmental data, such as temperature and pressure, are taken from the standard meteorology from iBMB at each day, when the experiments have been performed.

**Tab. 2-10** Measurement abbreviations

| Parameter | Abbreviation | Location | Unit |
|---|---|---|---|
| Temperature | TP<br>TR<br>TW, TWO<br>TCI<br>TCO<br>TE<br>TB<br>TH | plume<br>compartment<br>wall, wall outside<br>inside cable<br>on cable surface<br>ethanol<br>bi-directional probes<br>environmental (hall) | [°C] |
| Mass loss | GVP, GVC | pool, cable tray | [kg] |
| Pressure difference | DP | opening, compartment | [Pa] |
| Gas analysis inside compartment | GA | compartment | [Vol.-%] |
| Pressure | PH | environmental (hall) | [Pa] |
| Heat flux density | WS | cable tray | [kW/m²] |
| (Total) Heat release rate * | HRR | outside compartment | [kW] |
| Smoke propagation velocity | RD | outside compartment | [m²/s] |
| Gas burner flow rate | RG | outside compartment | [l/min] |

* By means of oxygen consumption calorimetric method according to ISO 9705 /ISO 93/

**Tab. 2-11** List of measurements performed

| | x [cm] | y [cm] | z [cm] |
|---|---|---|---|
| **TEMPERATURES** | | | |
| **Centerline plume** | | | |
| TP 1 | 290 | 180 | 040 |
| TP 2 | | | 120 |
| TP 3 | | | 200 |
| TP 4 | | | 280 |
| TP 5 | | | 360 |
| TP 6 | | | 440 |
| TP 7 | | | 520 |
| **Compartment chain 1** | | | |
| TR 1-1 | 60 | 60 | 040 |
| TR 1-2 | | | 120 |
| TR 1-3 | | | 200 |
| TR 1-4 | | | 280 |
| TR 1-5 | | | 360 |
| TR 1-6 | | | 440 |

| | x [cm] | y [cm] | z [cm] |
|---|---|---|---|
| TR 1-7 | | | 520 |
| **Compartment chain 2** | | | |
| TR 2-1 | 300 | 60 | 040 |
| TR 2-2 | | | 120 |
| TR 2-3 | | | 200 |
| TR 2-4 | | | 280 |
| TR 2-5 | | | 360 |
| TR 2-6 | | | 440 |
| TR 2-7 | | | 520 |
| **Compartment chain 3** | | | |
| TR 3-1 | 300 | 300 | 040 |
| TR 3-2 | | | 120 |
| TR 3-3 | | | 200 |
| TR 3-4 | | | 280 |
| TR 3-5 | | | 360 |
| TR 3-6 | | | 440 |
| TR 3-7 | | | 520 |
| **Compartment chain 4** | | | |
| TR 4-1 | 60 | 300 | 040 |
| TR 4-2 | | | 120 |
| TR 4-3 | | | 200 |
| TR 4-4 | | | 280 |
| TR 4-5 | | | 360 |
| TR 4-6 | | | 440 |
| TR 4-7 | | | 520 |
| **Compartment chain 5 – 40 cm in front of vertical tray** | | | |
| TR 5-1 | 85 | 220 | 040 |
| TR 5-2 | | | 120 |
| TR 5-3 | | | 200 |
| TR 5-4 | | | 280 |
| TR 5-5 | | | 360 |
| TR 5-6 | | | 440 |
| TR 5-7 | | | 520 |
| **Wall chain 1, thermocouple with little metal plate** | | | |
| TW 1-1 | 260 | 360 | 040 |
| TW 1-2 | | | 120 |

| | x [cm] | y [cm] | z [cm] |
|---|---|---|---|
| TW 1-3 | | | 200 |
| TW 1-4 | | | 280 |
| TW 1-5 | | | 360 |
| TW 1-6 | | | 440 |
| TW 1-7 | | | 520 |
| **Wall chain 2, thermocouple with little metal plate** | | | |
| TW 2-1 | 0 | 220 | 040 |
| TW 2-2 | | | 120 |
| TW 2-3 | | | 200 |
| TW 2-4 | | | 280 |
| TW 2-5 | | | 360 |
| TW 2-6 | | | 440 |
| TW 2-7 | | | 520 |
| **Ethanol, covered thermocouple** | | | |
| TE | 340 | 140 | 32 |
| **Door** | | | |
| TB 2-1 | 180 | -15 | 160 |
| TB 2-2 | | | 205 |
| TB 2-3 | | | 250 |
| TB 2-4 | | | 295 |
| TB 2-5 | | | 340 |
| **Opening side wall** | | | |
| TB 3 | 375 | 215 | 105 |
| **Exhaust duct** | | | |
| TB 4 | outside fire compartment | | |
| **Wall outside** | | | |
| TWO 1 | 260 | 390 | 120 |
| TWO 2 | -30 | 220 | 120 |
| **On surface of cable 1** | | | |
| TCO 1-1 | ~ 45 | ~225 | 120 |
| TCO 1-2 | | | 160 |
| TCO 1-3 | | | 200 |
| TCO 1-4 | | | 240 |
| TCO 1-5 | | | 280 |
| TCO 1-6 | | | 320 |
| TCO 1-7 | | | 360 |
| TCO 1-8 | | | 400 |

| | x [cm] | y [cm] | z [cm] |
|---|---|---|---|
| TCO 1-9 | | | 440 |
| **On surface of cable 2** | | | |
| TCO 2-1 | ~ 40 | ~225 | 120 |
| TCO 2-2 | | | 160 |
| TCO 2-3 | | | 200 |
| TCO 2-4 | | | 240 |
| TCO 2-5 | | | 280 |
| TCO 2-6 | | | 320 |
| TCO 2-7 | | | 360 |
| TCO 2-8 | | | 400 |
| TCO 2-9 | | | 440 |
| **On surface of cable 3** | | | |
| TCO 3-1 | ~45 | ~215 | 120 |
| TCO 3-2 | | | 160 |
| TCO 3-3 | | | 200 |
| TCO 3-4 | | | 240 |
| TCO 3-5 | | | 280 |
| TCO 3-6 | | | 320 |
| TCO 3-7 | | | 360 |
| TCO 3-8 | | | 400 |
| TCO 1-9 | | | 440 |
| **On surface of cable 4** | | | |
| TCO 4-1 | ~ 40 | ~215 | 120 |
| TCO 4-2 | | | 160 |
| TCO 4-3 | | | 200 |
| TCO 4-4 | | | 240 |
| TCO 4-5 | | | 280 |
| TCO 4-6 | | | 320 |
| TCO 4-7 | | | 360 |
| TCO 4-8 | | | 400 |
| TCO 4-9 | | | 440 |
| **In cable 1** | | | |
| TCI 1-1 | ~ 45 | ~230 | 120 |
| TCI 1-2 | | | 160 |
| TCI 1-3 | | | 200 |
| TCI 1-4 | | | 240 |

| | x [cm] | y [cm] | z [cm] |
|---|---|---|---|
| TCI 1-5 | | | 280 |
| TCI 1-6 | | | 320 |
| TCI 1-7 | | | 360 |
| TCI 1-8 | | | 400 |
| TCI 1-9 | | | 440 |
| **In cable 2** | | | |
| TCI 2-1 | ~ 40 | ~230 | 120 |
| TCI 2-2 | | | 160 |
| TCI 2-3 | | | 200 |
| TCI 2-4 | | | 240 |
| TCI 2-5 | | | 280 |
| TCI 2-6 | | | 320 |
| TCI 2-7 | | | 360 |
| TCI 2-8 | | | 400 |
| TCI 2-9 | | | 440 |
| **In cable 3** | | | |
| TCI 3-1 | ~ 45 | ~210 | 120 |
| TCI 3-2 | | | 160 |
| TCI 3-3 | | | 200 |
| TCI 3-4 | | | 240 |
| TCI 3-5 | | | 280 |
| TCI 3-6 | | | 320 |
| TCI 3-7 | | | 360 |
| TCI 3-6 | | | 400 |
| TCI 3-9 | | | 440 |
| **In cable 4** | | | |
| TCI 4-1 | ~ 40 | ~210 | 120 |
| TCI 4-2 | | | 160 |
| TCI 4-3 | | | 200 |
| TCI 4-4 | | | 240 |
| TCI 4-5 | | | 280 |
| TCI 4-6 | | | 320 |
| TCI 4-7 | | | 360 |
| TCI 4-8 | | | 400 |
| TCI 4-9 | | | 440 |
| **HEAT FLUX DENSITY** | | | |
| WS 1 | ~ 40 | 220 | 120 |
| WS 2 | | | 200 |

| | x [cm] | y [cm] | z [cm] |
|---|---|---|---|
| WS 3 | | | 280 |
| WS 4 | | | 360 |
| WS 5 | | | 440 |
| **MASS LOSS** | | | |
| GVP | Assembly below the pool | | |
| GVC | Assembly at the top of the compartment | | |
| **DIFFERENCE PRESSURE** | | | |
| **Centerline plume** | | | |
| DP 1-1 | 290 | 180 | 120 |
| DP 1-2 | | | 280 |
| DP 1-3 | | | 440 |
| **Door** | | | |
| DP 2-1 | 180 | -15 | 160 |
| DP 2-2 | | | 205 |
| DP 2-3 | | | 250 |
| DP 2-4 | | | 295 |
| DP 2-5 | | | 340 |
| **Exhaust duct** | | | |
| DP 4 | outside fire compartment | | |
| **Fire compartment** | | | |
| DP 5-1 | 10 | 65 | 55 |
| DP 5-2 | | | 275 |
| DP 5-3 | | | 495 |
| **GAS ANALYSIS** | | | |
| **Fire compartment** | | | |
| GA 1 | 30 | 195 | 120 |
| GA 2 | 30 | 195 | 440 |
| **Exhaust duct (oxygen consumption method and smoke production)** | | | |
| GA 3 | outside fire compartment | | |
| RD | outside fire compartment | | |

### 2.5.3 Instrumentation

**Tab. 2-12** gives an overview of the measuring equipment used for the test series.

**Tab. 2-12** Overview of the measuring equipment

| Location | Measuring equipment | Measured parameter | Name |
|---|---|---|---|
| Compart-ment | bare thermocouple, type K NiCrNi | temperature | TR 1-5 (1-7) |
| | Oxor 610 * | $O_2$ | GA 1 |
| | Binos 610 * | $CO$, $CO_2$ | GA 1 |
| | Multor 610 * | $O_2$, $CO$, $CO_2$ | GA 2 |
| | gardon gague detectors | total heat flux density (radiative + convective) | WS 1-5 |
| | pressure gauge | pressure difference | DP 5 (1-3) |
| Plume | bare thermocouple, type K NiCrNi | temperature | TP 1-7 and TB 1 (1-3) |
| | bi-directional probe | pressure difference | DP 1 (1-3) |
| Door ope-ning | bare thermocouple, type K NiCrNi | temperature | TB 2 (1-5) |
| | bi-directional probe | pressure difference | DP 2 (1-5) |
| Wall | thermocouple with little metal plate, type K NiCrNi | wall surface temperature | TW |
| Pool | load cell | mass loss | GVP |
| | sheathed thermocouple protected, type K NiCrNi | temperature | TE |
| Cable tray | bared thermocouple, type K NiCrNi | temperature | TCO, TCI |
| | load cell | mass loss | GVC |
| Off-gas flow | Ultramat 22 * | $CO$, $CO_2$ | GA 3 |
| | Servomex * | $O_2$ | GA 3 |
| | bi-directional probe | Pressure difference | DP 4 |
| | bare thermocouple, type K NiCrNi | temperature | TB 4 |
| | Maurer Light | smoke production | RD |

Note:Bared thermocouples type K have a diameter of 1.7 ± 0.1 mm

* All gas measurements are made with dry gas, $CO_2$ has been trapped out before the gas has been analyzed with the Servomex in case of the off-gas flow

# 3 Experimental Results

## 3.1 Results to Be Delivered

In Tab. 3-1 the values to be delivered and which are not directly measured are explained in more detail. In chapter 3.2 to chapter 3.7 the equations are given, which are used to calculate the derived data. The results of the tests and the additional data are given in an MS EXCEL©-sheet to the members of the international platform.

Tab. 3-1 Additional variables to be delivered

| Description | Name | Unit | Comment |
|---|---|---|---|
| | Tup | °C | Upper layer temperature |
| | Tlow | °C | Lower layer temperature |
| | Layer_height | m | Layer height |
| Wall surface temperature | TW (up) | °C | Wall temperature of the fire compartment in the upper layer region |
| | TW (low) | °C | Wall temperature of the fire compartment in the lower layer region |
| Combustion | Combustion rate ethanol | kg/s | Combustion rate of ethanol |
| | Combustion rate cable | kg/s | Combustion rate of cables |
| | Comb. Heat release | kW | Total combustion heat release |
| Mass flow rates | Gin (Door) | kg/s | Mass flow rate through front door into the fire compartment |
| | Gout (Door) | kg/s | Mass flow rate through front door from the fire compartment |
| Heat flux rates | Heat Loss (Walls) | kW | Heat loss into the walls of the fire compartment |
| | Heat Flow (Door) | kW | Total heat flux through the door |

## 3.2 Gas Velocities and Volume Flows

### 3.2.1 Exhaust Duct /ISO 93/

According to /ISO 93/, the flow rate $\dot{V}_{exhaust\ duct}$ is given by the equation (3.1), the velocity in the exhaust duct is given with equation (3.2):

$$\dot{V}_{exhaust\ duct} = A \cdot \overbrace{k_t \cdot \underbrace{\frac{1}{k_p} \cdot \frac{22{,}4}{T_{298}}}_{=0.07} \cdot \sqrt{T \cdot \Delta p}}^{corrected\ velocity} = A \cdot v_{exhaust\ duct} \tag{3.1}$$

$$v_{exhaust\ duct} = k_t \cdot 0.07 \cdot sign(\Delta p)\sqrt{T \cdot |\Delta p|} \tag{3.2}$$

$A =$ exhaust cross section area: 0.04 * $\pi$ [m²]

$\Delta p =$ pressure difference bidirectional-probe [Pa]

$T =$ temperature [K]

$k_p =$ calibration constant for bi-directional probe: 1.08

$k_t =$ correction factor for velocity profile: 0.9 [-]

### 3.2.2 Centerline Plume and Door

The velocity $v_{plume,\,door}$ in the centerline plume and the door are calculated with equation (3.3).

$$v_{plume,\,door} = 0.07 \cdot sign(\Delta p)\sqrt{T \cdot |\Delta p|} \tag{3.3}$$

No additional correction factor as in (3.2) been used.

## 3.3 Combustion

### 3.3.1 Calculation of the Heat Release Rate /ISO 93/

The heat release rate was calculated by using equations of /ISO 93/. With an appropriate measurement in the exhaust flow, the smoke gas volume flow $\dot{V}_{298}$ (standardized to 25 °C) is given using equation (3.4). With equation (3.5) the total heat release rate is given. For those analysts determining the net heat release rate of the cables equation (3.6) has to be used. The energy released by oxygen consumed per unit volume for propane and ethanol is taken from literature /DRY 99/ and standardized to 25 °C.

$$\dot{V}_{298} = \frac{T_{298}}{T} \cdot \dot{V}_{exhaust\ duct} \tag{3.4}$$

$$HRR = E^{V}_{O_2,M} \cdot \dot{V}_{298} \cdot X^{a}_{O_2} \cdot \frac{\phi}{\phi \cdot (\alpha - 1) + 1} \tag{3.5}$$

$$\dot{q}_m = HRR - \frac{E^{V}_{O_2,M}}{E^{V}_{O_2,C_3H_8}} \cdot \dot{q}_b - \frac{E^{V}_{O_2,M}}{E^{V}_{O_2,C_2H_6O}} \cdot \dot{q}_e \tag{3.6}$$

With

| | |
|---|---|
| $T$ | gas temperature in the exhaust duct [K] |
| $\dot{V}_{298}$ | standardized volume flow rate of gas in the exhaust duct [m³/s] |
| $\phi$ | oxygen depletion factor with carbon dioxide filtering |
| $E^{V}_{O_2,M}$ | = 17200 kJ/m³ consumed oxygen (standard, standardized to 25 °C) |
| $\alpha$ | = 1.105 (‘chemical expansion factor’) |
| $HRR$ | total heat release rate [kW] |
| $\dot{q}_b$ | power output of gas burner [kW] |
| $\dot{q}_e$ | power output of ethanol-pool [kW] |
| $E^{V}_{O_2,C_3H_8}$ | = 16752 kJ/m³ consumed oxygen (propane, standardized to 25 °C) |
| $E^{V}_{O_2,C_2H_6O}$ | = 16857 kJ/m³ consumed oxygen (ethanol, standardized to 25 °C) |
| $\dot{q}_m$ | heat release rate of the material [kW] |

### 3.3.2 Calculation of the Pool and Cables Mass Loss Rates /ISO 99/

The mass loss rate [kg/s] from the pool and the cable on the tray is calculated by applying the five point numerical differentiation equations published in ISO 5660, Part 1 /ISO 99/, page 21. The mass loss was therefore smoothed (sequential average over 8 values).

## 3.4 Smoke Production /ISO 93/

The smoke production rate SPR in the exhaust duct is calculated under consideration from the absolute volume flow:

$$SPR = \frac{1}{L} \cdot \ln\left(\frac{I_0}{I}\right) \cdot \dot{V}_{exhaust\ duct} \quad [\mathrm{m^2/s}] \tag{3.7}$$

$I_0$ light intensity without extinction /-/

$I$ light intensity with extinction /-/

$L$ = 0.4 m, diameter of exhaust duct

## 3.5 Experimental Data Reduction /NIS 03/

### 3.5.1 Layer Interfaces Height

The lower layer temperature $T_{low}$ is taken to be the average of the thermocouple readings of the lowest measuring points. The interface height and upper layer temperature were calculated from solving the integral equations, given in /NIS 03/. Combining these equations provides the equation for the interface height:

$$z_{\text{int}} = \frac{T_{low}\left(I_1 \cdot I_2 - H^2\right)}{I_1 + I_2 T_{low}^2 - 2T_{low}H} \tag{3.8}$$

with:

$z_{\text{int}}$ layer interface height [m]

$T_{low}$ temperature of the lowest measurement point [°C]

$H$ room height [m]

$I_1$ integral value – approximated by discrete summation

$$I_1 = \int_0^H T(z,t)dz \approx \sum_{i=1} T_i(t) \cdot \Delta h_i \tag{3.9}$$

$T_i(t)$ temperature at measurement point number i

$\Delta h_i$ layer height assigned to measurement point number i

$I_2$ integral value – approximated by discrete summation

$$I_2 = \int_0^H \frac{1}{T(z,t)} dz \approx \sum_{i=1} \frac{1}{T_i(t)} \cdot \Delta h_i \tag{3.10}$$

### 3.5.2 Upper Layer Temperatures

The upper layer temperature was approximated as mean value of the temperatures of all measurement points located above the layer interfaces:

$$T_{up} = \frac{\sum_{j=1}^{n} T_j(t)}{n} \quad \text{for} \quad \mathrm{z_j} > z_{\mathrm{int}} \tag{3.11}$$

with:

$T_{up}$ upper layer temperature [°C]

$T_j$ temperature of measurement point $j$

$z_j$ temperature of measurement point $j$

$n$ total number of measurement points above layer interface

### 3.5.3 Lower Layer Temperatures

The lower layer temperature was approximated as mean value of the temperatures of all measurement points located below the layer interfaces:

$$T_{low} = \frac{\sum_{k=1}^{m} T_k(t)}{m} \quad \text{for} \quad \mathrm{z_k} < z_{\mathrm{int}} \tag{3.12}$$

with:

$T_{up}$ lower layer temperature [°C]

$T_k$ temperature of measurement point $k$

$z_k$ temperature of measurement point $k$

$m$ total number of measurement points below the layer interface

### 3.5.4 Wall Layer Temperatures

The upper layer wall temperature was approximated as mean value of the wall temperatures of all measurement points located above the layer interfaces:

$$TW_{up} = \frac{\sum_{k=1}^{n} TW_k(t)}{n} \quad \text{for} \quad \mathrm{z_k} < z_{\text{int}} \tag{3.13}$$

The lower layer temperature was approximated as mean value of the wall temperatures of all measurement points located under the layer interfaces:

$$TW_{low} = \frac{\sum_{k=1}^{m} TW_k(t)}{m} \quad \text{for} \quad \mathrm{z_k} < z_{\text{int}} \tag{3.14}$$

with:

$TW_{up}$ upper layer wall temperature [°C]

$TW_{low}$ lower layer wall temperature [°C]

$TW_k$ wall temperature of measurement point $k$

$z_k$ temperature of measurement point $k$

$n$ total number of measurement points above layer interface

$m$ total number of measurement points under layer interface

## 3.6 Mass Flow Rates /EMM 02/

For a discrete measurement consisting of n (i = 1 to n) so-called "bidirectional probes" and gas temperature probes arranged in parallel the mass flow for the $i^{th}$ partial opening surface can calculated with

$$\dot{m}\left(z_i\right) = 16.79 \cdot b \cdot \frac{h}{n} \cdot \sqrt{\frac{\Delta p(z_i)}{T(z_i)}} \text{ [kg/s].} \tag{3.15}$$

with:

$z_i$ elevation in the opening [m]

$b$ width of the opening [m]

$h$ height of the opening [m]

$n$ number of measurement points

A balance of the mass flows ‘in’ and ‘out’ the fire compartment must be determined as a function of the neutral height, which can vary time dependently.

## 3.7 Heat Flow through the Door /HAM 06/

The total heat flow through the door was calculated using the temperature and velocity measurements at the door opening. The heat loss through the door was estimated from the following equation:

$$HFD = \sum \dot{m} C_p \Delta T = \sum \rho \bar{v} A C_p \Delta T \text{ [kW]} \tag{3.16}$$

$\rho$ density calculated from using the ideal gas law [kg/m³]

$\bar{v}$ mean gas velocity in the range of the opening [m/s]

$A$ opening area [m²]

$C_p$ $= 1.007 + 1.816 * 10^{-4} \cdot (T - 20)$ specific heat [J/kgK]

$\Delta T$ temperature difference between hall and opening [°C]

## 3.8 Heat Loss to Walls

The heat losses into the walls, floor and ceiling are determined with the following equation:

$$HLW = \sum_{w} \alpha_w A_w \left( T_r - T_w \right) \text{ [kW]} \tag{3.17}$$

$w$ index for wall, floor and ceiling

$\alpha_w$ = 7.69 walls and ceiling, 5.88 floor; convection heat transfer coefficient [W/m²K]

$A_w$ area of wall, floor and ceiling [m²]

$T_r$ lower or upper layer room temperature [°C]

$T_w$ lower or upper layer wall temperature [°C]

In case of the walls the upper and lower layer are considered separately. For the temperature at the surface of floor and ceiling, temperatures are taken from the lowest (TW1_1 and TW2_1) and highest wall surface measuring points (TW1_7 and TW2_7) accordingly, because no measurements have been taken at this boundaries.

## 3.9 Starting and Boundary Conditions

### 3.9.1 Test Recording Times and Gas Burner Power Output

The tests have shown that it was difficult to control the gas burner as a function of the ignition of the cable bundles as intended in the specification from Benchmark Exercise No. 5 (see paragraph **2.4.3**). It is possible that a bundle is already burning, although the other one has not yet clearly caught fire. For this reason, in Tab. 3-2 the exact control of the burner is shown so that this can be considered in the frame of any further simulation. Tab. 3-2 also gives information about the overall test time until the end of each record. The end of the data record gives no information about last flames at the cables. At least 20 min were recorded after the last flames.

**Tab. 3-2** Overview test run times and burner output

| Test parameters | Test 1 | Test 2 | Test 3 | Test 4 |
|---|---|---|---|---|
| Date 2003 | 12-09 | 12-12 | 12-16 | 12-18 |
| Material | FRNC | | PVC | |
| Start of data record | - 0:02:00 | - 0:02:00 | - 0:02:00 | - 0:02:00 |
| Pre-heating | Liquid quadratic ethanol pool: 0.7* 0.7 m², 62.5 Liter | | | |
| | No | yes | no | yes |
| At test time | - | 0:00:00 | - | 0:00:00 |
| Gas burner [kW] | At test time | | | |
| 50 | - | - | 0:00:00 | 0:20:10 |
| 100 | - | - | - | 0:35:20 |
| 150 | 0:00:30 | 0:20:20 | - | - |
| 300 | 0:40:00 | 0:50:00 | - | - |
| 0 | 1:10:40 | 1:02:00 | 0:13:50 | 0:38:20 |
| End of data record | 1:39:20 | 1:56:00 | 1:03:30 | 1:57:50 |

### 3.9.2 Pressure and Temperature at Test Start Time

Tab. 3-3 provides the temperatures at the start time of the tests and Tab. 3-4 the pressure values. For the fire compartment the temperature values are given in the upper and the lower region.

**Tab. 3-3** Initial fire compartment temperature for Test 1 to Test 4

| | Test 1 | Test 2 | Test 3 | Test 4 |
|---|---|---|---|---|
| **TEMPERATURE IN COMPARTEMENT [°C]** | | | | |
| Lower level: 1.2 m | | | | |
| TR 1-2 | 14.3 | 15.8 | 18.0 | 17.7 |
| TR 2-2 | 14.7 | 15.0 | 18.5 | 18.3 |
| TR 3-2 | 15.3 | 16.0 | 18.7 | 18.7 |
| TR 4-2 | 14.3 | 14.7 | 17.5 | 17.9 |
| TW 1-2 | 15.7 | 17.3 | 19.8 | 19.1 |
| TW 2-2 | 15.1 | 17.1 | 18.9 | 18.1 |
| Upper level: 4.4 m | | | | |
| TR 1-6 | 16.2 | 17.6 | 20.6 | 18.7 |
| TR 2-6 | 16.3 | 17.7 | 20.6 | 18.8 |
| TR 3-6 | 15.7 | 17.6 | 20.8 | 18.7 |
| TR 4-6 | 16.4 | 17.7 | 20.8 | 18.8 |
| TW 1-6 | 16.7 | 17.9 | 21.4 | 18.9 |
| TW 2-6 | 16.8 | 18.2 | 21.6 | 19.0 |
| **TEMPERATURE ON CABLE SURFACE [°C]** | | | | |
| Lower level: 1.2 m. side of bundle | | | | |
| TCO 1-1 (right) | 15.0 | 16.9 | 18.5 | 17.9 |
| TCO 3-1 (left) | 15.2 | 17.1 | 18.5 | 18.3 |
| Upper level: 4.4 m. side of bundle | | | | |
| TCO 1-9 (right) | 18.0 | 18.2 | 21.8 | 19.0 |
| TCO 3-9 (left) | 18.0 | 17.9 | 21.5 | 18.9 |

**Tab. 3-4** Hall pressure and temperature values for Test 1 to Test 4

| | Test 1 | Test 2 | Test 3 | Test 4 |
|---|---|---|---|---|
| **PRESSURE IN HALL [mbar]** | | | | |
| Start test | 1015.1 | 1015.6 | 1015.2 | 1015.0 |
| End test | 1014.5 | 1016.0 | 1015.6 | 1014.5 |
| **TEMPERATURE IN HALL [°C]** | | | | |
| Start test | 16.1 | 18.0 | 18.0 | 18.5 |
| End test | 16.6 | 18.1 | 16.9 | 18.0 |

### 3.9.3 Flow Rate Exhaust Duct

In Tab. 3-5 the mean values for the flow rates in the exhaust duct are given. The flow rate $\dot{V}$ is given with equation (3.1) according to ISO 9705 /ISO 93/, the velocity is given with equation (3.2).

**Tab. 3-5** Mean values flow rate during Test 1 to Test 4

| [m³/s] | Test 1 | Test 2 | Test 3 | Test 4 |
|---|---|---|---|---|
| Mean flow rate | 2.72 | 2.81 | 2.64 | 2.76 |

## 3.10 Test Results

### 3.10.1 Short Summary of the Tests

A short overview of the main characteristics of the test series is given in the following list of comments. For additional information to the comments of Test 1 – 4 see the results for the heat release rate of the cables and the burner power output for Test 1 & 2 in Fig. 3-1 and for Test 3 & 4 in Fig. 3-2. Some plots of interest for each test are given in the Appendix A. With TR_M1-7 a mean value of the thermocouple trees TR1-4 (level by level) is given.

**Comments to Test 1 (FRNC, no pre-heating):**

Ignition of both cables at 150 kW gas burner output, no continued flame spread, little blistering of the sheath surface, FRNC cables providing only a small contribution to the total heat release.

**Comments to Test 2 (FRNC, pre-heating):**

Ignition of both cables at 150 kW gas burner output, no continued flame spread, strong blistering of the sheath surface, FRNC cables providing only a small contribution to the total heat release.

**Comments to Test 3 (PVC, no pre-heating):**

Ignition of both cables at 50 kW gas burner output, continued flame spread on both cables.

**Comments to Test 4 (PVC, pre-heating):**

Ignition of cable A at 50 kW gas burner output with continued flame spread, no ignition of cable B at this output level. Ignition of cable B at a 100 kW gas burner output followed by a flash over of the cables.

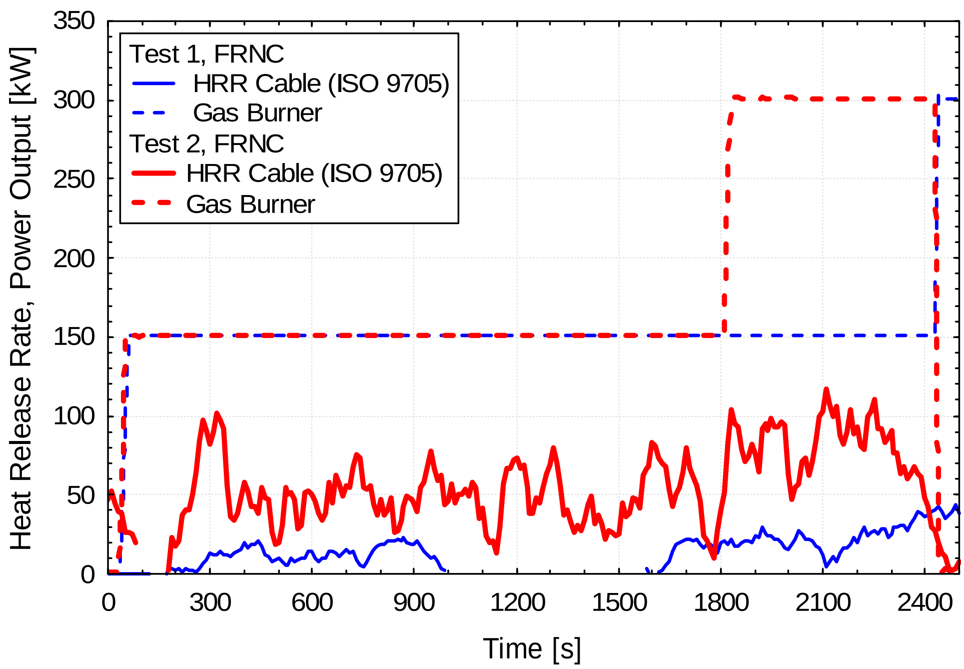


**Fig. 3-1** HRR cable and Gas Burner power output from Test 1 & Test 2 (FRNC cables), for better comparison of HHR results the pre-heating phase of Test 2 is not shown

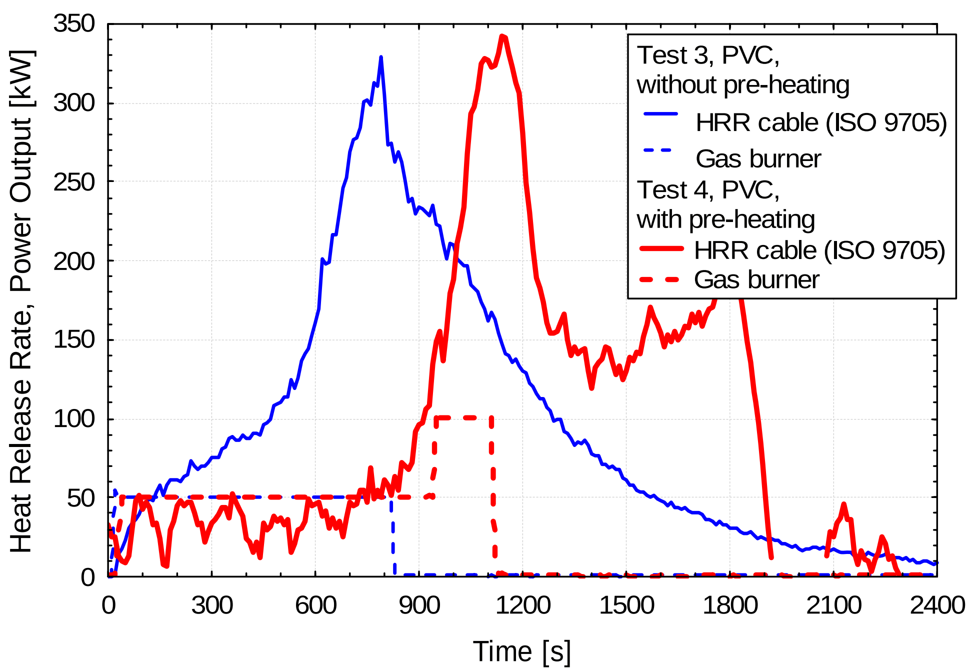


**Fig. 3-2** HRR cable and Gas Burner power output from Test 3 & Test 4 (PVC cables), for better comparison of HRR results the pre-heating phase of Test 4 is not shown

### 3.10.2 General Results

Fig. 3-3 shows the temperature 40 cm in front of the cable tray for Test 2 and Fig. 3-4 for Test 4 during the phase of pre-heating. Fig. 3-5 shows the measured heat flux in front of the cable tray for Test 2 and Fig. 3-6 for Test 4. The temperatures and the heat fluxes in Test 2 and Test 4 in the environment of the cable tray are in good agreement. The boundary conditions for both tests are nearly the same.

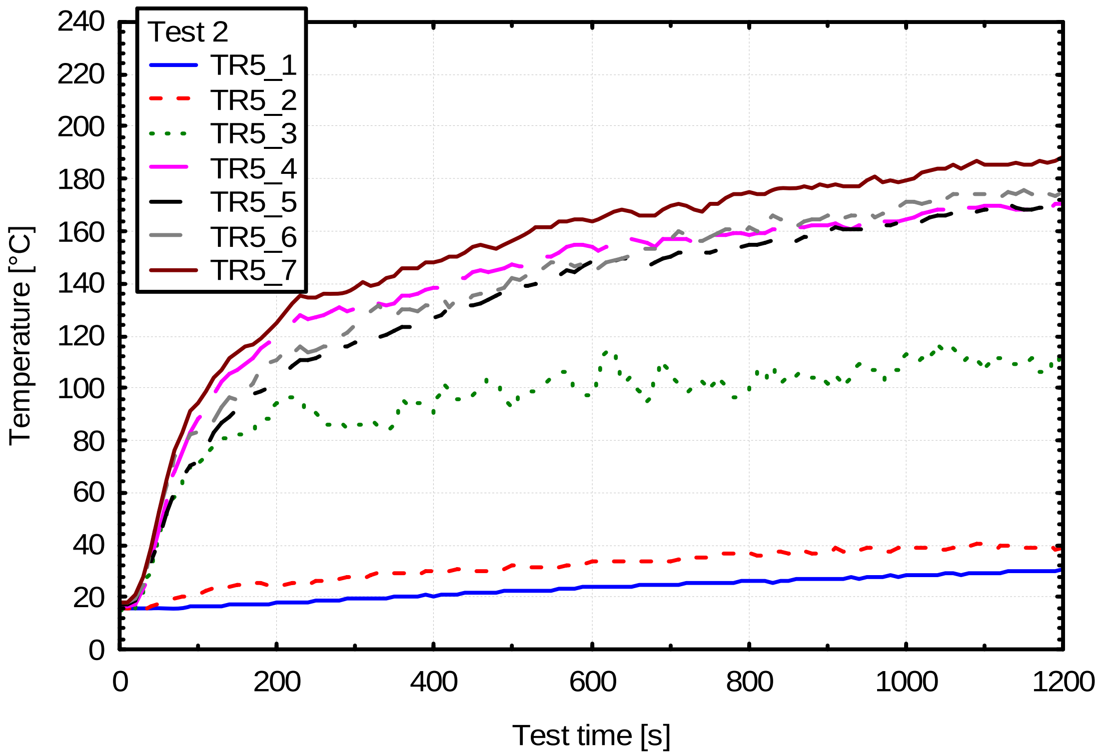


**Fig. 3-3** Temperature TR5, 40 cm in front of the cable tray levels 1-7, Test 2

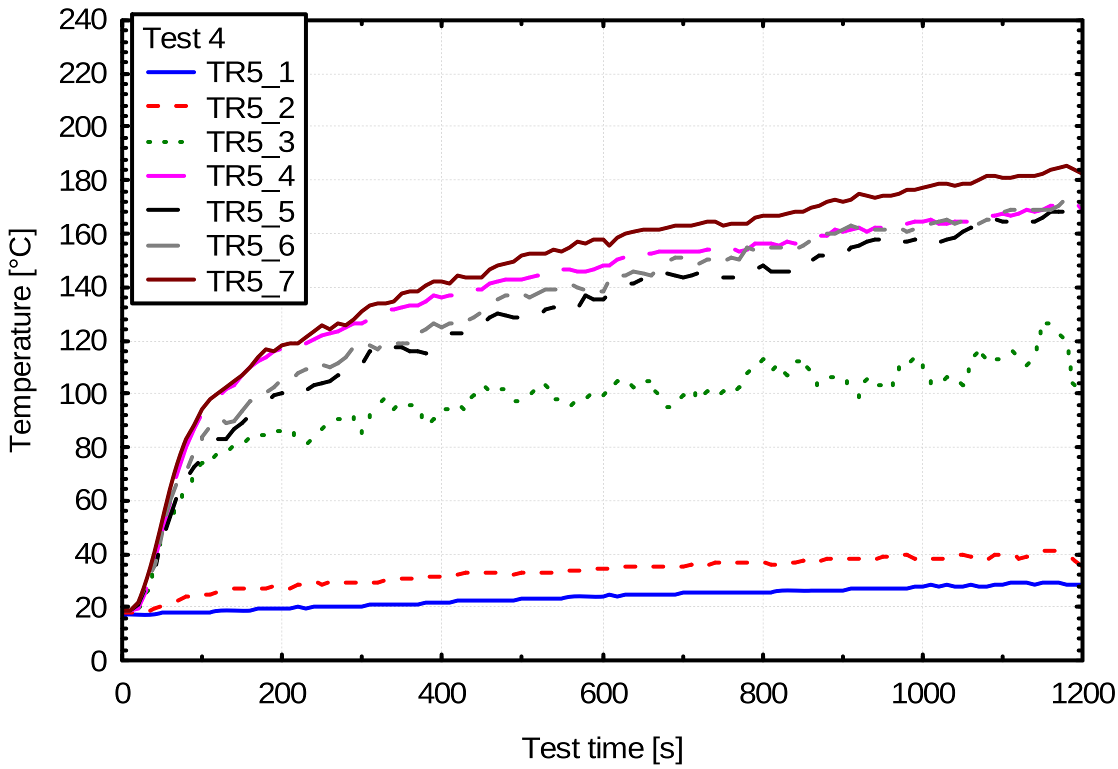


**Fig. 3-4** Temperature TR5, 40 cm in front of the cable tray levels 1-7, Test 4

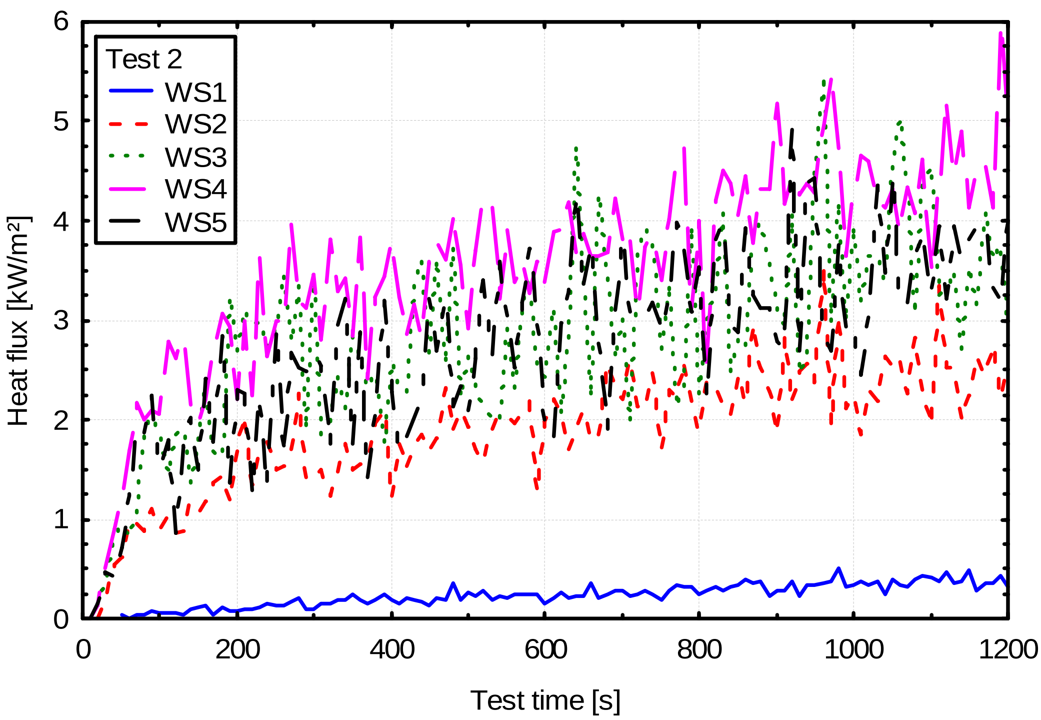


**Fig. 3-5** Heat flux WS, in front of the cable tray levels 1-5, Test 2

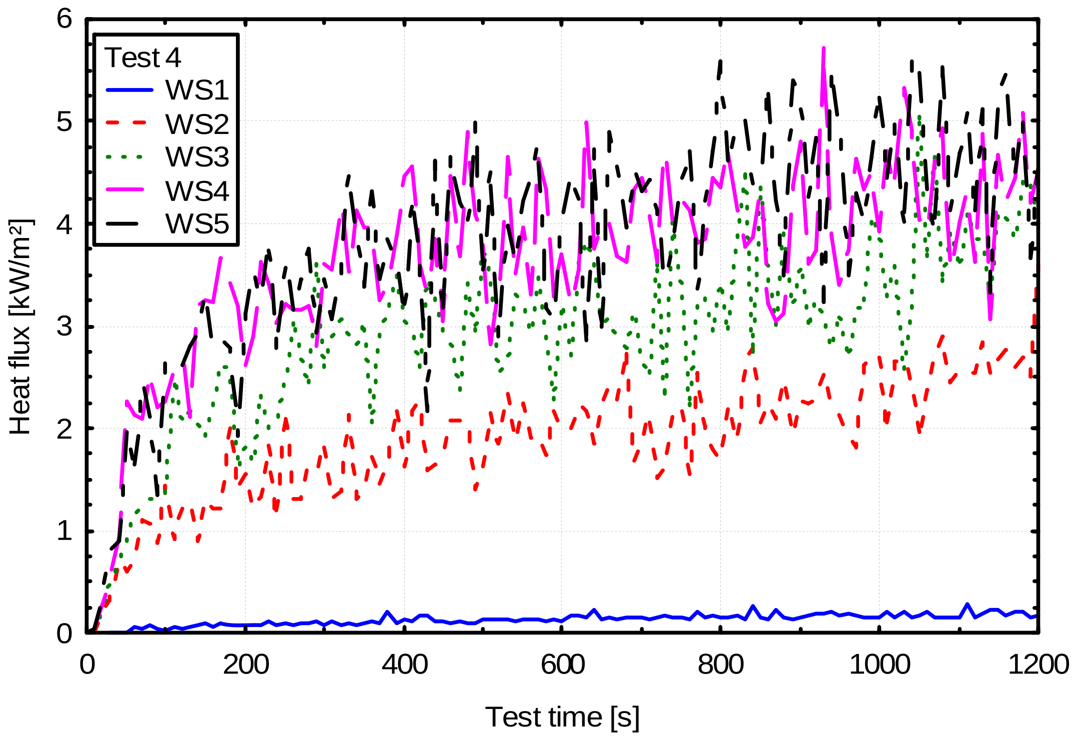


**Fig. 3-6** Heat flux WS, in front of the cable tray levels 1-5, Test 4

In Tab. 3-6 the ignition times observed for Test 1 to Test 4 are given. The ignition time is not accurately determined because the gas burner fire and the fire of the cables themselves are superimposed. The ignition times given here can only be used as an indicator for the fire behavior of the tested cables.

In case of Test 4, the power cables are not ignited at a burner output of 50 kW and ignited only when the burner is increased to 100 kW. This behavior has not been expected, because there was no problem to ignite the PVC power cables in case of Test 3 without pre-heating and the same burner output (see Fig. 3-1 and Fig. 3-2). One possibility for the cause of this effect could be that the ethanol pool produced a flow field in which the flame of the gas burner is pulled away from the cable to the side of the pool. The consequence could be that the gas burner output is not large enough to ignite the power cables. On the other hand, the oxygen concentration in the room changes because of the oxygen consumption of the burning ethanol. This may represent another reason for the difficulty to ignite the PVC insulated power cables.

In /HOS 03/ no systematic difference for the measured heat release rate of I&C and power cables from the same material in Cone-Calorimeter tests has been found if the same diameter of the cables is used. In Benchmark Exercise No. 5 the diameter of the PVC power cables is much larger than for the I&C cables. This should lead to different fire behavior from the I&C and power cables in this benchmark. During the pre-heating period of approx. 1200 s the cable insulation is probably pyrolysed to a certain degree, but the released gases are not ignited. In particular, flammable plasticizer could be released at low temperatures, what would be equivalent to an ageing of the insulation material. Secondarily it is possible that the pyrolysis gases are taken away through the door and an ignition is possible at a different place and at later time. This could be a hazardous effect.

**Tab. 3-6** Ignition times observed

| | Test 1 | Test 2 | Test 3 | Test 4 |
|---|---|---|---|---|
| Material | FRNC | | PVC | |
| Burner output [kW] | 150 | 150 + pre-heating | 50 | 50 + pre-heating |
| | Ignition time [s] | | | |
| power cables | 150 | 360 | 190 | - |
| I&C cables | 187 | 133 | 428 | 171 |

Fig. 3-7 and Fig. 3-8 show the ignition phase of Test 3 and Test 4, respectively. Fig. 3-9 to Fig. 3-12 show the cable insulation materials after Test 1 and Test 3 in the lower and upper part of the tray.

**Fig. 3-7** Ignition phase of Test 3, PVC I&C and power cables

**Fig. 3-8** Ignition phase of Test 4, no ignition of PVC power cables

**Fig. 3-9** FRNC cable material after Test 1, lower range of tray

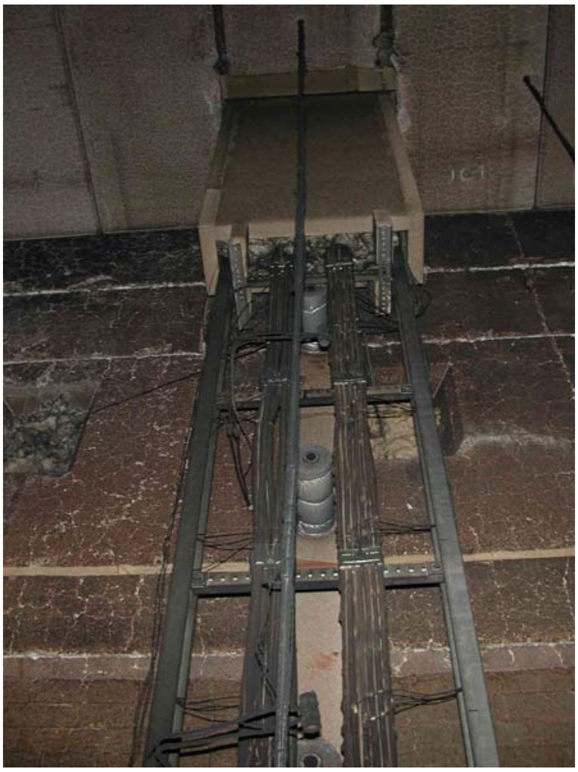

**Fig. 3-10** FRNC cable material after Test 1, upper range of tray

**Fig. 3-11** PVC cable material after Test 3, lower range of tray

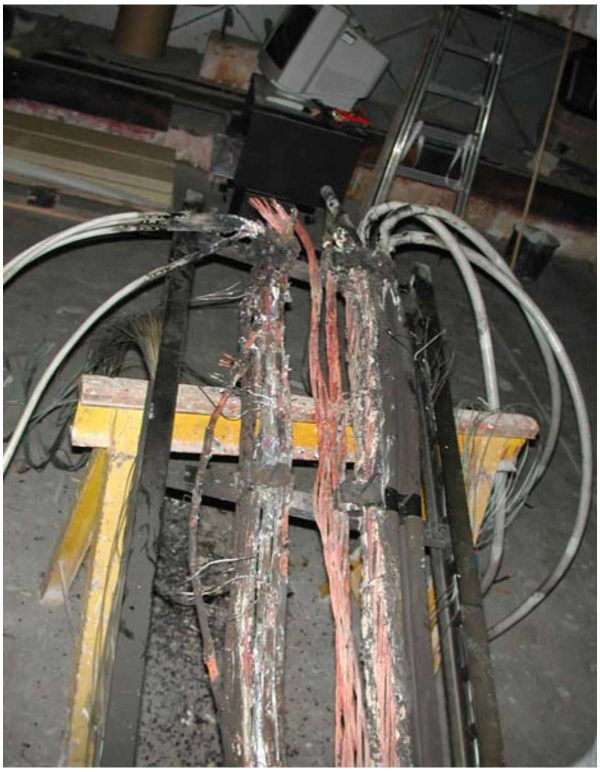

**Fig. 3-12** PVC cable material after Test 3, upper range of tray

### 3.10.3 Flame Spread

Major topic of Benchmark Exercise No. 5 is the flame spread on cables. In case of Test 1 and Test 2 (FRNC insulated cables) no substantial flame spread occurs. In the following paragraph, results of Test 3 (PVC insulated cables, without pre-heating) will be discussed. Fig. 3-13 shows the course over the time of the 9 temperature measuring points on the I&C cables (TCO3_1 to TCO3_9) and Fig. 3-15 on the power cables (TCO1_1 to TCO1_9) of Test 3. In all figures presented in this paragraph only the first 900 s are considered. A temperature plateau at about 220 C in nearly all measured heights has been found in case of power cables for about 100 s time period. After this interruption, the temperatures are increasing again.

A temperature on the cable from 350 °C is assumed to indicate a burning of the cable. In case of I&C cables, a relative continuous flame spread over the whole distance to the cable tray occurs. Fig. 3-14 shows the flame spread velocity from level to level on the cable tray for the I&C cables in Test 3. In the upper part of the tray (level 4 to level 8) a mean value for the flame spread velocity of 90 cm/min is found. For the whole distance on the tray (level 1 to level 9) the total flame spread velocity is given with 40 cm/min.

Fig. 3-16 shows the flame spread velocity from level to level on the cable tray for the power cables of Test 3. In case of the power cables, the flame spread velocity on the cable tray has strong variations, a continuous level by level flame spread is not found. With the simple assumption that the flames jump from level to level negative values for the flame spread velocity indicate a flame spread from a higher to a lower lever on the tray. For the power cables applied in Test 3 it is not meaningful to provide mean and total flame spread velocities. It is obvious that flame spread is a complex process and that boundary effects could even lead to a sudden flame jump over the whole distance. In particular, the separated cable bundles interact in their fire behavior.

The temperatures measured during Test 3 in front of the cable tray (TR5_1 to TR5_7) are presented in Fig. 3-17 and the heat flux densities (WS1-WS5) between the two cable bundles are presented in Fig. 3-18. For the exact location of the instrumentation see paragraph **2.4.4**.

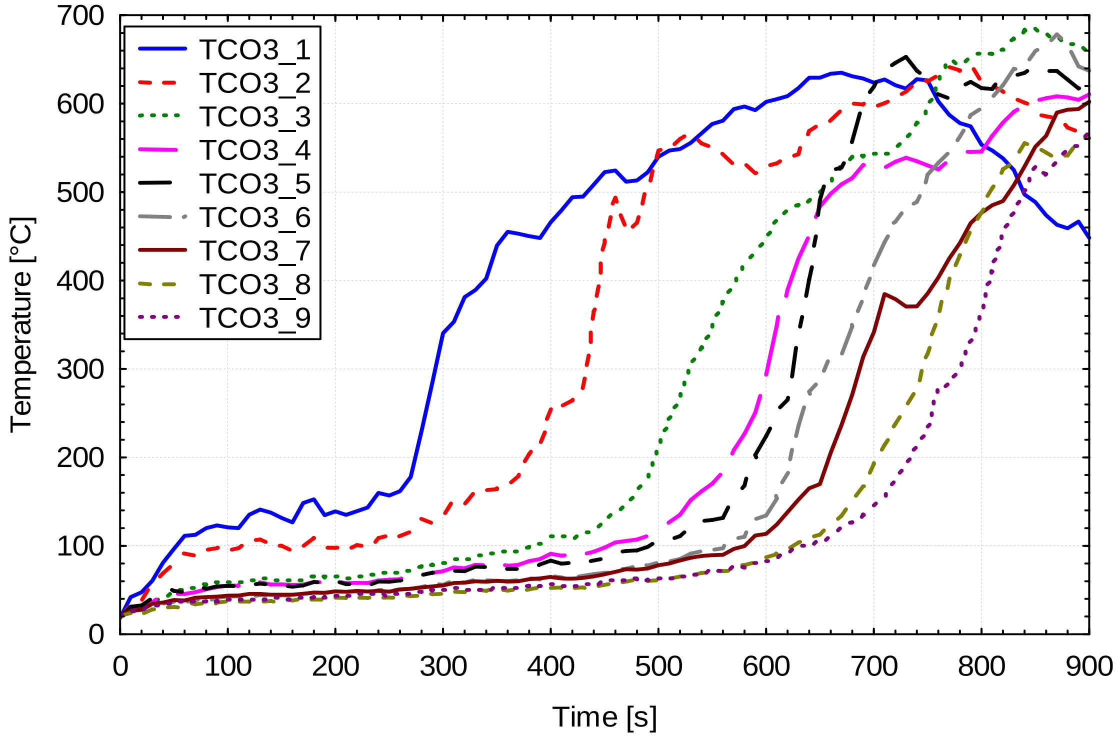


**Fig. 3-13** Temperatures on I&C cables (cable A, Test 3, without pre-heating)

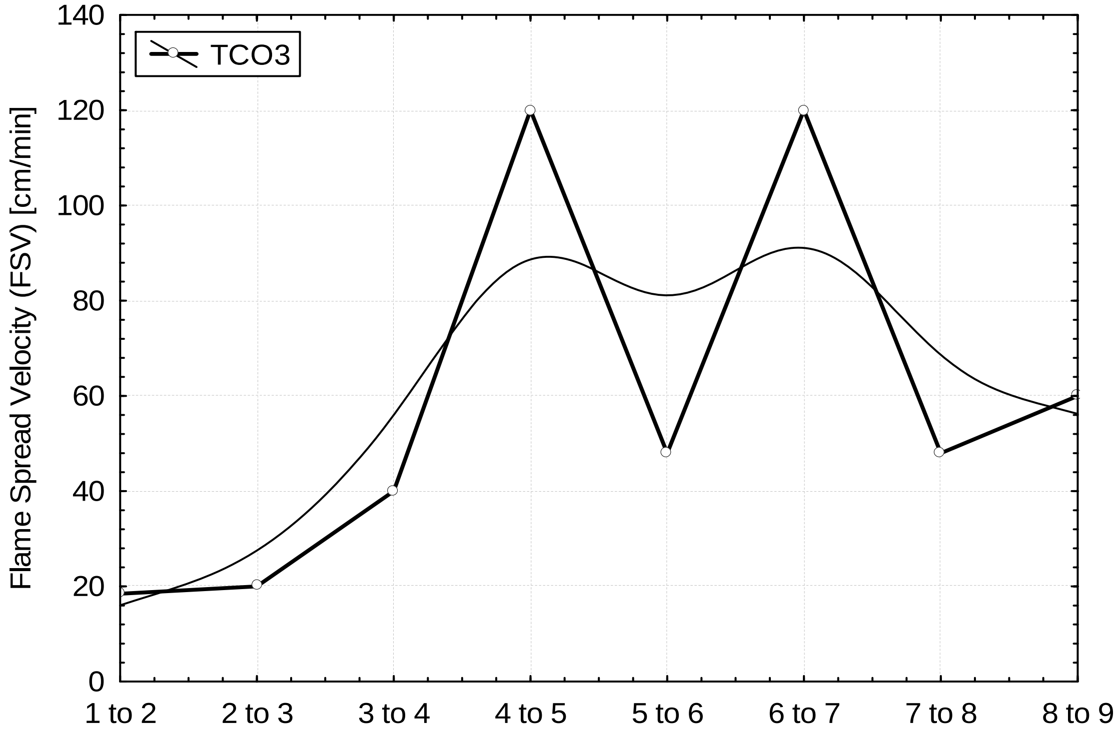


**Fig. 3-14** Flame spread velocity on I&C cables (cable A, Test 3, without pre-heating)

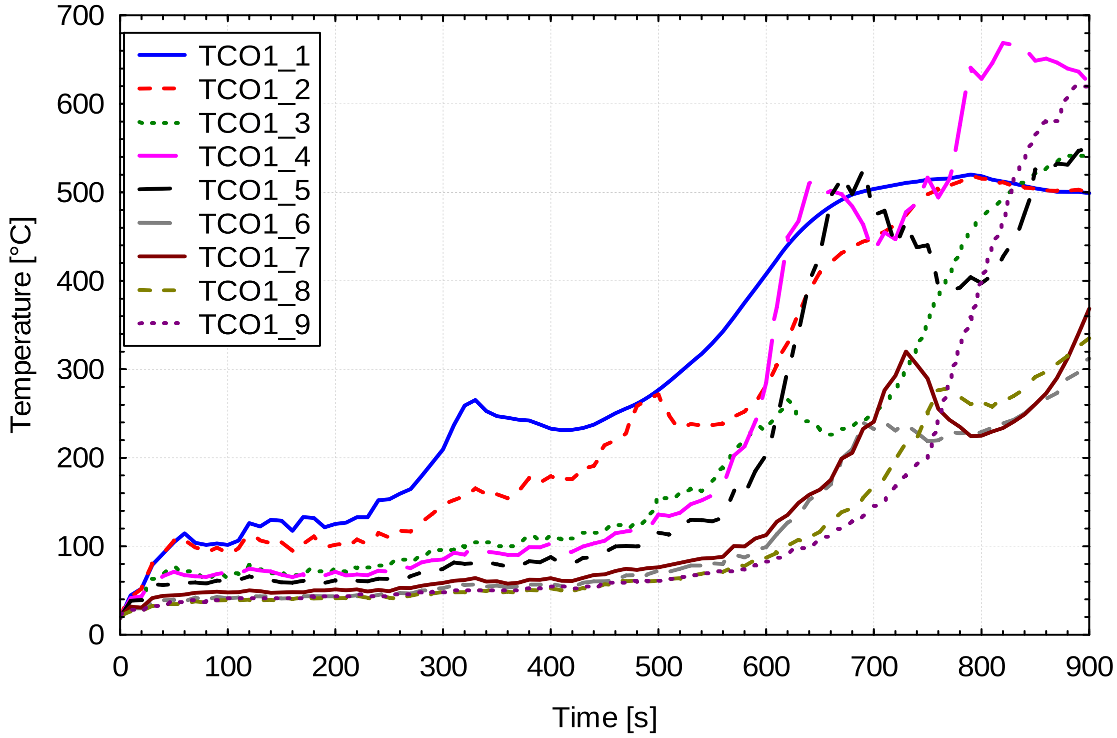


**Fig. 3-15** Temperatures on power cables (cable B, Test 3, without pre-heating)

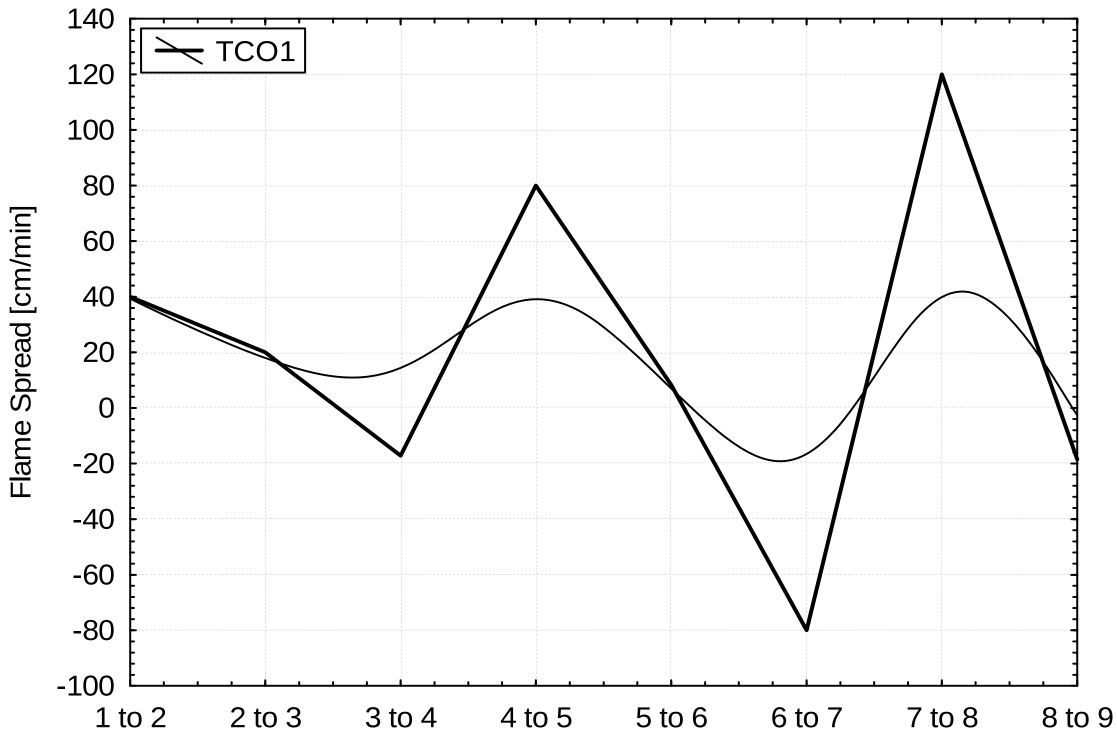


**Fig. 3-16** Flame spread velocity on power cables (cable B, Test 3, without pre-heating)

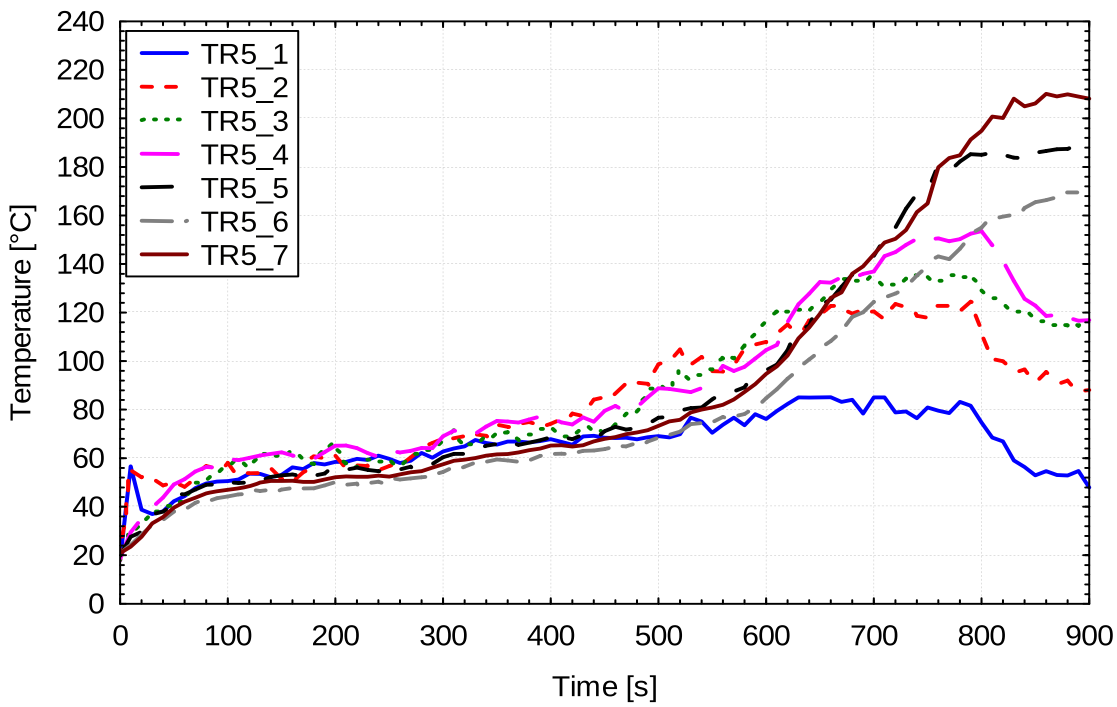


**Fig. 3-17** Temperatures in front of cable bundles A and B on the cable tray, Test 3

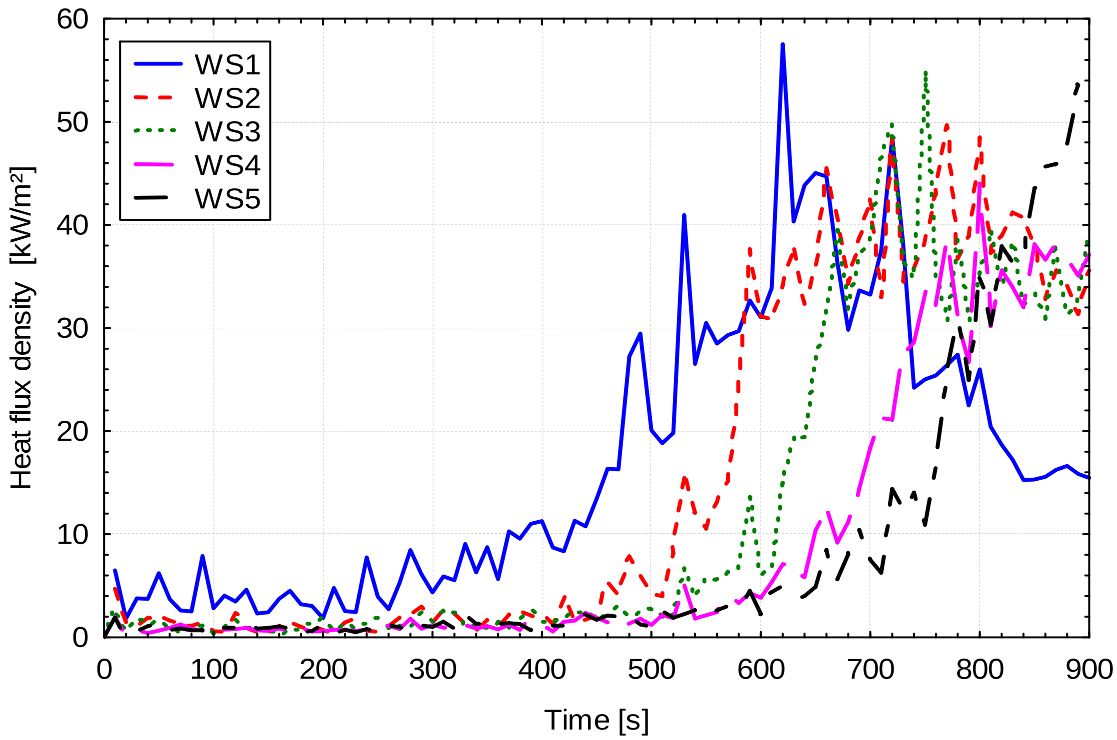


**Fig. 3-18** Heat flux density in front of cable bundles A and B on cable tray, Test 3

### 3.10.4 Functional Failure Results

An overview of the abbreviations used in the text and figures in this paragraph is given in paragraph **2.4.6**. Fig. 3-19 to Fig. 3-22 show the short circuit times for the Tests 1 to 4. Each plot involves a curve of the burner output during the test. In Tab. 3-7 and Tab. 3-8 data on the first short circuit, the mean value and the standard deviations of all short circuit times for the first burner output level are given. For Test 2 and Test 4 the pre-heating time of 1200 s is neglected.

Fig. 3-23 shows the functional failure results for I&C cables during all tests. A significant difference in short circuit times is found between FRNC and PVC insulated cables. The tests show a significant effect of pre-heating on the functional failure times of the cables. This behavior is a result of the effects of the thermo-physical data from the PVC insulated and the FRNC cables, respectively, which are documented in Appendix A. The thermal inertia ($\lambda\rho c_p$) from the FRNC cables is higher than that from the PVC cables, so that the temperatures at the cable centre are lower in case of the FRNC cables (Test 2) then in case of the PVC cable in Test 4 after pre-heating time. The temperatures at the cable centre of the I&C PVC cables after 20 min pre-heating are approx. 30 – 40 °C higher. This effect is diagrammed in Fig. 3-25 for Test 2 and Test 4. It is remarkable that the PVC cables are ignited with a burner output of 50 kW, while, in contrary, the FRNC cable are ignited with 150 kW.

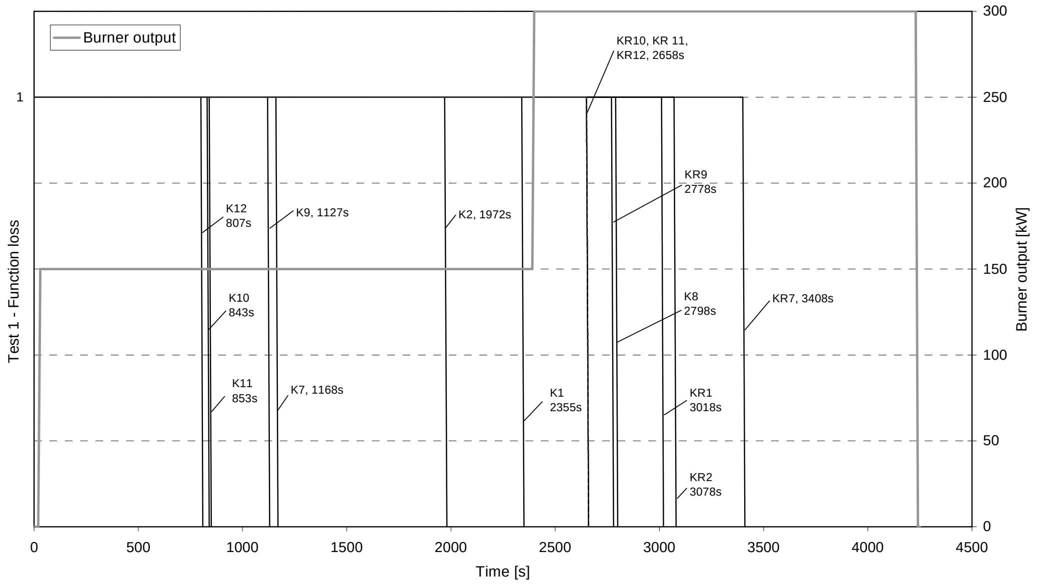


**Fig. 3-19** Burner output and short circuits of FRNC cables (Test 1, without pre-heating)

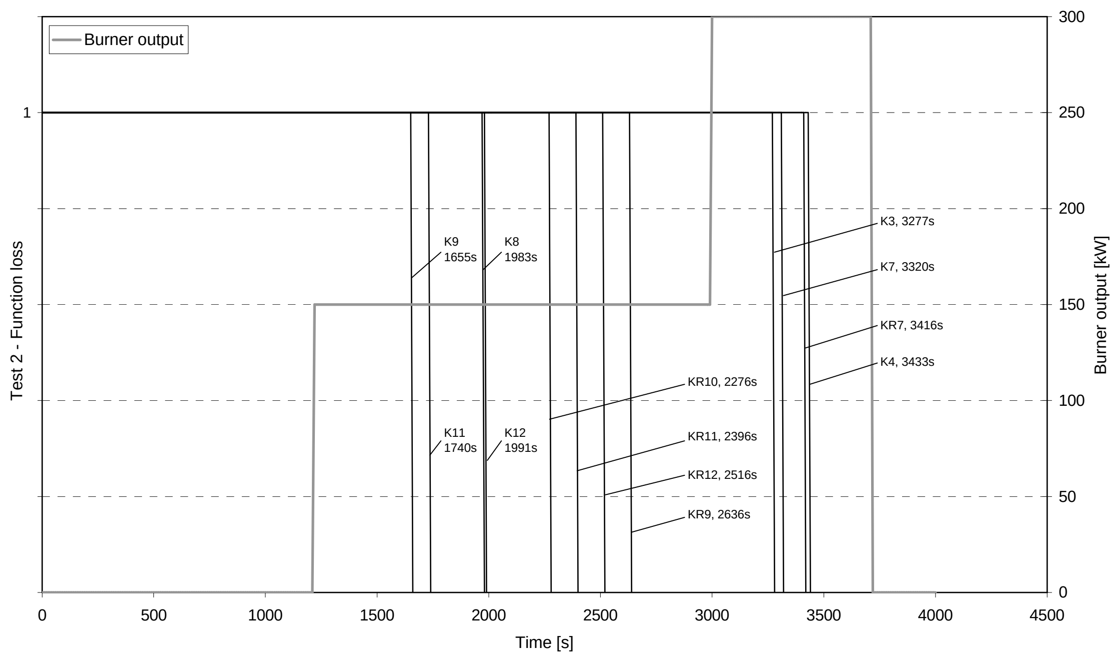


**Fig. 3-20** Burner output and short circuits of FRNC cables (Test 2, pre-heating 1200 s)

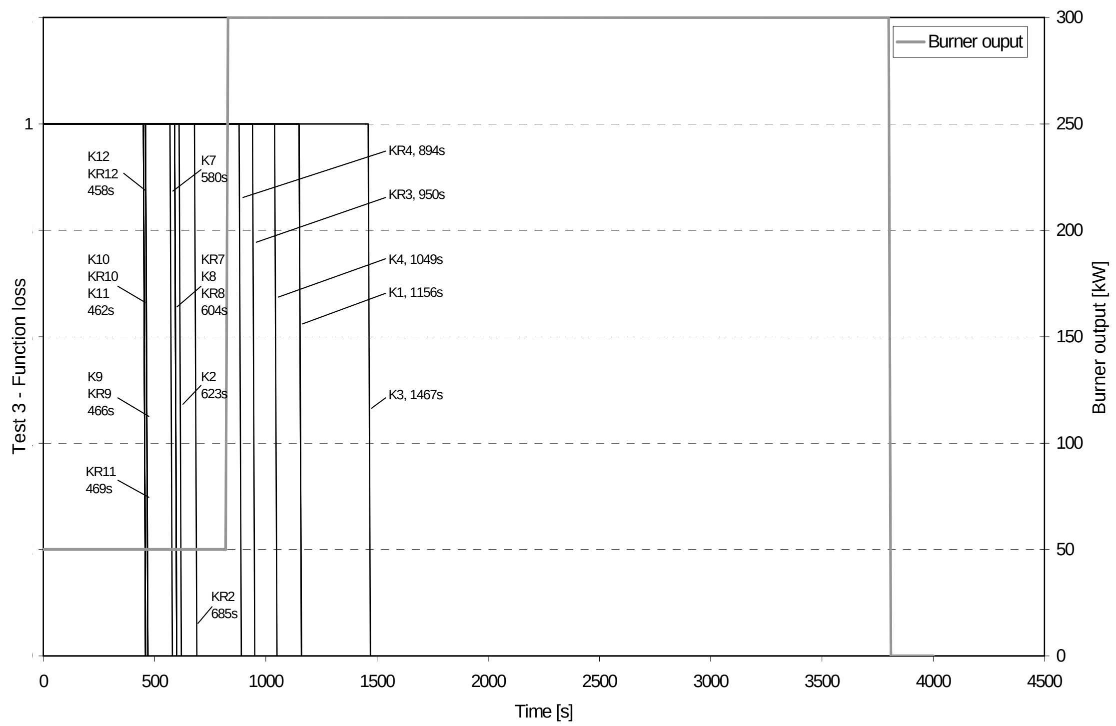


**Fig. 3-21** Burner output and short circuits of PVC cables (Test 3, without pre-heating)

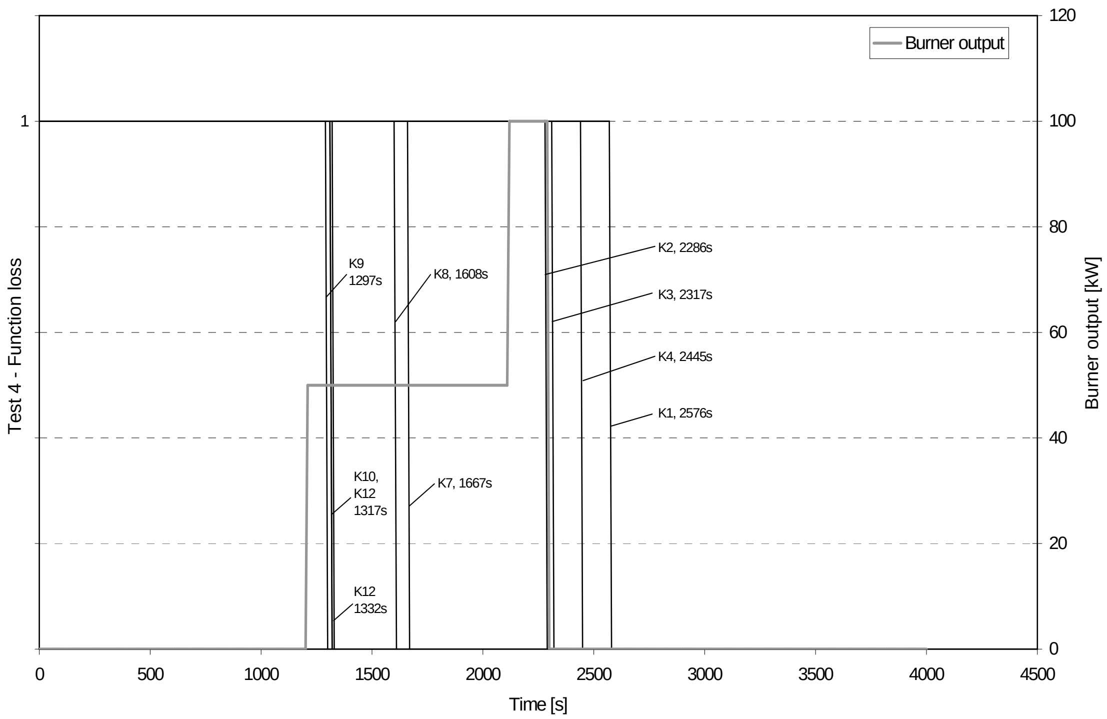


**Fig. 3-22** Burner output and short circuits of PVC cables (Test 4, pre-heating 1200 s)

**Tab. 3-7** Short circuit times, Test 1 and Test 2, FRNC cables

| **Burner output [kW]** | | **Test 1: no pre-heating [s]** | | **Test 2: pre-heating [s]** | |
|---|---|---|---|---|---|
| | | **I&C cable C** | **Power cable D** | **I&C cable C** | **Power cable D** |
| conductor to conductor (K) | | | | | |
| 150 | minimum | 807 | 1972 | 455 | - |
| | failure index | K12 | K2 | K9 | - |
| | mean value and standard deviation | $959 \pm 173$ | $2163 \pm 270$ | $642 \pm 171$ | - |
| conductor to tray (KR) | | | | | |
| 150 | Minimum | - | - | 1076 | - |
| | failure index | - | - | KR10 | - |
| | mean value and standard deviation | - | - | $1236 \pm 183$ | - |

**Tab. 3-8** Short circuit times Test 3 and Test 4, PVC cables

| Burner output [kW] | | Test 3: no pre-heating [s] | | Test 4: pre-heating [s] | |
|---|---|---|---|---|---|
| | | **I&C cable A** | **Power cable B** | **I&C cable A** | **Power cable B** |
| conductor to conductor (K) | | | | | |
| 50 | minimum | 458 | 623 | 97 | 1117 |
| | failure index | K12 | K2 | K9 | K3 |
| | mean value and standard deviation | 547 ± 78 | 1074 ± 349 | 223 ± 158 | 1207 ± 134 |
| conductor to tray (KR) | | | | | |
| 50 | minimum | 458 | 685 | - | - |
| | failure index | KR12 | KR2 | - | - |
| | mean value and standard deviation | 531 ± 103 | 921 ± 194 | - | - |

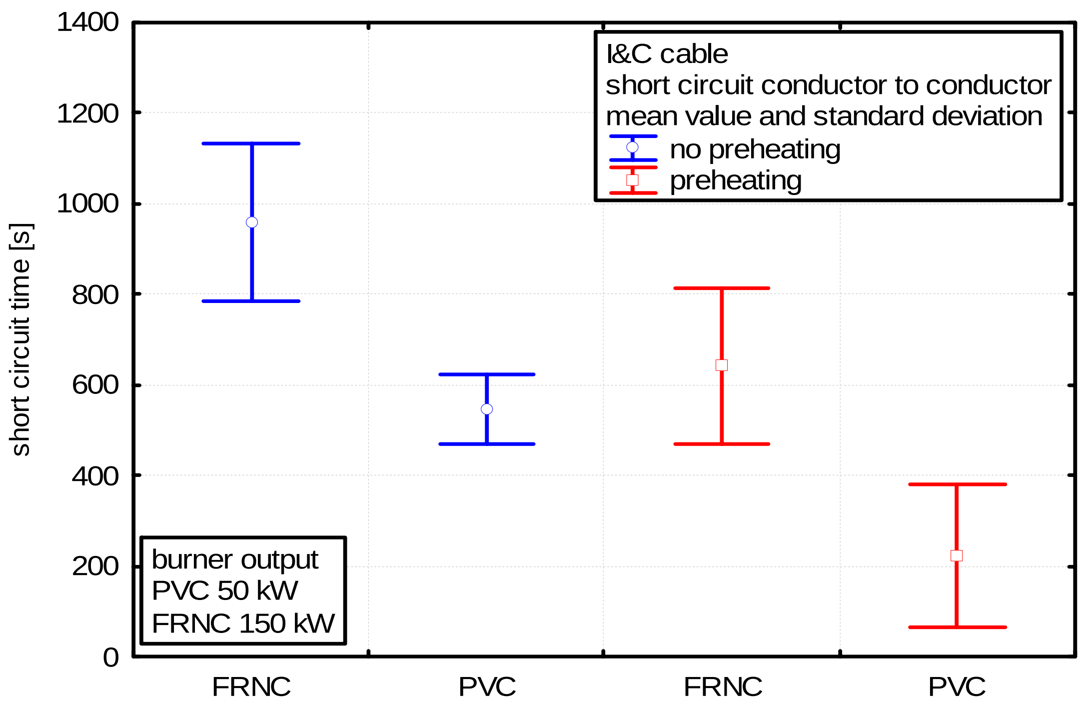


**Fig. 3-23** Short circuit times, Tests 1 to 4, I&C cables

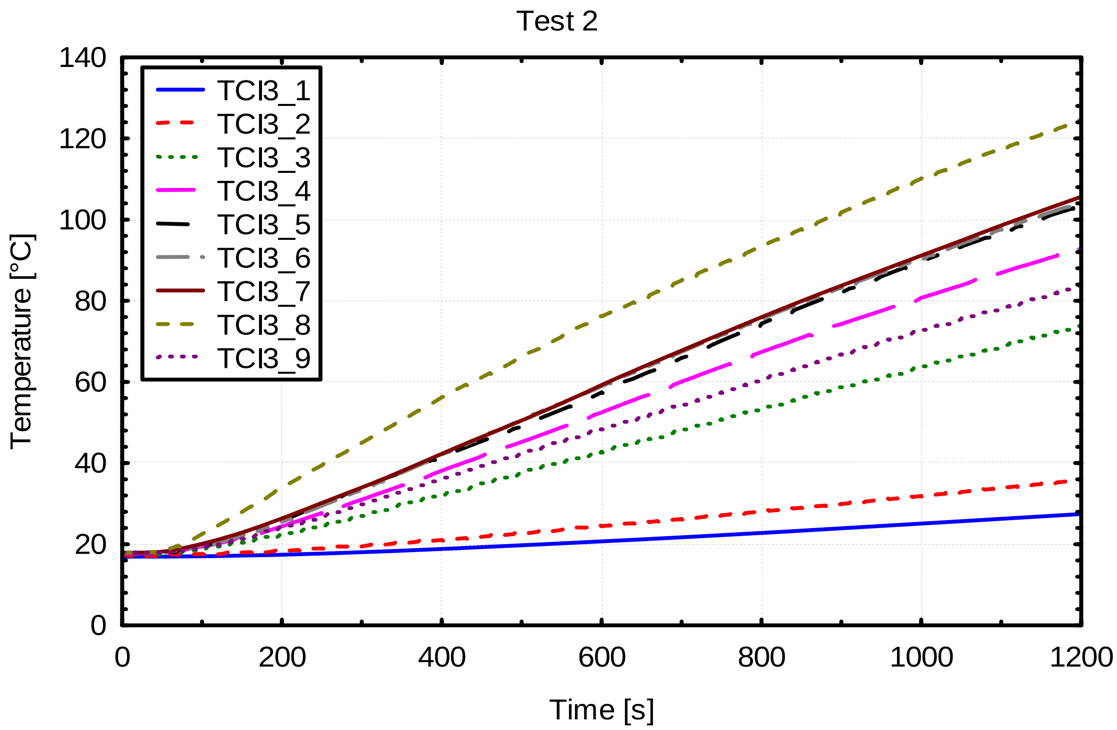


**Fig. 3-24** Temperature cable centre TCI3, pre-heating 1200 s, Test 2

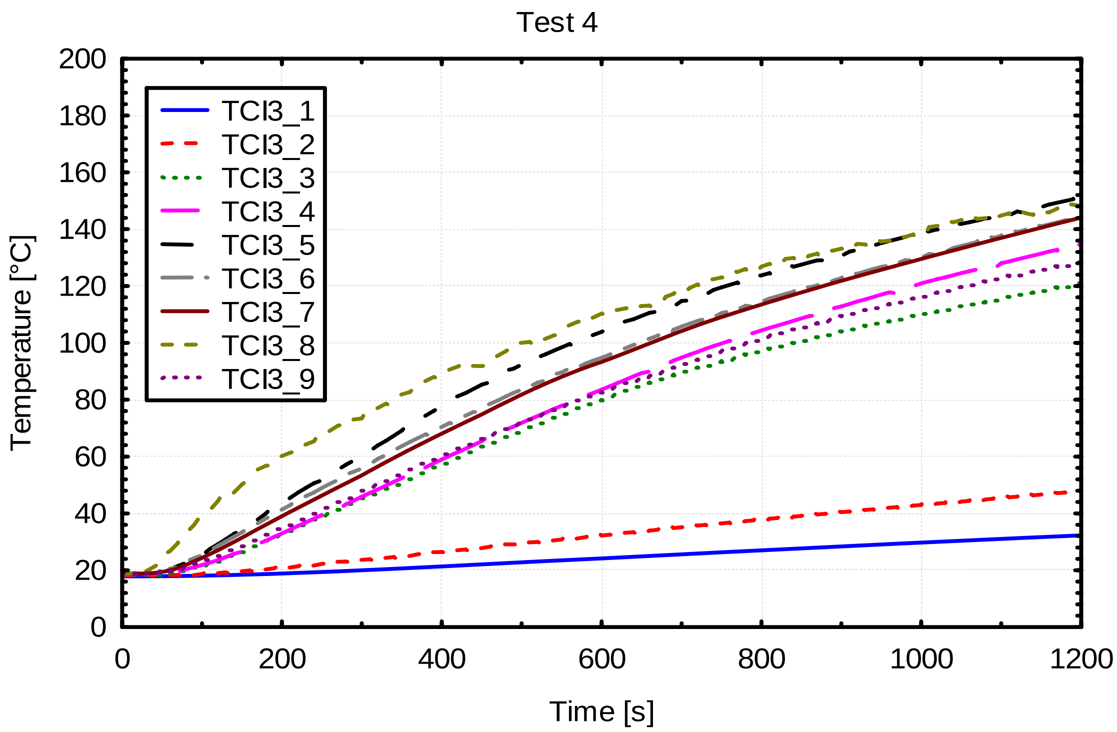


**Fig. 3-25** Temperature cable centre TCI3, pre-heating 1200 s, Test 4

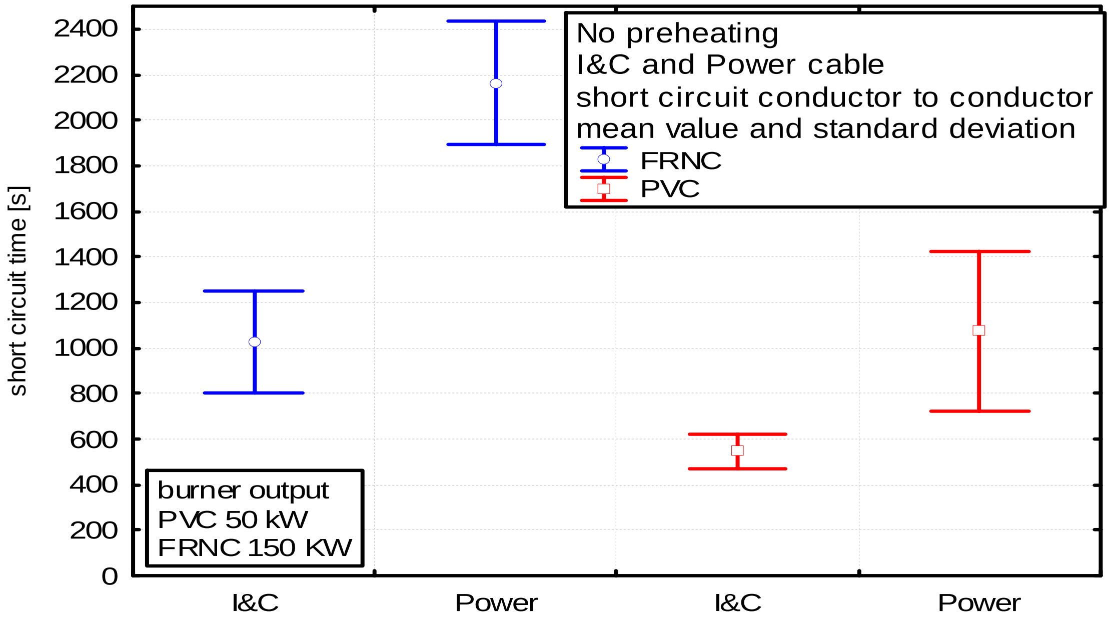


**Fig. 3-26** Short circuit times, Tests 1 to 4, no pre-heating

Fig. 3-26 shows the results for I&C cables for both insulation materials in case of no pre-heating (Test 1 and Test 3). It is obvious that power cables have better fire characteristics than I&C cables of the same cable insulation material. This effect can be explained by the higher fraction of metal in case of the power cables so that heat could dissipate. This process results in later times of ignition. In /HOS 03/, high voltage power cables as well as low voltage I&C cables from different cable insulation materials have been tested with similar results.

In /HOS 03/ it has also been demonstrated that a fundamental distinction between horizontal and vertically oriented cable has to be made. For the horizontal cable arrangement, there is a significant dependence between the fire propagation, the cable quantity, the cable density, and the location in the fire area. For vertically oriented cables the influence of the quantity of cables in a bundle on the vertical propagation is not so clearly stated. That means that it is not possible to transfer the functional failure results from the vertical to the horizontal cable tray arrangement. Nevertheless, the vertical configuration leads to significant higher flame spread velocities /HOS 03/. This effect significantly impacts the heat input to the room. As a consequence, the temperatures in the close vicinity of the cable increase. In this case, it is possible that vertically oriented cable trays show worse fire characteristics compared to horizontally oriented cable trays.

# 4 Input Parameters and Assumptions

This section gives information about input parameters and assumptions made to provide the participants with input data for conducting blind and open predictions. A comprehensive specification of the Benchmark Exercise has been given and various thermo-physical data for the compartment as well for the fire scenario (e.g. data on the wall, on the ethanol pool for pre-heating and on the ignition burner output).

Important measurements are provided by the oxygen calorimetric that are used to derive the total heat release rate (HRR) from the test. The accuracy of the given HRR is about 20 %. Another fundamental measurement is the mass loss directly from the cable during the test.

Typical thermo-physical data and the fire characteristics of the cables must be known for the different codes as input values. **Tab. 4-1** gives an overview over the methods used to gain several of these data. The data from a Cone Calorimeter test are needed to be converted to the properties listed in **Tab. 4-1**. This list is neither complete nor are the methods chosen necessarily the best for each property. No data are provided for the conductivity, for the specific heat and for the emissivity of the cable insulation materials. These data have to be taken from the literature.

The main procedure applied is the Cone Calorimeter test /ISO 99/, which is used to obtain the most desired properties from the cable materials. To determine the ignition temperature $T_{ig}$, the critical heat flux (*CHF*) and the thermal inertia ($\lambda \rho c_p$) the method from Janssens /JAN 92/ has been used. The procedure has been developed for a material with thermally thick behavior (that means with low heat conductivity, for example in case of an insulation material). The approach of Janssens solvthe case of a semi-infinite slab heated by radiation and cooled by convection. The result from a statistical approach derived the following relation

$$\dot{q}''_e = CHF\left[1 + 0.73\left(\frac{\lambda \rho c_p}{h_{eff}^2 t_{ig}}\right)^{0,547}\right], \qquad (4.1)$$

with $\dot{q}''_e$ representing the external heat flux from the Cone Calorimeter. An effective convective heat coefficient is given by

$$h_{eff} = \frac{\alpha_s CHF}{\left(T_{ig} - T_0\right)} \tag{4.2}$$

where $\alpha_s$ is the absorption coefficient of the solid surface and $T_0$ the ambient temperature. The absorption coefficient is assumed to be equal to the surface emissivity. Equation (4.1) has great significance for the practical application of radiant ignition data. It implies that if experimental data are plotted such that $\dot{q}_e''$ is on the x-axis and $1/t_{ign^{0.547}}$ on the y-axis, the data will fall in a straight line with the x-axis intercept being the critical heat flux. In the measured times of ignition at different heat flux densities are given. For further details see /JAN 92/.

The effective heat of combustion is given by means of dividing the heat release rate by the mass loss rate:

$$\Delta H_{c,eff}\left(t\right) = \frac{\dot{q}''\left(t\right)}{\dot{m}''\left(t\right)} \tag{4.3}$$

The most problematic parameter is the effective heat of gasification $\Delta H_{g,eff}$, since this parameter is not a constant in time, particularly for charring materials. However, a average effective value can be determined by analyzing Cone Calorimeter data in terms of the peak heat release rate as a function of the external heat flux. The equation is

$$\dot{q}'' = \dot{q}''_{net} \frac{\overline{\Delta H_{c,eff}}}{\Delta H_{g,eff}} . \tag{4.4}$$

The net heat flux is a function of the external radiant heat flux provided the flame heat flux in the Cone test and the re-radiation flux or surface temperature is constant. These are reasonable as long as the flame is large, and the long-term charring effects are small, accordingly /QUI 02/.

**Tab. 4-1** Input data, properties and methods

| | Property | Symbol | Unit | Method or source |
|---|---|---|---|---|
| 1 | Ignition temperature | $t_{ign}$ | °C | Cone, Janssens /JAN 92/ |
| 2 | Critical Heat flux | $CHF$ | kW/m² | Cone, Janssens /JAN 92/ |
| 3 | Thermal inertia | $\lambda\rho c_p$ | kJ²/K²/m⁴/s | Cone, Janssens /JAN 92/ |
| 4 | Average effective heat of gasification | $\overline{\Delta H_{g,eff}}$ | kJ/kg | Cone, Quintiere /QUI 02/ |
| 5 | Average effective heat of combustion | $\overline{\Delta H_{c,eff}}$ | kJ/kg | Cone |
| 6 | Average heat release rate | $\overline{HRR}$ | kW/m² | Cone |
| 7 | Maximum burning rate | $\dot{m}''_{\max}$ | kg/s/m² | Cone |
| 8 | Average $CO_2$ – Yield | $\overline{Y_{CO_2}}$ | kg/kg | Cone, average over MLR* |
| 9 | Average CO – Yield | $\overline{Y_{CO}}$ | kg/kg | Cone, average over MLR* |
| 10 | Average soot – Yield | $\overline{Y_{Soot}}$ | kg/kg | Cone, average over 300 s |
| 12 | Density | $\rho$ | kg/m³ | Manufacturer |
| 11 | Conductivity | $\lambda$ | W/m/K | No reference |
| 13 | Specific heat | $c_s$ | kJ/kg/K | No reference |
| 14 | Emissivity | $\varepsilon$ | - | No reference |

* MLR 10-90% according to ISO 5660 /ISO 99/

**Tab. 4-2** Time to ignition for cables

| Cable Index | Time to ignition $t_{ign}$ [s] | | | | |
|---|---|---|---|---|---|
| | Heat flux density [kW/m²] | | | | |
| | 18 | 20 | 25 | 35 | 50 |
| A | 198 | 141 | 60 | 44 | 8 |
| B | 365 | 239 | 137 | 43 | 16 |
| C | ∞ | ∞ | 355 | 109 | 47 |
| D | ∞ | 986 | 492 | 157 | 62 |

∞: no ignition until 45 min, at 18 and 20 kW/m² only measurement of ignition time;
the given ignition times are an average value from two tests each; results of later measurements reveal a minimum heat flux of 11 kW/m² for cable A, and of 9 kW/m² for cable B; the minimum heat flux is the one between the lowest heat flux, for which no ignition occurs after 45 min, and the heat flux, for which ignition occurs within a time period of 45 min; with this approach the minimum heat flux for cables C and D would be 22.5 kW/m² and 19 kW/m² respectively

All the results with respect to the thermo-physical data and additional information according to the cables are given in Appendix A.

# 5 Comparison of Code Calculations and Experimental Results

The fire simulation codes have been applied within the Benchmark Exercise No. 5 by the expert institutions are listed in **Tab. 5-1**. A description of the various models, with references, is presented in the individual reports (where provided) in the appendicies.

Two different types of calculations have been performed by the individual modellers as written in **Tab. 5-1**. “Blind” means with only the detailed information of the given specification, and “open” means with all information from results of the measurements that have been made.

**Tab. 5-1** Fire simulation codes applied by expert institutions

| | Institution | Code | Code type | Calculations | Individual report |
|---|---|---|---|---|---|
| 1 | EPRI | MAGIC 3.4.8 | Zone | blind | not available[2] |
| 2 | NRC | FDS 3.1.5 | CFD | (blind), open[1] | Appendix C |
| 3 | NRC | CFAST 3.1.7 | Zone | (blind), open[1] | Appendix C |
| 4 | NIST | FDS 4.0 | CFD | blind, open | Appendix D[3] |
| 5 | GRS | COCOSYS (Developer Version) | Lumped parameter | blind, open | Appendix E |
| 6 | GRS | CFX | CFD | open | Appendix F |

[1] Tests are simulated only for the first 20 minutes (phase of pre-heating). No calculations concerning flame spread have been made. Because the calculations have done with the precribed HRR from the experiments as an input, the calculations have “open” character in this regard.

[2] Only Excel data sheet in incorrect data format provided.

[3] Only for the open calculations.

## 5.1 Blind Calculations

Presentations of the results of blind calculations were given by M. K. Dey (USNRC), K. McGrattan (NIST), and W. Klein-Hessling (GRS) at the 8th ICFMP meeting in ESPOO, Finland in 2004. The presentations are summarized in the following paragraphs to give an overview on the results and findings.

### 5.1.1 CFAST (Zone Model) and FDS (CFD Code) Applied by M. K. Dey (NRC, U.S.)

A validation study with the zone model CFAST as well as with the CFD code FDS code has been performed using compartment conditions and prescribed heat release rates measured during the experiments. The study was limited to the validation of the codes for predicting compartment conditions for a simple ethanol pool fire. Test 4 has been taken for this study. Open calculations were presented during the meeting because they are more representative then the blind predictions. The validation of models available for predicting cable ignition and flame spread will be conducted by USNRC in the future.

In the following, some remarks are given to the simulations with CFAST and FDS.

- Remarks to the simulations with CFAST:
  - Problems were faced in specifying the O2/C ratio input for CFAST. An inconsistency existed between the source code and directions in the CFAST User's Guide /JON 04/.
  - The layer of insulation covering the walls could not be modeled directly and was neglected.
  - The exhaust duct was not modeled.
  - CFAST general over-predicts compartment temperatures.
- Remarks to the simulations with FDS:
  - A grid size of 10 cm was used, but no grid size sensitivity study was conducted.
  - The modeling of the hood was found to have only minor effects to the simulation results, and therefore no attempt was made to account for the hood in the simulations.
  - The walls were simulated as 'backing insulated", which means that there will be no heat losses from the walls to the environment.
- General remarks:
  - No detailed heat transfer model for a cable or cable tray exists in both codes.
  - No attempts to predict flame spread in cable trays are made.

– Heat flux comparisons are difficult because the definition of the heat flux in the codes differs from the method used to measure the heat flux in the tests (cooled flux gauges).

A comparison of the code predictions and the experimental results from Test 4 for the lower layer temperature is given in Fig. 5-1 and for the hot gas layer temperature in Fig. 5-2. The predicted temperatures provided by the FDS code are in a good agreement to the results from the experiment. The results from the blind calculations with FDS from NIST are included. The compartment temperatures predicted by CFAST are higher then the temperatures measured during the experiment. For a more detailed analysis to the accuracy of CFAST temperature predictions see /KLE 06/.

Fig. 5-3 gives a comparison of code predictions and experimental results from the heat flux density (WS3) of Test 4. The results from the blind calculations with FDS from NIST are also included. The heat flux predicted by the CFAST code is in a better agreement to the measured heat flux during the test. For more details see Appendix C.

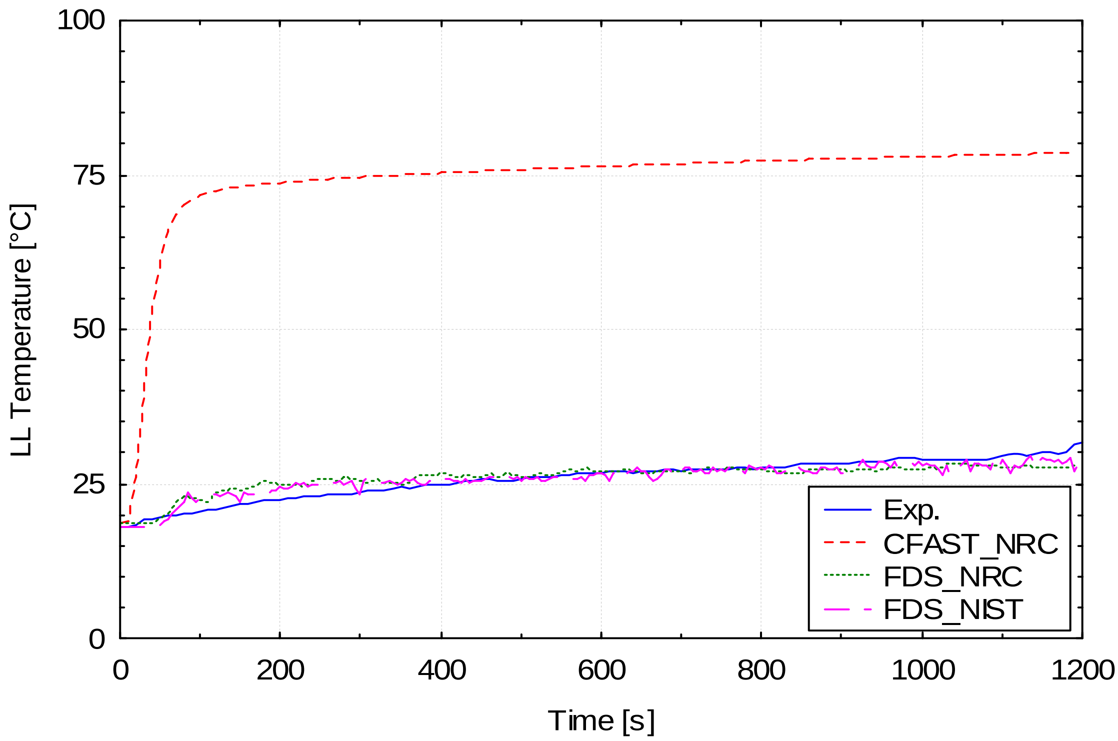


**Fig. 5-1** Lower layer temperatures, code predictions and Test 4 results

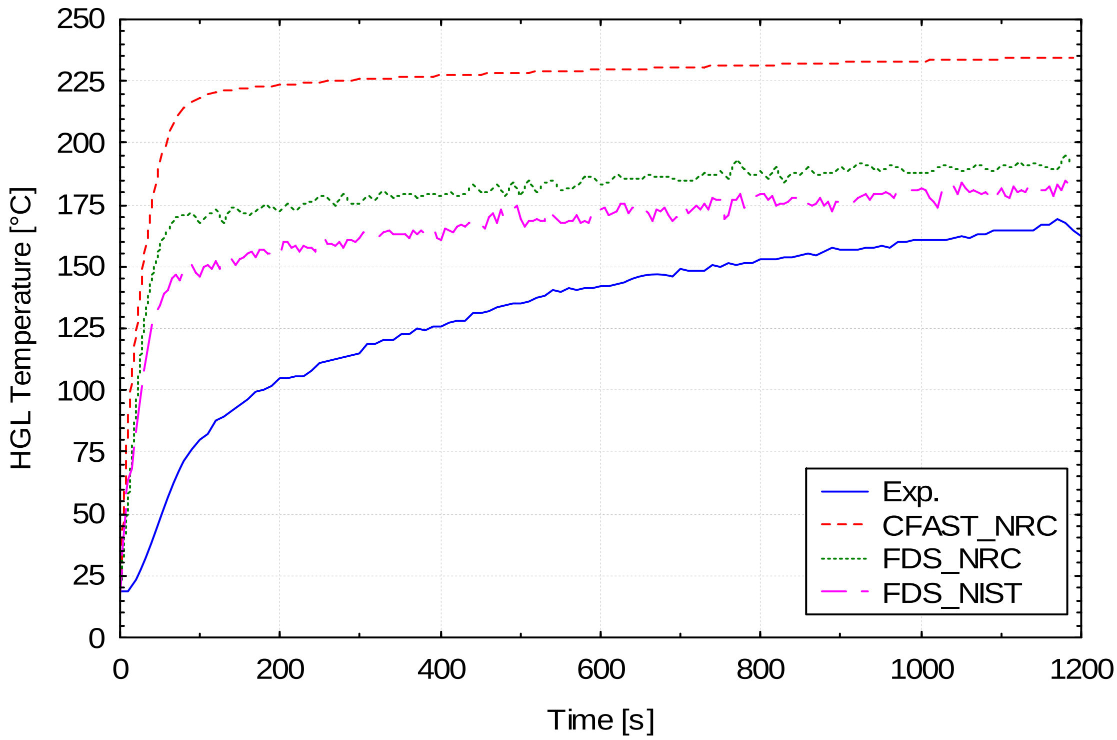


**Fig. 5-2** Hot gas layer (upper layer) temperatures, code predictions and Test 4 results

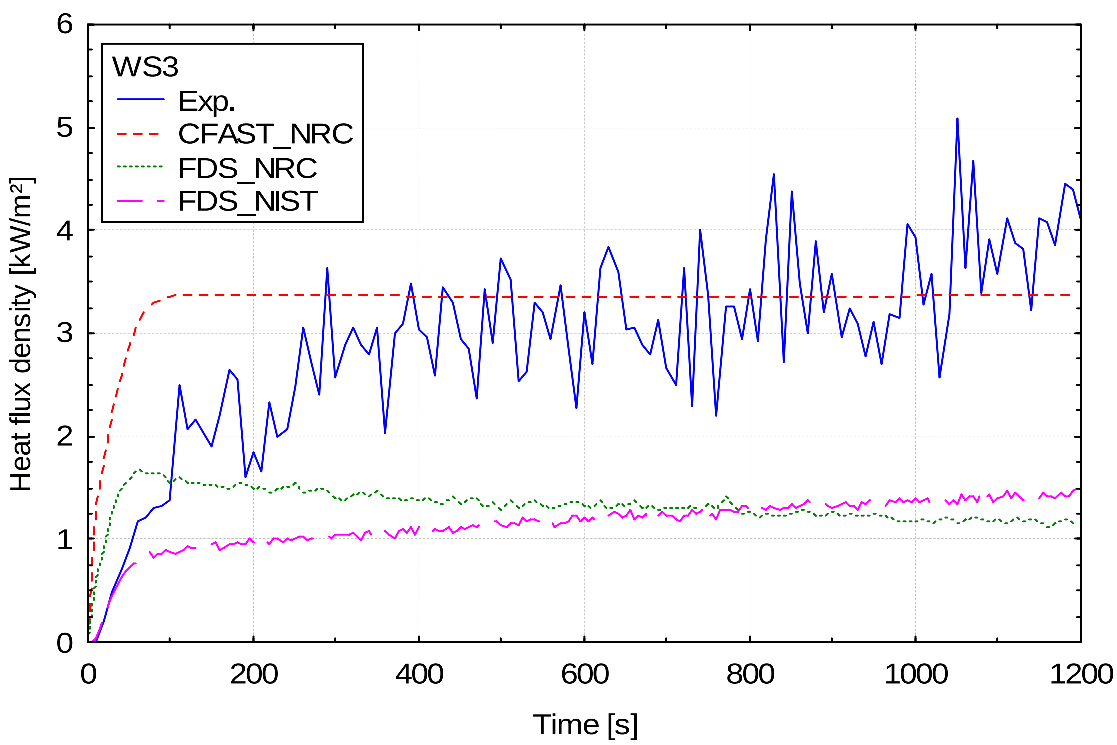


**Fig. 5-3** Heat flux density, code predictions and Test 4 results

### 5.1.2 FDS (CFD Code) Applied by K. McGrattan (NIST, U.S.)

Blind simulations of Test 1 to Test 4 have been conducted. A computational domain with two grid regions has been used. The overall enclosure has been built up by a rectangular grid, with a grid of 10 cm in size throughout. A finer grid of 5 cm resolution has been superposed on the 10 cm grid in the near vicinity of the cables. The heat release from the pool and the gas burner has been prescribed. In the simulations, the cables are assumed to be a solid slab and a one dimensional heat transfer calculation into assumed homogenous material of given thickness has been performed. A pyrolysis model for a thermoplastic has been used to predict the burning rate of the cable bundles. For more details see Appendix D.

A first conclusion of the work with FDS:

- There is no pyrolysis model in FDS to simulate a complex cable bundle.
- The convective/radiative transport in FDS works well.
- The under-ventilation algorithm is too simplistic.
- There is no possibility to characterize small objects as something other than large objects.

Fig. 5-4 shows the course of the temperature at three levels in front of the cable tray during the first 1200 s. The energy flux to the cables predicted by is not high enough so the cables do not burn in a way comparable to that the cables do during the test. The temperature in front of the cable therefore does not increase as much as observed in the experiment. **Fig. 5-5** shows the same situation for the heat flux densities after ignition of the cables in the experiment. The heat flux densities calculated by the FDS code do not increase as in the experiment because no sustained flaming occurs in the simulation. **Fig. 5-6** shows this situation for the surface temperature of the power cables. The surface temperature of the cables increases during the period of the ignition burner being in operation, but because of no sustained ignition in case of simulation the surface temperature is below the temperature measured during the test.

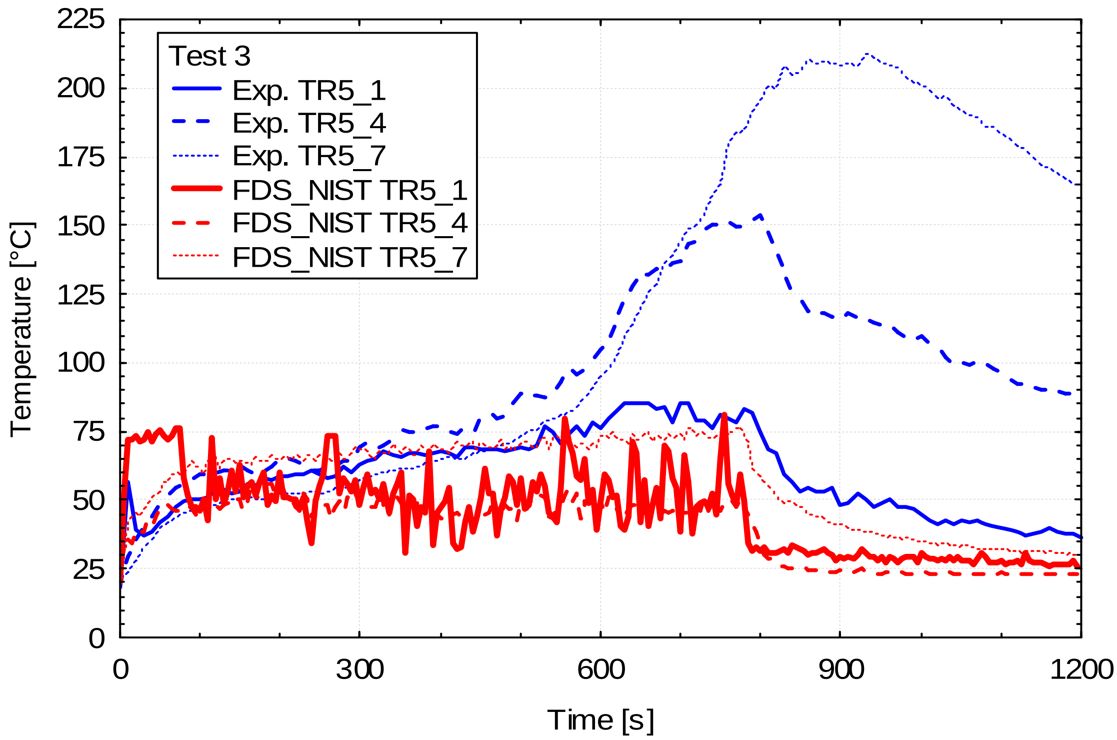


**Fig. 5-4** Temperatures in front of the cables, code predictions and Test 3 results

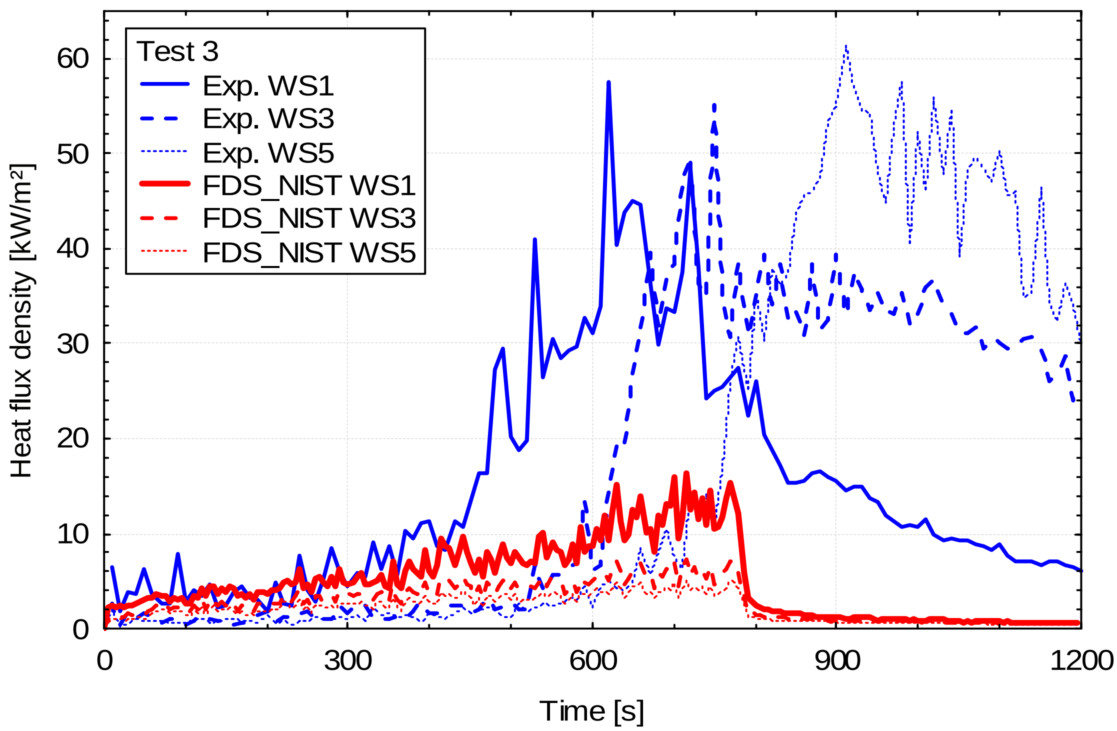


**Fig. 5-5** Heat flux densities in front of the cables, code predictions and Test 3 results

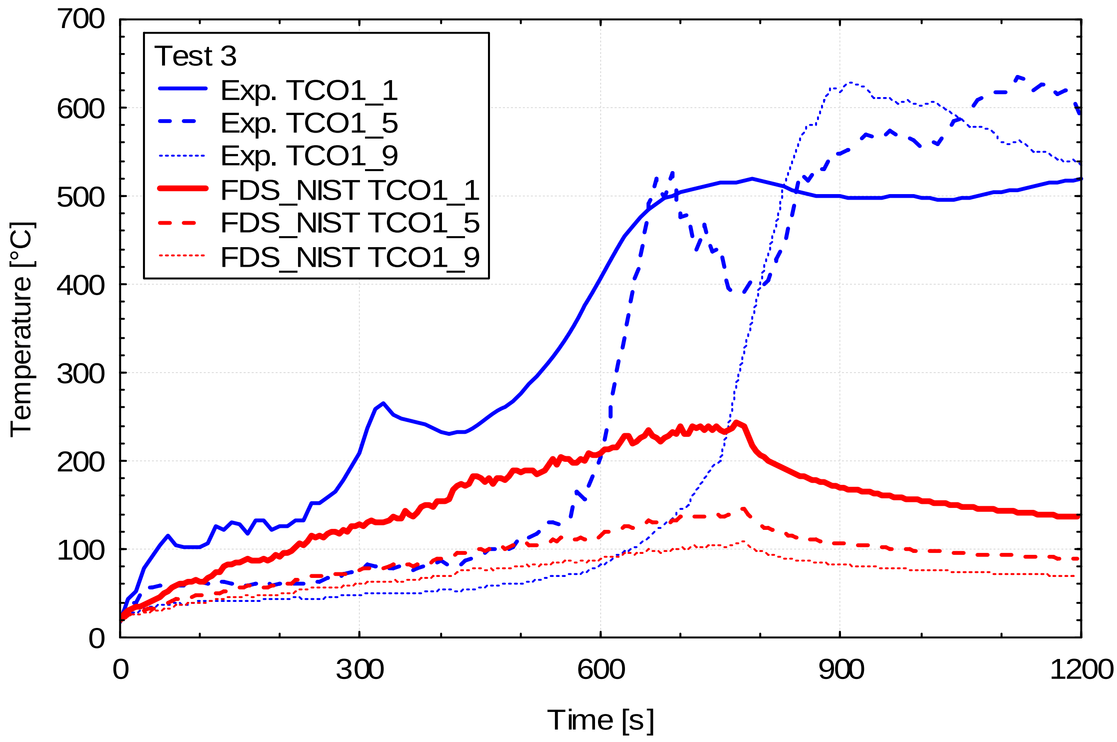


**Fig. 5-6** Surface temperatures power cables, code predictions and Test 3 results

### 5.1.3 COCOSYS (Lumped Parameter Code) Applied by W. Klein-Hessling (GRS, Germany)

Blind simulations of Test 1 and Test 3 have been conducted. A number of 48 zones, 1250 junctions and 368 wall structures have been used to build up the computational domain of the specified test. The hood has not been simulated. The code has performed a one dimensional heat conduction through walls and the flow through the opening has been simulated by 2 atmospheric junctions. The cable bundles have been simulated as rectangular slabs using corresponding material properties. A one dimensional heat conduction has been calculated, but the heating is only considered from one side. The radiation fraction has been set to 0.35 and 95 % reaction efficiency has been used. For more details see Appendix E.

Strong stability problems occurred during simulations which were not clarified at that time. The main results observed are:

– Good simulation of the temperature increase inside fire compartment,

– poor simulation of the temperature distribution inside the fire plume (no plume model available in COCOSYS),

– temperatures at the cable tray were strongly underestimated,

– temperature increase inside the cable is much too low,

– difficulties to simulate incomplete burning of cables with the simple pyrolysis model.

**Fig. 5-7** shows the mass loss rate of the cables provided by the code (based on empirical data) and that from the cables in the experiment. **Fig. 5-8** depicts the predicted temperature in front of the cables. Code instabilities appeared as mentioned above. **Fig. 5-9** shows the course of the temperature in the cable center predicted by the code in comparison to the test measurements. In comparison to the surface temperature, the calculated temperature inside the I&C cables are too low. The main reason is that there is no consideration of the thermal input coming from the fire at the backside of the cable tray.

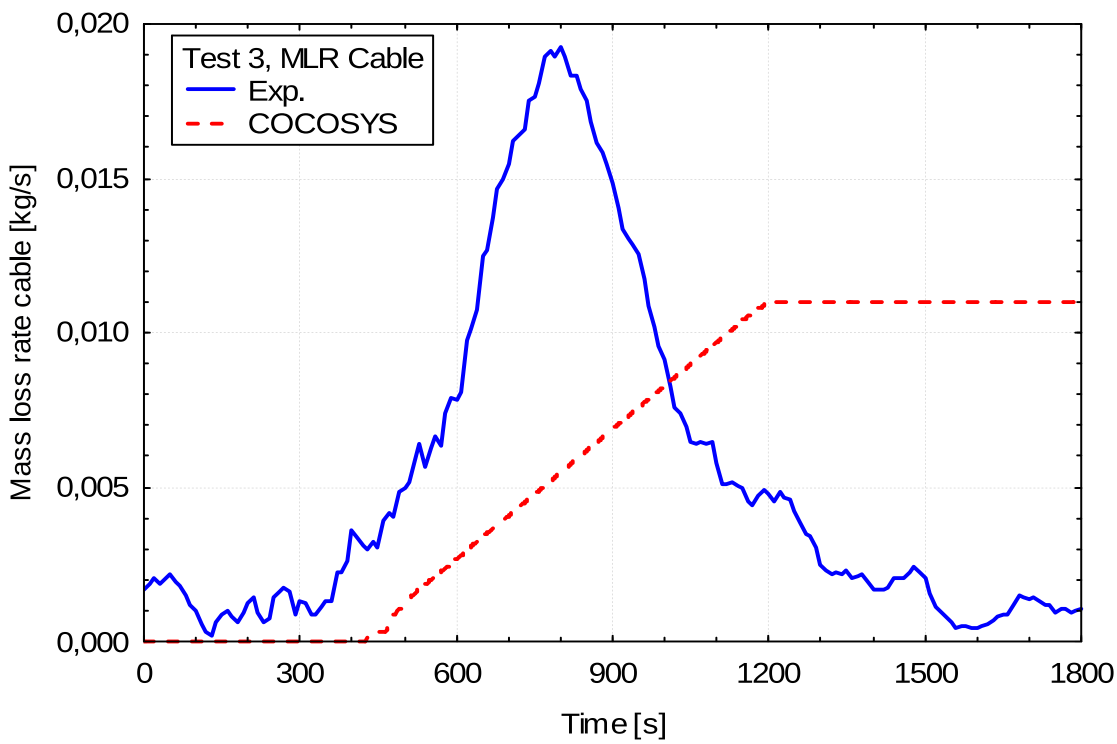


**Fig. 5-7** Mass loss rate cables, code predictions and Test 3 results

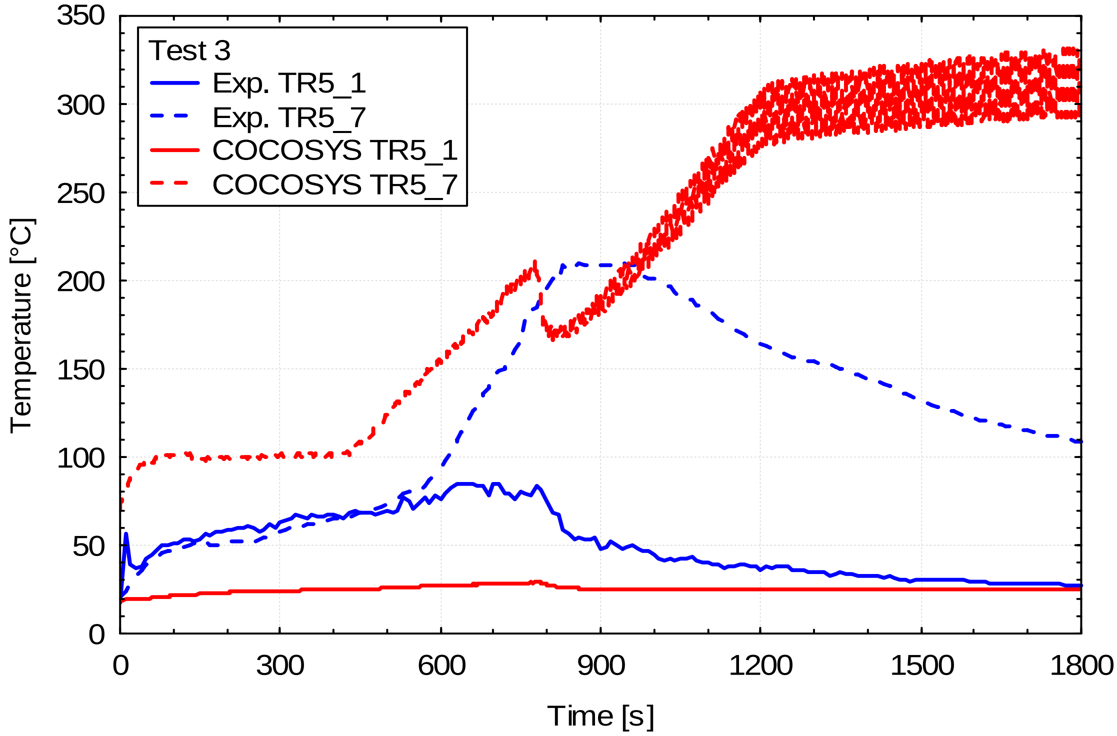


**Fig. 5-8** Temperatures in front of the cables, code predictions and Test 3 results

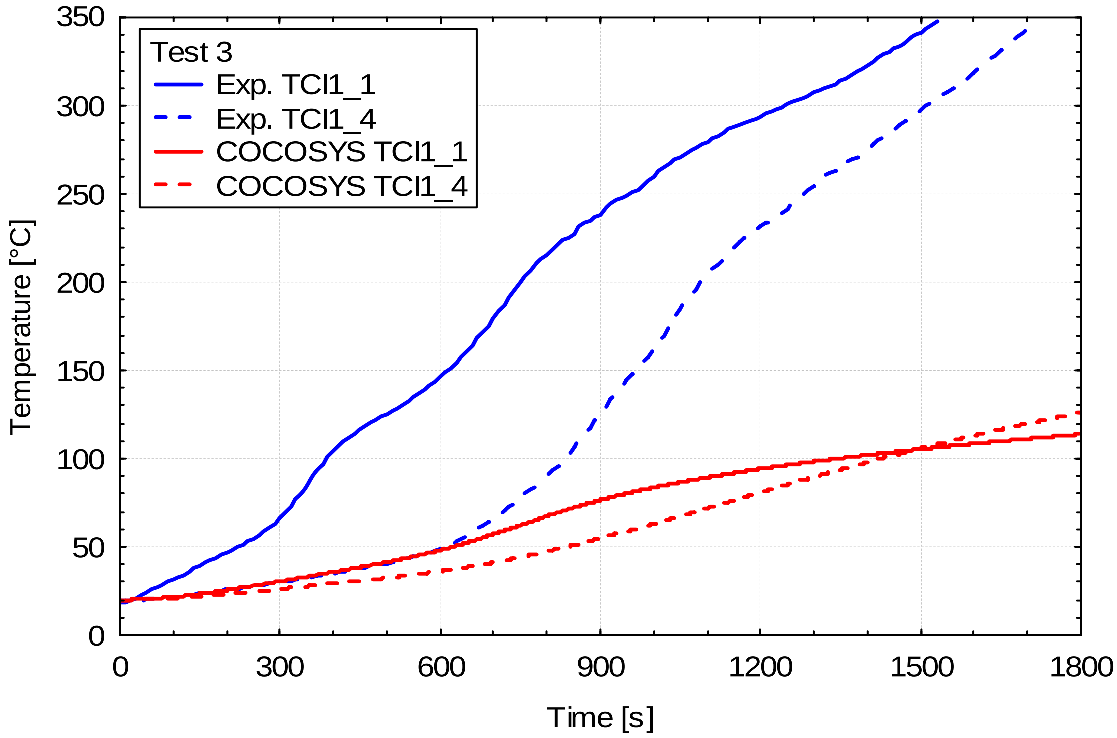


**Fig. 5-9** Cable center temperatures, code predictions and Test 3 results

## 5.2 Open Calculations

A significant contribution to the open calculations comes from the same participants having performed blind simulations. A detailed analysis of the work and the results of open calculations from M. K. Dey (USNRC), K. McGrattan (NIST), W. Klein-Hessling (GRS) and Matthias Heitsch (GRS) is given in the corresponding Appendices. The following paragraphs will give a short summary of the main results and conclusions from the individual reports given in the appendices.

### 5.2.1 CFAST (Zone Model) and FDS(CFD Code) Applied by M. K. Dey (NRC, U.S.)

This work gives basic statements on the experiences made with the multi-compartment zone model CFAST (Version 3.7.1), and the three dimensional CFD code (field model) FDS (Version 3.1.5). The study was limited to the validation of the codes for predicting compartment conditions for a simple pool fire. Therefore, the study was restricted to Test 4, which includes a pool fire used to preheat the compartment and the PVC cables. A summary of this work is already given in chapter 5.1. Because of the limitation of the calculations to the time of pre-heating (first 1200 s) the simulation type is practically an open one, as the heat release rate measured during the fire is taken as an input for the simulations.

The report gives an overview of results coming from the codes compared with data from the measurements of several quantities. The most interesting issue of this Benchmark Exercise is, with which accuracy the codes can predict the quantities in the direct environment of the cable tray. These are the gas temperature in front of the cables, the heat flux to the targets and the target temperatures. Fig. 5-10 shows the model build-up with FDS. The isosurface of the flame sheet of the ethanol pool computed at the 442 s is shown. Fig. 5-11 shows the heat flux on the cables (WS, FDS and experiment) and **Fig. 5-12** the compartment temperature in front of the cables (TR5, FDS and experiment). **Fig. 5-13** shows the surface temperature on the power cables (FDS, CFAST and experiment) and **Fig. 5-14** the surface temperature on the I&C cables (FDS, CFAST and experiment).

The heat flux predicted by FDS is lower than the measured value, but it is pointed out that different definitions and the way of comparing the heat flux may be a problem of the comparison to the code results. The predicted compartment temperatures from FDS are in good agreement with the experimental results. The surface temperatures on the cables computed from FDS are lower than the experimental results. The results for the surface temperatures from the CFAST simulations are in a better agreement to the measurements but most of them are also lower than the experimental data. For more details see Appendix C. There results from hand calculation tools (Fire Dynamics Tools) also based on the Society of Fire Protection Engineers (SFPE) Handbook /SFP 95/ can be found. In the following, a brief list of general conclusions of this work is given:

– The FDS manuals in conjunction with the Smokeview /FOR 04/ graphical interface provide a comprehensive, understandable interface for the user.
– The CFAST graphical interface (GUI) is outdated and does not function in more recent operating platforms such as MS Windows 2000.
– The calculations of heat flux to the targets and walls are a potential area of improvement for both CFAST and FDS.
– FDS predicted that the flows in the fire trench effect plume development and tilting.
– More studies of this phenomenon would be beneficial, especially for NPP scenarios.

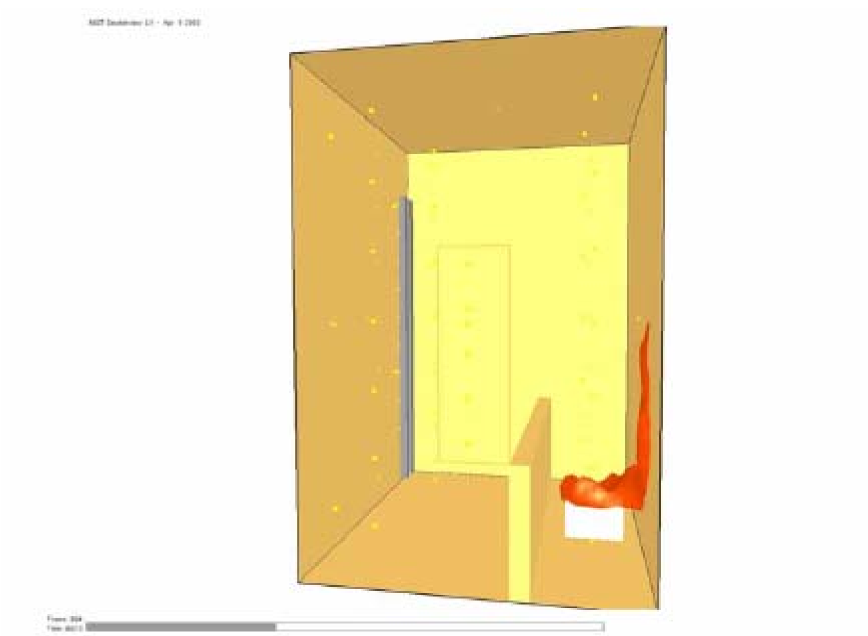

**Fig. 5-10** Isosurface of flame sheet 442 s in Smokeview – Test 4 (from Appendix C)

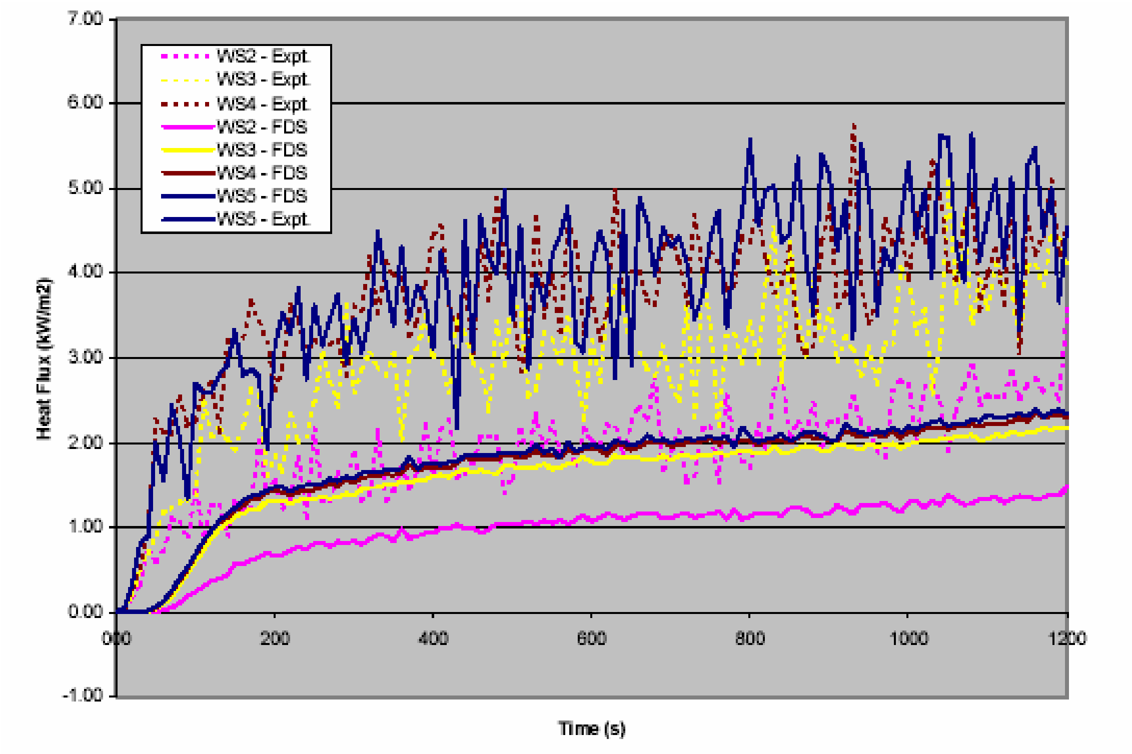


**Fig. 5-11** Heat flux on cables (WS) – Test 4 (from Appendix C)

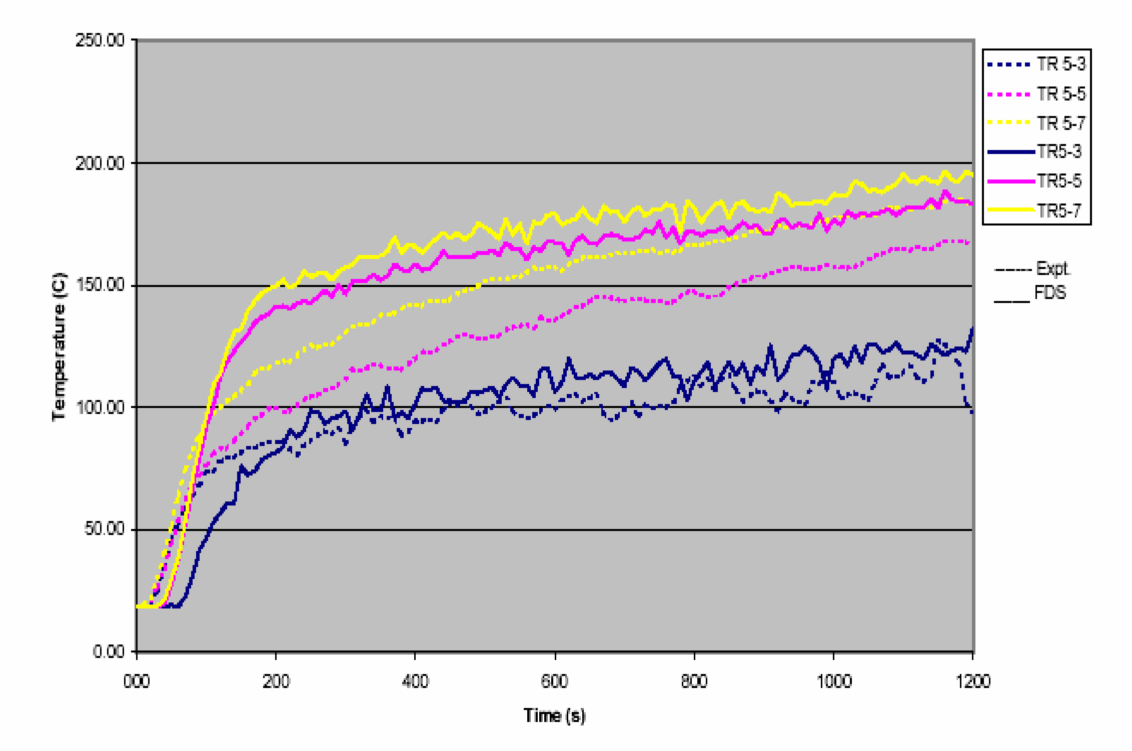


**Fig. 5-12** Compartment temperature (TR5) – Test 4 (from Appendix C)

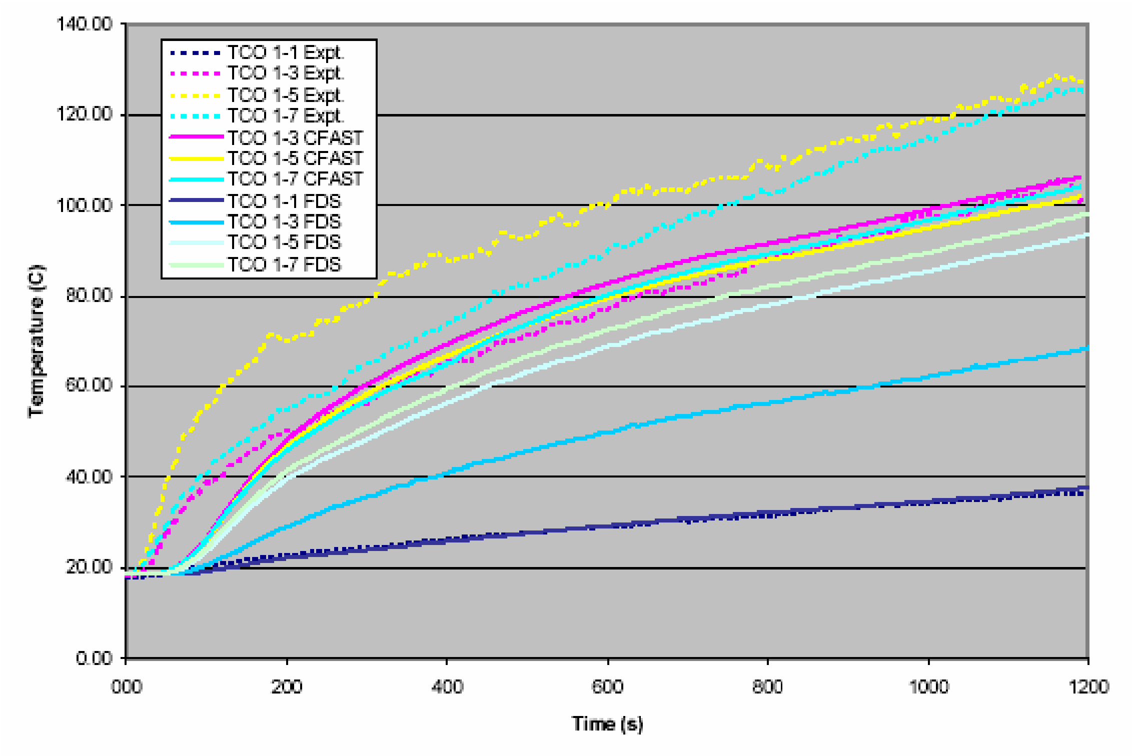


**Fig. 5-13** Power cable surface temperature (TCO1) – Test 4 (from Appendix C)

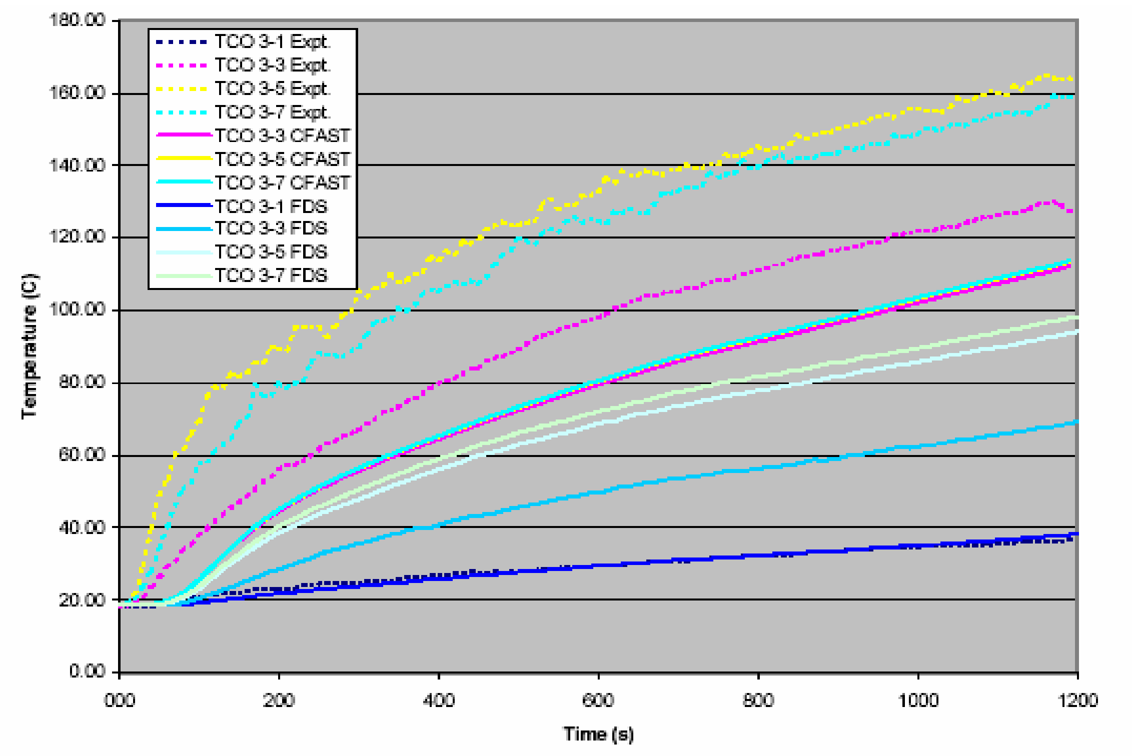


**Fig. 5-14** I&C cable surface temperature (TCO3) – Test 4 (from Appendix C)

### 5.2.2 FDS (CFD Code) Applied by K. McGrattan (NIST, U.S.)

FDS /MCG 04/ is a computational fluid dynamics code that solves the Navier-Stokes equations in low Mach number, or thermally-expandable form. The transport algorithm is based on Large Eddy Simulation (LES) techniques; radiation is modeled using a gray-gas approximation and a finite volume method is used to solve the radiation transport equation. Combustion is modeled using a mixture fraction approach, in which a single transport equation is solved for a scalar variable representing the fraction of gas originating in the fuel stream.

**FDS Code Description and Input Assumptions**

**Fig. 5-15** shows the fire and the smoke in Smokeview /FOR 04/ from the simulation of Test 4. The geometry is built up with a single, rectilinear grid, plus a comparable volume under the hood outside the door. The cells are exactly 10 cm size throughout. A second numerical grid is superposed on the 10 cm grid near the cables. This second grid is made up of cells of 5 cm each. The two cable bundles are approximated as solid slabs of plastic.

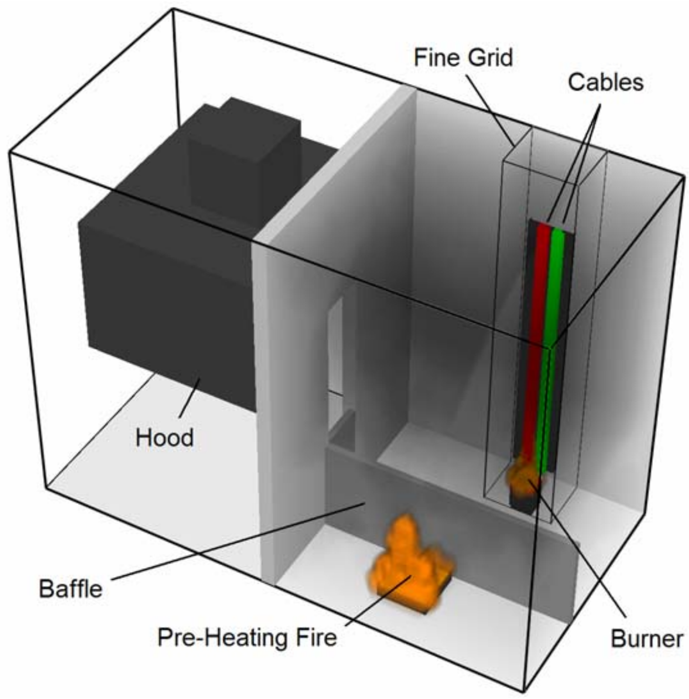


**Fig. 5-15** Simulation of Test 4, showing the fires and smoke in Smokeview (from Appendix D)

FDS performs a one-dimensional heat transfer calculation into an assumed homogeneous material of given thickness and (temperature dependent) thermal properties. Solid constructions within the computational domain must conform to the underlying gas phase grid. The thickness of the solids is not tied to the gas phase grid, only the exposed surface area. Thus, the solid phase heat transfer calculation is partially decoupled from the gas phase – heat transfer in the normal direction can be modeled with as fine grid as needed, but mass and heat transfer between the solid and the gas is constrained by the gas phase grid.

In the simulations, the cable bundles are assumed to be solid slabs, covered by 5 cm x 5 cm x 2 mm thick 'tiles' with the given thermal properties of the PVC or FRNC cable coating. The 'tiles' are assumed to have an insulated backing. Nothing in the model could account for the lateral heat conducting along the metal conductors. In all simulations the HRR from the pool and from the ignition burner is prescribed and the pyrolysis from the cable is predicted. A pyrolysis model of a thermoplastic is taken although it is suggested that PVC cables behave more like charring solids. For more details see Appendix D.

**FDS Code Results**

The following figures give some comparisons of code predictions and experimental results to Test 3, as an example. **Fig. 5-16** shows the predicted and measured heat release rate from Test 3 and Fig. 5-17 shows the predicted as well as the measured gas temperature in front of the cables at 4.4 m over the ground (TR5-6). Although the simulated heat flux to the cables is not too low at the beginning (Fig. 5-18), the pyrolysis model does not predict the behavior of the cables in the experiment after time of ignition. The measured temperatures rose steadily to the prescribed ignition temperature, resulting in burning at low rate, not high enough to induce spreading and a comparable pyrolysis rate as measured in the experiment.

Fig. 5-19 shows the predicted and the experimental data of the surface temperature of the power cables and Fig. 5-20 the surface temperature of the I&C cables. As mentioned above the predicted temperatures could not follow the experimental results, particularly after ignition of the cables in the tests. For more details see Appendix D.

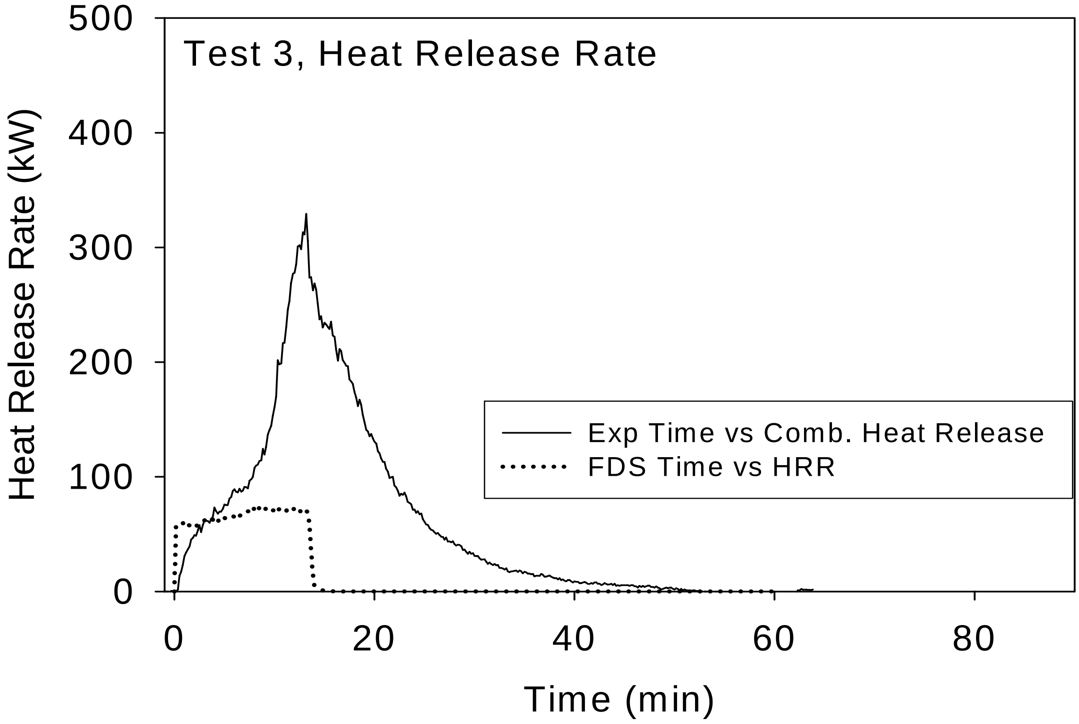


**Fig. 5-16** Heat release rates in front of the cables - Test 3 (from Appendix D)

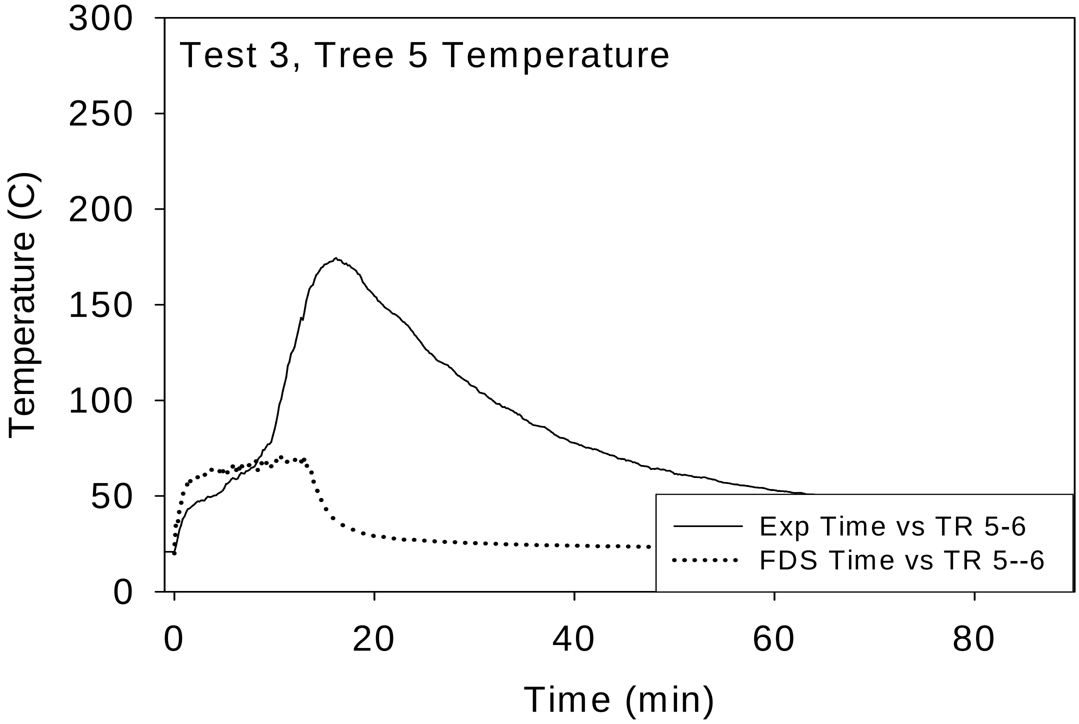


**Fig. 5-17** Gas temperature in front of the cables - Test 3 (from Appendix D)

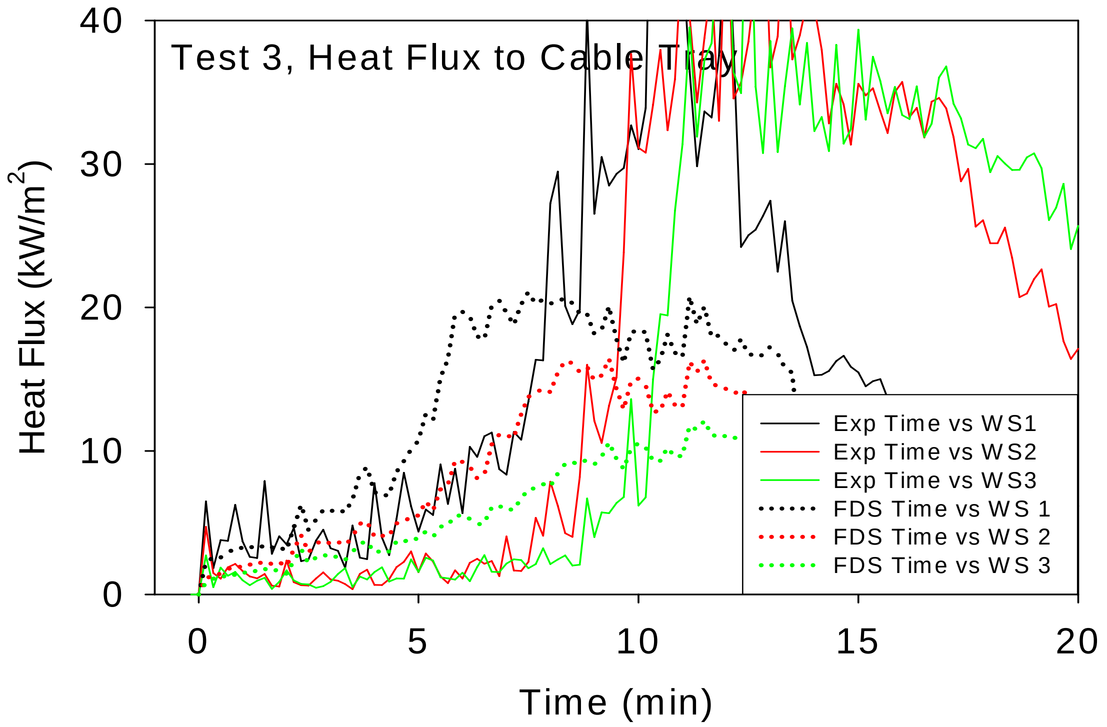


**Fig. 5-18** Heat flux in front of cables (WS) - Test 3 (from Appendix D)

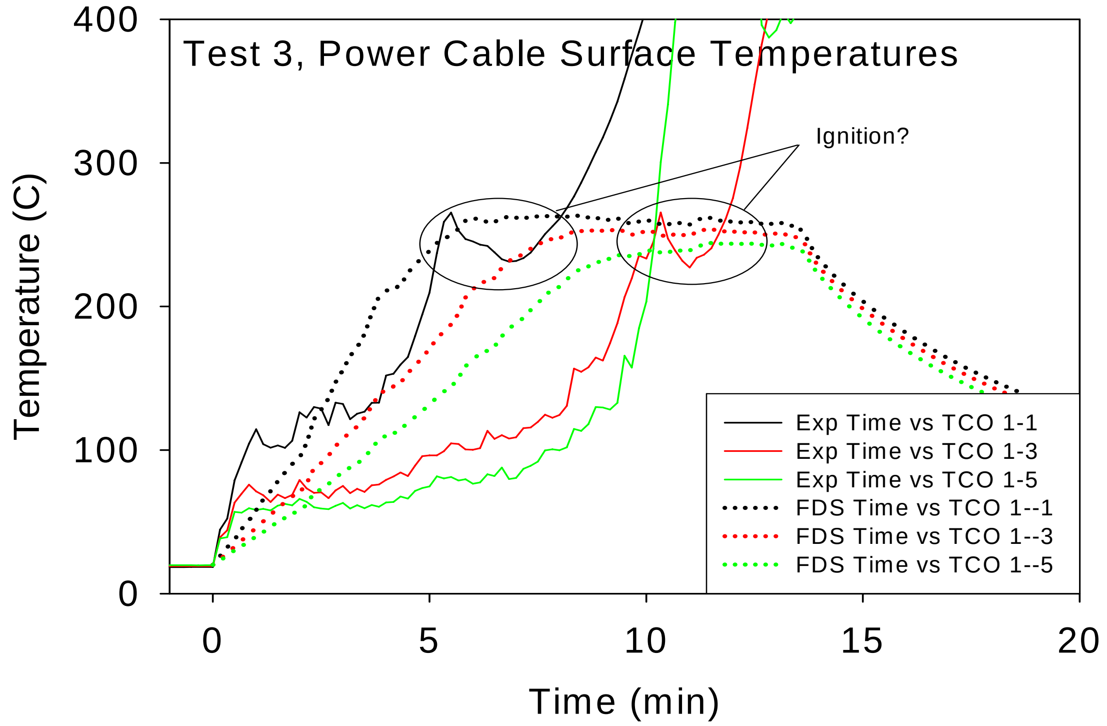


**Fig. 5-19** Surface temperature of the power cables – Test 3 (from Appendix D)

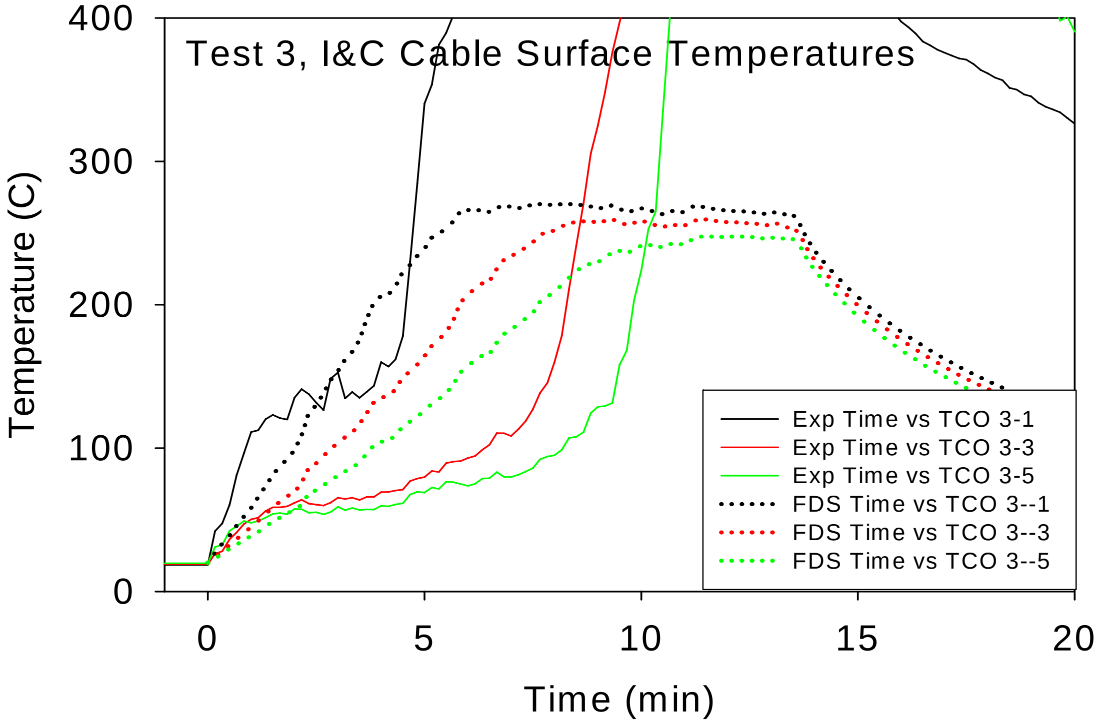


**Fig. 5-20** Surface temperature of the I&C cables– Test 3 (from Appendix D)

In the following, a brief list of the general conclusions of the open calculations with FDS is given:

– FDS in its current form is not suitable for this type of prediction.

– No pyrolysis model for cables is included in FDS.

– A purely deterministic model is not practicable because of the complexity.

– Complex objects may be modeled in the future as a collection of small ‘particles”, for example as cylinders.

– There are no set rules on how to measure the different properties as main input, such as heat of gasification, ignition temperature or heat of combustion.

– The models available should be used to simulate the experiments performed to obtain the properties (like Cone Calorimeter tests).

– Thermal properties should be consistent and from a single source.

### 5.2.3 COCOSYS (Lumped Parameter Code) Applied by W. Klein-Hessling (GRS, Germany)

COCOSYS /ALL 05/ is a so-called lumped parameter code. To simulate the local conditions (natural convection, temperature stratification) the fire compartment has been divided into a quite large number of control volumes. The main idea is to have a separate control volume for each temperature measurement or temperature point for comparison and to have separate control volumes around the fire plume, the ventilation system, and the doors and openings, respectively.

**COCOSYS Code Description and Input Assumptions**

Test 1 to Test 4 has been simulated and most of the measured quantities have been modeled and compared with the experimental results. To overcome the problems for heating up the cables by the gas burner and to handle the remaining cable mass fractions, the models in COCOSYS have been improved to some extent. The gas burner is simulated by the fuel fire pyrolysis model in COCOSYS with a user defined pyrolysis rate. The radiation fraction is assumed to be 40 %. In the open calculation the combustion model parameters have been adjusted to get a more realistic height of the fire and more complete combustion of the propane. The cable trays are simulated with the so-called simplified cable burning model. For the open calculations, the COCOSYS program has been extended at two points:

- The heat transfer into the cables close to the gas burner fire has been improved,
- A remaining mass fraction for incomplete burn down of cables has been introduced.

**Fig. 5-21** shows the 3D view of the experimental setup. The next figures are taken from Appendix E and show the results of Benchmark Exercise No. 5, Test 3. In these figures the experimental results and the code predictions from the ‘blind’ and ‘open” calculations are compared to each other.

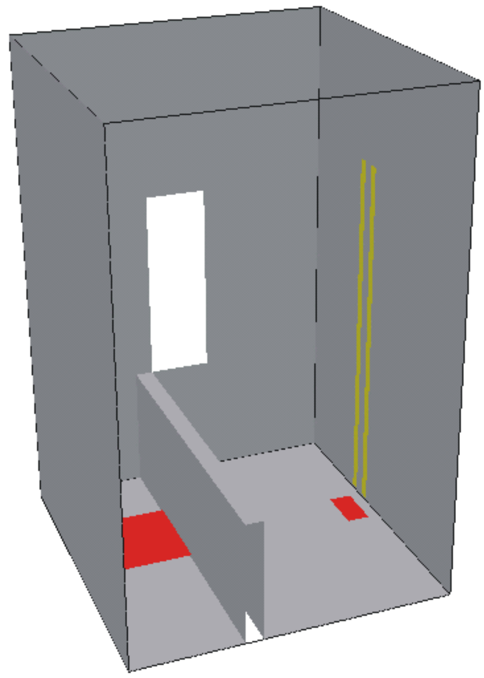

**Fig. 5-21** 3D view of the experimental set up (from Appendix E)

**COCOSYS Code Results**

In **Fig. 5-22** the course of the HRR is shown. The model is working with a specified pyrolysis rate [kg/sm²] for the cables. The propagation velocity is depending on the assigned surrounding temperature of the target structure temperature. The database for this property comes from earlier experimental results, made in the same compartment. In the open calculation the combustion model parameters have been adjusted to get a more realistic height of the ignition gas burner, so that the results for the open calculations (indicate with blue lines in the plots) are in better agreement with the experimental data. **Fig. 5-23** shows the gas temperatures in front of the cable tray at three different height levels. The code instabilities have been reduced (see the open calculations in chapter 5.2), but the model over-predicts the gas temperatures compared to the experimental results.

**Fig. 5-24** shows the predicted as well as the experimental data of the surface temperature of the power cables and **Fig. 5-25** shows the surface temperature of the I&C cables. The surface temperature increase of the power cables as well as of the I&C cables are much better calculated in the open calculations. This work is extended to a comparison of computational results to most quantities measured during the experiments. For more details see Appendix E. In the following, a brief list of general conclusions of the calculational efforts with COCOSYS is provided:

– The improvements in the model gave better results e.g. in case of the inner and surface temperatures of the cables.

– A plume model is lacking in COCOSYS and has to be supplemented in the future.

– Practically, cables not burning (FRNC) are difficult to model, because with the existing model the cables will start to burn at defined temperatures.

– Local effects, such as blistering of cable material and small local fires, cannot be simulated.

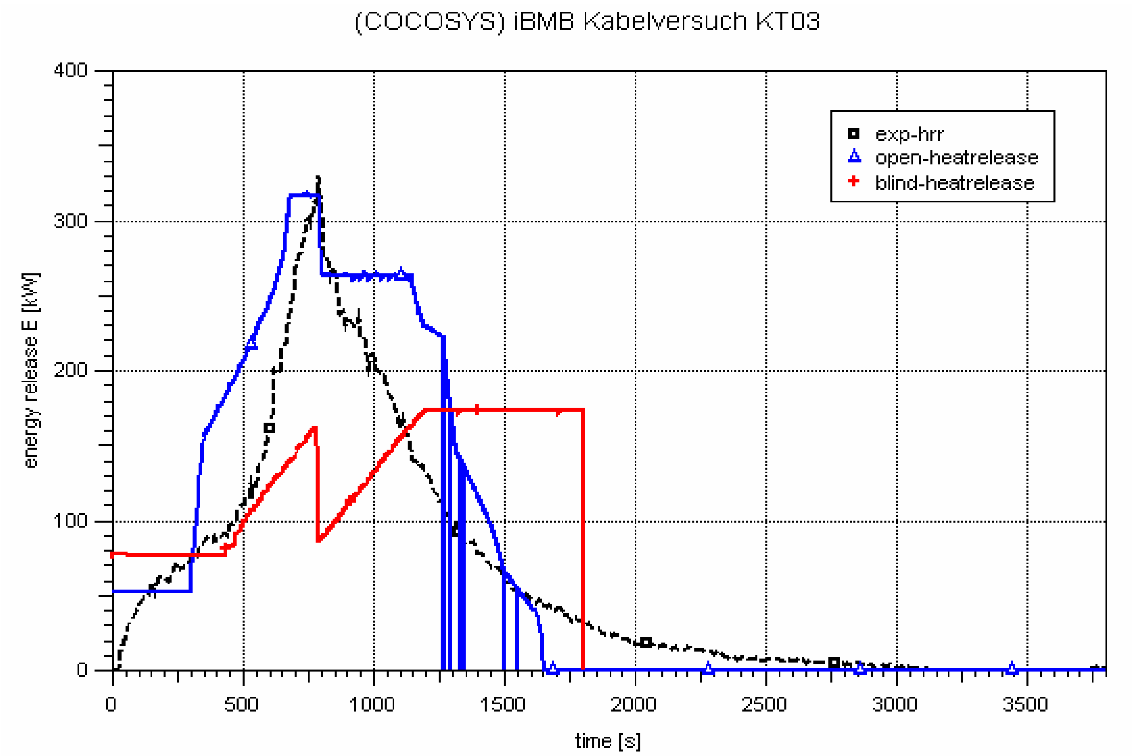


**Fig. 5-22** Test 3: Energy release due to combustion (from Appendix E)

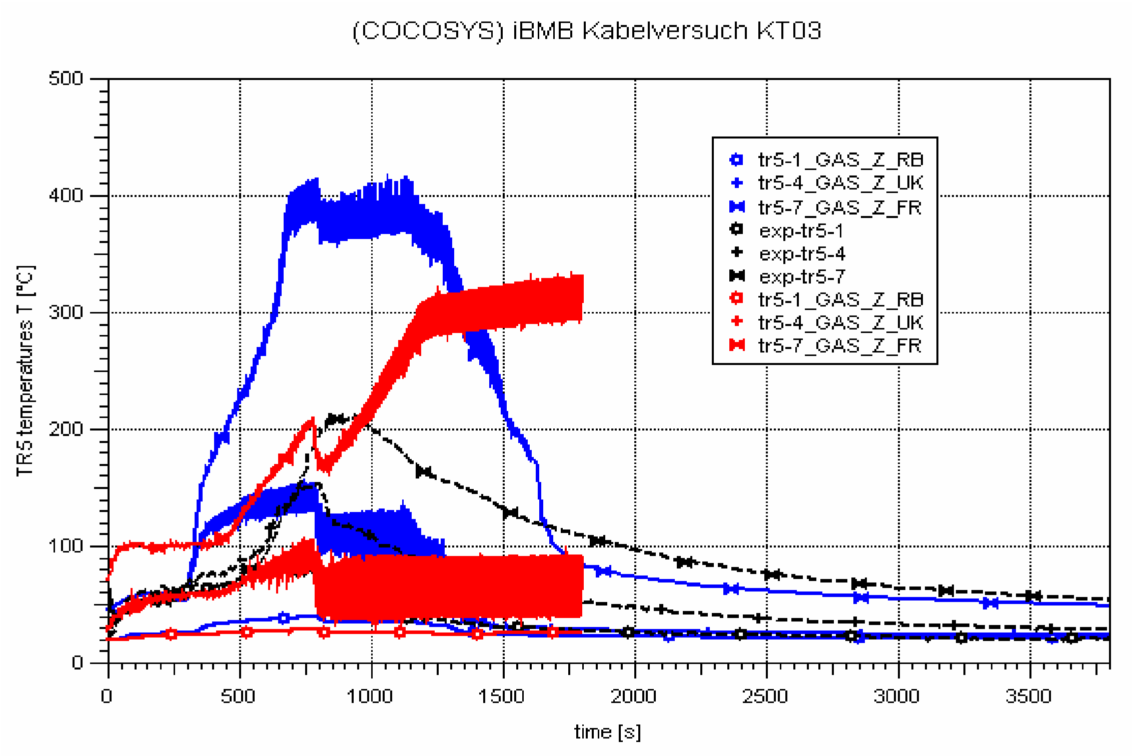


**Fig. 5-23** Test 3: Temperature at tree TR5 close to gas burner (from Appendix E)

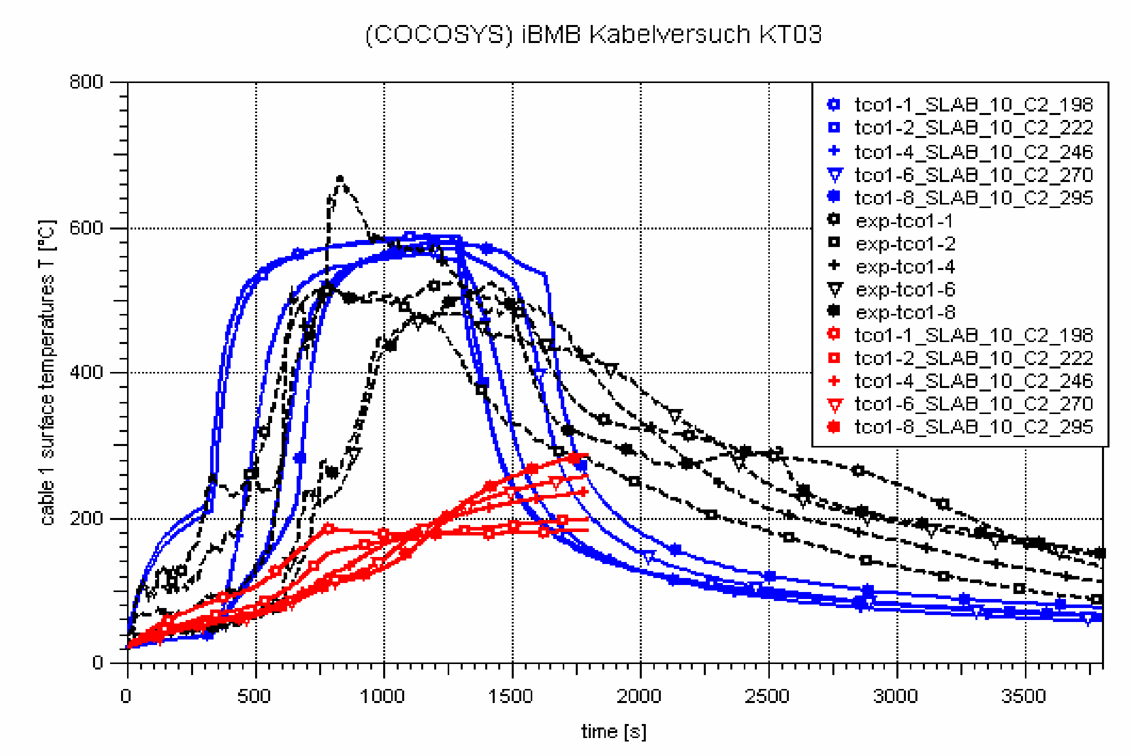


**Fig. 5-24** Test 3: Power cable surface temperature at TCO1 (from Appendix E)

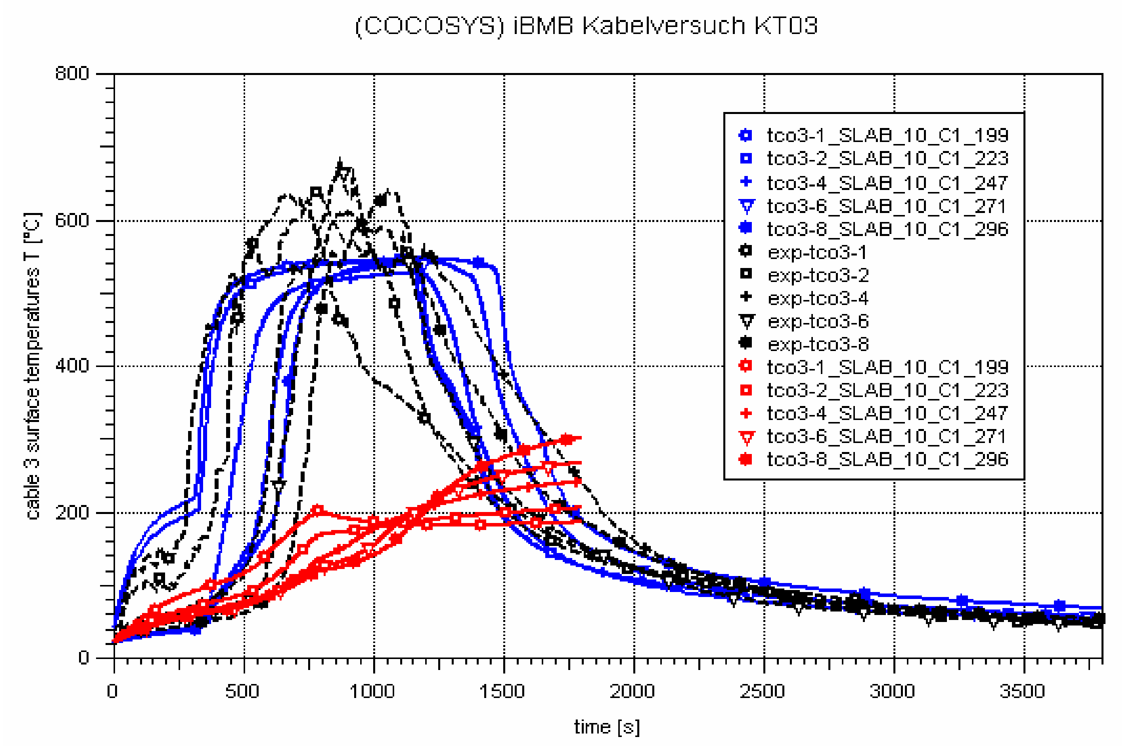


**Fig. 5-25** Test 3: I&C cable surface temperature at TCO3 (from Appendix E)

### 5.2.4 CFX (CFD Code) Applied by M. Heitsch (GRS, Germany)

Calculations with the commercial CFD code CFX have been carried out for Benchmark Exercise No. 5. The code version 10 of the CFX family /ANS 05/ represents a completely new code structure compared with previous versions and offers new features.

Benchmark No. 5 focuses on the pyrolysis from sufficiently heated cable trays. This complex process is not available as a kind of model in CFX. However, the basic elements for including arbitrary models are provided in the code concept. Therefore, first steps were made to implement a pyrolysis model in CFX. Taking into account the large effort, which has been made with other codes to implement and validate such a model, only Test 1 from the available tests has been analyzed.

**CFX Code Description and Input Assumptions**

The code version 10 of CFX offers the ability to use a mixture of structured (hexahedral) and unstructured (tetras, pyramids) cells to represent a given geometry. This provides the flexibility to model any kind of arrangement and is important if complex flow patterns are expected. CFX is capable of modeling steady-state and transient flows, laminar and turbulent flows, subsonic, transonic and supersonic flows, heat transfer and thermal radiation, buoyancy, non-Newtonian flows, transport of non-reacting scalar components, multiphase flows, combustion, flows in multiple frames of reference, and particle tracking.

The gas mixture of air and the fuel propane is modeled by the individual species, which are propane, oxygen, nitrogen, carbon-monoxide, carbon-dioxide and steam. Soot is also created according to the Magnusson soot model implemented in CFX-10. In this model, a number of constants are used, which are not further investigated in the given context. Nitrogen represents a background fluid, not participating in any reaction. The chemical reaction itself is represented by a single-step mixing controlled reaction within the Eddy Dissipation model. A complete combustion is assumed.

CFX offers the possibility of specifying sources of mass and energy in volumes and at boundaries. Boundaries can also be interfaces between fluid and solid domains. In the general case, each cell close to the boundary can be checked if a given ignition temperature is passed. If this is the case, the pyrolysis of the solid body depending on a given (probably temperature dependent) reaction rate can be invoked. Oxygen from the surrounding atmosphere is consumed. The total amount of carbon in the solid is the upper limit which can be consumed.

In the given context of Benchmark Exercise No. 5, the basic idea of checking each individual cell along the interface of the cable bundles could not be implemented for practical reasons. The limitation is that this model can only be implemented by extra FORTRAN routines which need a certain 64-Bit compiler. This compiler is not yet available. Consequently, a more simple approach was chosen, which does not need extra routines. Only the maximum temperature of the cable is checked and a constant pyrolysis rate of 0.002 kg/s (derived from the experiment) is used as basis for releases of energy, CO and $CO_2$. **Fig. 5-26** shows the model CFX configuration used for Benchmark Exercise No. 5 and **Fig. 5-27** the structured mesh to represent the cable bundles in detail.

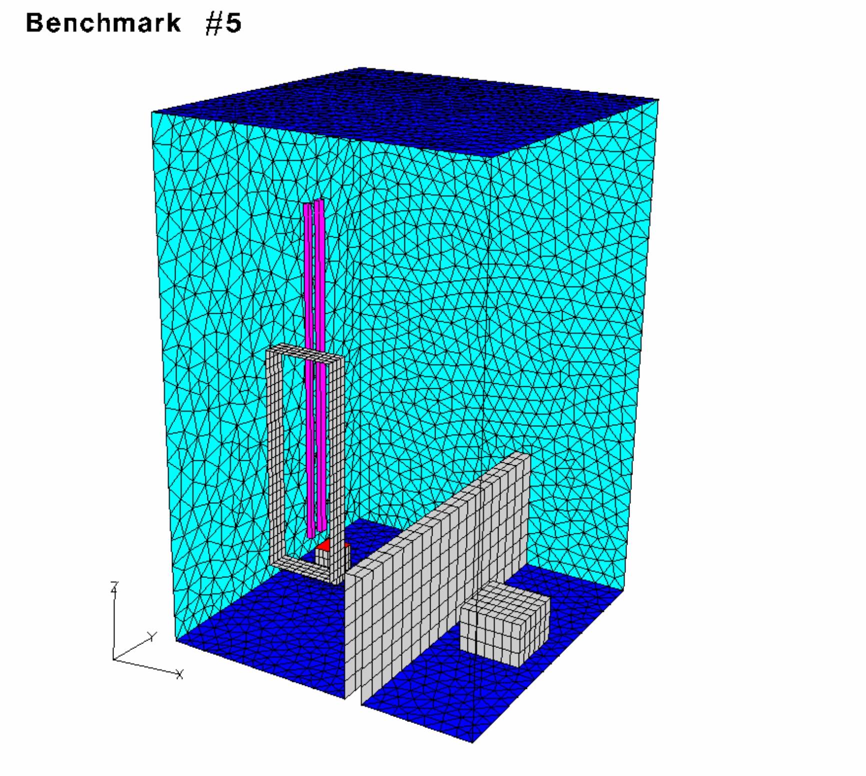


**Fig. 5-26** Cut through the CFX model of the test facility in configuration for Benchmark No. 5 (from Appendix F)

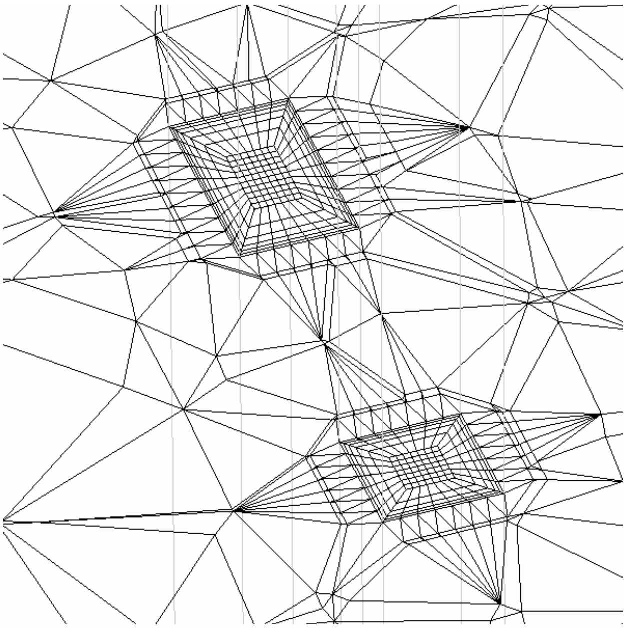

**Fig. 5-27** Structured mesh to represent cable bundles (from Appendix F)

**CFX Code Results**

For a first overview on the results from the CFX calculations the calculated gas temperatures (TR1-2, TR1-4 und TR1-7) in front of the cable tray are given in **Fig. 5-28**. The temperatures are in a reasonable agreement to the measured ones during the first phase of burner output (150 kW), but too low in the second phase of the burner with a power output of 300 kW.

In **Fig. 5-29**, the maximum temperatures on both cable bundle surfaces are given. The given ignition temperature is only reached for the power cable (bundle D) in the second phase of the burner output. The I&C cables (bundle C) will not burn in the CFX simulation. For more details and further information see Appendix F.

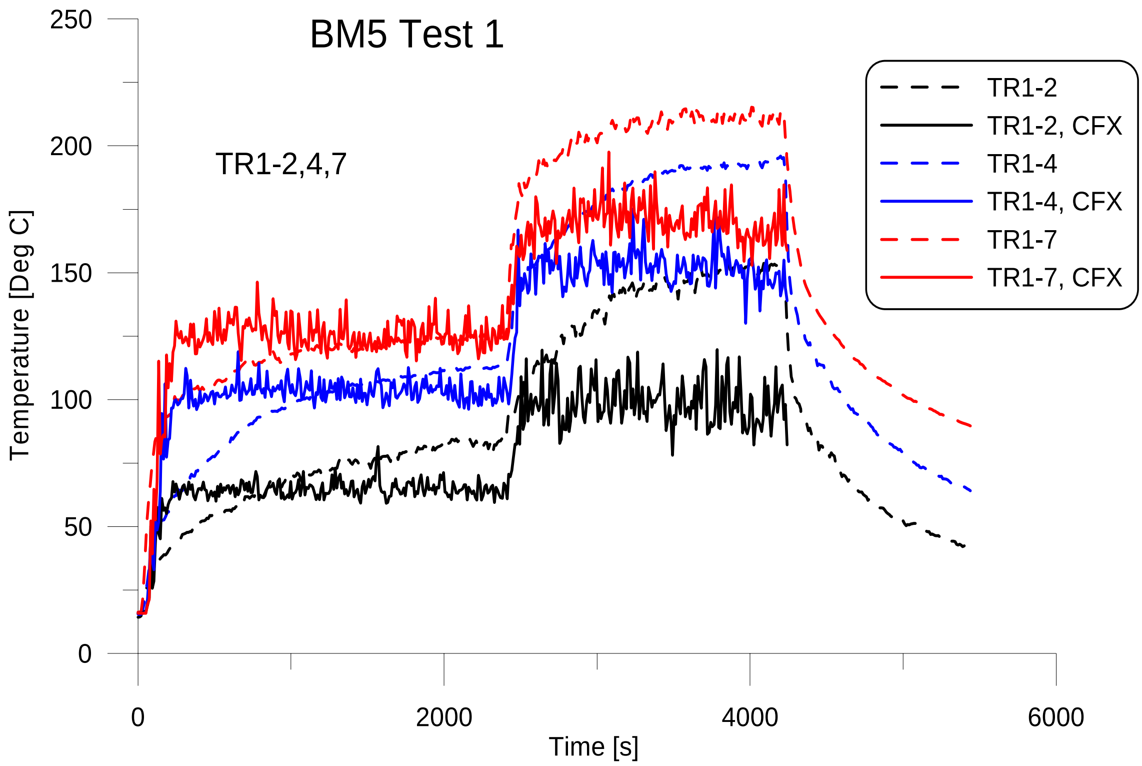


**Fig. 5-28** Gas temperatures along line TR1 (from Appendix F)

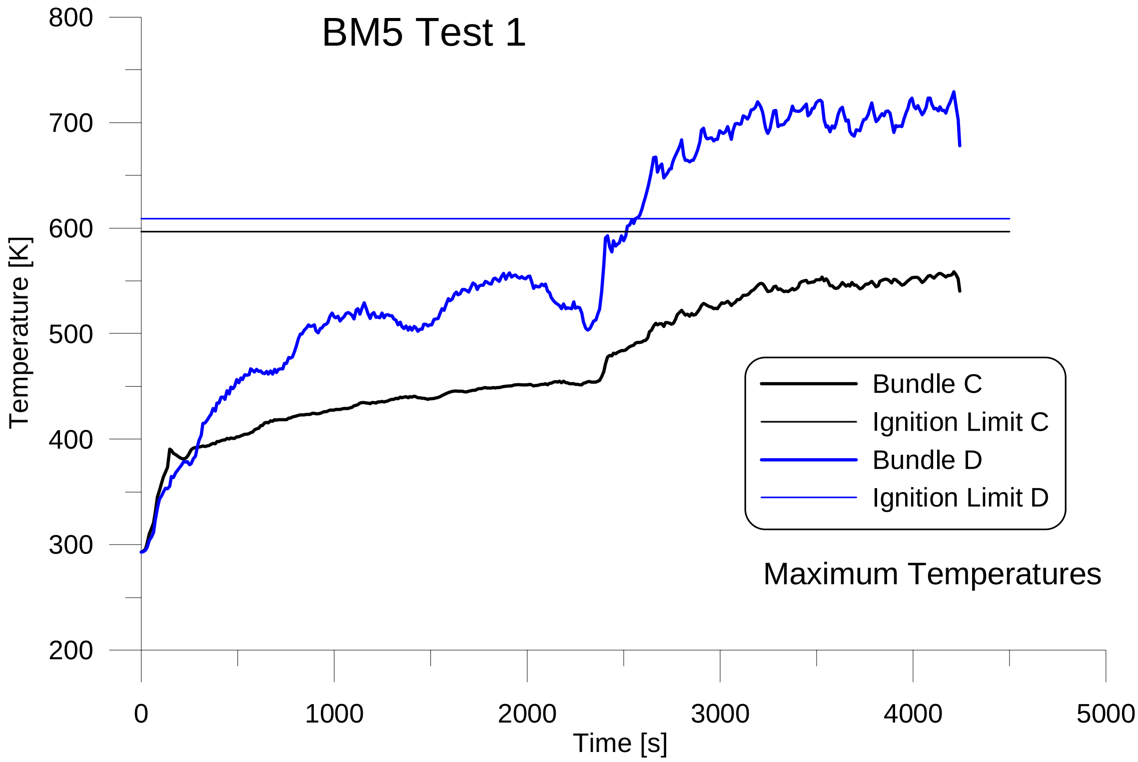


**Fig. 5-29** Maximum temperatures [°C] of cable bundles (from Appendix F)

A brief list of the general conclusions of this work is given in the following:

- Basic structures such as cable bundles, walls, and the gas burner are composed of structured cells; the rest space is filled up by unstructured cells.
- The use of unstructured cells is an easement to older versions of CFX to the possibility to build up the model, but end up with more cells.
- In the current version of CFX no pyrolysis model is implemented.
- Basic elements for the inclusion of arbitrary models are provided in the code concept.
- First steps were made to implement a pyrolysis model in CFX, however the work at the pyrolysis model is not yet finished.
- The calculations presented are based on a simple approach to the pyrolysis of the cables. If the ignition temperature is reached at one point of the cable bundle, the complete bundle burned at the assumed (maximum) pyrolysis rate given from the experimental data.

## 5.3 Code to Code Comparison

In this chapter, specific results of the open calculations with the lumped parameter code COCOSYS and the CFD codes FDS and CFX are compared against each other as well as with the experimental results. In the previous chapters it has been pointed out that these codes have no deterministic pyrolysis sub-models for complex cable bundles and that the task of simulating flame spread is an extremely challenging one.

On the one hand, it is evident that the results of simulation tools strongly depend on the quality and capability of the models and the experience of the user. On the other hand, some notable work has been performed by the individual modelers to improve some features of the codes concerning a pyrolysis model or the way to handle the modeling of flame spread on cables. At the time being, only results for Test 1 are available from all codes so that the comparison is restricted to this experiment. The accuracy for predicting the major physical quantities for a given heat release rate in an assumed fire scenario has been discussed in previous ICFMP Benchmark Exercises (see /MIL 04, MCG 06, KLE 06/). One of the most difficult parameters to calculate (and to measure) is found to be the heat flux density. The difficulties in calculating the heat flux density with high accuracy represents a big handicap for the prediction of complex processes at a target such as a cable bundle.

Benchmark Exercise No. 5 focuses on the impact from a given power output of a gas burner on two separated cable bundles on a vertical tray. Therefore, the measured and calculated variables of the direct environment and of the cables themselves are of common interest although several other important variables have been measured in the fire compartment. In Test 1 no ethanol pool has been used for pre-heating of the room and the cables. The total heat release rate is equal to the sum of the energy released from the gas burner and of the energy released from the burning cables.

Test 1 is a extreme difficult exercise in terms of the investigation of a pyrolysis model. This is due to the fact that the pyrolysis rate of the FRNC cables is very low in the experiment, even with a relatively high power output from the gas burner (300 kW after 2400 s) as shown in Fig. 5-30. At a level of 300 kW power output the pyrolysis rate in the experiment reaches a maximum of about 0,003 kg/s.

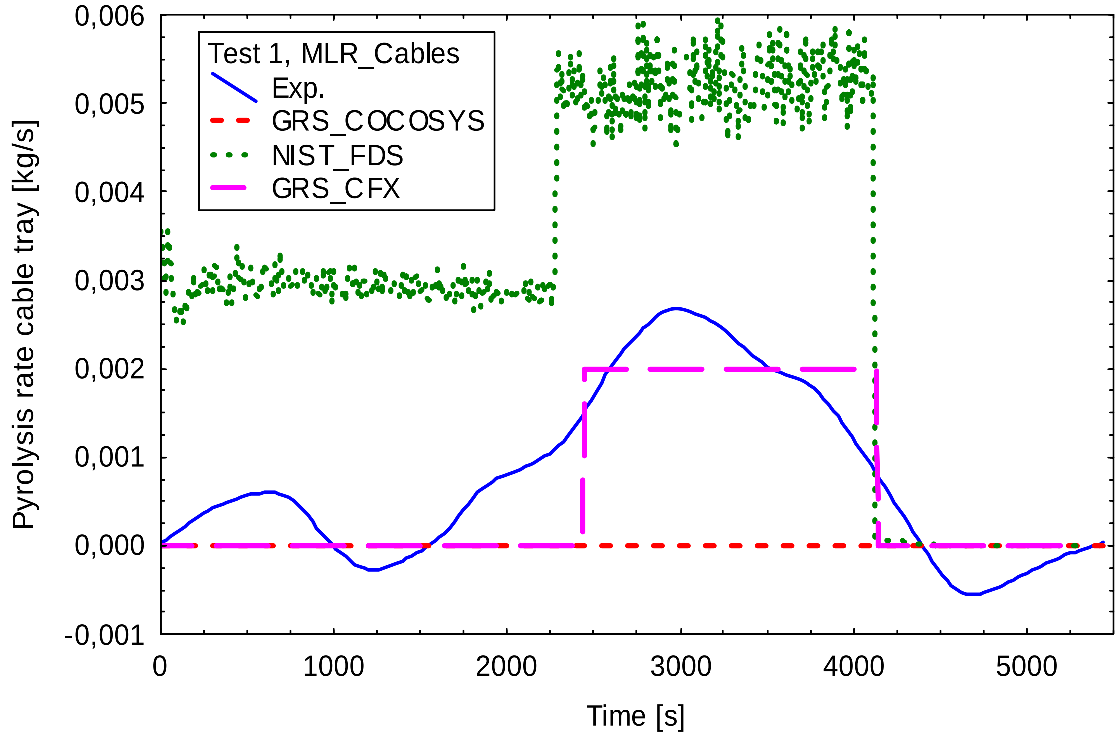


**Fig. 5-30** Pyrolysis rate of cables (MLR_Cables), Test 1 - measurement and code calculation results or inputs (only FDS has a (simple) sub-model to *predict* the pyrolysis rate of a burning object)

Note that only the FDS code has a sub-model to predict the pyrolysis rate of a solid object. The calculated pyrolysis rate coming from the FDS code is slightly too high in comparison with the experimental data. In COCOSYS the pyrolysis rate of the cables is set to zero (as an user input) and in CFX the pyrolysis is activated only when the surface temperature of the cables is reached. In this case the code used the given average pyrolysis rate (~0.002 kg/s) from the experimental data of Test 1 to simulate the individual burning cable bundles.

The corresponding total heat release rate for Test 1 (with the HRR from the gas burner) is shown in Fig. 5-31. A simple hand calculation can be made to check the measured total HRR for the second burner output phase with 300 kW. Assuming that both cable bundles burn at a maximum pyrolysis rate of 0.003 kg/s with a average effective heat of combustion of 16 MW/s (see Appendix A for cable C and cable D ), a maximum energy of nearly 0,003 kg/s * 16 MW/s = 48 KW will be released from both cable bundles. Fig. 5-31 shows the maximum total HRR derived in Test 1 with the oxygen consumption method of approx. 60 kW (if the offset from the gas burner is subtracted). This is in a good agreement to the simple approach.

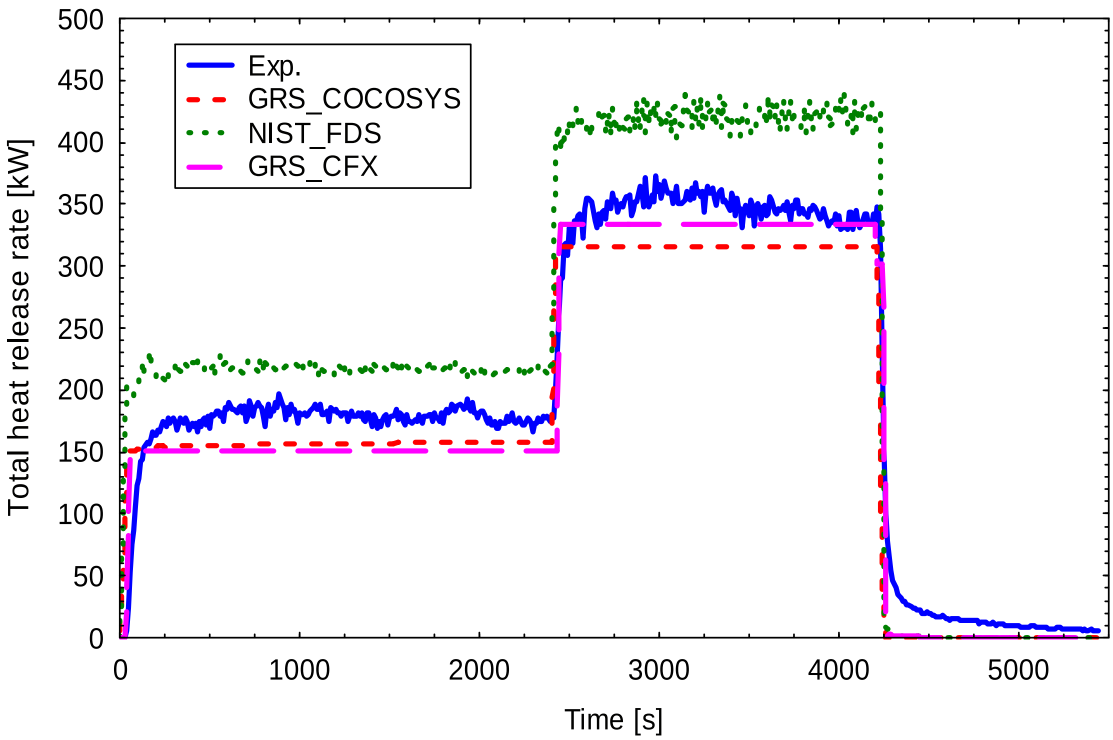


**Fig. 5-31** Total heat release rate (HRR), Test 1 - measurement and code calculation results

Fig. 5-32 shows the measured as well as the calculated gas temperatures in front of the cables (TR5_1) 0.4 m above the floor (lower layer) and Fig. 5-33 the one 3.6 m above the floor (upper layer), each value 40 cm in front of the surface of the cable bundles. The FDS code slightly over-predicts the measured temperatures in the lower layer, CFX and COCOSYS under-predict the measured values. The deviations from the calculated values to the measured ones in the upper layer are smaller for FDS and COCOSYS, but in case of the CFX code the values are much too high in the first phase of burner output (until 2400 s). Besides this, the calculated values from CFX becomes extremely noisy.

Fig. 5-34 shows the measured and the calculated surface temperatures for the power cables (TCO1_3) at 2.0 m above the floor and Fig. 5-35 shows the temperatures for the I&C cables (TCO3_3) respectively. Fig. 5-37 shows the measured and calculated surface temperatures for the power cables (TCO1_7) at 3.6 m above the floor and Fig. 5-36 for the I&C cables (TCO3_7) respectively. The interpretation of the individual calculated cable bundle surface temperatures is given code by code later.

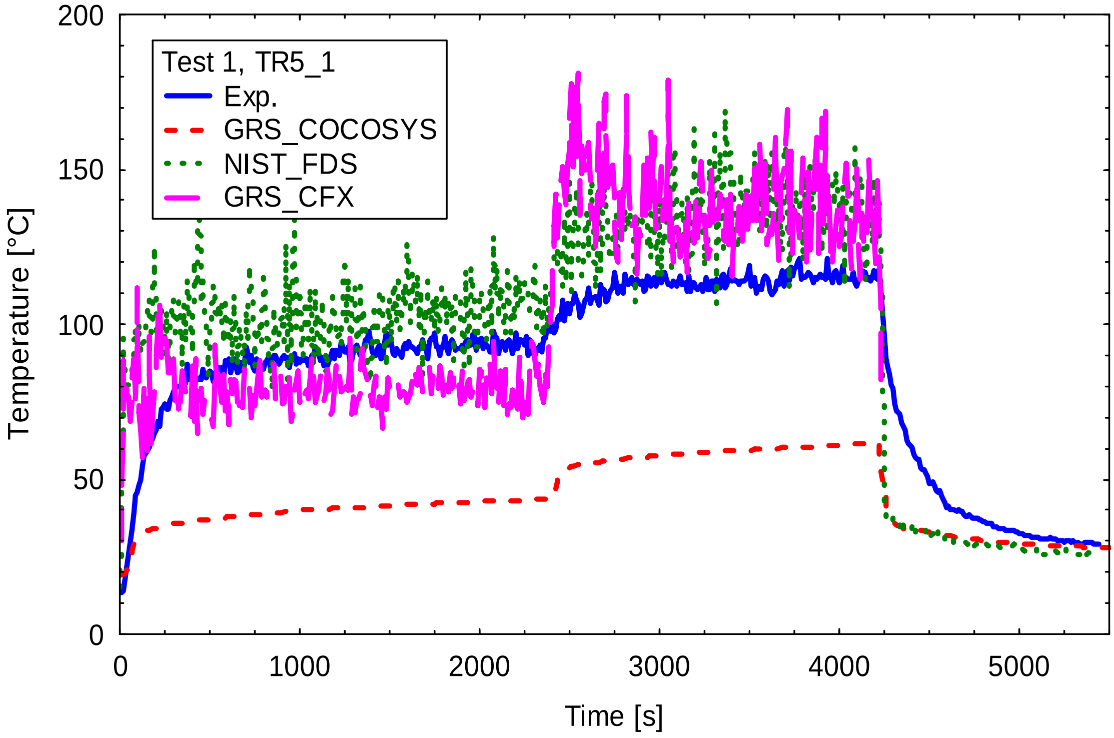


**Fig. 5-32** Gas temperatures in front of cables (TR5_1), Test 1 - measurement and code calculation results (lower compartment)

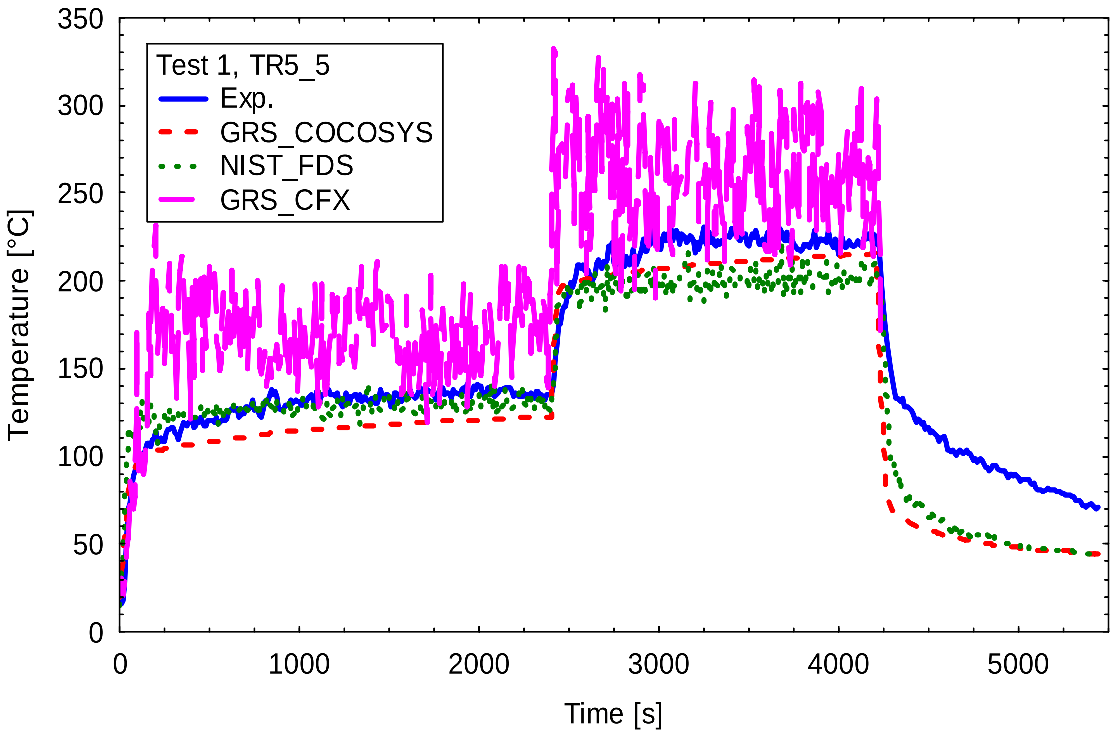


**Fig. 5-33** Gas temperatures in front of the cables (TR5_5), Test 1 - measurement and code calculation results (upper compartment)

**COCOSYS**

The calculated gas temperatures in front of the cables in the lower compartment (Fig. 5-32, TR5_1) are lower than the measured temperatures. The gas temperatures in front of the cables in the upper compartment (Fig. 5-33, TR5_5) are in a good agreement with the experimental data. If using the empirical sub-model for pyrolysis in COCOSYS the FRNC cables are found to be completely burned out. To avoid this behavior it has been decided not to use this model for FRNC cables (Tests 1 & 2). This decision means that the cables are just treated as heat sinks in both tests, and the pyrolysis rate will be zero (see Fig. 5-30). Furthermore, it has been found that the performance of the code regarding the surface temperatures in the upper layer in Test 1 is good, looking at Fig. 5-36 and Fig. 5-37. Some problems results from the missing plume model in COCOSYS, leading to a wrong air entrainment and plume size. Therefore, as usual, the deviations of the result close to the fire are larger.

**FDS**

Due to the burner output and the given thermo-physical data of the cable insulation material, the energy needed to vaporize the cable material (assumed to be a thermoplastic) is high enough so that a steady burning behavior of the cables occurs at a temperature level that is in the region of the given ignition temperature. No surface temperatures at higher levels occur as long as the material still burns. Due to the pyrolysis of the cables, the total heat release rate found in Test 1 is significantly higher than the measured one as shown in Fig. 5-31. FDS is the only code used with an implemented pyrolysis model for predicting the pyrolysis of a given material.

**CFX**

The calculations presented are based on a simple approach to the pyrolysis of the cables. If the ignition temperature is reached at one point of the cable bundle, the complete bundle starts burning at the assumed pyrolysis rate given from the experimental data. In the calculation, the I&C cable bundle would not burn, because the ignition temperature is only reached for the power cable bundle (cable D). Therefore the increase of the power cable surface temperatures (Fig. 5-34 and Fig. 5-36) is remarkably higher than that of the I&C cables (Fig. 5-35 and Fig. 5-37) in the second phase. As mentioned above, the development of a CFX sub-model for a better representation of the pyrolysis has not yet been finished so that more work with CFX has to be performed for additional conclusions in the future.

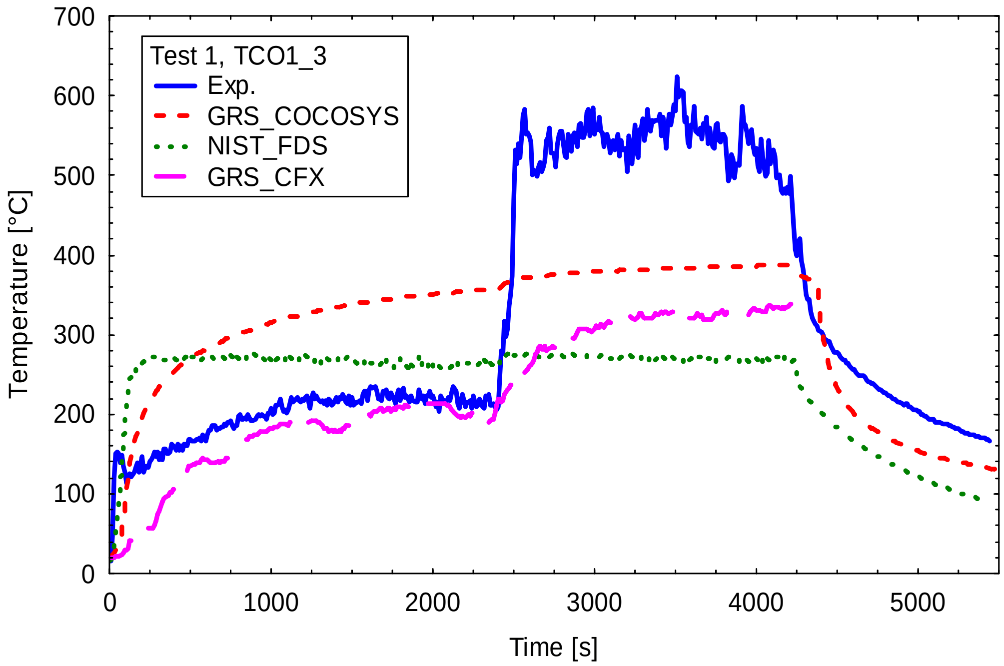


**Fig. 5-34** Power cable surface temperatures (TCO1_3), Test 1 - measurement and code calculation results, lower layer

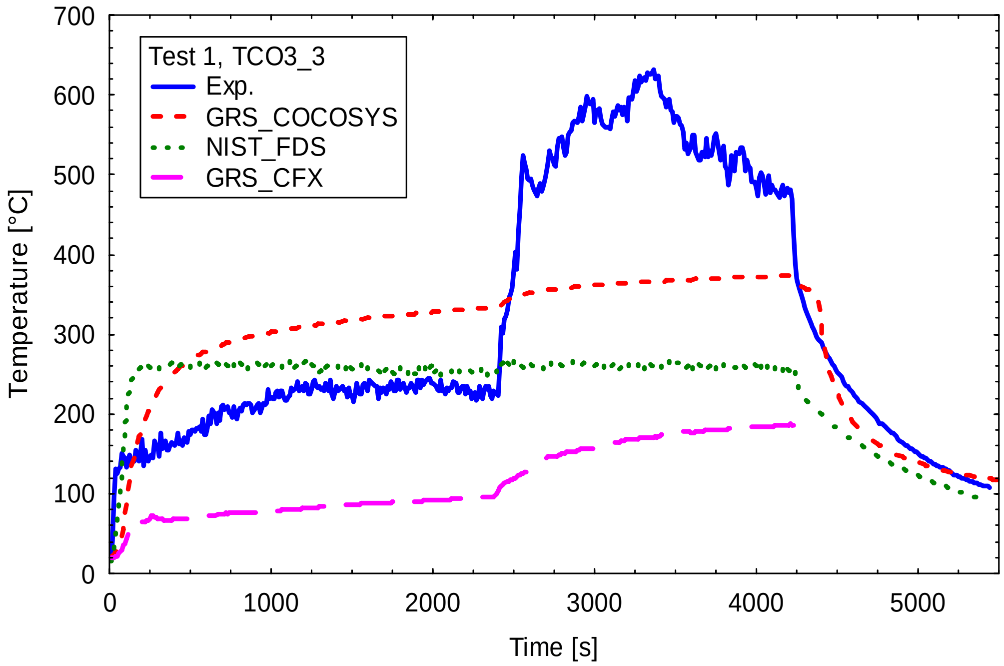


**Fig. 5-35** I&C cable surface temperatures (TCO3_3), Test 1 - measurement and code calculation results, lower layer

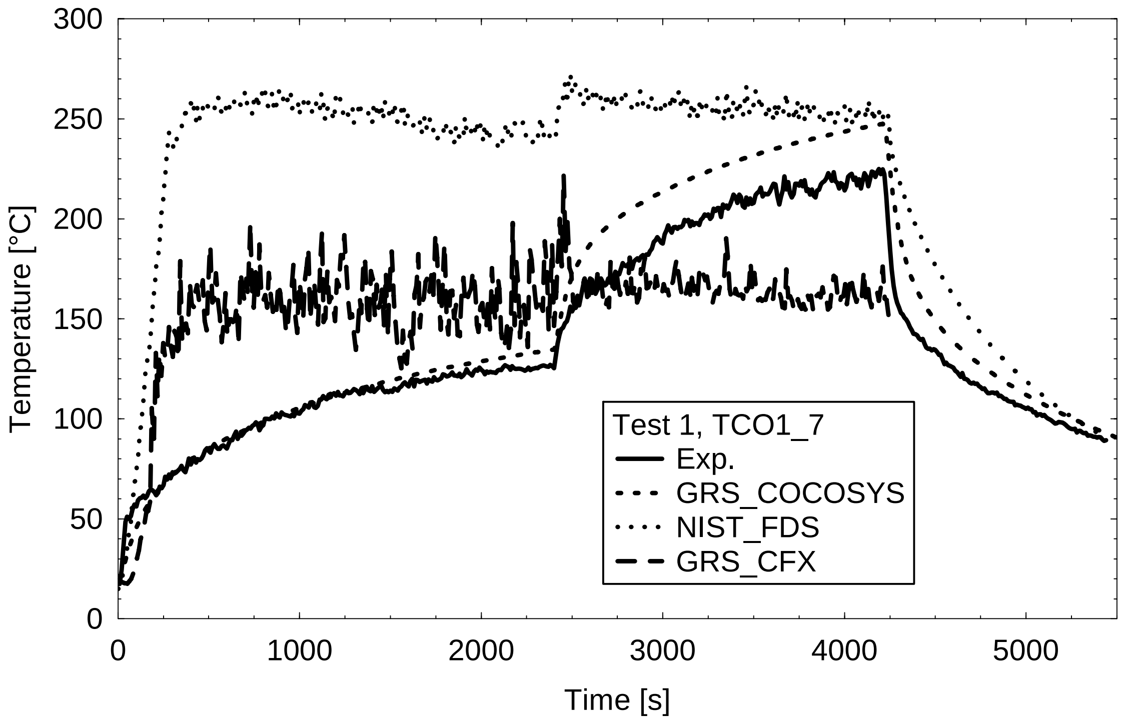


**Fig. 5-36** Power cable surface temperatures (TCO1_7), Test 1 - measurement and code calculation results, upper layer

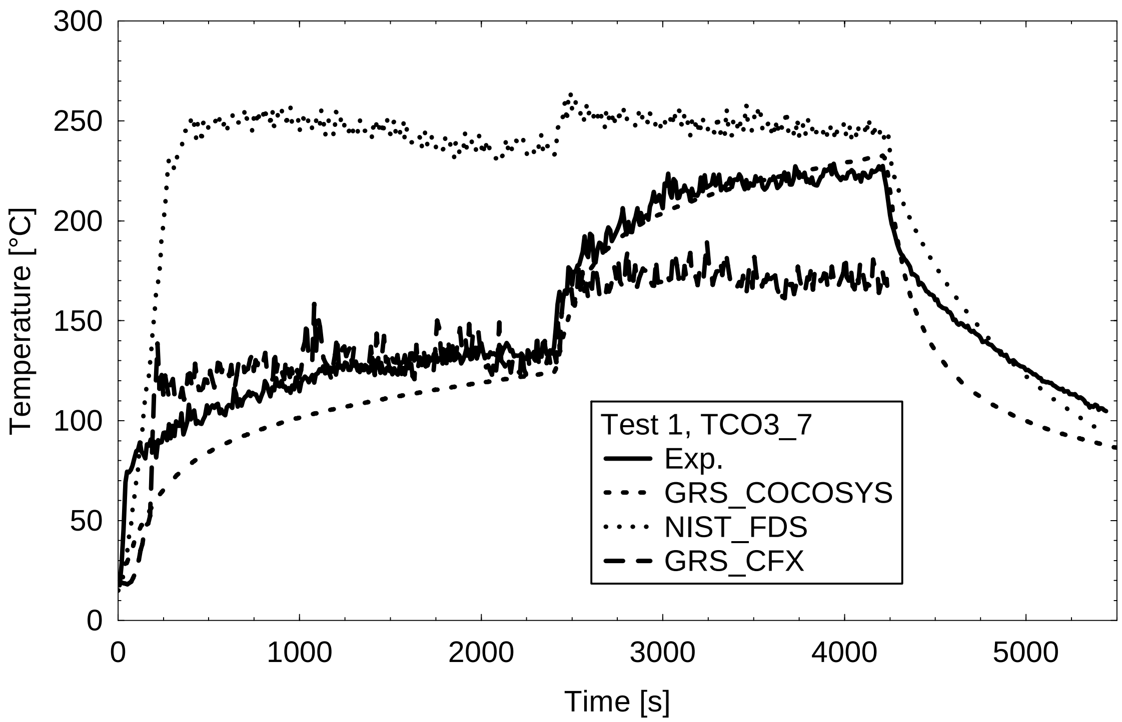


**Fig. 5-37** I&C cable surface temperatures (TCO3_7), Test 1 - measurement and code calculation results, upper layer

# 6 General Conclusions

A series of four real scale vertical cable tray fire experiments in a naturally ventilated compartment has been performed at iBMB of Braunschweig University of Technology in the frame of the ‘International Project to Evaluate Fire Models for NPP Applications” (ICFMP) to gain more insights on the consequences and effects of cable fires, in particular with respect to the functional failures of electric equipment, as well as for validation of state-of-the-art fire simulation codes. The test series considers pre-heating effects and includes time dependent electrical function loss measurements.

## 6.1 Conclusions Regarding Experimental Results

During the pre-heating phase of approximately 20 min, the temperature in the near vicinity of the cable insulation is found to reach a maximum of 200 °C. The major issue of the tests for the Benchmark Exercise No. 5 calculations is the flame spread on the cables. Two different cable insulation materials have been used: PVC and FRNC. High voltage power cables as well as low voltage I&C cables have been investigated separately in two bundles on the cable tray. The pre-heating of the compartment has been conducted by means of an ethanol pool fire; a propane gas burner has been used as ignition source.

The tests show that FRNC cables have significantly better characteristics in case of fire than PVC coated ones. No substantial flame spread takes place even in case of pre-heating. PVC cables could be ignited with a burner output of 50 kW. In contrast, the FRNC cables could be ignited at a burner output of 150 kW. The pre-heating has a complex effect on the fire behavior of the cables. It may occur that gases are pyrolysed, which are not ignited during the phase of pre-heating. These gases are transported to the cable surroundings and may leave the fire compartment.

In Test 3 a continuous average flame spread rate of 40 cm/min over the length of the cable tray in case of the I&C cables has been derived from the experimental data. A minimum surface temperature of 350 °C has been used as a indicator for a burning cable.

Short circuits occur first as ‘conductor to conductor’ shorts and later as ‘conductor to tray” shorts (short to ground). The time period when short circuits occur strongly depends on the pre-heating of the cables. In case of no pre-heating, the short circuit times are a factor two higher than in the case of pre-heating. In one case, a PVC insulated I&C cable had already failed after nearly 100 s in case of pre-heating. A mean value for the time to loss of function of a PVC insulated I&C cable with pre-heating has been estimated from the experiments to be approx. 220 s. The short circuit times of power cables are nearly two times higher then those of I&C cables independent from the cable insulation material. FRNC insulated cables have better characteristics in all tests and they are ignited with a substantially higher burner output as mentioned above. A mean value for the time to loss of electrical function of a FRNC insulated I&C cable in case of pre-heating has been estimated from the experiments to be 640 s.

The tests have been prepared and performed with high accuracy and by using instrumentation according to international standards. For a better understanding of the fire propagation, in particular on vertical cable trays, more tests are necessary: On one hand, repetition of the tests is necessary to get fundamental validation data that can be used for theortical comparisons. On the other hand, various parameters have to be adjusted. Major parameters should be the pre-heating time and the burner output. Potential ageing effects of the cables and the variation of materials of the same type ("PVC is not equal PVC") are other parameters to be examined.

## 6.2 Conclusions With Respect to the Calculations

Different fire simulation codes of differing code types have been used to calculate flame spread in a cable tray fire. None of the models applied in this ICFMP Benchmark Exercise No. 5 could predict the cable flame spread in an adequate way. There are significant differences in the way of performing flame spread calculations in the codes.

In FDS, a thermoplastic pyrolysis model has been deployed and the specified thermophysical data coming from experimental Cone Calorimeter measurements have been used as input. In the model, nothing accounts for charring or for the lateral heat conduction in the metal core. Furthermore, the complex cable bundle structure must be replaced with a rectangular slab because of the structure of the underlying numerical grid. The thickness of the solid is not tied to the gas phase grid, only the exposed surface area. As there are no standards to derive thermo-physical data from a set of Cone Calorimeter tests, it will be necessary to have clear guidelines, for the procedure for determining such data.

It should be pointed out that most of the codes could predict the main quantities (e.g. gas temperature, heat flux, gas velocities, etc.) for a given scenario, if the heat release rate from the fire is given as an input. This has been shown in the frame of other ICFMP Benchmark Exercises (see /DEY 02, KLE 06/). However, to predict the HRR and the flame spread for a given application, such as Benchmark Exercise No. 5, is a completely different task.

As a first step, it would be useful to add some general features to FDS that would be useful also in other applications. One of these is the limitation to rectangular structures and the connection to the underlying grid. One possibility is to model a complex object as a collection of small ‘particles”, each of them having properties similar to the solid material. Cable bundles could be treated as a collection of small cylinders, for which the interaction with each other would be almost completely separate from the gas phase grid.

In COCOSYS, an empirical approach has been chosen to calculate the heat release rate and the flame spread of a given cable tray fire scenario. The model uses a specified pyrolysis rate for the cables being represented by a rectangular slab as well. The propagation velocity depends on the assigned surrounding temperature of the target. A database for this property is derived from earlier experimental results, gained in the same compartment under similar conditions and consideration of different pre-heating temperatures. Therefore, the COCOSYS results are of a preliminary character and more calculations for different fire scenarios have to be performed to show the universality of the database applied.

During the calculations, the COCOSYS code has further developed in various respects. The heat transfer into the cables works considerably better now. Some problems still exist concerning the stability in those zones close to the vertical trays. This problem has to be solved in the future.

In CFX, while no pyrolysis model is included, the basic elements for checking the ignition temperature at each boundary cell of a solid does exist, and this can be coupled to a specified pyrolysis rate. The work to build up such a model has been started but is not yet finished. Because of some problems with this approach only Test 1 of Benchmark Exercise No. 5 has been calculated. The exercise to model a burning cable has therefore been simplified in that a constant pyrolysis rate (from the experimental data) is initiated once the ignition temperature at any one of the CFD cells at the cable bundle is reached.

The calculated gas temperatures are in better agreement to the experimental data in the direct environment of the cables for the first level of the gas burner with 150 kW power output. However, the predicted gas temperatures are too low for the second phase with 300 kW power output. In consequence, the resulting surface temperatures of the cables do not follow the experimental data in this second phase of the burner output.

The original question to be answered by this Benchmark Exercise was to predict the pyrolysis and not to prescribe it. For the future. it will be of great interest if the designed sub-tools for modeling the pyrolysis of a complex cable will work in a more sufficient way.

### 6.3 Recommendations

At the current time, none of the codes applied in the Benchmark Exercise No. 5 for calculating the ignition, the pyrolysis and the flame spread of realistically routed cables work at a level such that it is possible to use them as a reliable predictive tool for answering such a question. It is obvious that there is a need for the development and enhancement of sub-models for pyrolysis.

Because of continued flame spread, the data of Test 3 (PVC, no pre-heating) are particulary appropriate for the validation of fire spread models. The pyrolysis models have to demonstrate that they can predict the results of Test 1 as well as those of Test 2, because no flame spread occurs in case of FRNC cables. This may indicate that a computer code, which just performs well if flame spread occurs, may not be suitable to handle complex materials.

The examination with Benchmark Exercise No. 5 also shows that the input parameters for a pyrolysis model are highly significant, since a model will work only with the correct input of thermo-physical data of the used material. Up to now, there are no set rules how to measure the different properties as main input, such as heat of gasification, ignition temperature, or heat of combustion.

Because of the complexity to develop a complete deterministic flame spread model for cables there is a need for further measurement of empirical data for fire spread (pyrolysis growth) on complex items, e.g. cable trays.

# 7 Acknowledments

In addition to the analysts identified in the appendices of this report, who performed the calculations for Benchmark Exercise No. 5, several experts from various organizations contributed to this Benchmark Exercise in many ways. The test series used for this Benchmark Exercise was co-sponsored by the German Federal Ministry for the Environment, Nature Conservation and Nuclear Safety (BMU) and the German Federal Authority for Radiation Protection (BfS) within the frame of the projects SR 2449 and SR 2491. The tests were performed by Institut für Baustoffe, Massivbau und Brandschutz (iBMB) of Braunschweig University of Technology sub-contracted by GRS.

Dietmar Hosser, Olaf Riese, Hans-Joachim Wolff and Mark Klingenberg were the key iBMB staff for the test series. Jonathan Barnett at WPI, USA, Olavi Keski-Rahkonen and Simo Hostikka at VTT, Finland, and James Oldham and Doug Brandes (retired) at Duke Energy, USA hosted the 7th, 8th and 9th ICFMP meetings, where this Benchmark Exercise was planned in more detail and discussed, and also technical support. Monideep Dey at NRC/NIST, USA and Marina Roewekamp at GRS, Germany provided project management and technical support to the ICFMP group.

Heinz Peter Berg from BfS, Germany, Walter-Klein-Hessling from GRS, Germany, Monideep Dey, USA, Stewart Miles from BRE, GB and other members of the institutions participating in the ICFMP project all contributed to this Benchmark Exercise either by providing peer comments, participating in meetings to discuss the test plan and results, or indirectly by sponsoring participants for the project. Benchmark Exercise No. 5 and its corresponding documentation would not have been possible without the help and expertise of all the above.

# 8 References

/ALL 05/ Allelein, H.-J., et al.:
Weiterentwicklung der Rechenprogramme COCOSYS und ASTEC, Abschlussbericht, GRS-A-3266, Gesellschaft für Anlagen- und Reaktorsicherheit, April 2005

/ANS 05/ ANSYS Inc.:
CFX-10, User Documentation,. ANSYS Inc., USA, 2005

/AST 04/ American Society of Testing and Materials (ASTM):
Evaluating the Predictive Capability of Deterministic Fire Models,
ASTM E1355-04, West Conshohocken, PA , 2004

/BAB 03/ Babrauskas, V.:
Ignition Handbook, Fire Science Publishers, Society of Fire Protection Engineers, ISBN 0-9728111-3-3, USA, 2003

/DEY 02/ Dey, M. K.:
Evaluation of Fire Models for Nuclear Power Plant Applications: International Panel Report on Benchmark Exercise No. 1, Cable Tray Fires, U.S. Nuclear Regulatory Commission, Office of Nuclear Regulatory Research, NUREG 1758, Washington, June 2002, also National Institute of Standards and Technology, NISTIR 6872, June 2002

/DIN 85/ Deutsches Institut für Normung e.V. (DIN):
DIN 51622: Flüssiggase: Propan, Propen, Butan, Buten und deren Gemische, Anforderungen, Berlin, 1985

/DIN 95/ Deutsches Institut für Normung e.V. (DIN):
DIN 4102 – Teil 12: Brandverhalten von Baustoffen und Bauteilen, Teil 12: Funktionserhalt von elektrischen Kabelanlagen, Anforderungen und Prüfungen, Berlin, February 1995

/DRY 99/ Drysdale, D.:
An Introduction to Fire Dynamics, 2nd Edition, John Wiley & Sons Ltd., 1999

/EMM 02/ Emmons, H. W.:
Vent Flows, SFPE Handbook of Fire Protection Engineering, Section Two, Chapter 3, National Fire Protection Association, Quincy, Massachusetts, Society of Fire Protection Engineers, Bethesda, Maryland, 2003

/FOR 04/ Forney, G. P., K. McGrattan:
User's Guide for Smokeview Version 4 – A Tool for Visualizing Fire Dynamics Simulation Data, Fire Research Division, Building and Fire Research Laboratory, NIST Special Publication 1017, August 2004

/HAM 06/ Hamins, A., A. Maranghides, R. Johnssonm M. Donnelly, J, Yang, G. Mulholland, R. L. Antleitner:
Report of Experimental Results for the International Fire Model Benchmarking and Validation Exercise #. 3, National Institute of Standards and Technology, NIST SP 1013-1 and NUREG/CR-6905, May 2006

/HOS 98/ Hosser, D., W. Siegfriedm J. Will:
Untersuchungen zum Brandverhalten von Kabelanlagen und zur Schutzfunktion von dämmschichtbildenden Anstrichen und Kabeln, Bericht Nr. U 97 073 iBMB, Auftrags-Nr. SR 2207 – 81030 –UA-1313 BMU, February 1998

/HOS 02/ Hosser, D., O. Riese:
Proposal for large scale fire tests, 4th International Collaborative Project Meeting to Evaluate Fire Models for Nuclear Power Plants Applications, GRS Berlin,
October 17-18, 2001, In: International Collaborative Project Meeting to Evaluate Fire Models for NPP Applications – Proceedings, GRS-A-3106, Technical Report, 2002

/HOS 03/ Hosser, D., O. Riese, M. Schmeling:
Durchführung von vergleichenden Brandversuchen mit unterschiedlichen Kabelmaterialien und Kabelschutzsystemen, VGB Kraftwerkstechnik GmbH, VGB-Kennziffer SA 'AT' 11/00, June 2003

/HOS 05/ Hosser, D., O. Riese, M. Klingenberg:
Durchführung von weiterführenden Kabelbrandversuchen einschließlich der Präsentation der Ergebnisse im Rahmen des internationalen Projektes ICFMP, Vorhaben SR 2449, Unterauftrag UA-2298, Schriftenreihe Reaktorsicherheit und Strahlenschutz, BMU-2005-663, 2005

/ISO 93/ International Standards Organization (ISO):
ISO 9705-1: Fire Tests - Full-scale Room Test for Surface Products (Room Corner Test), International Organization for Standardization, 1993

/ISO 99/ International Standards Organization (ISO):
ISO 5660-1: Reaction to fire tests – Heat release, smoke production and mass loss rate; Part 1: Heat Release Rate (Cone Calorimeter method), International Organization for Standardization, 1999

/JAN 92/ Janssens, M.:
Determining flame spread properties from Cone Calorimeter measurements, Heat Release in Fires, Edited by V. Babrauskas and S. Grayson, 1992

/JON 04/ Jones, W., Ed.:
CFAST - Consolidated Model of Fire Growth and Smoke Transport (Version 5),
National Institute of Standards and Technology, NIST Special Publication 1030,
October 2004

/KAN 03/ Kanury, A. M.:
Flaming Ignition of Liquid Fuels, The SFPE Handbook of Fire Protection Engineering, Third Edition, Section Two, Chapter 2-11, National Fire Protection Association, Quincy, Massachusetts, Society of Fire Protection Engineers, Bethesda,
Maryland, 2003

/KLE 06/ Klein-Hessling, W., M. Roewekamp, O. Riese:
Evaluation of Fire Models for Nuclear Power Plant Applications: Large Fires in Compartments, International Panel Report on Benchmark Exercise No. 4,
Gesellschaft für Anlagen- und Reaktorsicherheit (GRS), Report Number GRS-213, ISBN-Nr.: 978-3-931995-80-5, to be published, 2006

/MCG 04/ McGrattan, K., Ed.:
Fire Dynamics Simulator (Version 4), Technical Reference Guide, National Institute of Standards and Technology, NIST Special Publication 1018, September 2004

/MCG 06/ McGrattan, K. B.:
Evaluation of Fire Models for Nuclear Power Plant Applications: Benchmark Exercise #3, NISTIR 7338, National Institute of Standards and Technology, Gaithersburg, Maryland, 2006 (to be published)

/MIL 04/ Miles, S.:
Evaluation of Fire Models for Nuclear Power Plant Applications: International Panel Report on Benchmark Exercise No. 4, Pool Fires in Large Halls, Building Research Establishment Ltd., BRE Report Number 212214, May 2004

/NIS 03/ National Institute of Standards and Technology (NIST):
International Collaborative Project to Evacuate Fire Models for Nuclear Power Plant Applications: Summary of 5$^{th}$ Meeting, NISTIR 6986, C-62-64, National
Institute of Standards and Technology, September 2003, also U.S. Nuclear Regulatory Commission, NUREG/CP-0181, October 2003

/NOW 03/ Nowlen, S. P.:
Cable Failure Modes and Effects Risk Analysis Perspectives, Presented at: Structural Mechanics in Reactor Technology Post Conference Seminar 21 (SMIRT), Fire Safety in Nuclear Power Plants and Installations, August 25-28, 2003, Piestany, Slovak Republic, 2003

/QUI 01/ Quintiere, J. G.:
Models for Fire Growth and Spread, Published in “Engineering Methods for Fire Safety”, Proceedings of 9th International Fire Protection Symposium, Edited by
D. Hosser, iBMB, Braunschweig, 2001

/RIE 03/ Riese, O.:
Versuche zum Brandverhalten von verschiedenen Arten und Anordnungen von Kabeln, Publisher in „Braunschweiger Brandschutz-Tage ‚03“, 10. Fachseminar Brandschutz – Forschung und Praxis, 30. September und 1. Oktober 2003 in Braunschweig, iBMB (Institut für Baustoffe, Massivbau und Brandschutz), Heft 168, Braunschweig, 32003

/ROE 03/ Roewekamp, M., O. Riese, D. Hosser:
Foreseen German Real Scale Cable Tray Fire Tests and Functional Failure Tests, 5th International Collaborative Project Meeting to Evaluate Fire Models for Nuclear Power Plants Applications, NIST Gaithersburg, MD, May 2 – 3, 2002, NISTIR 6986, 569 p., NIST Gaithersburg, MD, D/303-306 pp September 2003

/SFP 95/ Society of Fire Protection Engineers (SFPE):
The SFPE Handbook of Fire Protection Engineering, 2nd Edition, National Fire Protection Association, Bethesda, Maryland, 1995

/TEW 03/ Tewarson, A.:
Generation of Heat and Chemical Compounds in Fires, The SFPE Handbook of Fire Protection Engineering, Third Edition, Section Three, Chapter 3-5, National Fire Protection Association, Quincy, Massachusetts, Society of Fire Protection Engineers, Bethesda, Maryland, 2003

/USN 04/ U.S. Nuclear Regulatory Commission (USNRC):
Fire Dynamics Tools (FDTs) Quantitative Fire Hazard Analysis Methods for the U.S. Nuclear Regulatory Commission Fire Protection Inspection Program, NUREG-1805, Washington DC, USA, November 2004

/WOO 03/ Woods, H. W.:
Draft of the United (US) Nuclear Regulatory Commission (NRC) Final Report for the “Fire-Induced to Electrical Cables and Circuits Working Group (FIDECC_WG)’ of the ‘Cooperative PRA (COOPRA) International Effort’, 2002

## List of Figures

## List of Tables

## Acronyms and Initialisms

| | |
|---|---|
| BE | Benchmark Exercise |
| BfS | Bundesamt für Strahlenschutz |
| CFAST | Consolidated Model for Fire and Smoke Transport |
| CFD | Computational Fluid Dynamic |
| COCOSYS | Containment Code System |
| EdF | Electricité de France |
| EPRI | Electric Power Research Institute |
| FDS | Fire Dynamics Simulator |
| FRNC | Fire retardant non-corrosive |
| GRS | Gesellschaft für Anlagen- und Reaktorsicherheit |
| HGL | Hot gas layer (or upper layer) |
| iBMB | Institut für Baustoffe Massivbau und Brandschutz |
| I&C | Instrumentation and control |
| LL | Lower layer |
| MAGIC | Zone Model for simulation of fire compartment building by EdF |
| MLR | Mass loss rate |
| NIST | National Institute of Standards and Technology |
| NPP | Nuclear Power Plant |
| PVC | Polyvinyl chloride |
| SNL | Sandia National Laboratories |
| USNRC | United States Nuclear Regulatory Commission |

# Appendix A: Cable Data

**Tab. A-1** Detailed information regarding cable type A

| **Labeling** | | |
|---|---|---|
| Index | A |  |
| Cable type | PVC - I&C cable<br><br>∅ ≈14.0 mm | |
| Type label due to VDE 0815/16 | | JE-Y(St)Y 16 x 2 x 0,8 mm |
| Labeling details | | J - installation cable<br>E - electronic<br>Y - PVC insulation<br>(St) - static foil screen<br>Y - PVC outer sheath<br>- wires => 32 wires<br>- diameter =>0.8 mm<br>- cross section => 0,5 mm² |

**Tab. A-2** Detailed information regarding cable type B

| **Labeling** | | |
|---|---|---|
| Index | B | 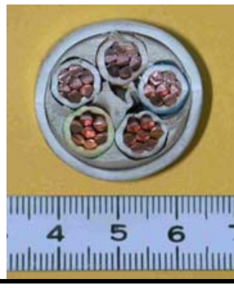 |
| Cable type | PVC - Power cable<br><br>∅ ≈ 30.0 mm | |
| Type label due to VDE 0250 | | NYM-J 5 x 25 |
| Labeling details | | N - VDE-type<br>Y - PVC insulation<br>M - sheathed cable<br>J - with protective wire<br>- wires => 5 wires<br>- cross section => 25 mm² |

**Tab. A-3** Detailed information regarding cable type C

<table>
<tr><th colspan="3">Labeling</th></tr>
<tr><td>Index</td><td>C</td><td rowspan="2">
</td></tr>
<tr><td>Cable type</td><td>FRNC– I&C cable<br><br>∅ ≈16.0 mm</td></tr>
<tr><td colspan="2">Type label due to VDE 0250</td><td>JE-LIHCH (Bd) 16 × 2 × 0.5</td></tr>
<tr><td colspan="2">Labeling details</td><td>J - installation cable<br>E - electronic<br>LI - stranded wire<br>H - non-corrosive (non-halogen) insulation<br>C - shielding by copper wire mesh<br>H - non-corrosive (non-halogen) sheath<br>- wires => 32 wires<br>- cross section => 0.5 mm²</td></tr>
</table>

**Tab. A-4** Detailed information regarding cable type D

<table>
<tr><th colspan="3">Labeling</th></tr>
<tr><td>Index</td><td>D</td><td rowspan="2">
</td></tr>
<tr><td>Cable type</td><td>FRNC– Power cable<br><br>∅ ≈12.5 mm</td></tr>
<tr><td colspan="2">Type label due to VDE 0250</td><td>NHXMH-J 5 x 2,5</td></tr>
<tr><td colspan="2">Labeling details</td><td>N - VDE-type<br>HX - non-corrosive (non-halogen) materials<br>MH - connection wire of medium mechanical<br>- load<br>J - with protective wire<br>- wires => 5 wires<br>- cross section => 2.5 mm²</td></tr>
</table>

**Tab. A-5** Thermo-physical data of cable type A

<table>
<tr><td>Cable A</td><td>PVC - I&C cable</td><td colspan="4">JE-Y(St)Y 16 x 2 x 0,8 mm</td></tr>
<tr><td colspan="6">Thermo-physical cable data from Cone Calorimeter at iBMB</td></tr>
<tr><td colspan="2"></td><td colspan="2">Value</td><td>Reference</td><td>Unit</td></tr>
<tr><td colspan="2">Critical heat flux</td><td colspan="2">12.5</td><td rowspan="3">theory by Janssens *</td><td>kW/m²</td></tr>
<tr><td colspan="2">Ignition temperature</td><td colspan="2">313.6</td><td>°C</td></tr>
<tr><td colspan="2">$\lambda\rho c_p$</td><td colspan="2">0.12</td><td>$kW^2s/K^2m^4$</td></tr>
<tr><td colspan="2">Heat flux (two tests each)</td><td>35 kW/m²</td><td>50 kW/m²</td><td colspan="2">two tests each</td></tr>
<tr><td colspan="2">Maximum heat release rate</td><td>207.5</td><td>257.6</td><td></td><td>kW/m²</td></tr>
<tr><td colspan="2">Average heat release rate</td><td>155.8</td><td>193.6</td><td rowspan="4">mass loss rate 10 – 90 % according to ISO 5660 fire tests - reaction to fire, part 1</td><td>kW/m²</td></tr>
<tr><td colspan="2">Average effective heat of combustion</td><td>11.2</td><td>13.9</td><td>MJ/kg</td></tr>
<tr><td colspan="2">Average $CO_2$ -yield</td><td>1.065</td><td>0.486</td><td>kg/kg</td></tr>
<tr><td colspan="2">Average CO-yield</td><td>0.049</td><td>0.054</td><td>kg/kg</td></tr>
<tr><td colspan="2">Average soot-yield</td><td>0.047</td><td>0.100</td><td>(average 300 s)</td><td>kg/kg</td></tr>
<tr><td colspan="2">Average effective heat of gasification</td><td colspan="2">3910</td><td>obtained from reciprocal slope of a plot of peak mass loss rate versus external heat flux</td><td>kJ/kg</td></tr>
<tr><td colspan="6">Other methods and sources</td></tr>
<tr><td colspan="2">HCl-yield</td><td colspan="2">0.5</td><td>NUREG – 1758</td><td>kg/kg</td></tr>
<tr><td colspan="2">Fraction of flame heat released as radiation</td><td colspan="2">0.48</td><td>NUREG – 1758</td><td>-</td></tr>
<tr><td colspan="2">Emissivity</td><td colspan="2">0.8</td><td>NUREG – 1758</td><td>-</td></tr>
<tr><td colspan="2">Specific heat $c_p$</td><td colspan="2">1040</td><td>NUREG – 1758</td><td>J/kgK</td></tr>
<tr><td colspan="2">Thermal conductivity $\lambda$</td><td colspan="2">0.092</td><td>NUREG – 1758</td><td>W/mK</td></tr>
<tr><td colspan="2">Heat of combustion core insulation</td><td colspan="2">21.547</td><td rowspan="2">iBMB, oxygen bomb calorimeter</td><td>MJ/kg</td></tr>
<tr><td colspan="2">Heat of combustion sheath insulation</td><td colspan="2">13.878</td><td>MJ/kg</td></tr>
<tr><td colspan="2">Non-combustible volume</td><td colspan="2">0.017</td><td rowspan="4">iBMB</td><td>l/m</td></tr>
<tr><td colspan="2">Combustible volume</td><td colspan="2">0.116</td><td>l/m</td></tr>
<tr><td colspan="2">Density non-combustible volume</td><td colspan="2">8726</td><td>kg/m³</td></tr>
<tr><td colspan="2">Density combustible volume $\rho$</td><td colspan="2">1458</td><td>kg/m³</td></tr>
</table>

* M. Janssens:
Determining flame spread properties from Cone Calorimeter measurements, Heat Release in Fires, Edited by V. Babrauskas and S. Grayson, 1992

**Tab. A-6** Thermo-physical data of cable type B

| **Cable B** | **PVC – power cable** | **NYM-J 5 x 25** | | | |
|---|---|---|---|---|---|
| **Thermo-physical cable data from Cone Calorimeter at iBMB (each heat flux two tests)** | | | | | |
| | | Value | | Reference | Unit |
| Critical heat flux | | 12.4 | | theory by Janssens * | kW/m² |
| Ignition temperature | | 312.6 | | | °C |
| $\lambda\rho c_p$ | | 0.24 | | | $kW^2s/K^2m^4$ |
| Heat flux (two tests each) | | 35 kW/m² | 50 kW/m² | two tests each | |
| Maximum heat release rate | | 157.8 | 216.8 | | kW/m² |
| Average heat release rate | | 67.6 | 123.2 | mass loss rate 10 -9 0 % according to ISO 5660 fire tests - reaction to fire, part 1 | kW/m² |
| Average effective heat of combustion | | 18.1 | 20.7 | | MJ/kg |
| Average $CO_2$ -yield | | 1.276 | 0.468 | | kg/kg |
| Average CO-yield | | 0.022 | 0.027 | | kg/kg |
| Average soot-yield | | 0.038 | 0.055 | (average 300 s) | kg/kg |
| Average effective heat of gasification | | 4930 | | obtained from reciprocal slope of a plot of peak mass loss rate versus external heat flux | kJ/kg |
| **Other methods and source** | | | | | |
| HCl-yield | | 0.5 | | NUREG - 1758 | kg/kg |
| Fraction of flame heat released as radiation | | 0.48 | | NUREG - 1758 | - |
| Emissivity | | 0.8 | | NUREG - 1758 | - |
| Specific heat $c_p$ | | 1040 | | NUREG - 1758 | J/kgK |
| Thermal conductivity $\lambda$ | | 0.092 | | NUREG - 1758 | W/mK |
| Heat of combustion core insulation | | 15.099 | | iBMB, oxygen bomb calorimeter | MJ/kg |
| Heat of combustion sheath insulation | | 15.421 | | | MJ/kg |
| Non-combustible volume | | 0.122 | | iBMB | l/m |
| Combustible volume | | 0.484 | | | l/m |
| Density non-combustible volume | | 8879 | | | kg/m³ |
| Density combustible volume $\rho$ | | 1504 | | | kg/m³ |

* M. Janssens:
Determining flame spread properties from Cone Calorimeter measurements, Heat Release in Fires, Edited by V. Babrauskas and S. Grayson, 1992

**Tab. A-7** Thermo-physical data of cable type C

| **Cable C** | **FRNC – I&C cable** | **JE-LIHCH (Bd) 16 × 2 × 0.5** | | | |
|---|---|---|---|---|---|
| **Thermo-physical cable data from Cone Calorimeter at iBMB (each heat flux two tests)** | | | | | |
| | Value | | Reference | Unit | |
| Critical heat flux | 12.1 | | theory by Janssens* | kW/m² | |
| Ignition temperature | 323.4 | | | °C | |
| $\lambda\rho c_p$ | 0.96 | | | $kW^2s/K^2m^4$ | |
| Heat flux (two tests each) | 35 kW/m² | 50 kW/m² | two tests each | | |
| Maximum heat release rate | 99.4 | 170.5 | | kW/m² | |
| Average heat release rate | 39.5 | 78.2 | mass loss rate 10 – 90 % according to ISO 5660 fire tests - reaction to fire, part 1 | kW/m² | |
| Average effective heat of combustion | 18.1 | 22.5 | | MJ/kg | |
| Average $CO_2$ -yield | 0.916 | 0.170 | | kg/kg | |
| Average CO-yield | 0.076 | 0.017 | | kg/kg | |
| Average soot-yield | 0.017 | 0.001 | (average 300 s) | kg/kg | |
| Average effective heat of gasification | 4281 | | obtained from reciprocal slope of a plot of peak mass loss rate versus external heat flux | kJ/kg | |
| **Other methods and source** | | | | | |
| Fraction of flame heat released as radiation | - | | - | - | |
| Emissivity | 0.95 | | no reference | - | |
| Specific heat $c_p$ | - | | - | J/kgK | |
| Thermal conductivity $\lambda$ | - | | - | W/mK | |
| Heat of combustion core insulation | 23.264 | | iBMB, oxygen bomb calorimeter | MJ/kg | |
| Heat of combustion sheath insulation | 17.389 | | | MJ/kg | |
| Non-combustible volume | 0.017 | | iBMB | l/m | |
| Combustible volume | 0.160 | | | l/m | |
| Density non-combustible volume | 8691 | | | kg/m³ | |
| Density combustible volume $\rho$ | 1615 | | | kg/m³ | |

* M. Janssens:
Determining flame spread properties from Cone Calorimeter measurements, Heat Release in Fires, Edited by V. Babrauskas and S. Grayson, 1992

**Tab. A-8** Thermo-physical data of cable type D

<table>
<tr><td>Cable D</td><td>FRNC – power cable</td><td colspan="4">NHXMH-J 5 x 2,5</td></tr>
<tr><td colspan="6">Thermo-physical cable data from Cone Calorimeter at iBMB (each heat flux two tests)</td></tr>
<tr><td colspan="2"></td><td colspan="2">Value</td><td>Reference</td><td>Unit</td></tr>
<tr><td colspan="2">Critical heat flux</td><td colspan="2">13.0</td><td rowspan="3">theory by Janssens *</td><td>kW/m²</td></tr>
<tr><td colspan="2">Ignition temperature</td><td colspan="2">335.7</td><td>°C</td></tr>
<tr><td colspan="2">$\lambda \rho c_p$</td><td colspan="2">1.14</td><td>kW²s/K²m$^4$</td></tr>
<tr><td colspan="2">Heat flux (two tests each)</td><td>35 kW/m²</td><td>50kW/m²</td><td colspan="2"></td></tr>
<tr><td colspan="2">Maximum heat release rate</td><td>113.5 **</td><td>133.0</td><td></td><td>kW/m²</td></tr>
<tr><td colspan="2">Average heat release rate</td><td>41.1</td><td>59.5</td><td rowspan="4">mass loss rate 10 – 90 % according to ISO 5660 fire tests - reaction to fire, part 1</td><td>kW/m²</td></tr>
<tr><td colspan="2">Average effective heat of combustion</td><td>25.4</td><td>27.8</td><td>MJ/kg</td></tr>
<tr><td colspan="2">Average $CO_2$ -yield</td><td>1.105</td><td>0.012</td><td>kg/kg</td></tr>
<tr><td colspan="2">Average CO-yield</td><td>0.028</td><td>0.002</td><td>kg/kg</td></tr>
<tr><td colspan="2">Average soot-yield</td><td>0.026</td><td>0.028</td><td>(average 300 s)</td><td>kg/kg</td></tr>
<tr><td colspan="2">Average effective heat of gasification</td><td colspan="2">18361</td><td>obtained from reciprocal slope of a plot of peak mass loss rate versus external heat flux</td><td>kJ/kg</td></tr>
<tr><td colspan="6">Other methods and source</td></tr>
<tr><td colspan="2">Fraction of flame heat released as radiation</td><td colspan="2">-</td><td>-</td><td>-</td></tr>
<tr><td colspan="2">Emissivity</td><td colspan="2">0.95</td><td>no reference</td><td>-</td></tr>
<tr><td colspan="2">Specific heat $c_p$</td><td colspan="2">-</td><td>-</td><td>J/kgK</td></tr>
<tr><td colspan="2">Thermal conductivity $\lambda$</td><td colspan="2">-</td><td>-</td><td>W/mK</td></tr>
<tr><td colspan="2">Heat of combustion core insulation</td><td colspan="2">46.082</td><td rowspan="2">iBMB, oxygen bomb calorimeter</td><td>MJ/kg</td></tr>
<tr><td colspan="2">Heat of combustion sheath insulation</td><td colspan="2">16.802</td><td>MJ/kg</td></tr>
<tr><td colspan="2">Non-combustible volume</td><td colspan="2">0.012</td><td rowspan="4">iBMB</td><td>l/m</td></tr>
<tr><td colspan="2">Combustible volume</td><td colspan="2">0.095</td><td>l/m</td></tr>
<tr><td colspan="2">Density non-combustible volume</td><td colspan="2">8674</td><td>kg/m³</td></tr>
<tr><td colspan="2">Density combustible volume $\rho$</td><td colspan="2">1428</td><td>kg/m³</td></tr>
</table>

* M. Janssens:
Determining flame spread properties from Cone Calorimeter measurements, Heat Release in Fires, Edited by V. Babrauskas and S. Grayson, 1992,

** only one value

## Appendix B: Plots of Test 1 to Test 4

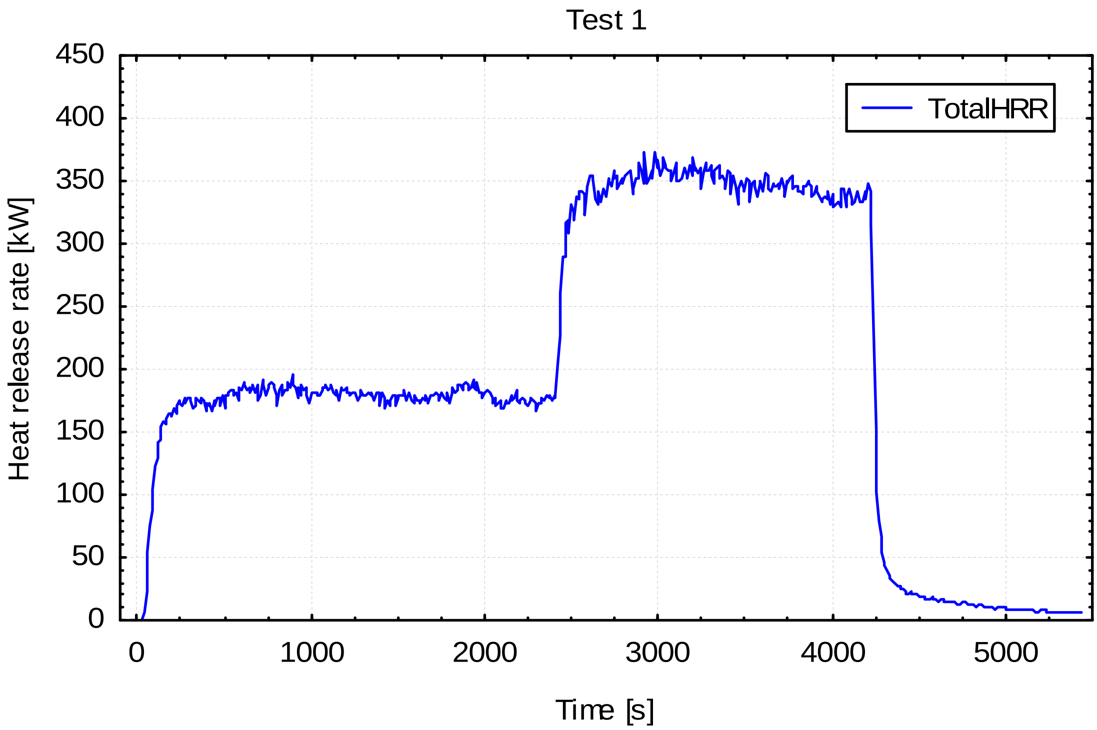


**Fig. B-1** Test 1: Total heat release rate (ISO 9705) exhaust duct

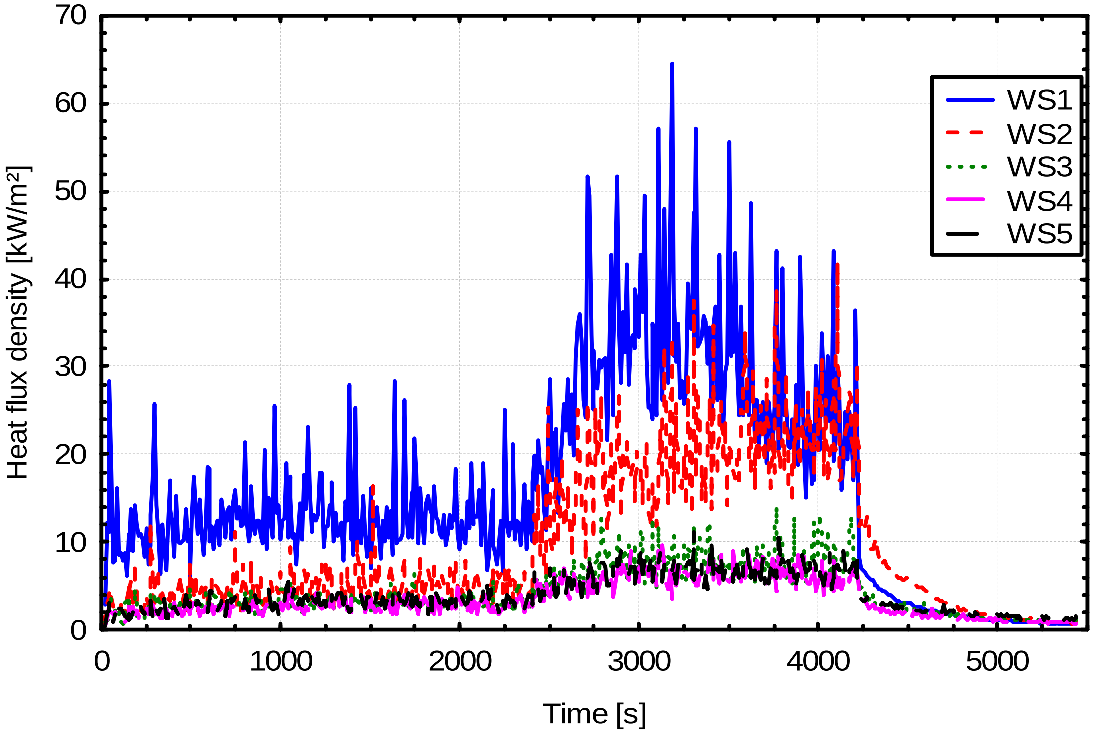


**Fig. B-2** Test 1: Heat flux density in front of the FRNC cable bundles

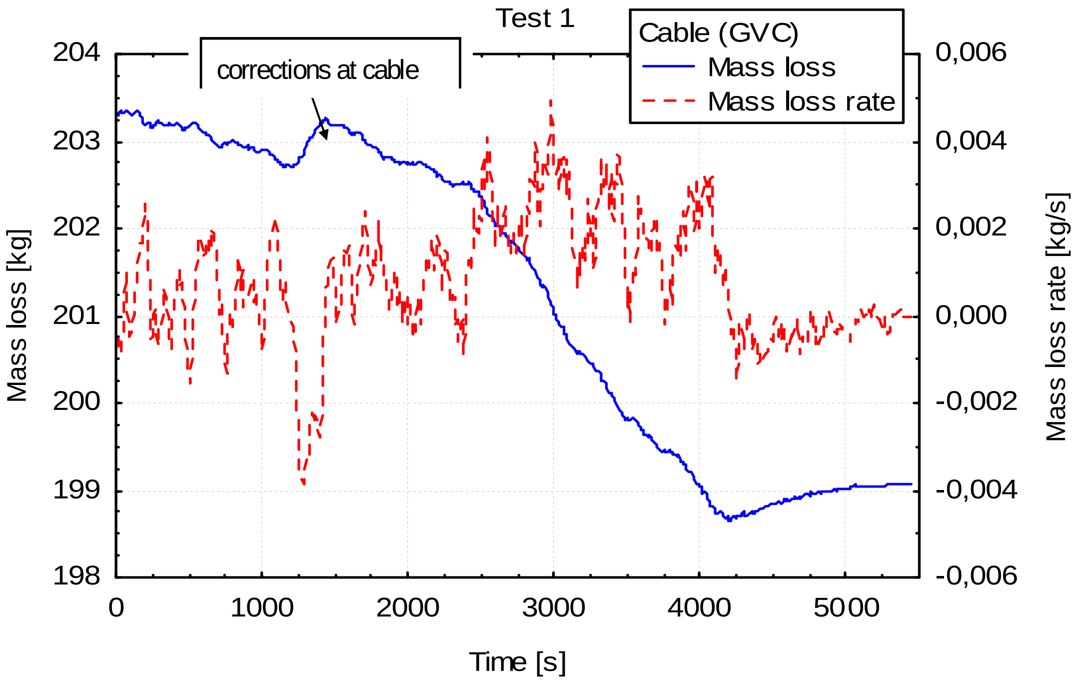


**Fig. B-3** Test 1: Mass loss and mass loss rate for FRNC cable bundles

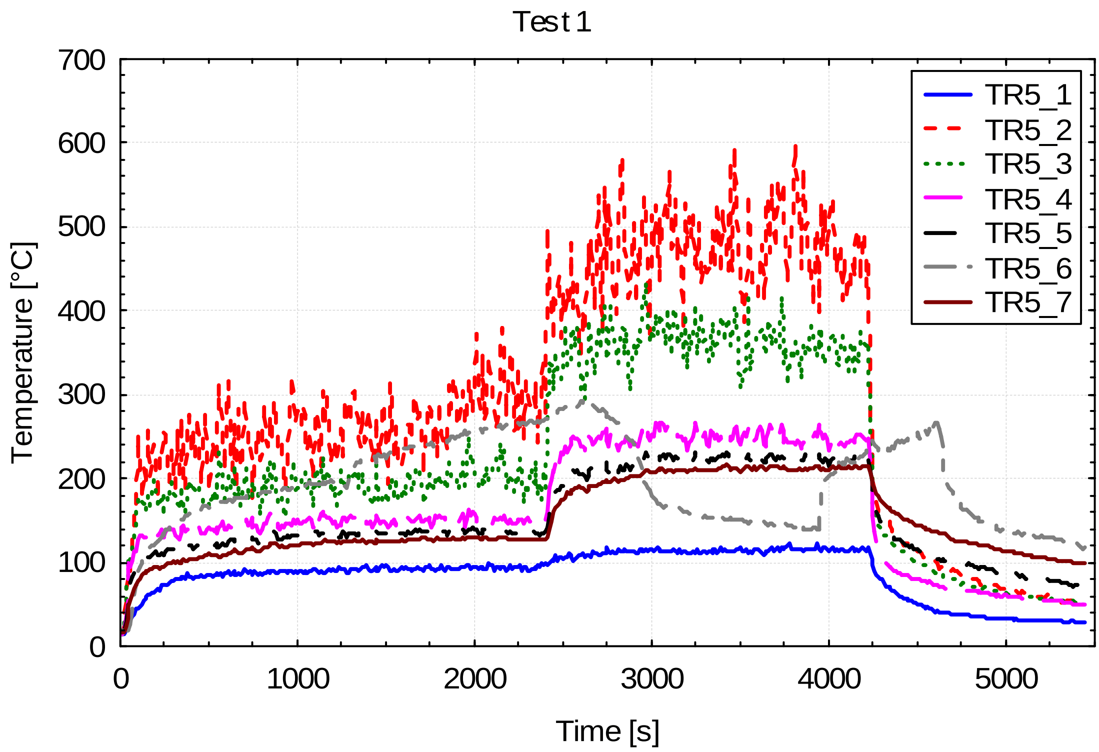


**Fig. B-4** Test 1: Gas temperatures at 40 cm from FRNC cable bundles

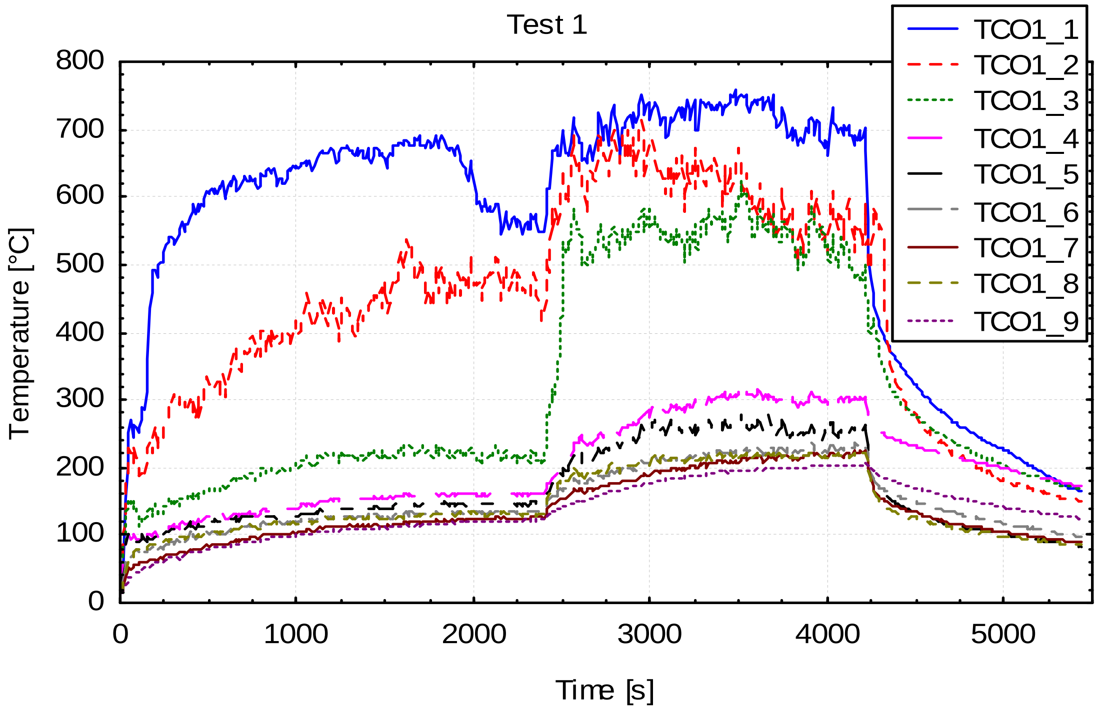


**Fig. B-5** Test 1: Surface temperatures at FRNC power cable bundle

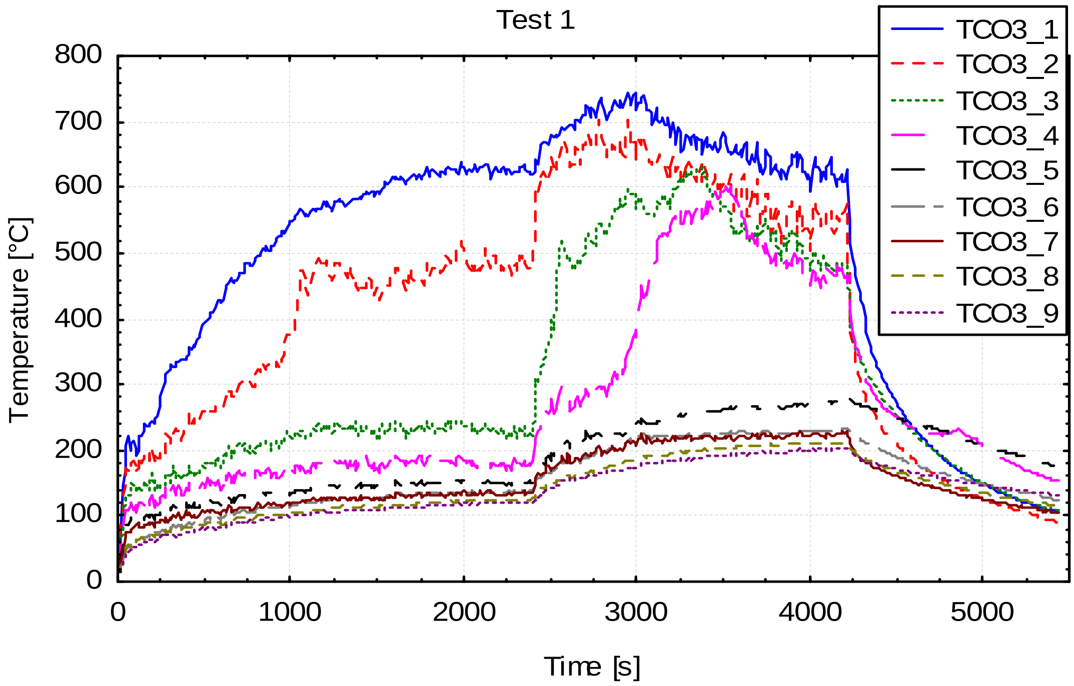


**Fig. B-6** Test 1: Surface temperatures at FRNC I&C cable bundle

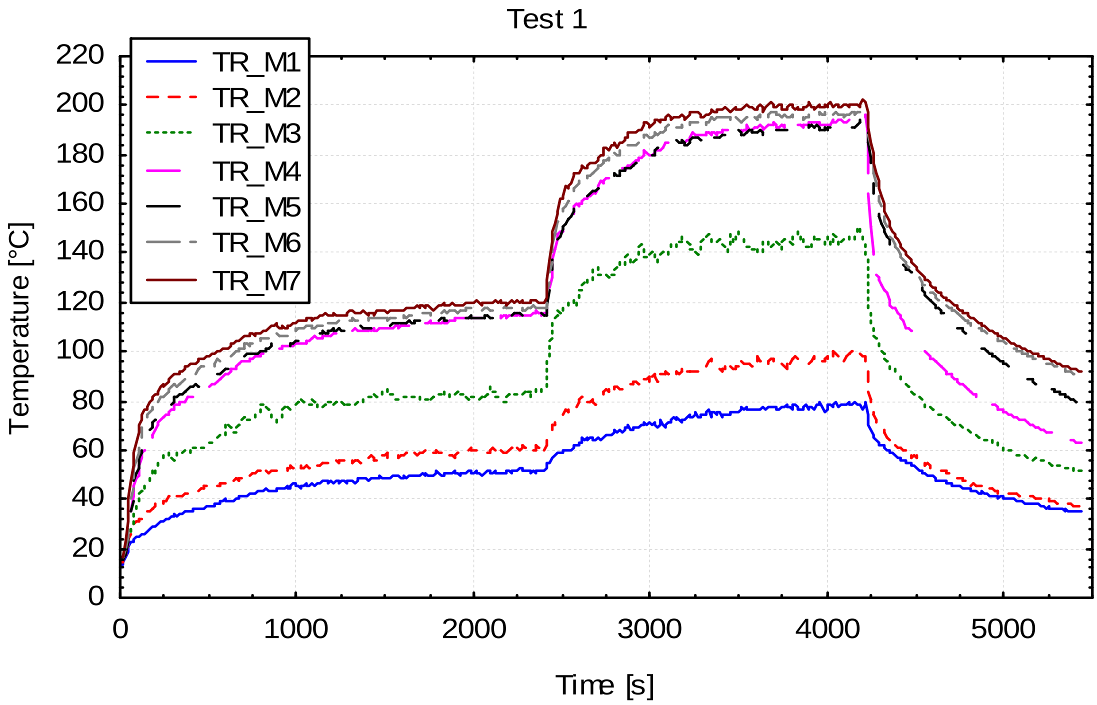


**Fig. B-7** Test 1: Average gas temperature for compartment chain 1-4

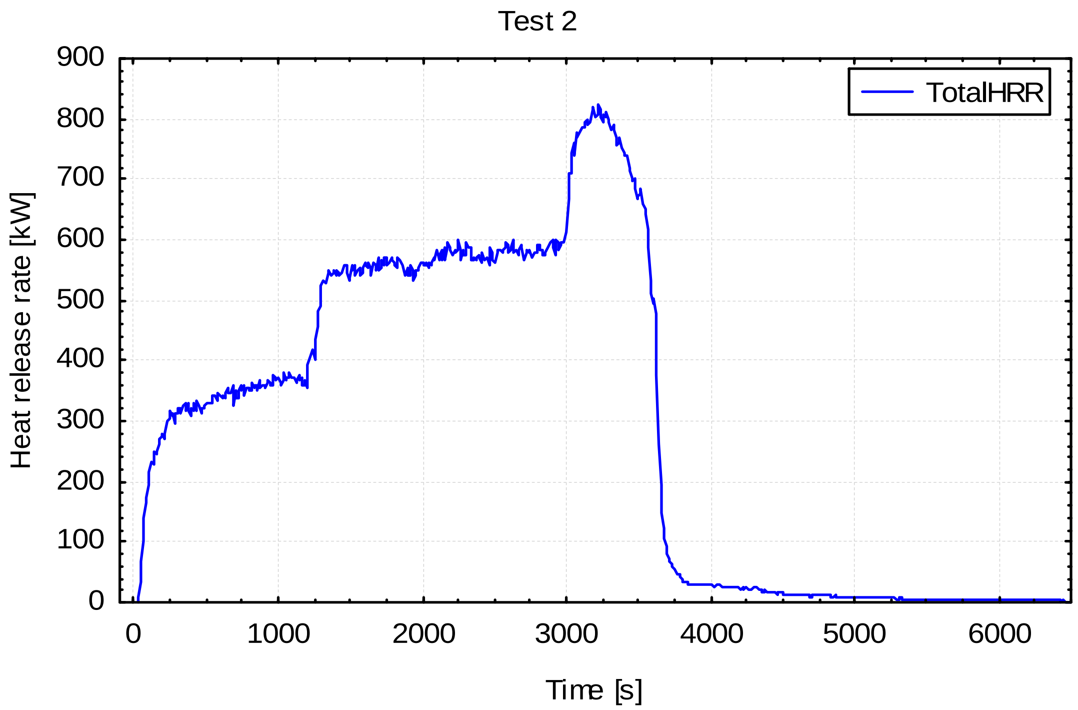


**Fig. B-8** Test 2: Total heat release rate (ISO 9705) exhaust duct

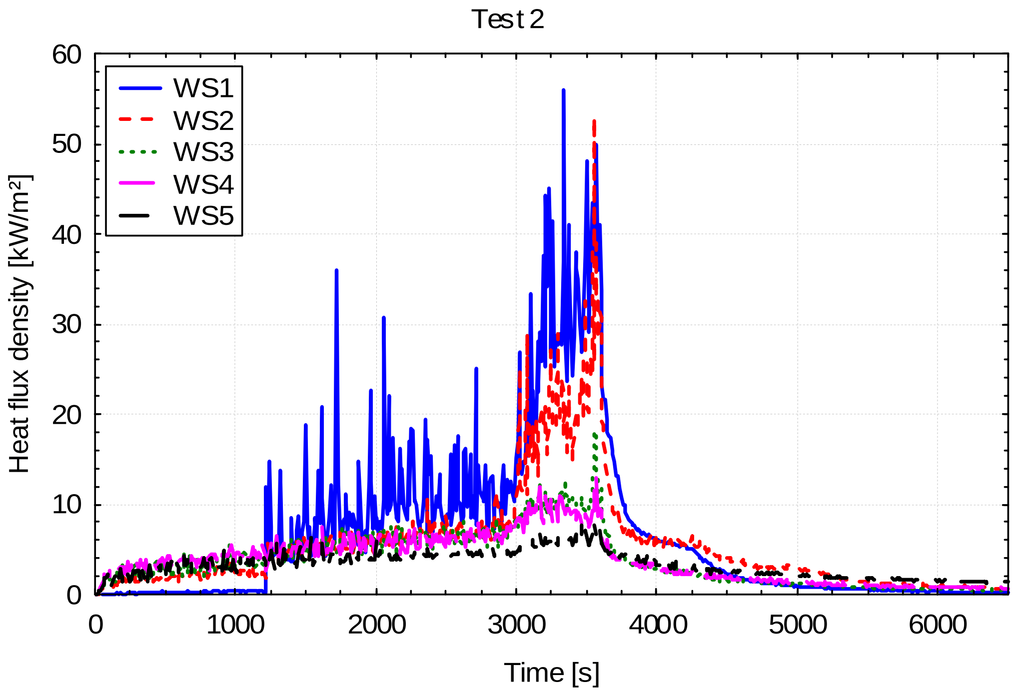


**Fig. B-9** Test 2: Heat flux density in front of the FRNC cable bundles

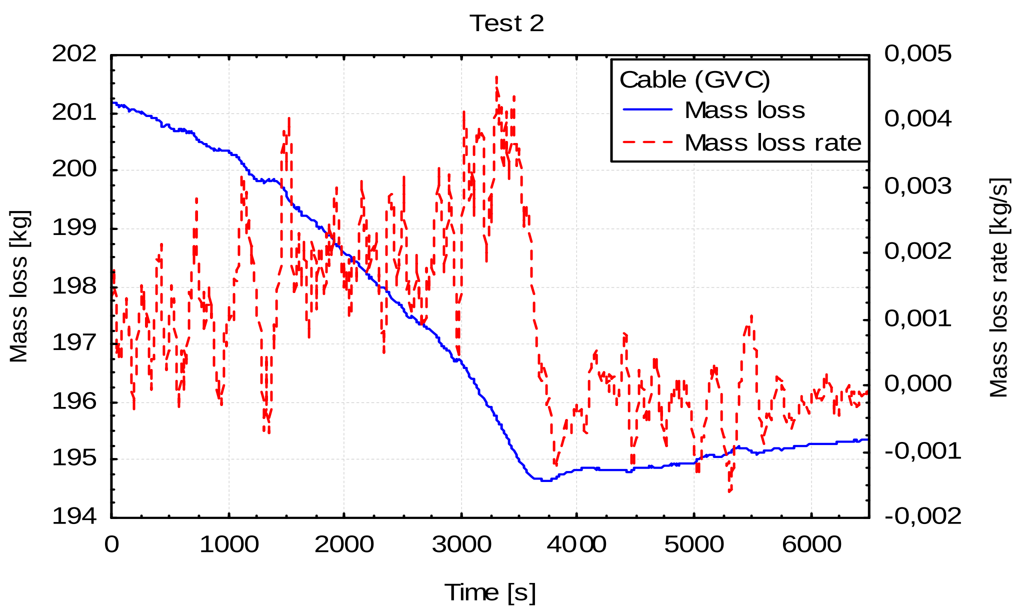


**Fig. B-10** Test 2: Mass loss and mass loss rate at FRNC cable bundles

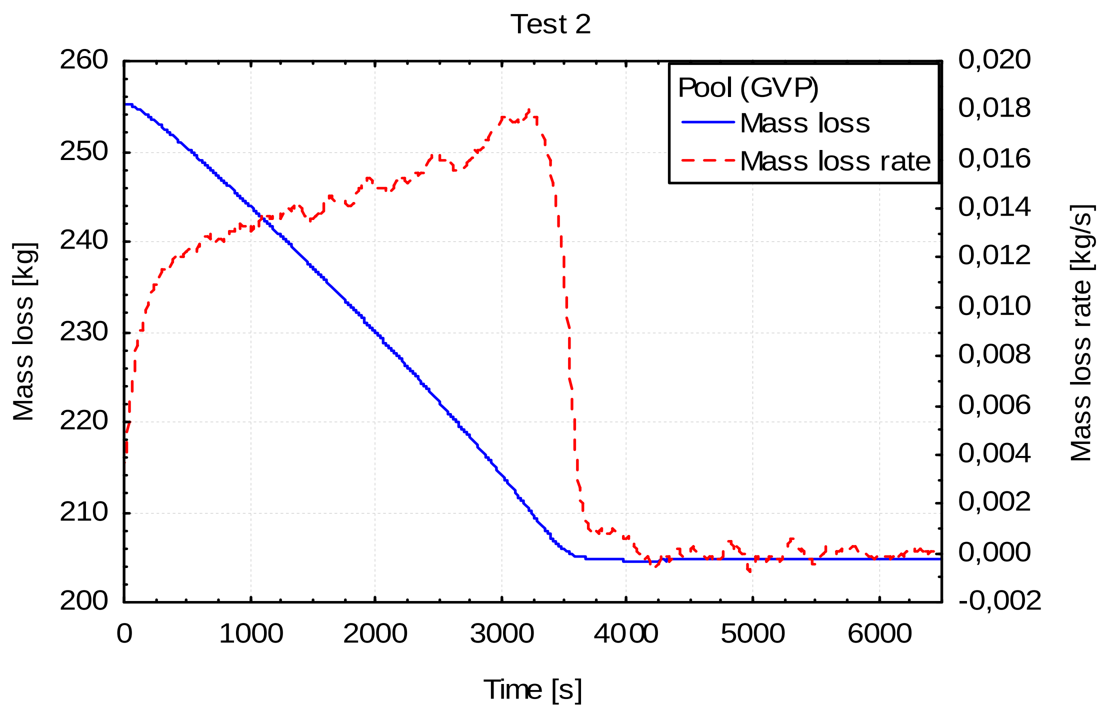


**Fig. B-11** Test 2: Mass loss and mass loss rate of ethanol fuel

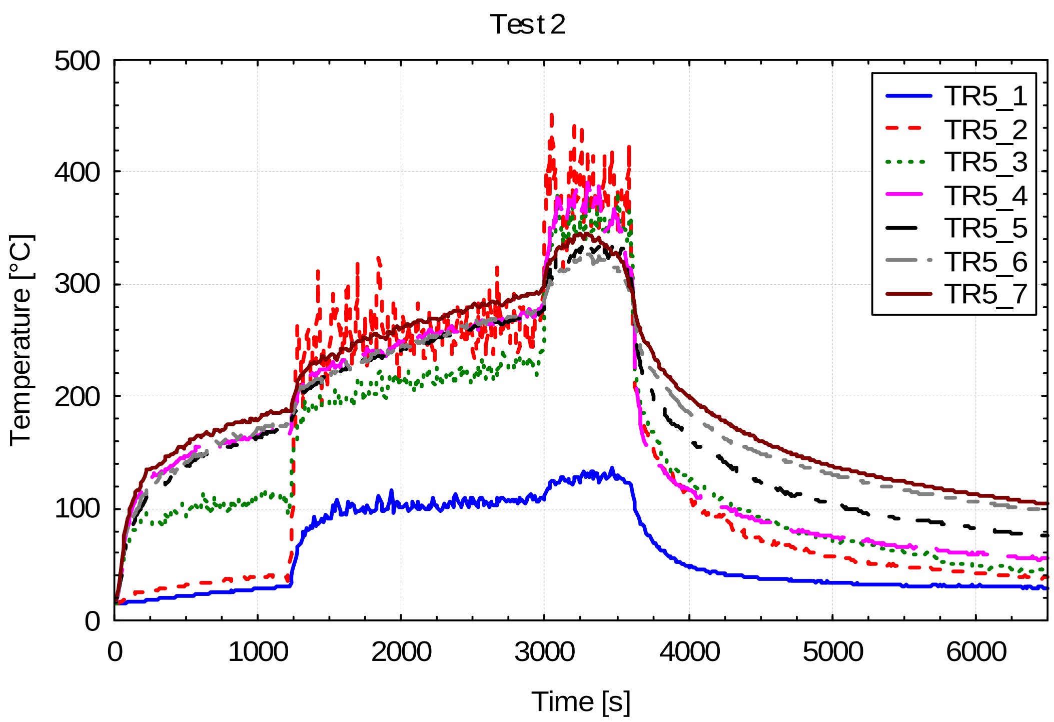


**Fig. B-12** Test 2: Gas temperatures at 40 cm from FRNC cable bundles

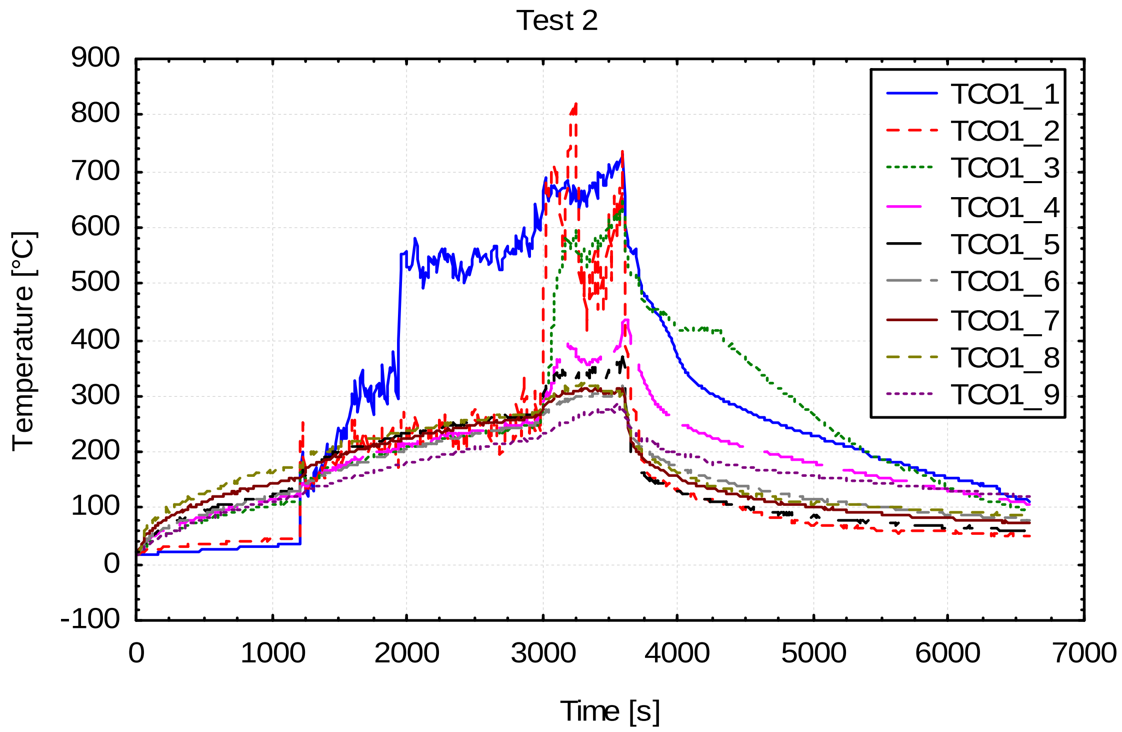


**Fig. B-13** Test 2: Surface temperatures at FRNC power cable bundle

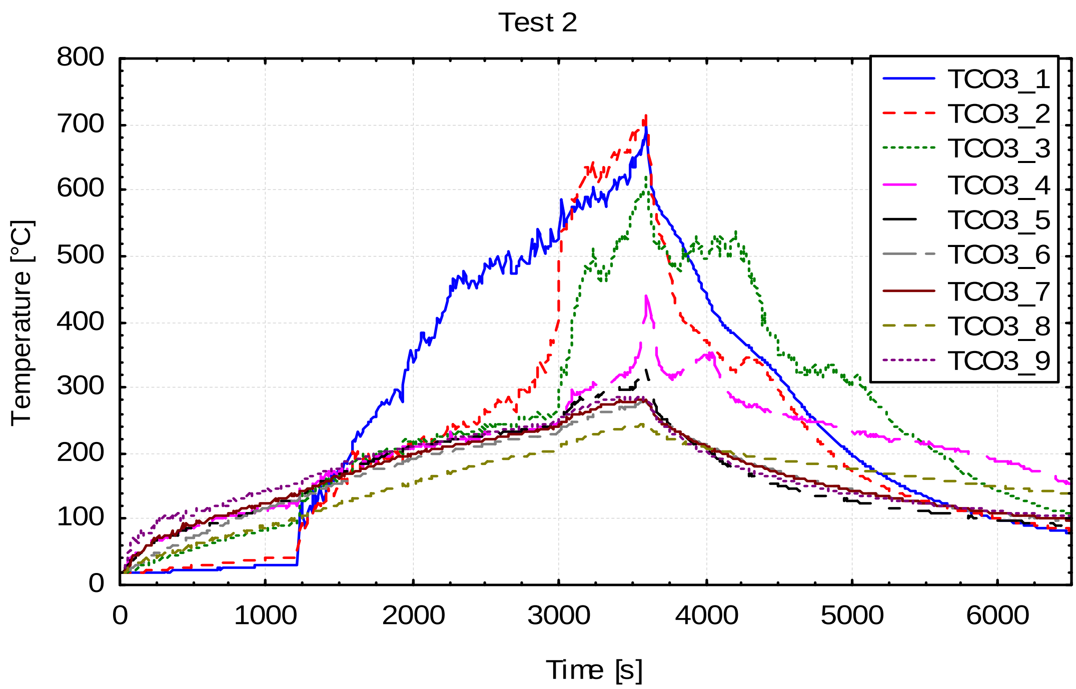


**Fig. B-14** Test 2: Surface temperatures at FRNC I&C cable bundle

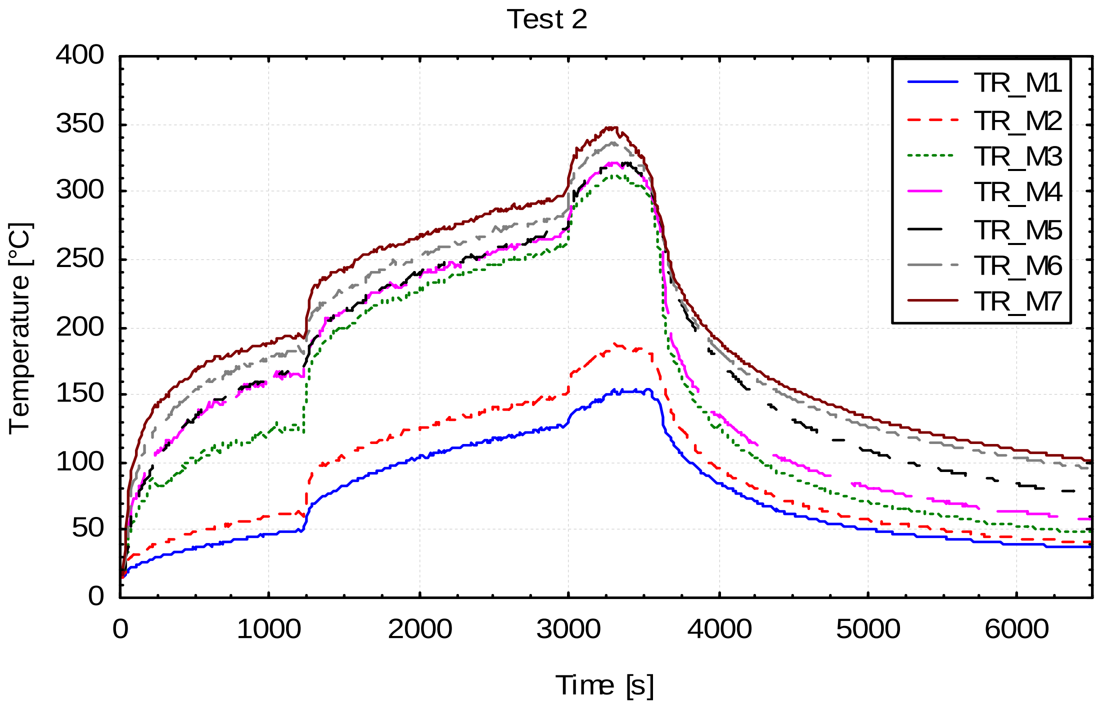


**Fig. B-15** Test 2: Average gas temperature for compartment chain 1-4

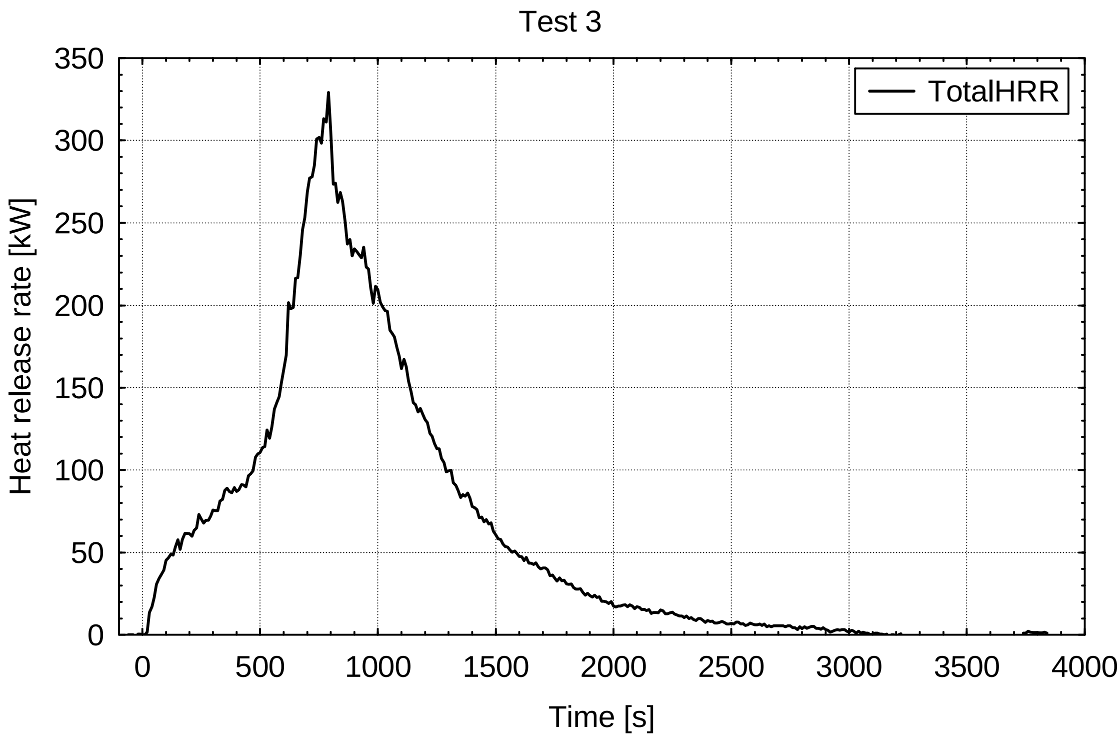


**Fig. B-16** Test 3: Total heat release rate (ISO 9705) exhaust duct

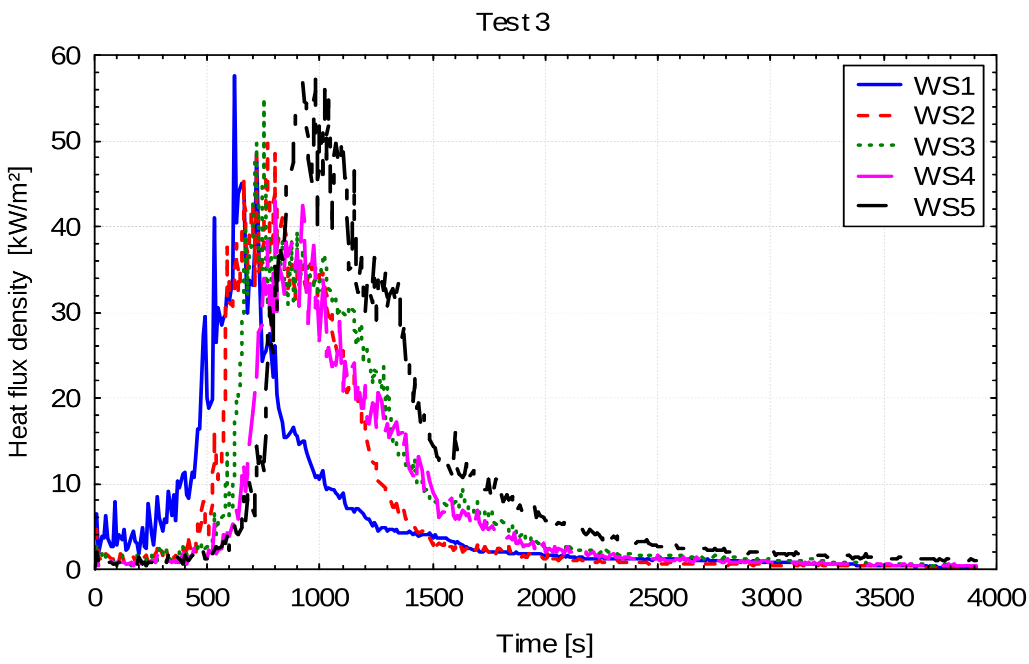


**Fig. B-17** Test 3: Heat flux density in front of the PVC cable bundles

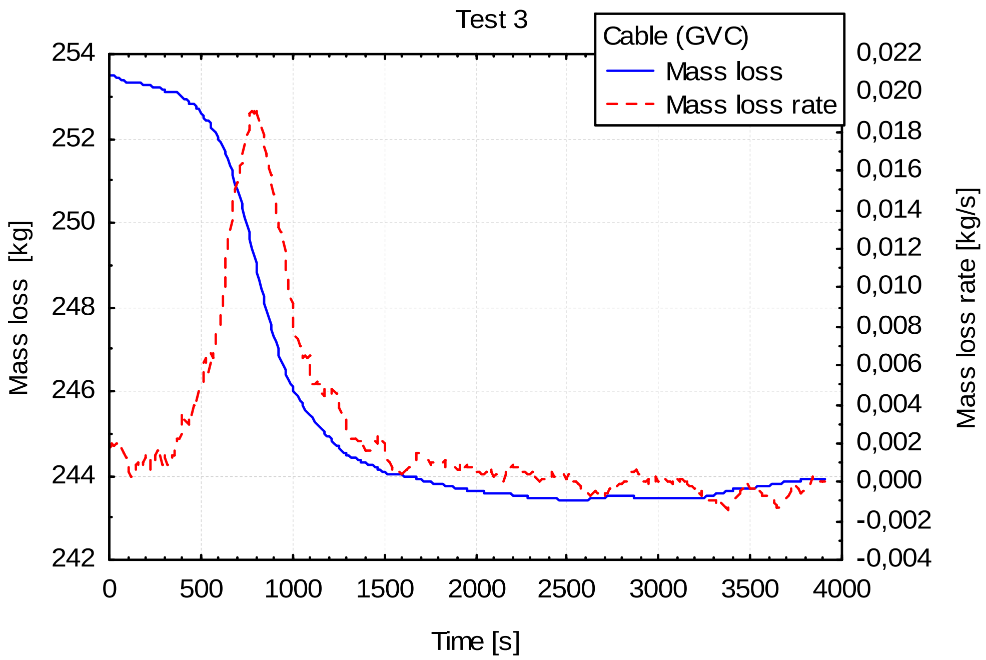


**Fig. B-18** Test 3: Mass loss and mass loss rate of PVC cable bundles

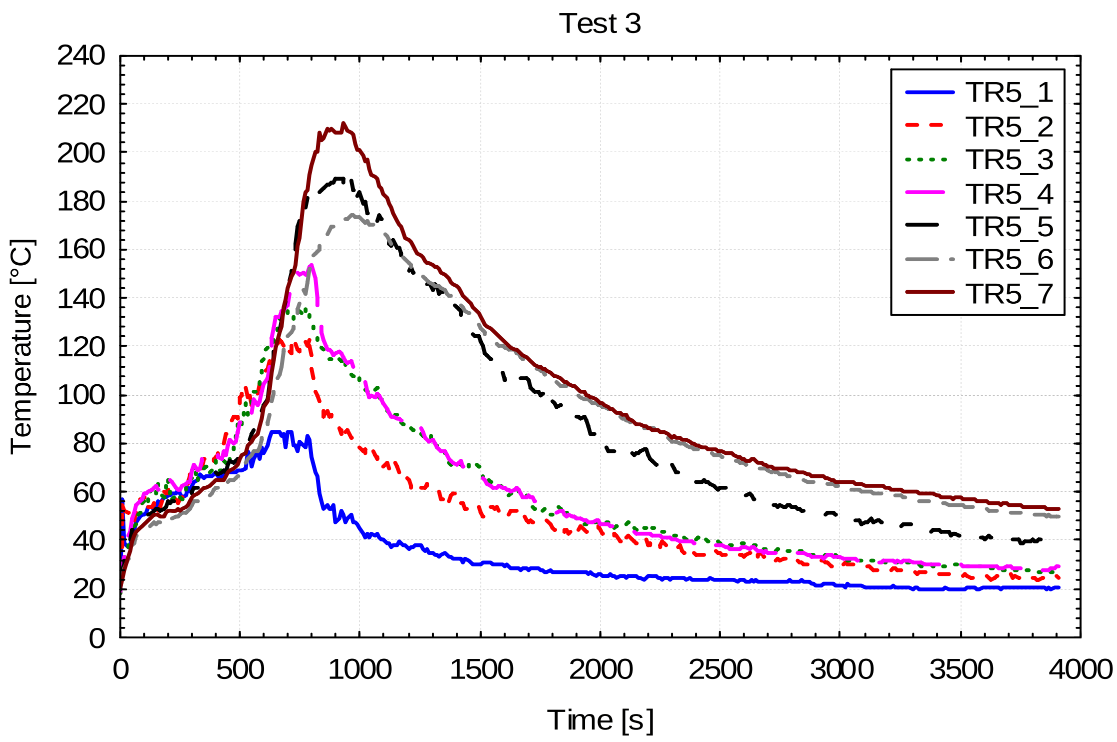


**Fig. B-19** Test 3: Gas temperatures at 40 cm from PVC cable bundles

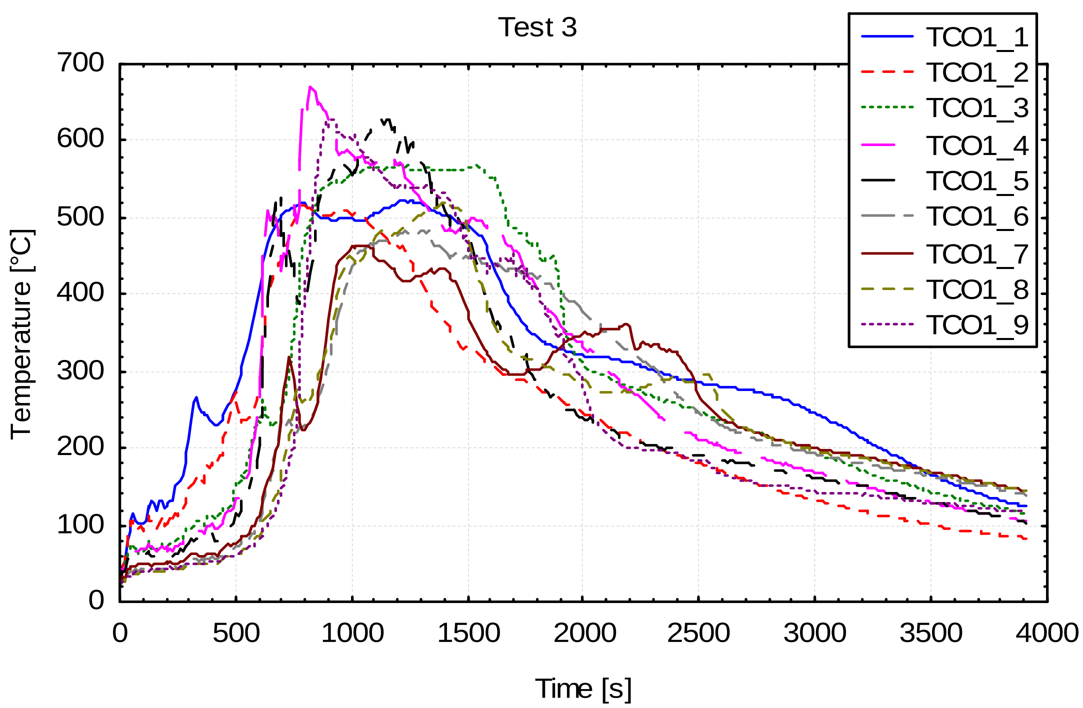


**Fig. B-20** Test 3: Surface temperatures at PVC power cable bundle

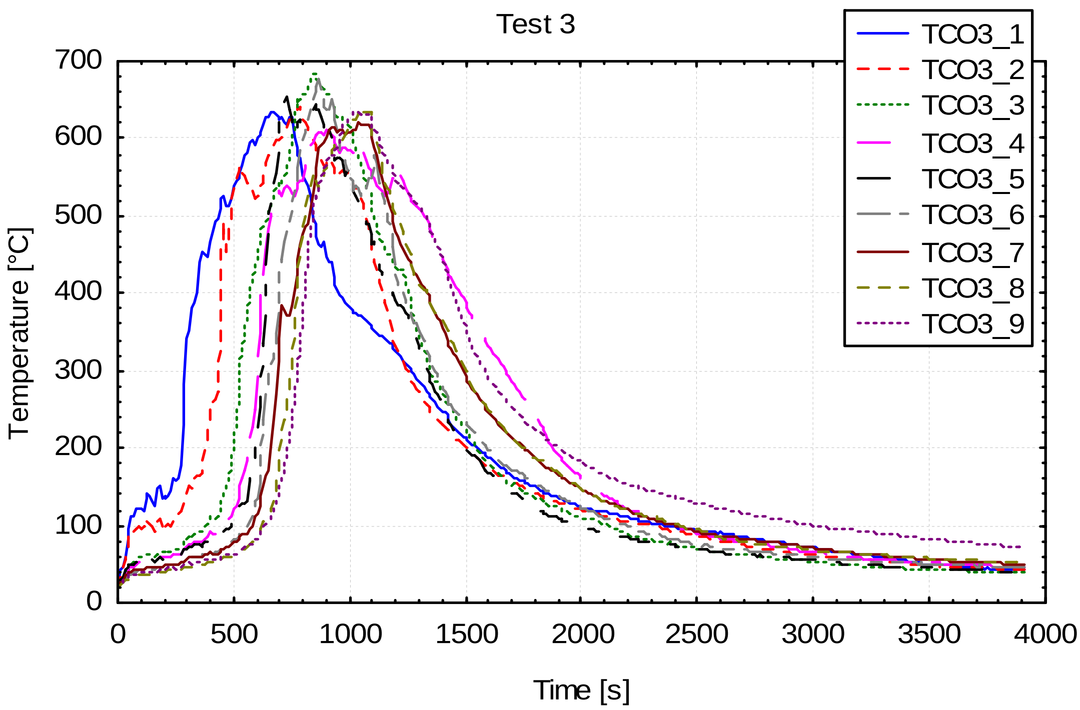


**Fig. B-21** Test 3: Surface temperatures at PVC I&C cable bundle

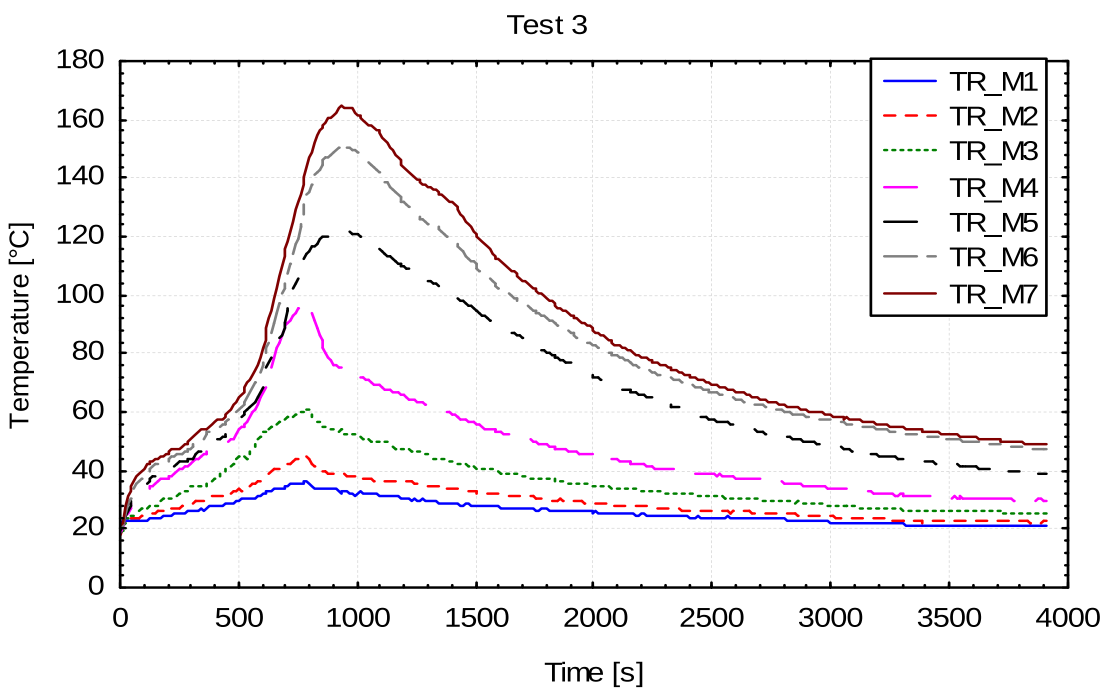


**Fig. B-22** Test 3: Average gas temperature for compartment chain 1-4

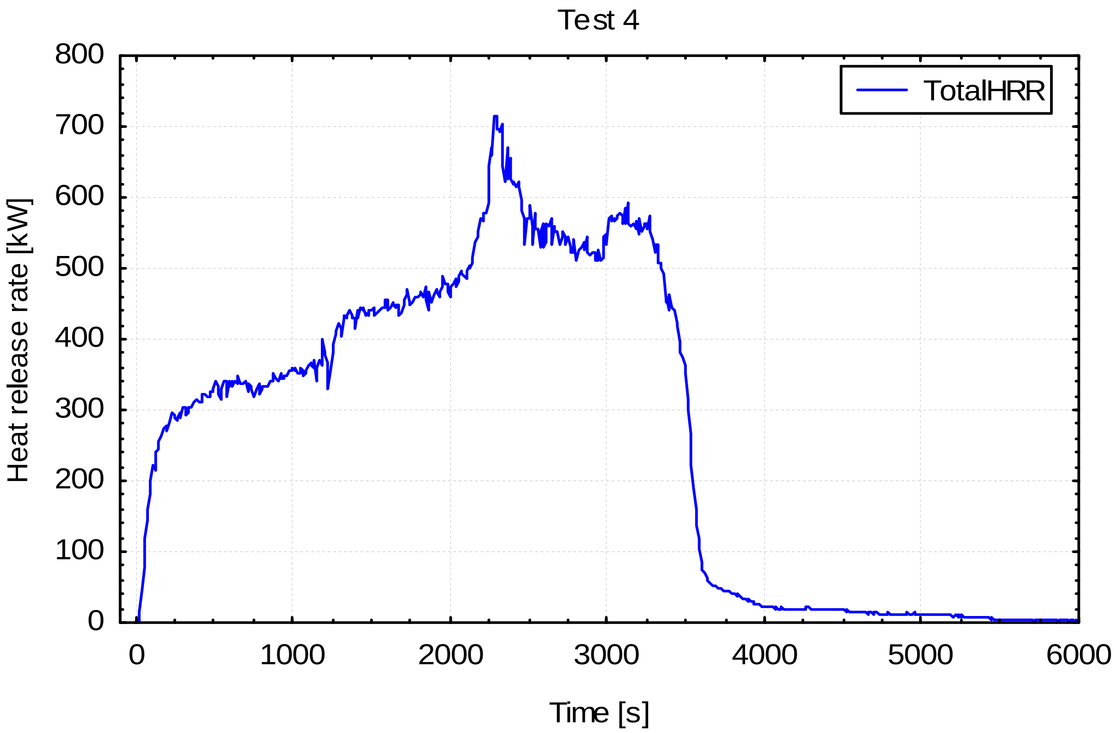


**Fig. B-23** Test 4: Total heat release rate (ISO 9705) exhaust duct

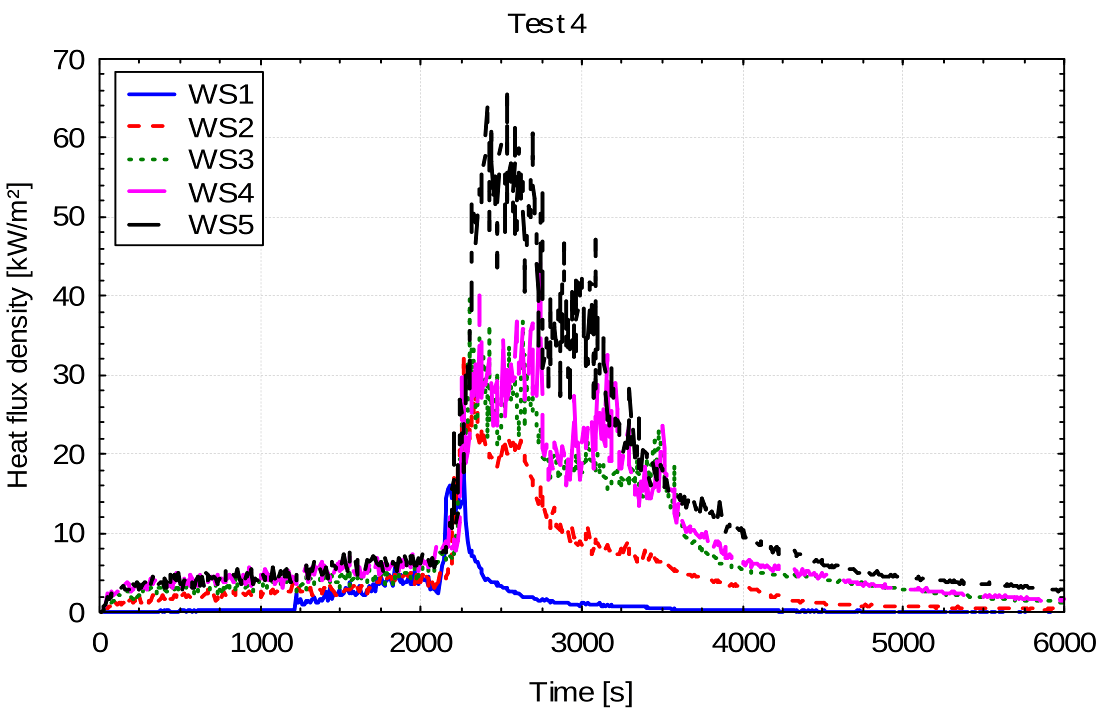


**Fig. B-24** Test4: Heat flux density in front of the PVC cable bundles

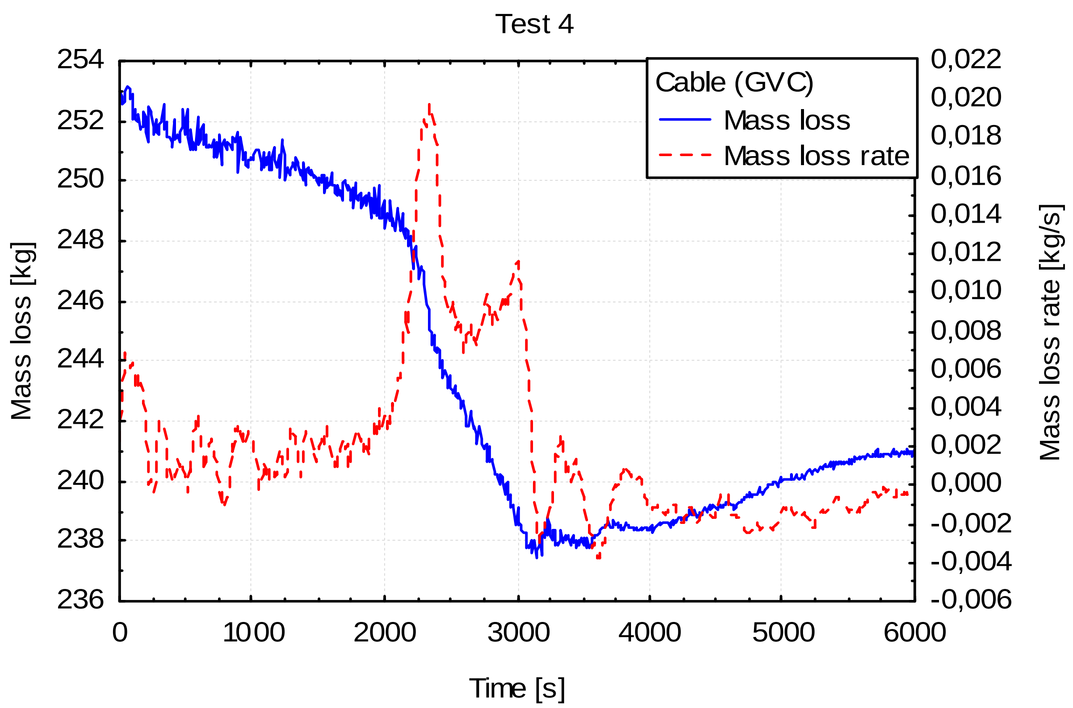


**Fig. B-25** Test 4: Mass loss and mass loss rate of PVC cable bundles

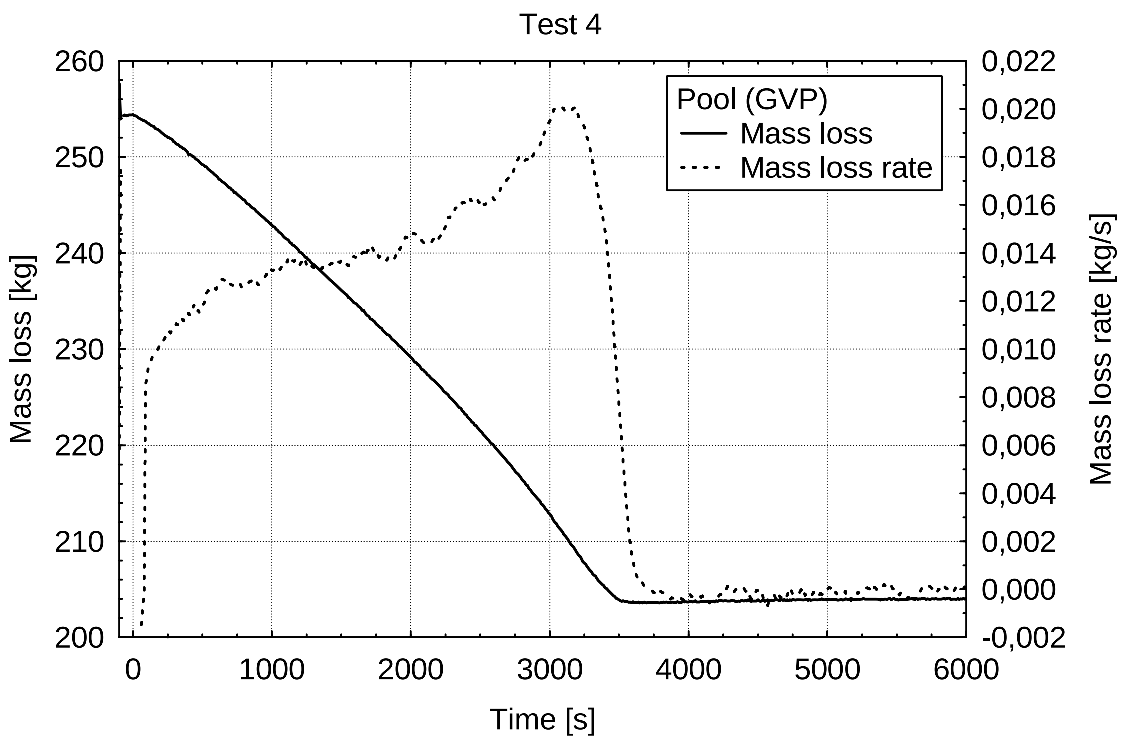


**Fig. B-26** Test 4: Mass loss and mass loss rate of ethanol fuel

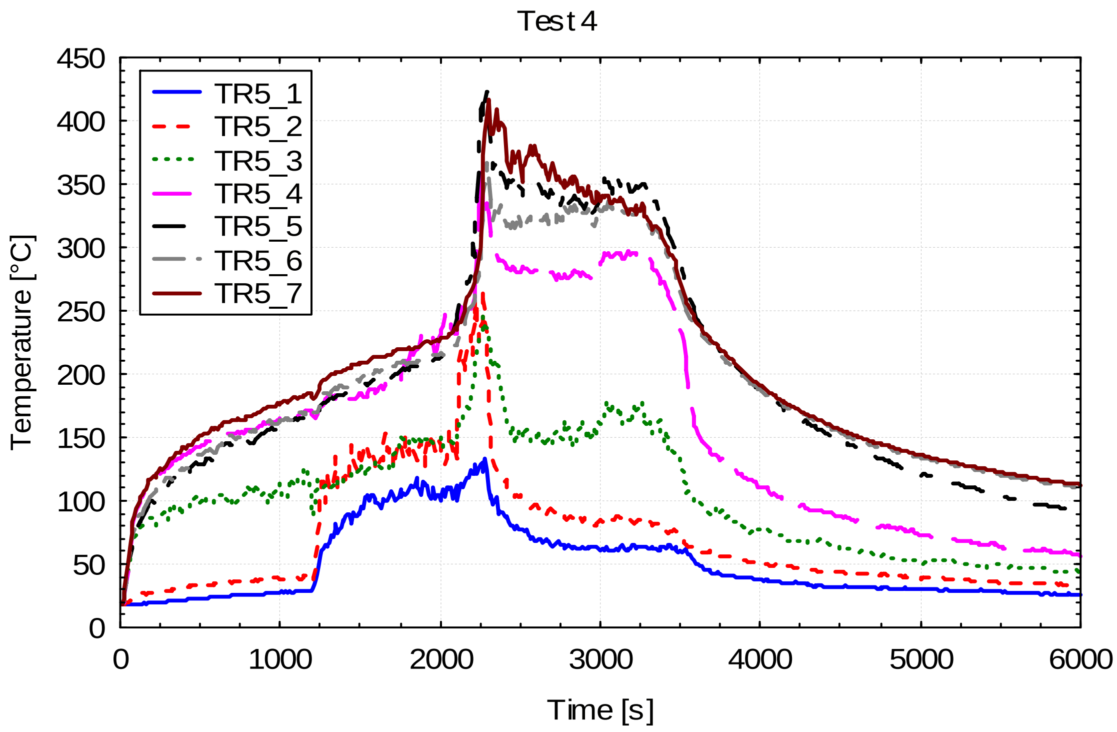


**Fig. B-27** Test 4: Gas temperatures at 40 cm from PVC cable bundles

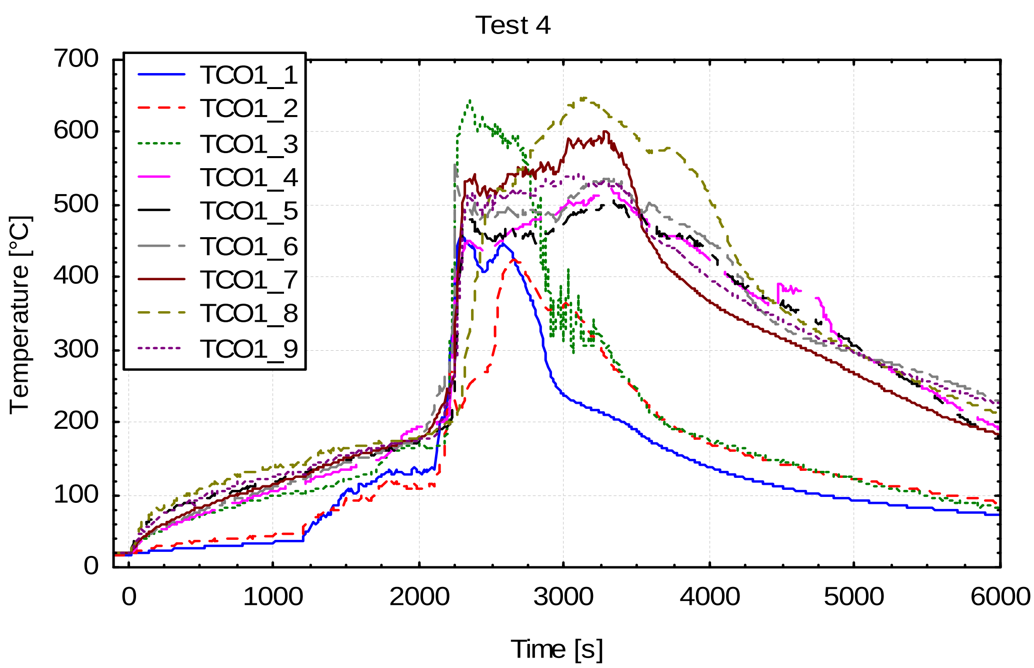


**Fig. B-28** Test 4: Surface temperatures at PVC power cable bundle

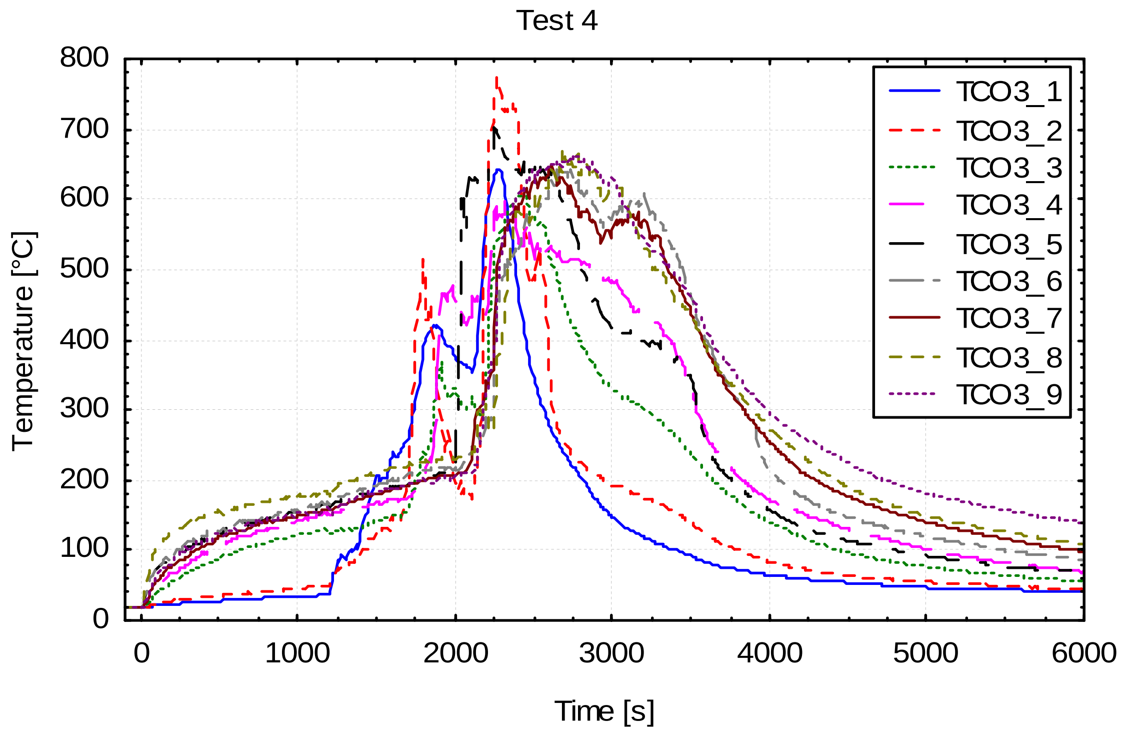


**Fig. B-29** Test 4: Surface temperatures at PVC I&C cable bundle

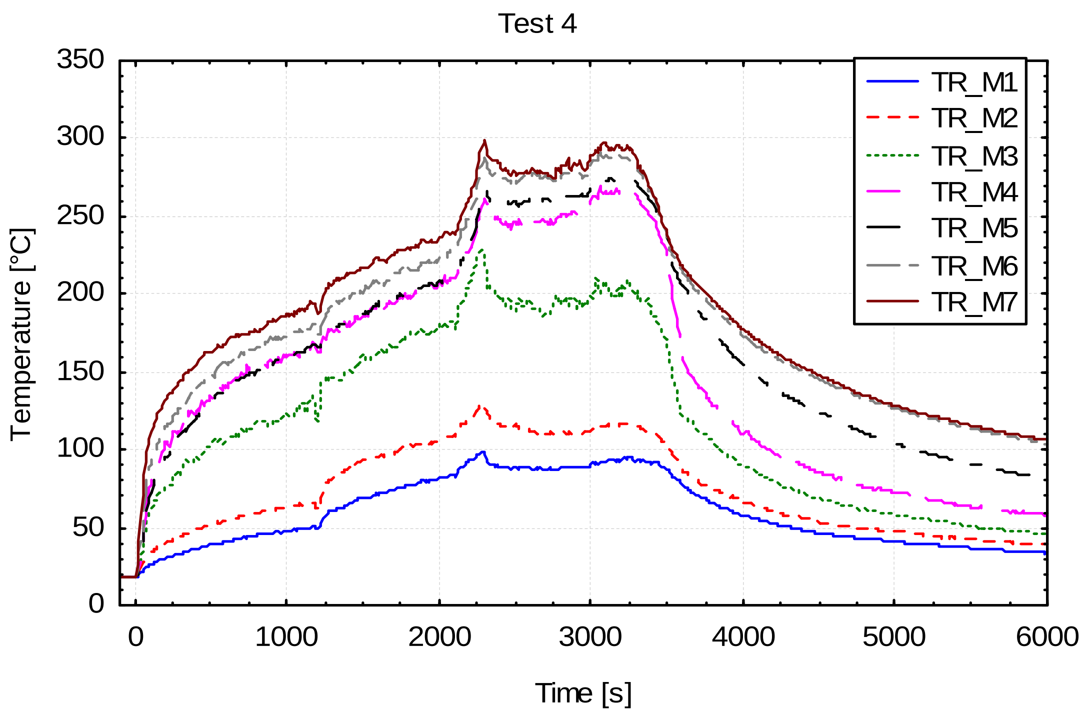


**Fig. B-30** Test 4: Average gas temperature for compartment chain 1-4

# Appendix C: CFAST and FDS Calculations for Benchmark Exercise No. 5

**Presented by**

Dr. Monideep K. Dey

U. S. Nuclear Regulatory Commission (USNRC[1]),

Office of Nuclear Regulatory Research

Mail Stop T 10 E 50, Washington, D.C. 20555, U.S.A.

---

[1] The above analyses were conducted while Dr. Dey served as a Guest Researcher in the Building Fire Research Laboratory, National Institute of Standards and Technology.

## Acknowledgments

The author wishes to acknowledge the efforts of IBMB and GRS for developing the specification of this exercise for the International Collaborative Fire Model Project. It is recognized that development of such a specification and experimental data requires considerable resources from these organizations. Specifically, the efforts of Olaf Riese and Dietmar Hosser at iBMB, and Marina Roewekamp at GRS, are greatly acknowledged and appreciated.

## C1 Introduction

The validation study of the CFAST and FDS fire computer codes presented here was conducted as part of Benchmark Exercise No. 5 of the International Collaborative Fire Model Project (ICFMP). The USNRC exercised the CFAST and FDS codes, developed by the National Institute of Standards and Technology (NIST), as part of its program to evaluate and validate these computer codes for use in NRC's regulatory framework. A complete specification of the exercise and description of the experimental results are presented and discussed in the main section of this report.

The validation study was conducted using compartment conditions and prescribed heat release rates measured during the experiments. The study was limited to the validation of the codes for predicting compartment conditions for simple pool fires. Therefore, the study was limited to Test 4 which included a pool fire used to preheat the compartment and PVC cables. Test 1 was not simulated since FRNC cables are not utilized in US NPPs. No attempt was made in this study to model cable ignition and flame spread and to use the entire extent of data available from these comprehensive and useful experiments. Validation of models available for predicting cable ignition and flame spread will be conducted in the future by the USNRC using the data set provided for this benchmark exercise.

## C2 Input Parameters and Assumptions

A comprehensive specification of Benchmark Exercise No. 5 was developed such that there would be a minimal amount of unspecified parameters and assumptions for the analysts conducting blind predictions for the exercise. However, there were still some parameters for which values had to be assumed for conducting the blind calculations. These are listed and discussed below:

1. **Heat Release Rate (HRR):**
   The HRRs of the fire measured during the experiments are used for this validation study. The measured HRR deviated from the HRR planned and stated in the specification of the exercise by ~ 20 %. Therefore, the calculations made for the specified HRR were redone with the measured values after the release of experimental data.

2. **Oxygen Content in Fuel:**
   Ethanol ($CH_3CH_2OH$) is the 1$^{st}$ fuel used in the ICFMP benchmark exercises that contained oxygen. Problems were faced in specifying the $O_2$/C ratio input for CFAST. Specifying the $O_2$/C ratio based on directions in the CFAST User's Guide resulted in an inadvertent increase of the specified HRR. An inconsistency existed between the source code and directions in the User's Guide which had to be resolved for correct implementation of the input data.

3. **Target Specification:**
   A detailed heat transfer model for a cable or cable tray will be fairly complex. Cable trays generally have a number of cables bundled together in layers, and most cables consist of several conductors. Cables configured in a single layer will get damaged and ignite at a lower flux than cables in a multilayer configuration because the flux to a single layer will not be shielded by cables above that layer. The damage or ignition temperature for cables in a multilayer configuration will depend on the volume-to-surface area ratio. The CFAST and FDS fire models are not capable of modeling complex cable configurations. The target in these models is represented as rectangular slabs, the slabs were assumed to be of the same thickness as the cables. Similar limitations of CFAST and FDS for modeling cable targets were noted in ICFMP Benchmark Exercise No. 1 /DEY 02/.

4. **Material Properties of Walls and Targets:**
   The material properties of the walls, ceiling, floor, and targets were specified for the exercise using values available in the literature for these materials. The properties

of the specific materials used in the experiments may vary from the generic values reported in the literature. This may a source of uncertainty in the predicted results.

5. **Radiative Fraction:**

   The radiative fraction of the fuel was specified based on values in the FDS database for ethanol. The radiative fraction for ethanol in the specific configuration for the benchmark exercise may vary from the value in the FDS database. The value of 0.2 for the radiative fraction in the FDS database seemed low, therefore, the value of 0.25 from a fire protection handbook /SFP 95/ was used for the calculations. This assumption may have an impact on the predicted results since this parameter determines the convective and radiative heat flow from the plume in both CFAST and FDS fire codes. This parameter was identified as a key parameter effecting fire compartment conditions in ICFMP Benchmark Exercise No. 2 /MIL 04/.

6. **Grid Size:**

   A grid size of 10 cm was used for the FDS calculations. It is recognized that CFD calculations are generally sensitive to the grid used. A grid size of 10 cm may be optimal for the type of scenarios simulated; however, this was not confirmed through a grid sensitivity analysis.

7. **Multi-Layer Boundaries:**

   The layer of insulation covering the walls was neglected in the CFAST calculation since it could not be directly modeled in CFAST. An insulated or adiabatic boundary condition was imposed on the walls for the FDS calculations.

8. **Exhaust Hood:**

   FDS calculations were conducted with and without the exhaust hood above the door of the compartment to determine its effect on the compartment conditions. It was determined that modeling the hood had very little effect on the compartment conditions. Therefore, no attempt was made to account for the exhaust hood as part of a ventilation system in the CFAST calculations.

9. **Heat Flux Comparisons:**

   The comparison of heat flux prediction with measured data poses several challenges. It is important that equivalent measures of heat flux are used in the comparison. The flux gauges in the experiments in Benchmark Exercise No. 5 were cooled and maintained at a constant temperature (20 °C). The CFAST and FDS codes normally output the net heat flux on targets based on the target temperature. It is important that these fluxes be modified to the incident radiative heat flux and the convective heat flux to a block at constant temperature for comparison with measured heat fluxes. Even with the modifications to account for the differences between measured and predicted values, an exact comparison is not possible due to the lack of ability to exactly measure the calculated values from models. Therefore, the comparison of heat fluxes will have some additional uncertainty due to this limitation.

## C3 Evaluation of Blind Model Predictions

The following provides a comparison of predictions by CFAST and FDS with results of Test 4 conducted for ICFMP Benchmark Exercise No. 5. The results of CFAST, a zone model, and FDS, a CFD code, are presented together to allow a comparison and discussion of the capabilities and limitations of the two types of models. Predictions using CFAST and FDS were made blind using the specified HRR and sent to GRS before the experimental data was released by them. GRS has certified the authenticity of these blind calculations. However, as indicated above, the measured HRR deviated from that specified for the blind exercise. Therefore, the blind calculations were redone after the release of experimental data using exactly the same input data except for the measured HRR. These open predictions are compared with the experimental data and presented below. CFAST Version 3.1.7 and FDS Version 3.1.5 were used for the computations.

The following is a list of the major sub-models implemented in the two fire computer codes for modeling the physical phenomena in the scenarios:

- combustion chemistry (tracking concentrations of oxygen and combustion products);
- plume and ceiling jet flow;
- mass and energy balance;
- ventilation through doors;
- forced ventilation;
- heat transfer to boundaries;
- heat transfer to targets
- thermal response of the target.

The FDS code computes the flows from first principles based on fluid dynamic equations, whereas CFAST utilizes correlations developed from experimental data. The performance of these sub-models is discussed below based on comparison of predicted results with experimental measurements. The theoretical formulation of the two models may be found in /JON 04/ for CFAST, and /MCG 04/ for FDS. The theoretical formulation of these codes are presented in these reports according to the format and content required by ASTM - 1355, "Evaluating the Predictive Capability of Deterministic Fire Models", /AST 04/. These reports were sponsored by the U.S. Nuclear Regulatory Commission for referencing in its validation studies as that reported herein.

### C3.1 Test 4

The following presents the comparison of predictions by the CFAST and FDS code with experimental data for Test 4 of the series. The discussion is grouped in categories presented below to evaluate the predictive capability of the models according to the general features and sub-models of the codes:

– Global parameters

– Local gas temperature

– Heat flux to targets

– Target temperature

– Wall temperature

Fig. C-1 to Fig. C-30 show the comparison of the trends of the predictions of CFAST and FDS with experimental data, and **Tab. C-1** shows the peak values predicted by the models and that measured, and the uncertainty of the predictions. The uncertainty value tabulated is:

(model prediction at peak- measured value at peak)/(measured value at peak - initial measured value)

A + sign in the uncertainty value means that the model prediction was greater than the measured value, and a - sign means that the model prediction was less than the measured value.

#### C3.1.1 Global Compartment Parameters

The HRR measured during the test and prescribed as input to the CFAST and FDS models are shown in Fig. C-1 and Fig. C-2. The HRR increases rapidly to 250 kW in ~ 265 s, and then increases more gradually to ~ 350 kW. Both CFAST and FDS follow the prescribed HRRs based on experimental data. There is no decrease in the HRR after 1200 s because the second phase of this experiment for pilot ignition of the cables was initiated at this point. As indicated above, this second phase of the experiment was not modeled for this validation study.

Fig. C-3 shows the development of the hot gas layer. The CFAST and FDS predictions, and experimental measurement all show that the HGL interface height reaches a steady level of ~ 1.5 m (just above bottom of door) in ~ 60 s. Tab. C-1 shows the steady state HGL interface height predicted by the codes and measured, and the uncertainties in the CFAST and FDS predictions. CFAST and FDS over-predict the steady state HGL interface height by + 6 % and + 11 %, respectively.

Fig. C-4 compares the door mass flows predicted by the codes and measured. An error exists in the measured flow into the compartment since it should be equal to the flow out of the compartment. FDS prediction of flow in and out of the compartment at ~ 1 kg/s is the same as measurement. CFAST over predicts the flows at ~ 1.2 kg/s by + 20 %.

Fig. C-5 shows the hot gas layer (HGL) temperature. Both CFAST and FDS predictions are similar, rapidly reaching ~ 140 °C in ~ 60 s followed by a more gradual increase to 180 °C at the end of the transient. The experimental measurement is much less than predicted by both codes indicating a possible error in the reduction of data to determine the HGL temperature. Therefore, uncertainties for this parameter are not reported. (Editorial remark: The data reduction was corrected later, see Fig. 5-2 main report.)

Fig. C-6 compares the $O_2$ depletion predicted by CFAST and FDS with experiment. The trend is similar to the HRR which determines the $O_2$ consumption. The $O_2$ level at GA2, located at 4.4 m above the floor in the HGL, predicted by CFAST and FDS at the end of the transient is 18.4 % and 18.0 %, respectively. The measured $O_2$ level at the end of the transient is 18.9 %. Since the decrease in $O_2$ level is very small and close to measurement uncertainties, the uncertainties in the predicted quantities are not reported.

Fig. C-7 compares the $CO_2$ production predicted by CFAST and FDS with experiment. The trend is similar to the HRR which determines the $CO_2$ production. The $CO_2$ level at GA2, located at 4.4 m above the floor in the HGL, predicted by CFAST and FDS at the end of the transient is 0.8 % and 1.6 %, respectively. The measured $CO_2$ level at the end of the transient is 1.3 %. The uncertainties in the CFAST and FDS predictions are - 37 % and + 20 %, respectively.

Fig. C-8 compares the door heat flows predicted by FDS and measurement. The FDS prediction of heat flow out of the compartment at ~ 166 kW is the same as measured. The CFAST code does not output this parameter.

Fig. C-9 compares the pressure predicted by CFAST and FDS in the compartment with measurement. The pressures predicted and measured at or near the floor are very similar and small, in the order of 2 - 3 Pa. The negative pressure indicates that flow will be into the compartment, as discussed later. Since the pressures are small and within the measurement uncertainties, the uncertainties of the predicted quantities are not reported.

### C3.1.2 Local Gas Temperature

The local gas temperatures in the plume, ceiling jet, and compartment are only predicted by FDS. FDS outputs showing plume and HGL development is shown in Fig. C-10 to Fig. C-14. Fig. C-10 shows an isosurface of the mixture fraction (at a value of 0.099), which represents the flame sheet created by FDS at ~ 40 s. The figure shows that the plume is mainly vertical at this time. Fig. C-11 shows an isosurface of the mixture fraction (at a value of 0.099) at 442 s. The figure shows that the plume takes a different form and is drawn to the right wall at this point. A review of the isosurface of the mixture fraction through the transient with Smokeview indicates that the plume is vertical until ~ 90 s and then oscillates with random shapes between the right wall and the partial wall (1.4 m height) on the left. The fire plume seems to be effected by the trench geometry between the two walls. Fig. C-12 and Fig. C-13 show a temperature slice at y = 1.8 m at 20 s and 340 s, again indicating a vertical plume at the beginning of the transient followed by a plume which takes random shapes and is confined by the surrounding walls. Fig. C-14 shows a temperature slice at x = 1.8 m which illustrates the flow of ambient air into the compartment through the door. The figure also shows the HGL above the bottom of the door, and illustrates the temperature gradient in the HGL. Fig. C-15 shows the flow vectors in the fire trench between the partial and right walls. The figure shows that the flow into the compartment from the door predicted by FDS causes a reverse flow in the trench pushing the fire plume toward the front wall.

Fig. C-16 shows an isosurface of the flame sheet and confirms the tilting of the fire plume toward the front wall. This reverse flow of air into the fire plume results in its tilting and possibly also the random shapes. This behavior of the fire plume cannot be confirmed due to the lack of video data of the fire.

Fig. C-17 shows the comparison of measured plume temperatures at TP2 - TP7 with that predicted by FDS. As shown in Fig. C-17, FDS predicts peaks in the plume temperature at ~ 120 s. These peaks are explained by the plume development predicted by FDS. As discussed above, observations of the plume predicted by FDS through Smokeview (the graphical interface for FDS) indicates a steady vertical plume until ~ 90 s when the plume begins to oscillate with random shapes between the left partial wall and right wall. This results in the FDS predictions of peaks in the plume temperature, specifically at the lower level at TP2 and TP3. The experimental measurements at TP2 and TP3 show an oscillation in the temperature which indicates movement of the plume. Measurements indicate that TP4 - TP7 are sensing the HGL temperature and that the plume does not extend to the higher levels. The plume temperature measurement by itself cannot confirm the plume is behaving in the manner predicted by FDS. The measured data shows the plume to be fully developed at ~ 60 s after which the plume temperatures at TP2 increase to ~ 450 °C without any intermediate peaks. FDS predicts the plume temperatures to reach ~ 180 °C at the end of the transients indicating the temperature in the plume region at this time is the same as in the HGL. This again confirms the behavior of the plume predicted by FDS which results in the centerline of the plume above the fire to be at the temperature of the HGL. As shown in Tab. C-1, the uncertainty in the predicted values are - 46 %, - 10 %, and + 1 % for TP3, TP5, and TP7, respectively.

Fig. C-18 shows the local gas temperatures in the compartment at TR1. TR 1-3 is near the HGL interface and reads a lower temperature than TR 1-5 and TR 1-7. FDS predicts a higher temperature than measured at TR 1-3 and TR 1-5, and similar temperatures for TR 1-7. FDS predicts a very small temperature gradient between TR 1-5 and TR 1-7, whereas measurements indicate a steeper temperature gradient.

Fig. C-19 shows the local gas temperature in the compartment at TR 2. FDS predictions are similar to measurements at this location. **Fig. C-20** shows the local gas temperatures at TR 3 which is located near the back wall. The predicted values are similar to measurements. Oscillations in the temperature at this point are noted, especially at the lower levels for TR 3-3 and TR 3-5. These oscillations are possibly caused by the reversed flow in the trench as discussed above. Fig. C-21 shows the local gas temperatures at TR 4 which is also located near the back wall. Oscillations in the gas temperature at this point are also noted, especially at the lower level at TR 4-3. Finally, Fig. C-22 shows the local gas temperatures at TR 5 near the cables. Again, FDS predictions are similar to measurements with uncertainties of + 8 %, + 4 %, and + 5 % at TR 5-3, TR 5-5, and TR 5-7, respectively.

#### C3.1.3 Heat Flux to Cable Targets

Fig. C-23 shows a comparison of the total heat flux on the cables predicted by CFAST and experiment. The heat flux on the gauges WS2 and WS3 on the left wall are mainly due to the flux from the HGL since the 1.4 m wall shields the gauges from most of the radiative heat flux from the fire. The experimental measurement of heat flux at WS 1 is very small since it is not in the HGL, and the 1.4 m partial wall shields the radiative heat flux from the fire. The CFAST prediction at WS1 is not included since CFAST does not have the capability to include partial walls in the compartment geometry. The measured fluxes at WS2, WS3, and WS4 are increasingly higher due to the temperature gradient in the HGL. The heat fluxes predicted by CFAST for WS2, WS3, and WS4 are of similar magnitude since only the average HGL temperature is predicted in a zone model, and temperature gradients in the hot gas are not simulated in such a model. The large oscillations in the measured heat flux, especially at WS3 and WS4, may be due to the position of the flux gauges in between the vertical cable trays and disturbance of the flow field by the cable trays in those positions.

Fig. C-24 shows a comparison of the total heat flux on the cables predicted by FDS and experiment. Although the FDS prediction at WS2 is lower than at the other gauges, the predicted heat flux levels at WS3, WS4, and WS5 are similar in magnitude. FDS does not predict the variation and gradient in the heat flux versus elevation, as measured. The uncertainties of the peak predicted heat fluxes for WS2, WS3, and WS4 for CFAST are + 49 %, 0 %, and - 15 %, respectively; and for FDS are - 49 %, - 42 %, and - 45 %, respectively.

#### C3.1.4 Cable Temperature

Fig. C-25 shows a comparison of the surface temperature of the power cable predicted by CFAST and FDS with experiment. The measured cable surface temperature at different elevations shows a gradient similar to that observed for the heat flux. However, the measured temperature at TCO 1-5 is greater than at TCO 1-7, contrary to expectation. The predictions by CFAST at the different elevations are similar in magnitude, as discussed above. The predictions by FDS show variations in the temperature at TCO 1-1 and TCO 1-3, but the temperatures at the other elevations are of similar magnitude. The uncertainties of the peak predicted surface temperatures for the power cable at TCO 1-3, TCO 1-5, and TCO 1-7 for CFAST are + 2 %, - 23 %, and - 21 %, respectively; and for FDS are - 41 %, - 32 %, and - 26 %, respectively.

Fig. C-26 shows a comparison of the I&C cable surface temperature predicted by CFAST and FDS to the experiment. The measured cable surface temperature at different elevations shows a gradient similar to that observed for the heat flux. However, the measured temperature at TCO 3-5 is greater than at TCO 3-7, contrary to expectation. The predictions by CFAST at the different elevations are similar in magnitude, as discussed above. The predictions by FDS show variations in the temperature at TCO 3-1 and TCO 3-3, but the temperatures at the other elevations are of similar magnitude. The uncertainties of the peak predicted surface temperatures for the I&C cable at TCO 3-3, TCO 3-5, and TCO 3-7 for CFAST are - 16 %, - 35 %, and - 33 %, respectively; and for FDS they are - 55 %, - 48 %, and - 44 %, respectively.

### C3.1.5 Wall Temperature

Fig. C-27 shows a comparison of left wall temperatures at TW-2 predicted by CFAST with experiment. The measured wall surface temperature at different elevations shows a gradient similar to that observed for the heat flux. However, the measured temperature at TW 2-4 is greater than at TW 2-5, contrary to expectation. Although the predicted and measured values are similar in magnitude at TW 2-4 and TW 2-5, the prediction at TW 2-2 is much larger than the measurement. This is due to the lack of capability in CFAST to model the partial 1.4-m wall. CFAST is predicting a higher than actual radiative flux from the fire at TW 2-2 due to this limitation. The uncertainties of the peak wall surface temperatures at TW 2-2, TW 2-4, and TW 2-5 are + 250 % (see reason above), - 12 %, and 0 %, respectively.

Fig. C-28 shows a comparison of left wall temperatures at TW-2 predicted by FDS with experiment. The FDS predictions are similar in magnitude to measured values. The uncertainties of the peak wall surface temperatures at TW 2-2, TW 2-4, and TW 2-5 are - 42 %, - 30 %, and 11 %, respectively.

Fig. C-29 shows a comparison of the rear wall temperatures at TW-1 predicted by FDS with experiment. FDS predictions are ~ 20 % less than the measured values.

Finally, Fig. C-30 shows FDS predictions of the back wall temperature compared with experimental observations. Since an adiabatic assumption (see above) was adopted for the walls in FDS to compensate for the lack of ability to model multi-layer boundaries, the temperature predicted at the back wall is constant. The measured back wall temperatures at TW 2 and TW 1 essentially remain at a constant temperature, decreasing slightly only due to temperature fluctuations in the compartment. This confirms the validity of the adiabatic assumption adopted in the FDS calculation.

### C3.1.6 Conclusion

CFAST and FDS predictions were similar to experimental observations for most parameters. Global parameters such as the door mass and heat flows, interface height, and O2 concentration were within 20 % of experimental values. Except for TP3, the local gas temperatures in the compartment and in the plume predicted by FDS were generally within 10 % of experimental observations. The effect of flows in the trench impacted the characteristics of plume development and temperature predicted by FDS. The heat flux to the cables predicted by CFAST and FDS deviated by as much as + 49 % and - 49 % from experimental observation, respectively. The corresponding cable surface temperatures predicted by CFAST and FDS deviated by as much as 35 % and 55 % from experimental observation, respectively.

## C4 General Recommendations and Conclusions

The following provides conclusions and general recommendations as a result of this validation study.

### C4.1 Capabilities and Limitations

The fire scenarios in Benchmark Exercise No. 5 are considered to be of average severity that analysts would model for NPP applications.

This validation study shows that the major sub-models implemented in both fire computer codes for modeling the physical phenomena in the scenario predicted reasonable trends and magnitudes of output parameters of interest. The predictions of the sub-models for combustion chemistry (tracking concentrations of oxygen and combustion products such as $CO_2$) were reasonable. The plume flows predicted resulted in reasonable accuracy of global compartment parameters, and the mass and energy balance in and out of the compartment. Specifically, the sub-models in the codes for ventilation and heat flow through doors predicted accurate results.

The study shows the importance of modeling the plume development in CFD codes to adequately capture the entire fire phenomenon, and to evaluate target heat up and ignition near the plume. FDS predicted that the flows that develop in the fire trench effects plume development and tilting. This phenomenon and effect could not be confirmed due to lack of video data. It is an important phenomenon for evaluating fire effects in such geometries.

The validation results show that the computation of heat fluxes and cable temperatures is more challenging than the prediction of global parameters for both codes, and larger deviations from experimental values are noted.

### C4.2 User Interface

**FDS**

The FDS manuals (Technical Reference Guide and User’s Guide), in conjunction with the Smokeview graphical interface for reviewing results of the computations, provide a comprehensive, understandable, and clear interface for the user. The quality of this interface has positively impacted the capability to analyze and interpret the predicted results.

**CFAST**

Although the Technical Reference Guide for CFAST is detailed, its relationship to the User's Guide, and a useful and comprehensive User's Guide is lacking. Additionally, the graphical user interface (GUI) for CFAST is outdated and does not function in more recent operating platforms such as Windows 2000. It would be beneficial to have a comprehensive User's Guide and enhanced GUI to allow more accurate input of data for the simulations and understanding of output parameters such as their units.

The users of these codes should be knowledgeable of the complexities of the compartment conditions, such as plume development in specific geometries, to assess and utilize the results of their calculations. Editor's note: The CFAST GUI has been subsequently been upgraded /JON 05/.

### C4.3 Benefits of Hand Calculations

In order to evaluate the benefits of hand calculations, blind calculations with FDTs /USN 04/ were conducted. The comparisons (see **Tab. C-2**) show that hand calculations could provide a method to quickly calculate global parameters (such as interface height), as well as plume temperatures using simple correlations. Some large deviations for plume temperature are noted. The plume correlation is for fires in an open environment and does not include the effects of the surrounding walls. Since the ranges of validity of the correlations are narrow, the results are best suited for a screening calculation where a rough estimate is needed, while acknowledging the answers may contain inaccuracies.

### C4.4 Need for Model Improvements

Although relatively good performance is noted above for most parameters, the calculation of heat flux to targets and walls is a potential area for improvement for both CFAST and FDS to improve the accuracy of the predictions. Also, optimal values for the input for the number-of-radiation-angles parameter used in the FDS heat flux calculations could be assessed for different applications. The simulation of plume development and tilting due to varying flow conditions in the compartment could be evaluated to determine any potential modifications to improve accuracy.

### C4.5 Need for Advanced Models

Simple hand calculations and zone models may be suitable for simple scenarios as in this validation study. However, this study has showed that even for such simple and non-severe fires, the evaluation of target heat up and ignition near the plume region may require the use of CFD codes.

The computational requirements for CFD codes should be noted. The test in this benchmark exercise required 10 hours to compute with FDS, whereas, zone models can be executed in less than 10 s.

### C4.6 Need for Additional Test Programs

As discussed above, FDS predicted that the flows that develop in the fire trench effects plume development and tilting. It would be beneficial to confirm this phenomenon and effect with additional tests, potentially as part of a general study to examine fire plume development in various geometries for NPP scenarios.

## C5 References


/AST 04/ American Society of Testing and Materials (ASTM):
Evaluating the Predictive Capability of Deterministic Fire Models, ASTM E1355-04, West Conshohocken, PA , 2004

/DEY 02/ Dey, M ., Ed.:
Evaluation of Fire Models for Nuclear Power Plant Applications, U.S. Nuclear
Regulatory Commission, NUREG-1758, Washington DC, USA, June 2002

/JON 04/ Jones, W., Ed.:
CFAST - Consolidated Model of Fire Growth and Smoke Transport (Version 5),
National Institute of Standards and Technology, NIST Special Publication 1030,
October 2004

/JON 05/ Jones, W., Ed.:
CFAST - Consolidated Model of Fire Growth and Smoke Transport (Version 6) – User's Guide, National Institute of Standards and Technology, NIST Special Publication 1041, December 2005

/MCG 04/ McGrattan, K., Ed.:
Fire Dynamics Simulator (Version 4), Technical Reference Guide," National Institute of Standards and Technology, NIST Special Publication 1018, September 2004

/MIL 04/ Miles, S. Ed.:
Evaluation of Fire Models for Nuclear Power Plant Applications: Pool Fires In Large Halls, Building Research Establishment, BRE Report No. 212214, May 2004,
Watford, UK.

/SFP 95/ Society of Fire Protection Engineers (SFPE):
The SFPE Handbook of Fire Protection Engineering, 2nd Edition, Bethesda, Maryland, 1995

/USN 04/ U.S. Nuclear Regulatory Commission (USNRC):
Fire Dynamics Tools (FDTs) Quantitative Fire Hazard Analysis Methods for the U.S. Nuclear Regulatory Commission Fire Protection Inspection Program, NUREG-1805, Washington DC, USA, November 2004

**Tab. C-1** Summary of Predictions for Test 4 for CFAST and FDS

| Parameter | Sensor | Model Prediction at Peak CFAST | Model Prediction at Peak FDS | Measured Value at peak | Initial Measured Value | Uncertainty CFAST | Uncertainty FDS |
|---|---|---|---|---|---|---|---|
| **Global Parameters** | | | | | | | |
| HGL Interface Height | | 1.6 m | 1.8 m | 1.3 m | 5.7 m | + 6 % | + 11 % |
| HGL Temperature (average) | | 187 °C | 176 °C | Error | 19 °C | NA | NA |
| Door Mass Flow | | 1.2 kg/s | 1 kg/s | 1 kg/s | 0 | + 20 % | 0 % |
| Door Heat Flow | | NA | 166 kW | 166 kW | 0 | NA | 0 % |
| Smoke Concentration | NA | | | | | | |
| Pressare | DP 5-1 | - 1.7 Pa | - 3.2 Pa | - 2.4 Pa | 0 | NA | NA |
| Flame Height | NA | | | | | | |
| $O_2$ Concentration | GA 2 | 18.4 % | 18.0 % | 18.9 % | 20.6 % | NA | NA |
| $CO_2$ Concentration | GA 2 | 0.84 % | 1.6 % | 1.33 % | 0 % | - 37 % | + 20 % |
| CO Concentration | GA 2 | | | | | NA | NA |

| | | | | | | | |
|---|---|---|---|---|---|---|---|
| **Local Gas Temperature** | | | | | | | |
| Plume Temperature | TP 3 | | 159 °C | 272 °C | 19 °C | | - 46 % |
| | TP 5 | | 183 °C | 202 °C | 19 °C | | - 10 % |
| | TP 7 | | 192 °C | 190 °C | 19 °C | | + 1 % |
| Hot Gas Temperature. (point values) | TR 5-3 | | 122 °C | 114 °C | 19 °C | | + 8 % |
| | TR 5-5 | | 192 °C | 185 °C | 19 °C | | + 4 % |
| Ceiling Jet Tempera-ture | TR 5-7 | | 193 °C | 184 °C | 19 °C | | + 5 % |
| | TR 2-7 | | 185 °C | 185 °C | 19 °C | | 0 % |
| | TR 1-7 | | 195 °C | 195 °C | 19 °C | | 0 % |
| **Heat Flux to Cables** | | | | | | | |
| Radiative Heat Flux | NA | | | | | | |
| Total Heat Flux | WS 2 | 4 $kW/m^2$ | 1.4 $kW/m^2$ | 2.7 $kW/m^2$ | 0 | + 49 % | - 49 % |
| | WS 3 | 3.7 $kW/m^2$ | 2.1 $kW/m^2$ | 3.7 $kW/m^2$ | 0 | 0 % | - 42 % |
| | WS 4 | 3.6 $kW/m^2$ | 2.3 $kW/m^2$ | 4.3 $kW/m^2$ | 0 | - 15 % | - 45 % |
| Cable Temperature | | | | | | | |

Notes:
+ Model prediction was greater than measured value
- Model prediction was less than measured value
Value tabulated is: (model prediction at peak- measured value at peak)/(measured value at peak - initial measured value)

**Tab. C-2** Summary of predictions with FDTs - Test 4

| Parameter | Sensor | Model prediction at peak | Measured value at peak | Initial measured value | Uncertainty |
|---|---|---|---|---|---|
| **Global Parameters** | | | | | |
| HGL Interface Height | | 0.3 m @ 60 s | 1.3 m | 5.7 m | - 18 % |
| HGL Temperature (Average) | | 178 C @ 1200 s | NA | 19 °C | NA |
| Local Gas Temperature | | | | | |
| Plume Temperature | TP 3 | 410 | 272 °C | 19 °C | + 62 % |
| | TP 5 | 142 | 202 °C | 19 °C | - 22 % |
| | TP 7 | 84 | 190 °C | 19 °C | - 50 % |
| Target Heat Flux | NA | | | | |

Notes:
+ Model prediction was greater than measured value
- Model prediction was less than measured value
Value tabulated is: (model prediction at peak- measured value at peak)/(measured value at peak - initial measured value)

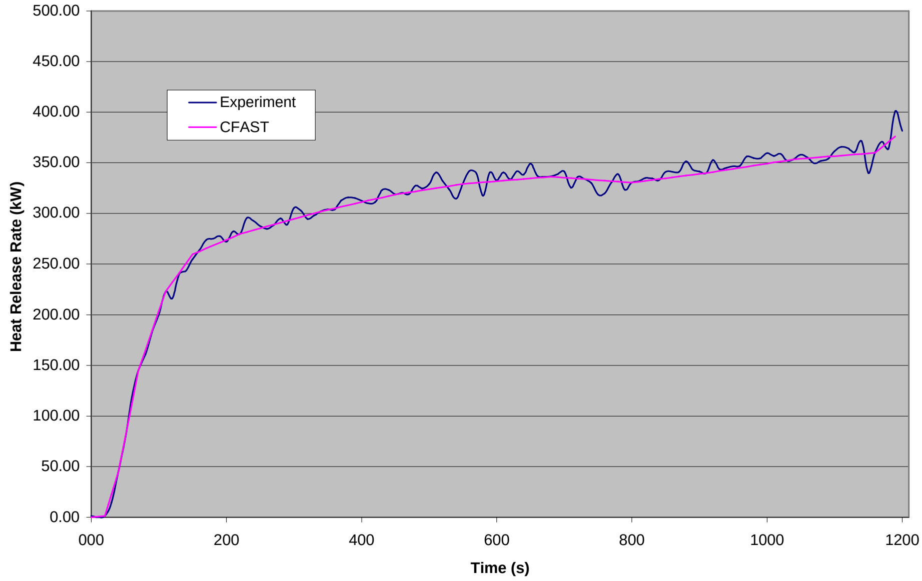


**Fig. C-1** Heat release rate (CFAST)

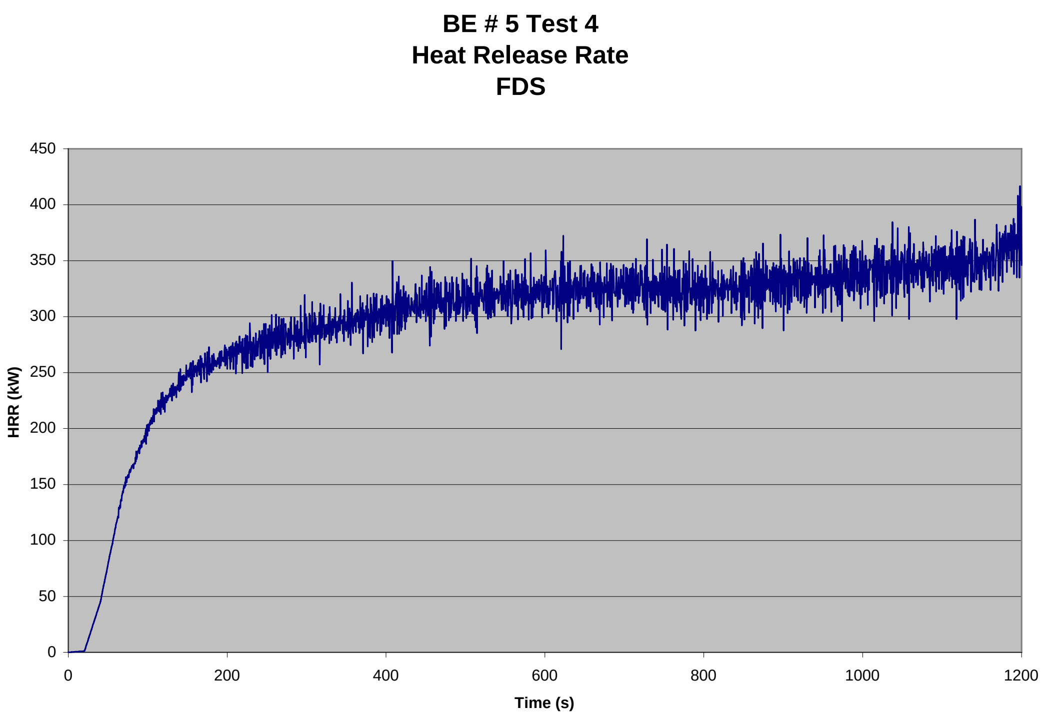


Fig. C-2 Heat release rate (FDS)

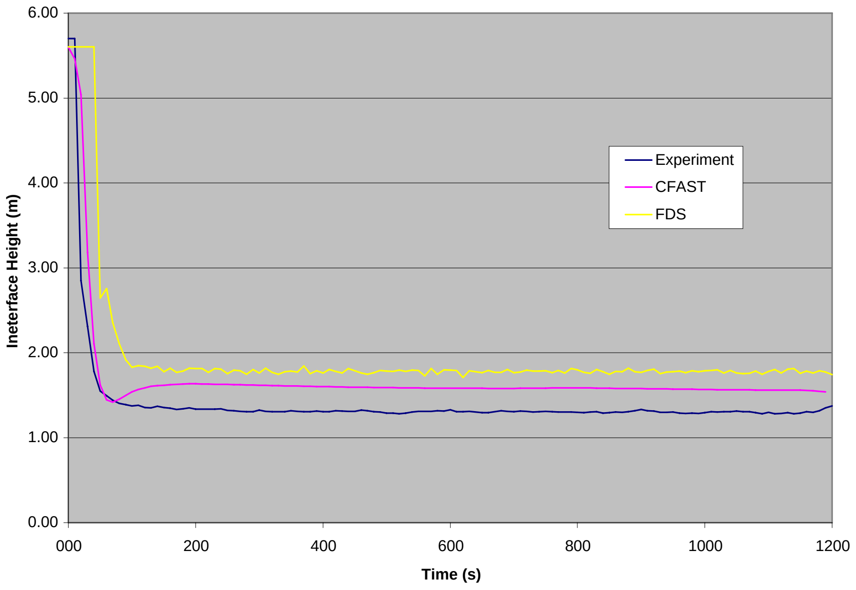


**Fig. C-3** HGL interface height

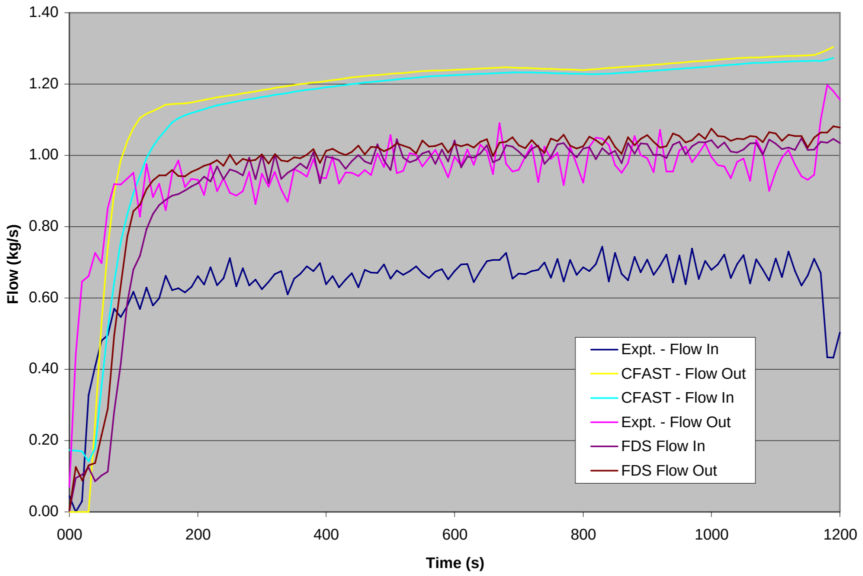


**Fig. C-4** Mass flow through door

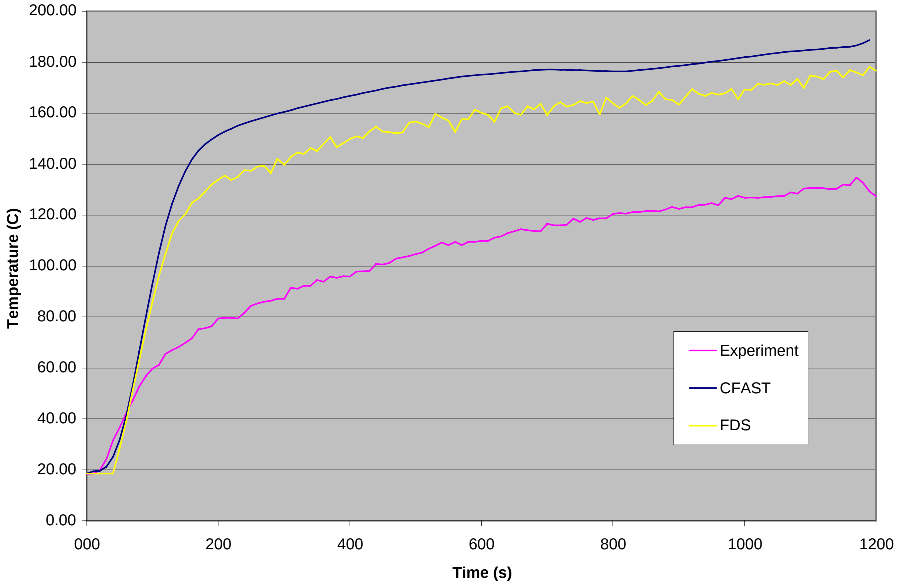


**Fig. C-5** HGL temperature

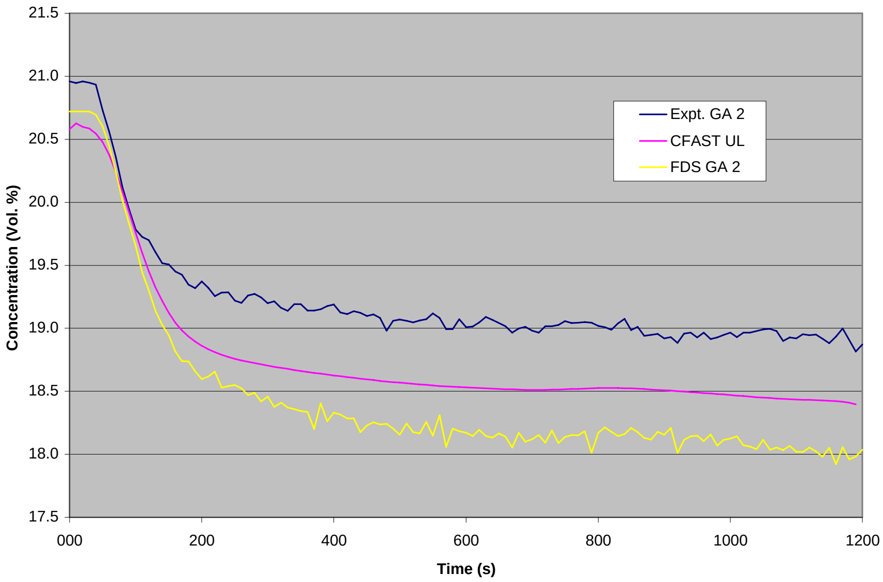


**Fig. C-6** Oxygen concentration

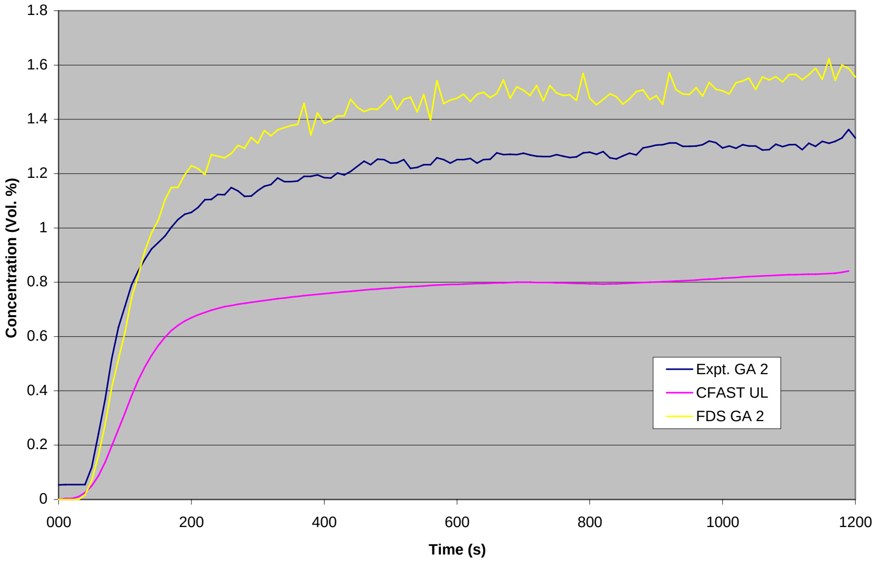


**Fig. C-7** CO2 concentration

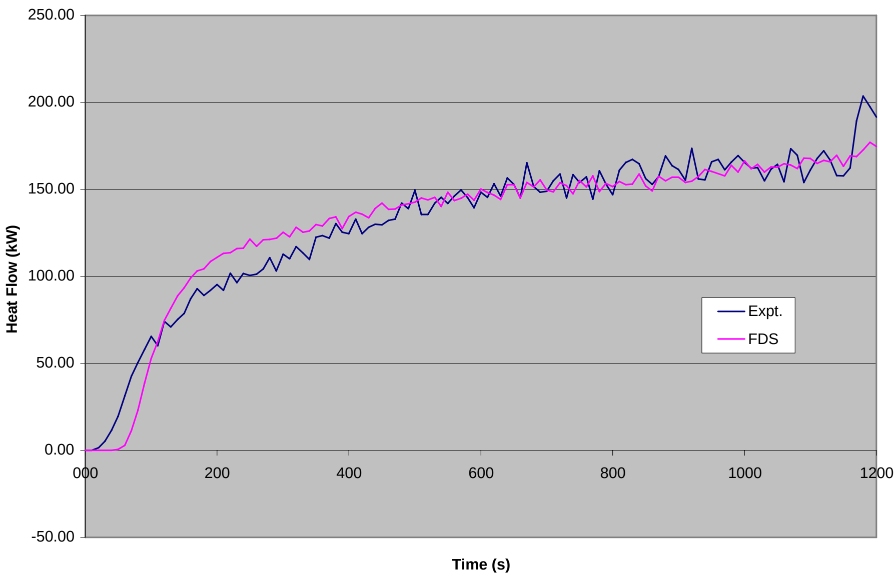


**Fig. C-8** Heat flow through door

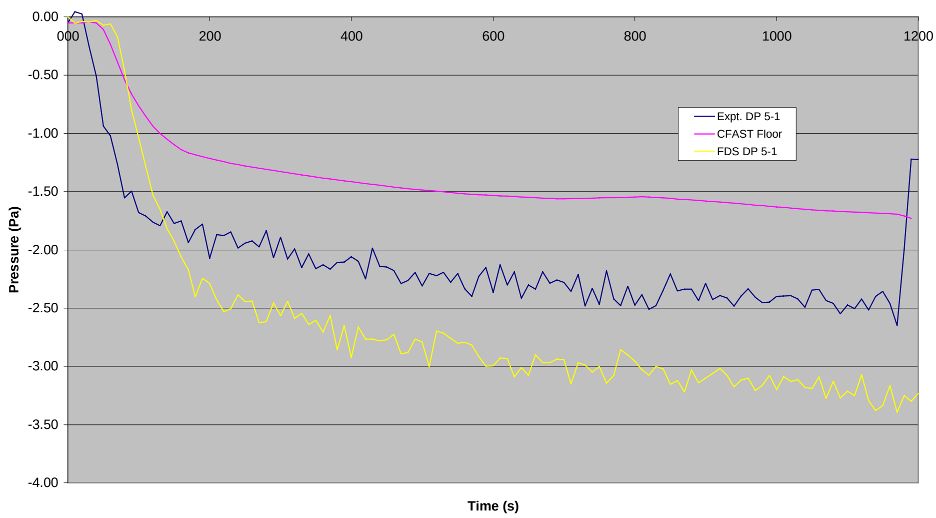


**Fig. C-9** Compartment pressure

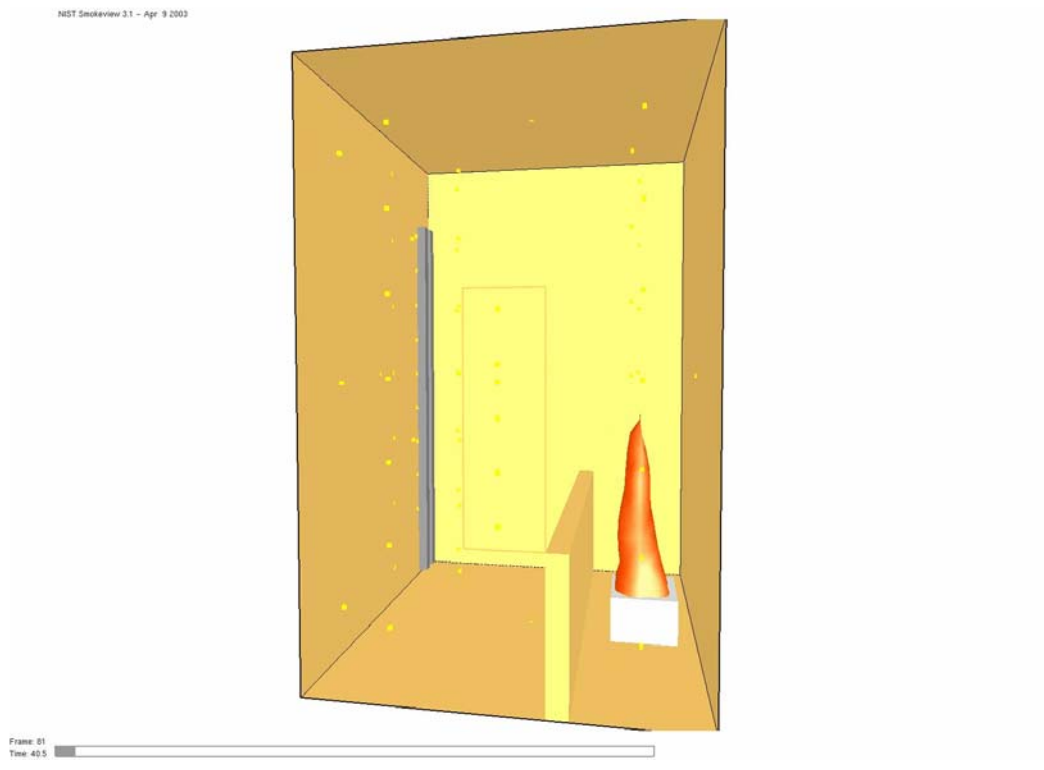


**Fig. C-10** FDS Isosurface of flame sheet (40 s)

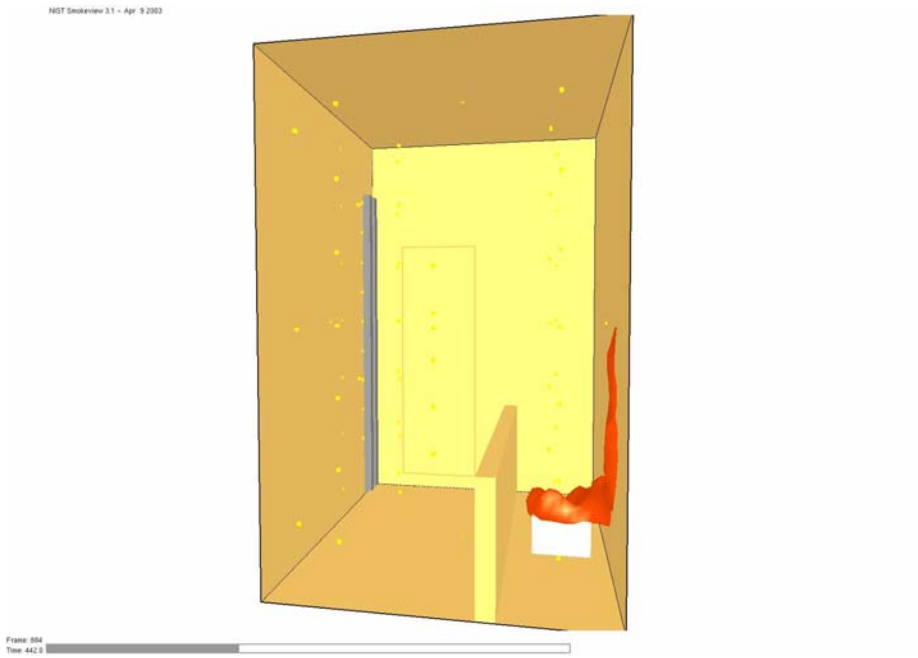

**Fig. C-11** FDS Isosurface of flame sheet (442 s)

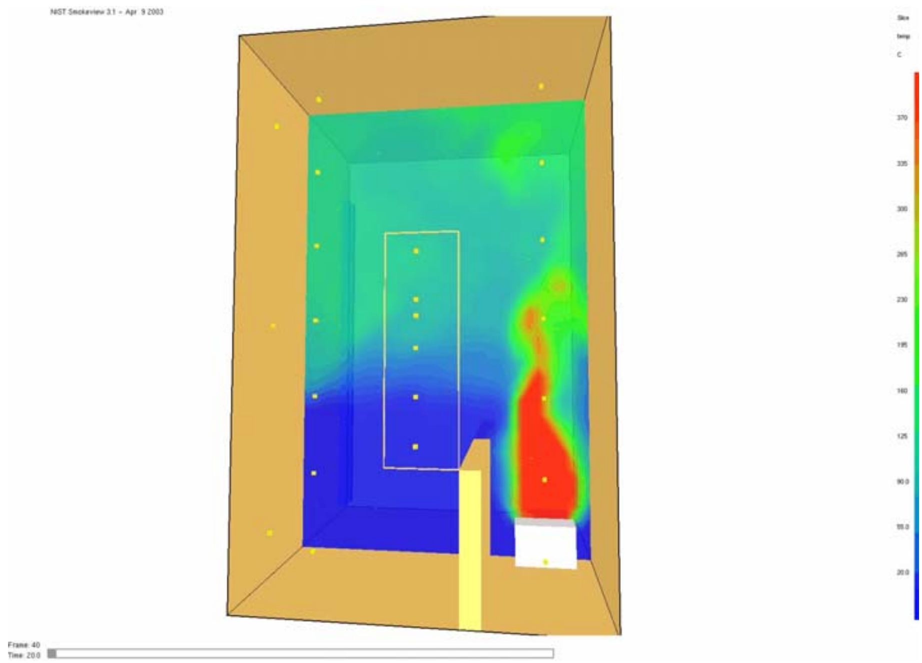

**Fig. C-12** FDS Temperature slice view (y=1.8 m, 20 s)

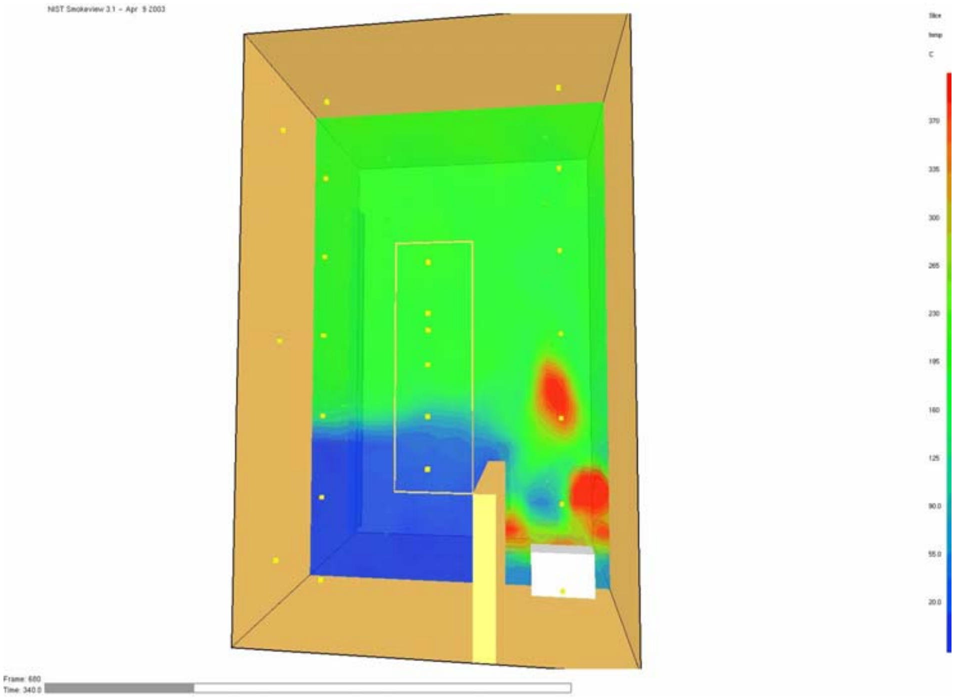


**Fig. C-13** FDS Temperature slice view (y = 1.8 m, 340 s)

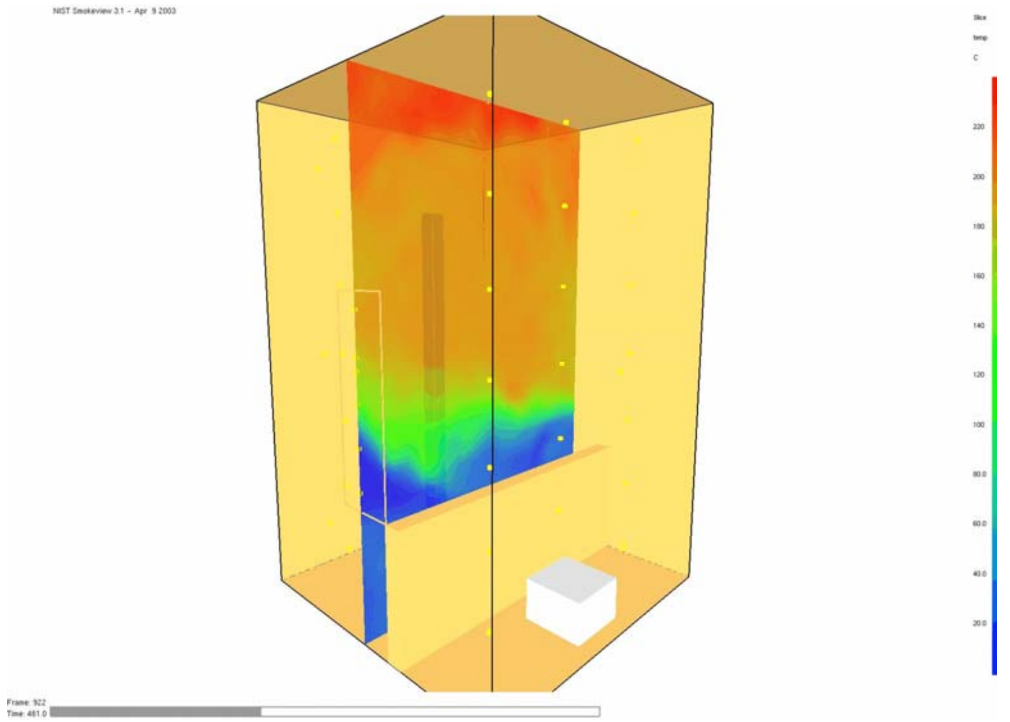


**Fig. C-14** FDS Temperature slice view (x = 1.8 m, 461 s)

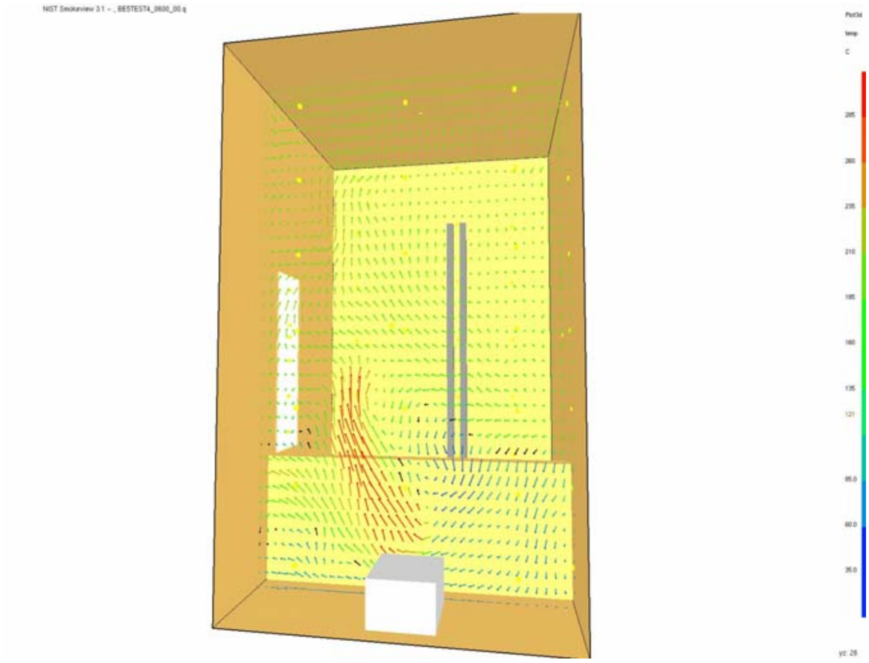

**Fig. C-15** FDS Flow vectors in trench (600 s)

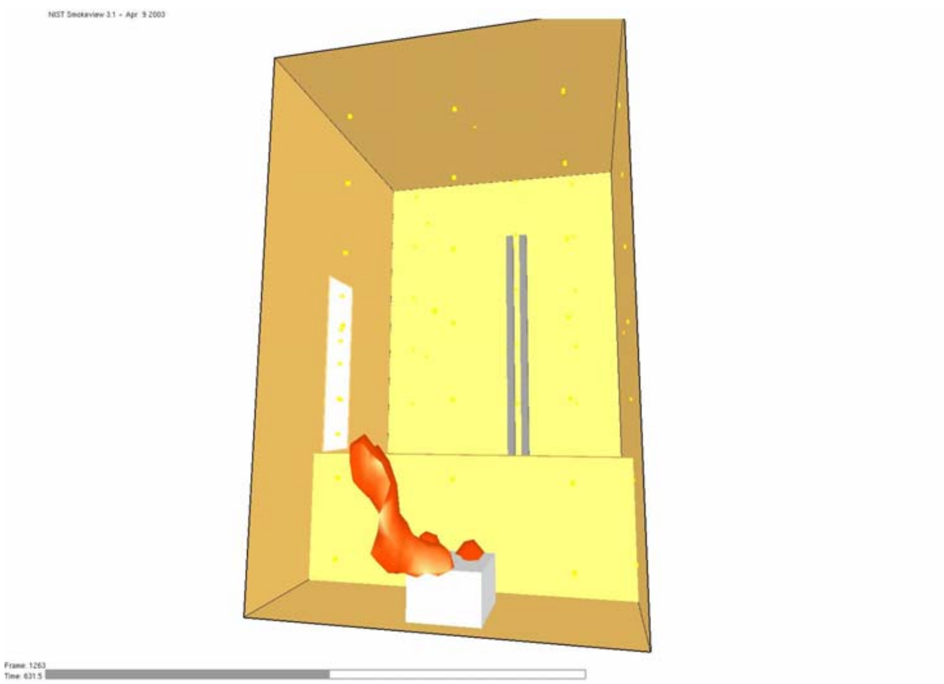

**Fig. C-16** FDS Isosurface of flame sheet (631 s)

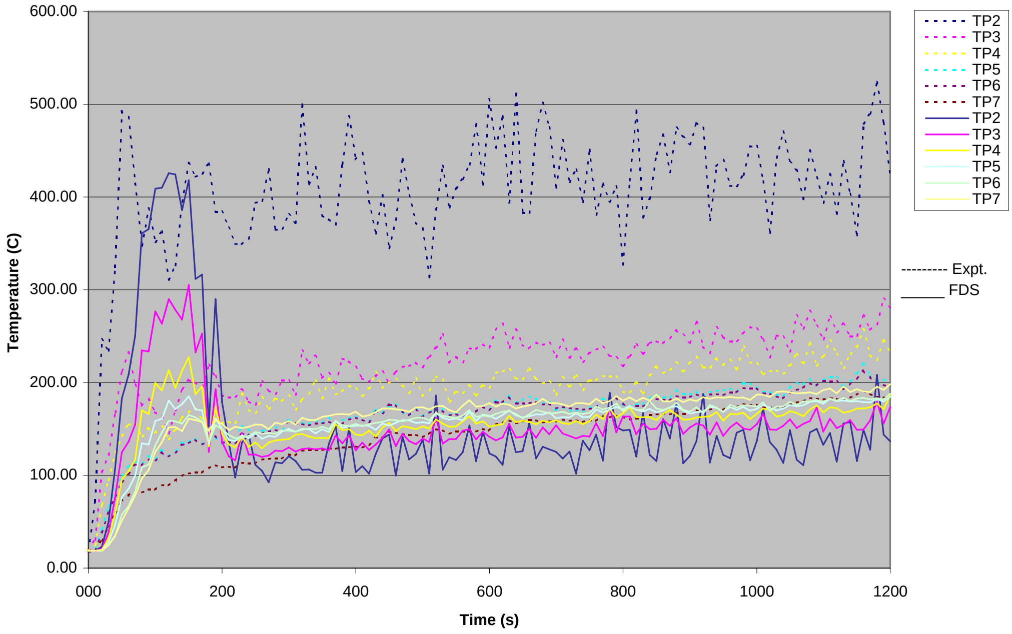


**Fig. C-17**　Plume temperature

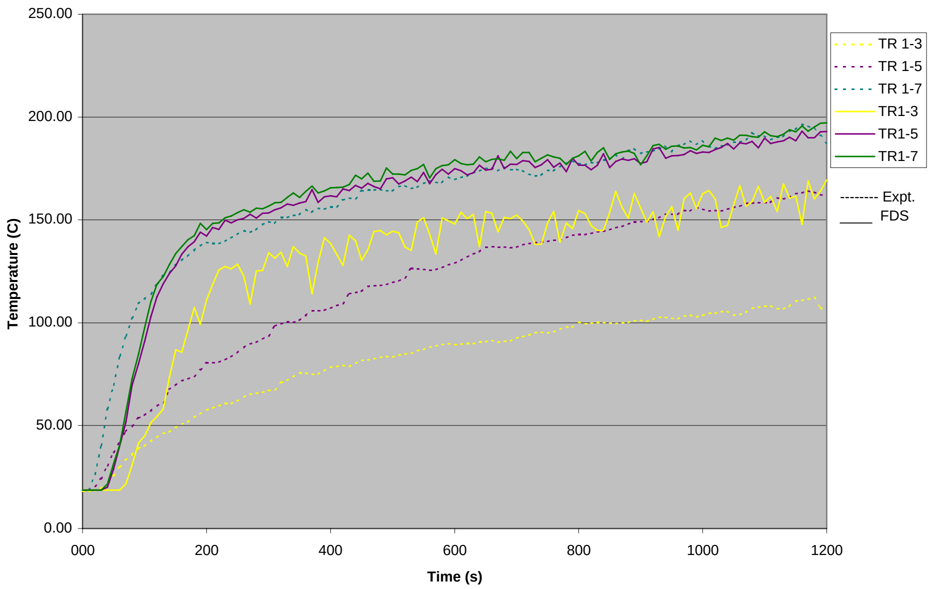


**Fig. C-18**　Compartment temperature (TR1)

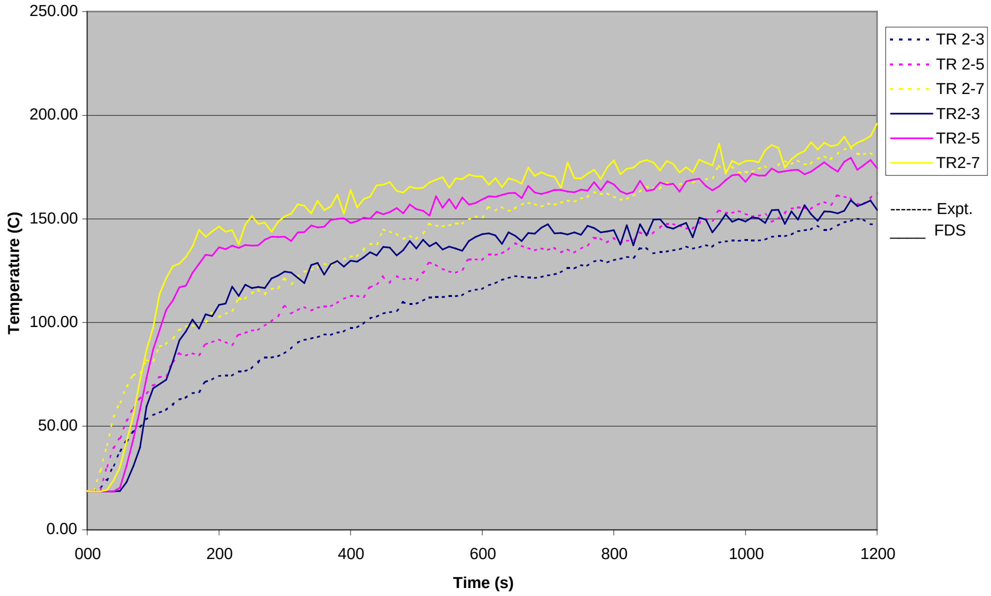


**Fig. C-19** Compartment temperature (TR2)

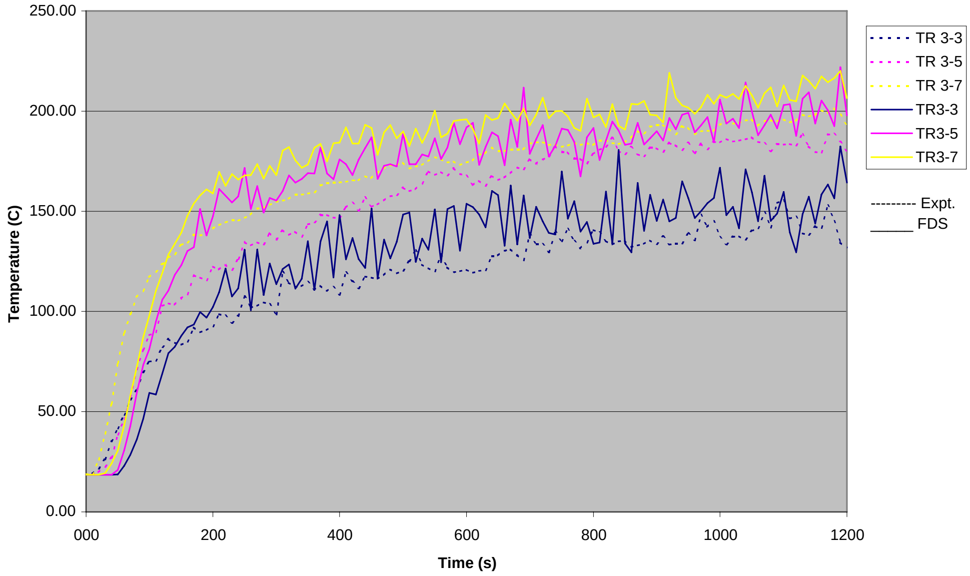


**Fig. C-20** Compartment temperature (TR3)

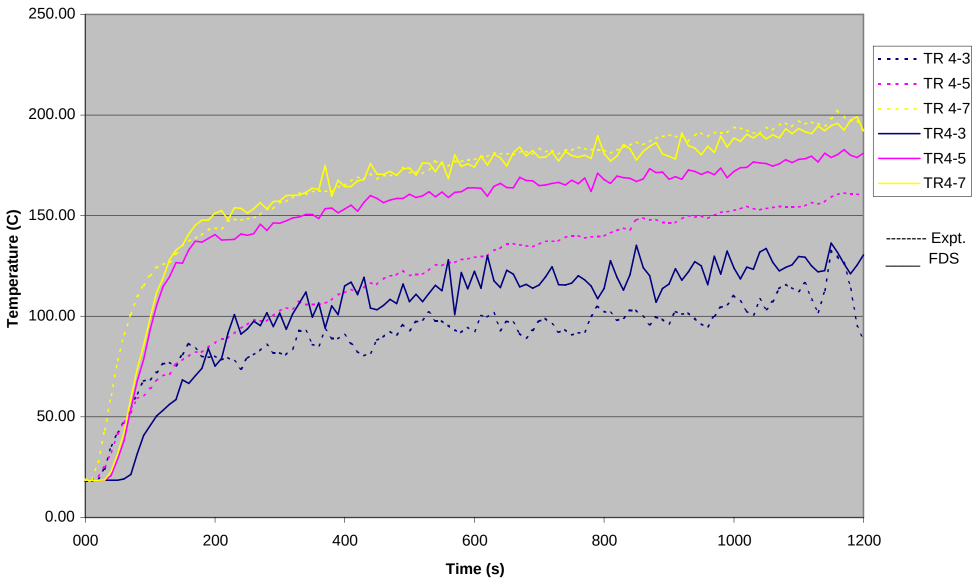


**Fig. C-21** Compartment temperature (TR4)

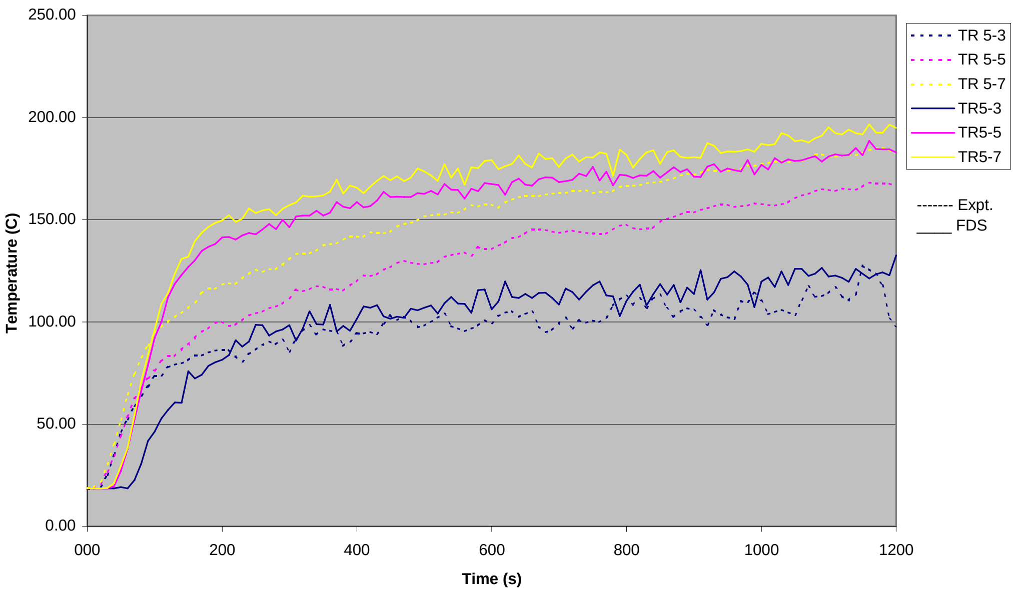


**Fig. C-22** Compartment temperature (TR5)

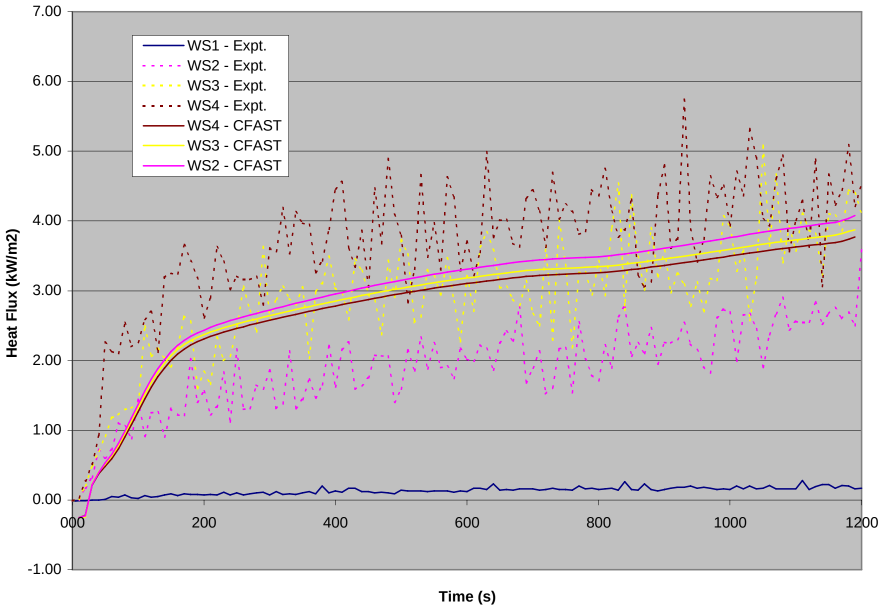


**Fig. C-23** Heat flux on cables (CFAST)

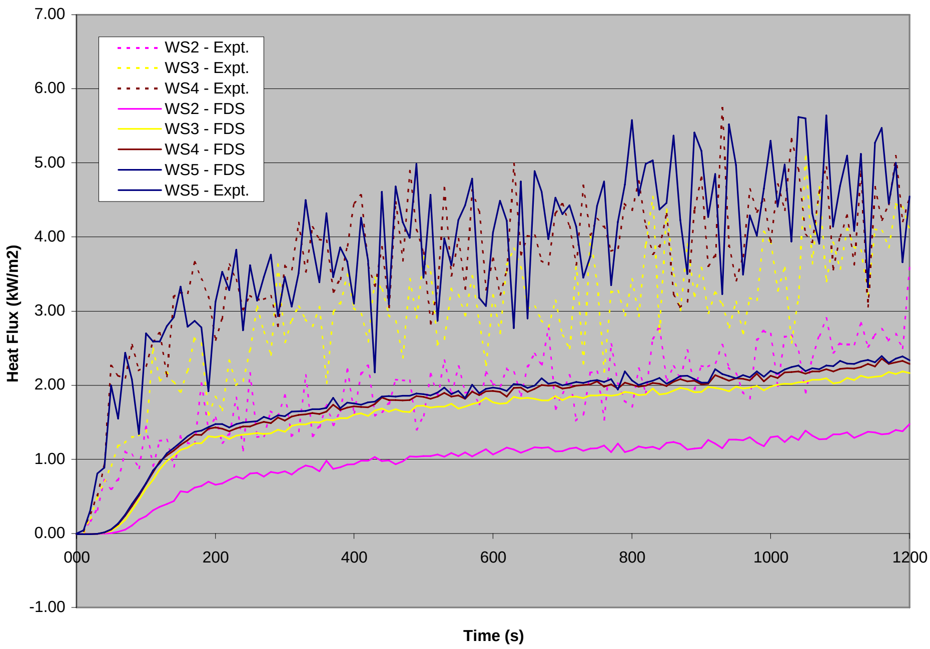


**Fig. C-24** Heat flux on cables (FDS)

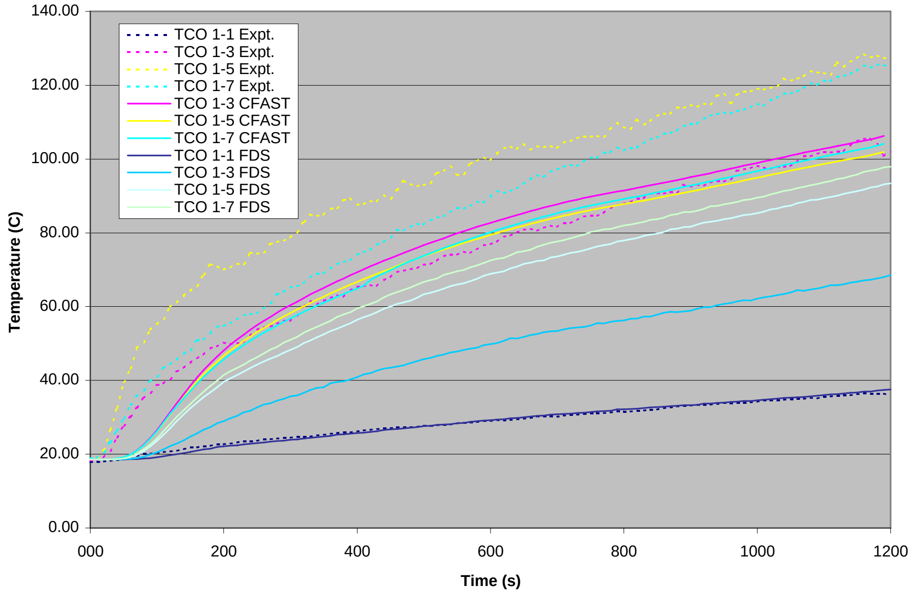


**Fig. C-25** Power cable temperature

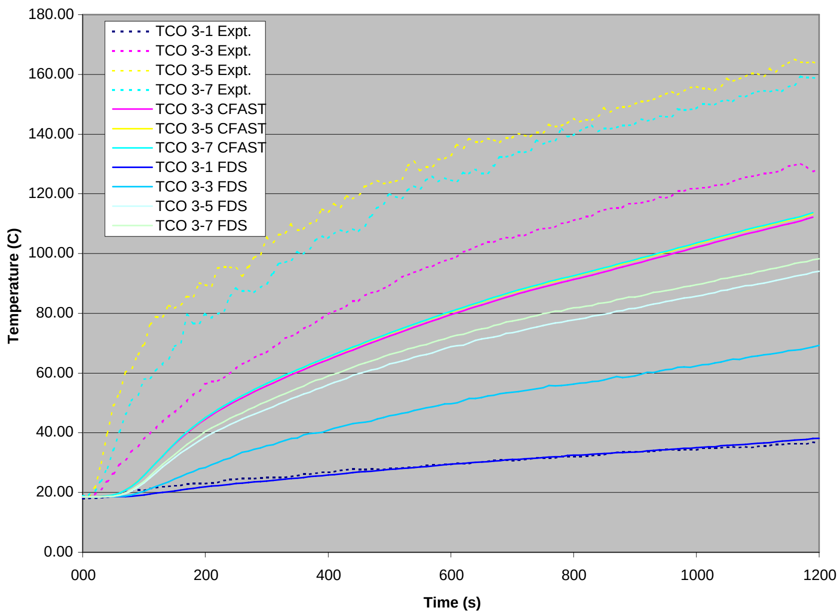


**Fig. C-26** I&C cable temperature

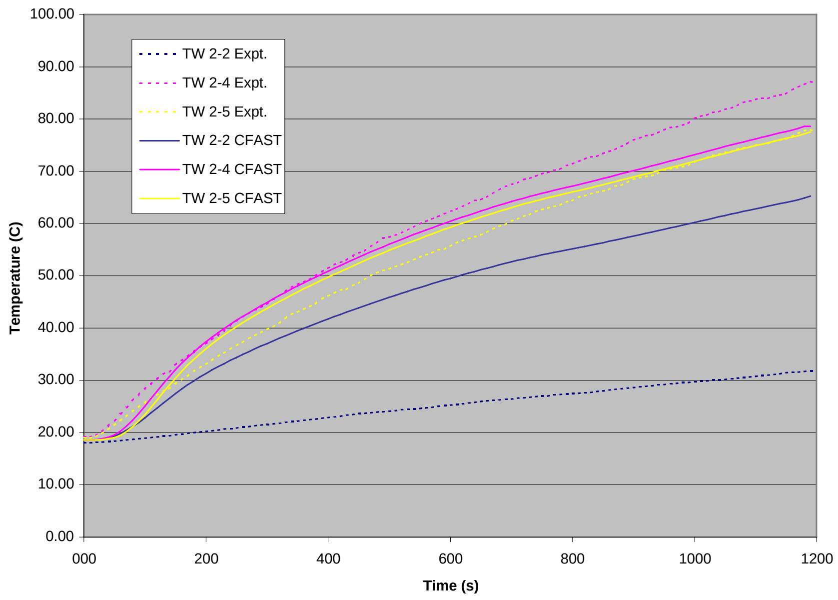


**Fig. C-27** Wall temperature (TW2)

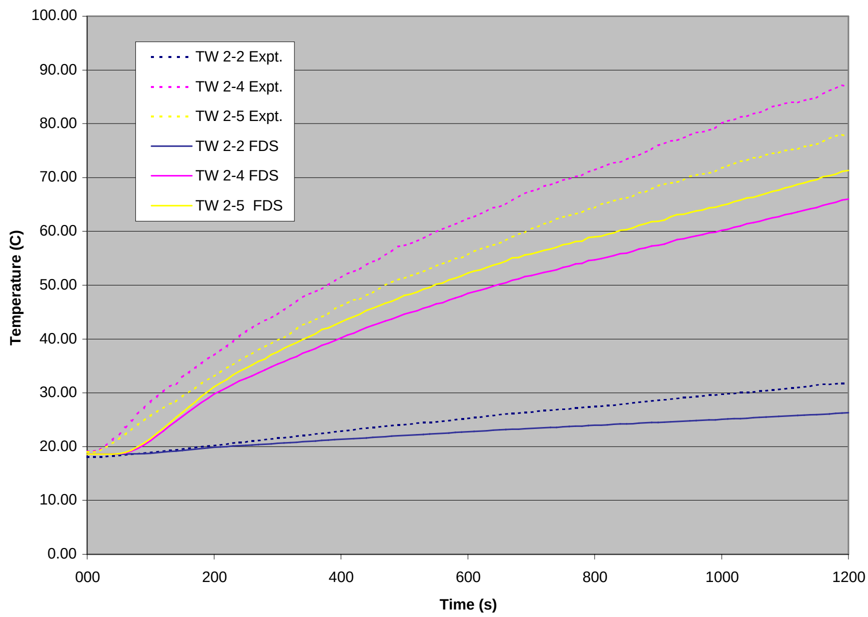


**Fig. C-28** Wall temperature figures

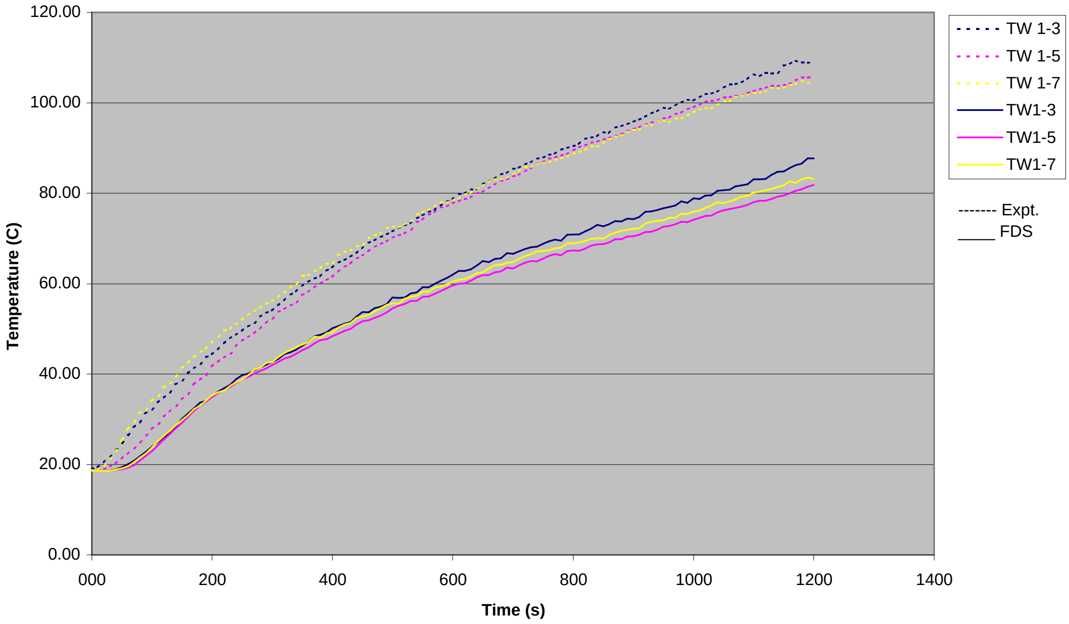


**Fig. C-29** Wall temperature (TW1)

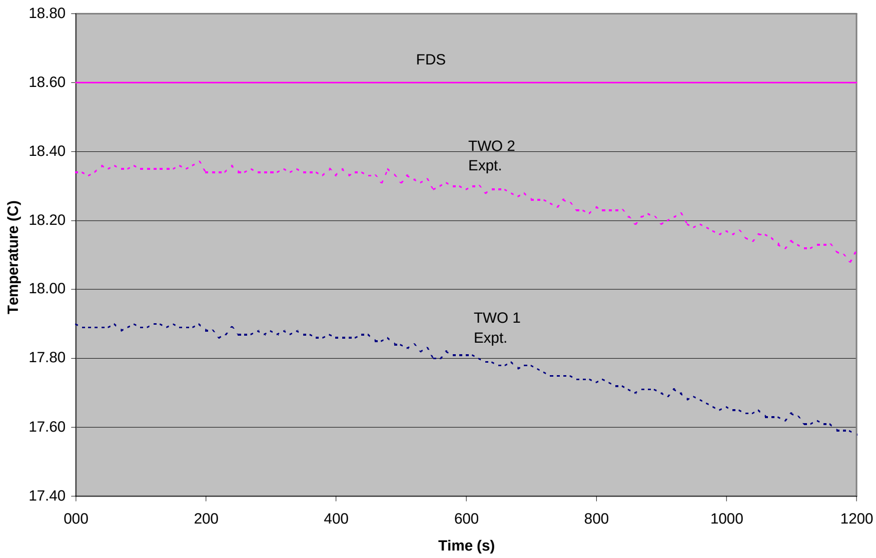


**Fig. C-30** Outside wall temperature

# Appendix D: FDS Calculations for Benchmark Exercise No. 5

**Presented by**

Kevin McGrattan
National Institute for Standards and Technology (NIST)
100 Bureau Drive, Gaithersburg, MD 20899, U.S.A.

## D1 Introduction

The primary intent of Benchmark Exercise No. 5 was to assess the ability of various models to predict the spread of fire on bundled power cables. Currently, there are no algorithms within the Fire Dynamics Simulator (FDS version 4) to model this process. At best, FDS can predict the heat flux to homogeneous solids that conform to the recti-linear numerical grid used to solve the gas phase conservation equations. The model does not account for the non-uniform composition of the cables or the geometric complexity of the cable bundles.

Nevertheless, FDS was used to model the four experiments that comprised BE No. 5 to point out what the model can and cannot do at the present time. In the chapters to follow, only the predictions and measurements relevant to flame spread will be shown. FDS was not run with a prescribed heat release rate (HRR), thus the predicted compartment temperatures and other quantities were in disagreement with the measurements simply because the HRR was not predicted accurately. Benchmark Exercises 3 and 4 are more suitable for assessing the transport algorithms within FDS, especially BE No. 4 which used the same compartment as BE No. 5.

## D2 Input Parameters and Assumptions

In cooperation with the fire protection engineering community, a computational fire model, Fire Dynamics Simulator (FDS), has been developed at the National Institute of Standards and Technology (NIST) in the USA to study fire behavior and to evaluate the performance of fire protection systems in buildings. The software was released into the public domain in 2000, and since then has been used for a wide variety of analyses by fire protection engineers. A complete description of the model can be found in /MCG 04/. Briefly, FDS is a computational fluid dynamics code that solves the Navier-Stokes equations in low Mach number, or thermally-expandable, form. The transport algorithm is based on large eddy simulation techniques, radiation is modeled using a gray-gas approximation and a finite-volume method is used to solve the radiation transport equation. Combustion is modeled using a mixture fraction approach, in which a single transport equation is solved for a scalar variable representing the fraction of gas originating in the fuel stream.

In this section, the most important features of the simulations of Benchmark Exercise No. 5 are described. Relevant features of the model for this application are described in more detail.

### D2.1 Compartment Geometry

The geometry of the compartment was relatively simple. The overall enclosure was rectangular, as were the vents and most of the obstructions. A single, rectilinear grid spanned the interior of the compartment, plus a comparable volume under the hood outside the door. The dimensions of the grid were 36 × 72 × 56, and the cells were exactly 10 cm in size throughout. All objects within the computational domain were approximated to the nearest 10 cm. The compartment walls and ceiling were made of various types of concrete, the thermal properties of which were input directly into the model.

A second numerical grid was superimposed on the 10 cm grid near the cables. This second grid was made up of 5 cm cells in an attempt to better resolve near-field phenomena. Even with this finer grid, however, the two cable bundles were approximated as solid slabs of plastic.

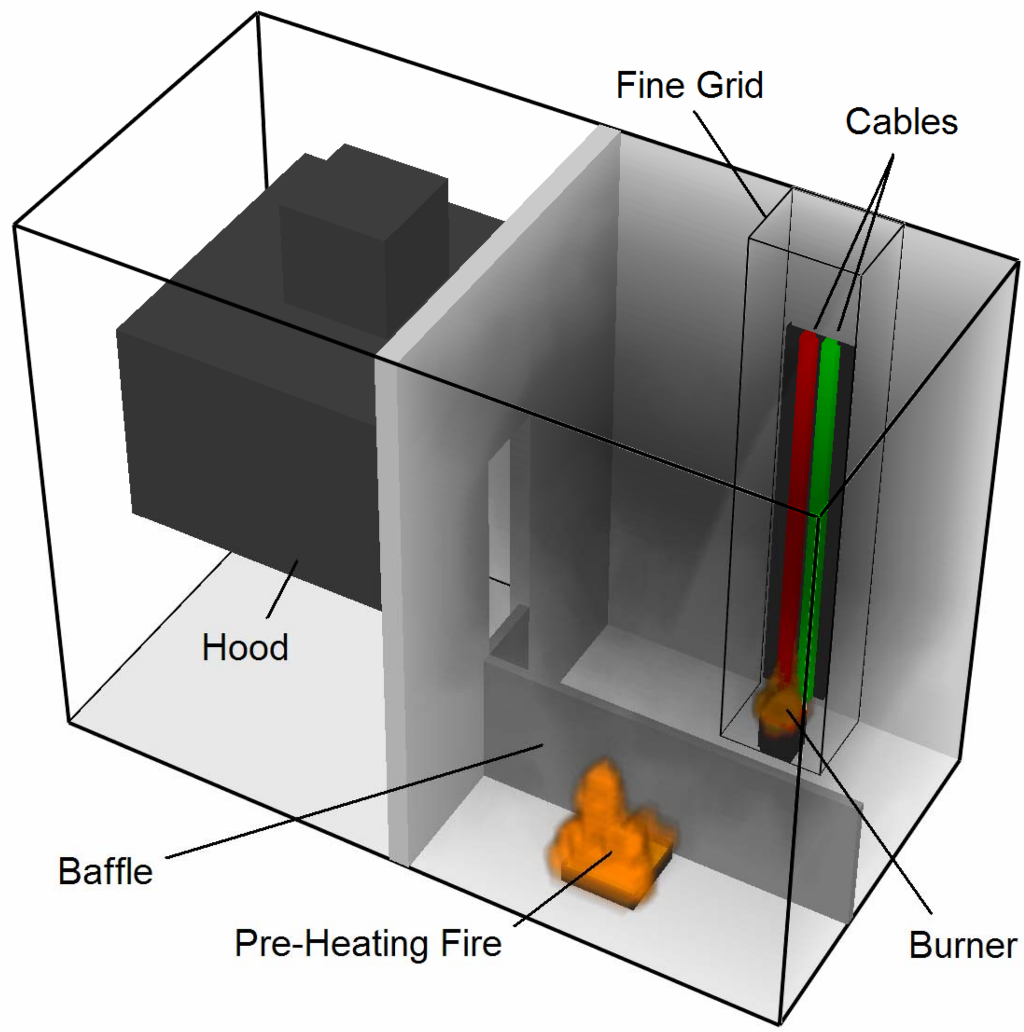


**Fig. D-1** Simulation of Test 4, showing the fires and smoke in Smokeview.

### D2.2 Cables

FDS performs a one-dimensional heat transfer calculation into an assumed homogenous material of given thickness and (temperature-dependent) thermal properties. Solid obstructions within the computational domain must conform to the underlying gas phase grid. In other words, the surface area of the solid is an integer multiple of the area of the face of a gas phase grid cell. The thickness of the solid is not tied to the gas phase grid, only the exposed surface area. Thus, the solid phase heat transfer calculation is partially decoupled from the gas phase – heat transfer in the normal direction can be modeled with as fine a grid as needed, but mass and heat transfer between the solid and the gas is constrained by the gas phase grid.

In the simulations, the cable bundles were assumed to be 10 cm × 10 cm solid slabs covered by 5 cm × 5 cm × 2 mm thick 'tiles' with the given thermal properties of the PVC or FRNC cable coating. The 'tiles' were assumed to have an insulated backing. This was an attempt to characterize the heat transfer through the covering of the outermost cables in the bundle which have a roughly 2 mm thick plastic coating surrounding insulated metal conductors. Nothing in the model could account for the lateral heat conduction along the metal conductors.

In the simulations, as the cable surface approached the prescribed 'ignition" temperature, the burning rate per unit area increased according to the Arrhenius expression:

$$\dot{m}'' = A\rho\, e^{-E/RT}$$

Here, $A$ and $E$ are the pre-exponential factor and activation energy, respectively, $\rho$ is the density of the solid, $R$ is a universal constant, and $T$ is the absolute temperature of the material surface. The activation energy and pre-exponential factor were chosen so that the material would burn at the rate measured in the Cone Calorimeter for a surface temperature near the given 'ignition" temperature. The burning rate is not sensitive to these various parameters, but it is sensitive to the heat of gasification. The heat of gasification dictates how much energy is required to liberate fuel gases from the solid. Given the simple pyrolysis model just described, the surface temperature never increases much beyond the prescribed 'ignition" temperature because the energy needed to gasify the fuel increases exponentially with temperature. In the simulations, the predicted surface temperature of the cables exhibited a steady increase until it reached the neighborhood of the 'ignition" temperature, at which point it remained more or less constant. This is characteristic of a *thermoplastic,* but it has been suggested that certain types of cables behave more like charring solids. In any event, all the cables were assumed to behave like thermoplastics.

### D2.3 Fire

Two fuels were used in the test: propane from a burner near the cables, and ethanol in a pan on the opposite side of the compartment to provide 'pre-heating". FDS only recognizes one fuel, and one set of stoichiometric parameters. For the simulations, the properties of propane were assigned to both fires, and the heat release rates were prescribed. However, the heat release rate from the burning cables was not prescribed, as the point of the exercise was to *predict* the burning rate.

### D2.4 Radiation

FDS uses a finite volume method to solve the radiation transport equation in the gray gas limit. By default, the radiation from the fire and hot gases is tracked in 100 directions. While this is adequate to predict the radiation heat flux to nearby targets (a few fire diameters away), it is not adequate to predict the flux to distant targets (greater than three diameters, roughly). Because all of the targets were relatively close to the fire, there was no need to modify the default settings of the radiation solver.

### D2.5 Output

During the simulation, values of temperature, heat flux and gas species concentrations, *etc*., were reported as 10 s averages. Linear interpolation was used to approximate values between the 10 cm grid cells. The results were saved in a text file and compared with the measurements. Details about each quantity saved are given in the next chapter.

## D3 Comparison of Model Prediction and Measurement

This section contains only comparisons of quantities that characterize the thermal environment near the cable tray. Comparisons of all other quantities were biased by the errors in the heat release rate prediction, not necessarily errors in the transport algorithm.

### D3.1 Heat Release Rate

**Fig. D-2** – **Fig. D-5** shows the predicted and measured heat release rates for Tests 1-4. For Tests 1 and 2, it was reported that there was no flame spread and a very low cable burning rate. The FDS simulations of Tests 1 and 2 predicted a slightly higher burning rate than was actually measured. This extra energy resulted from the cables near the propane burner getting hot enough to 'ignite", meaning that the simple pyrolysis model described above predicted a burning rate consistent with the predicted heat flux, surface temperature and assumed heat of gasification. In Tests 3 and 4, FDS again predicted a low cable burning rate, whereas in reality the cables burned readily and the fire spread upwards. The 'slabs' representing the cable bundles in FDS could not retain a sufficiently high surface temperature away from the burner to sustain flame spread. There was no interstitial space between the cables in the model, thus there was no way to 'trap" the heat needed to foster flame spread.

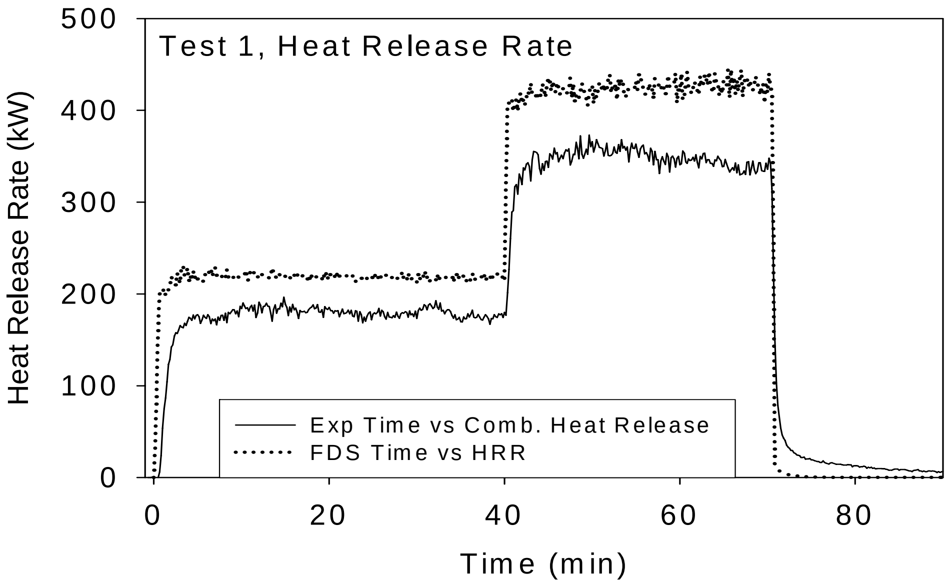


**Fig. D-2** Measured and predicted heat release rates for Test 1

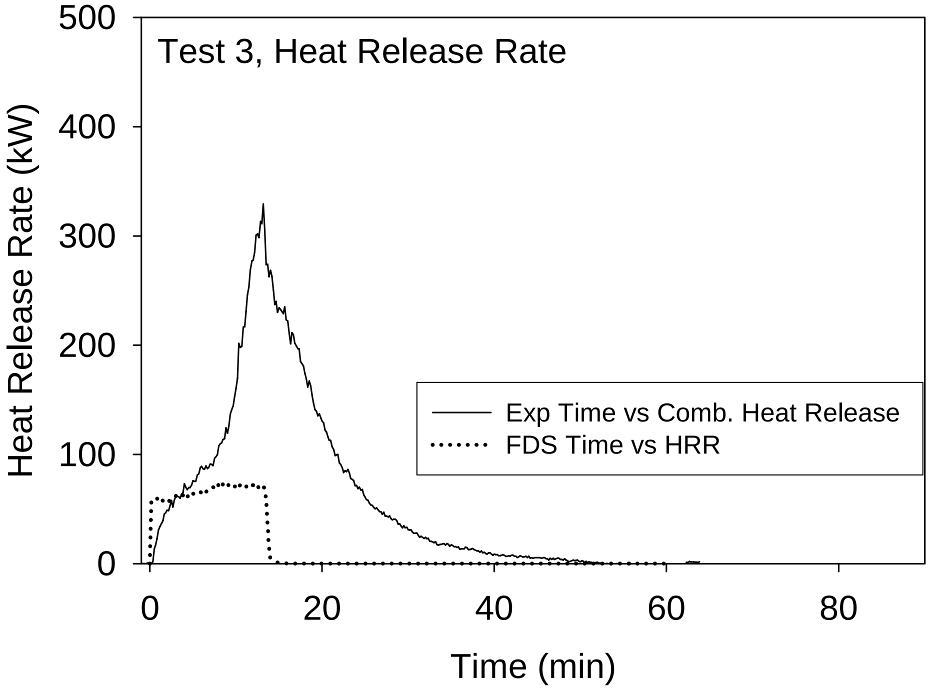


**Fig. D-3** Measured and predicted heat release rates for Test 2

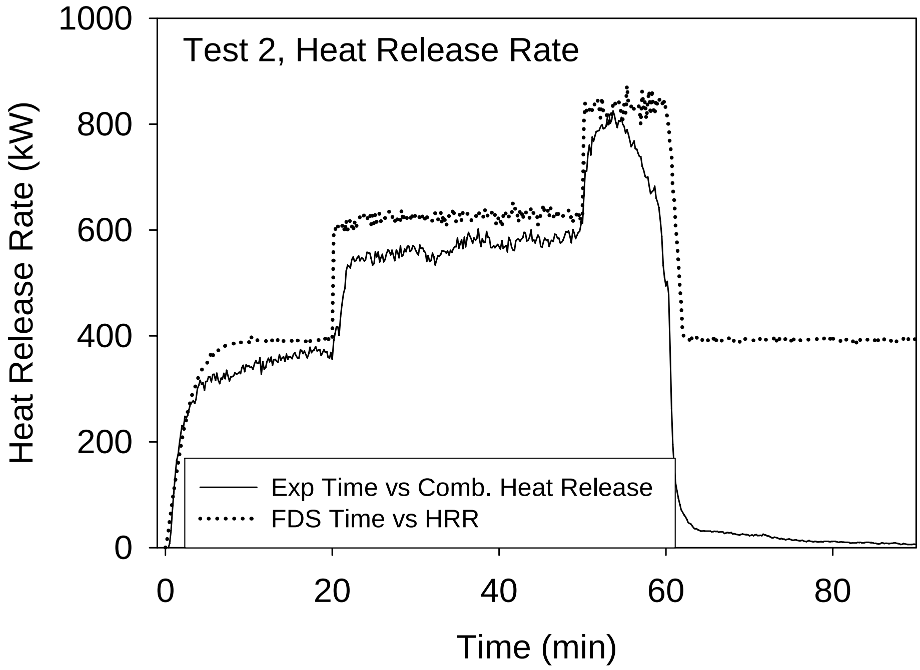


**Fig. D-4** Measured and predicted heat release rates for Test 3

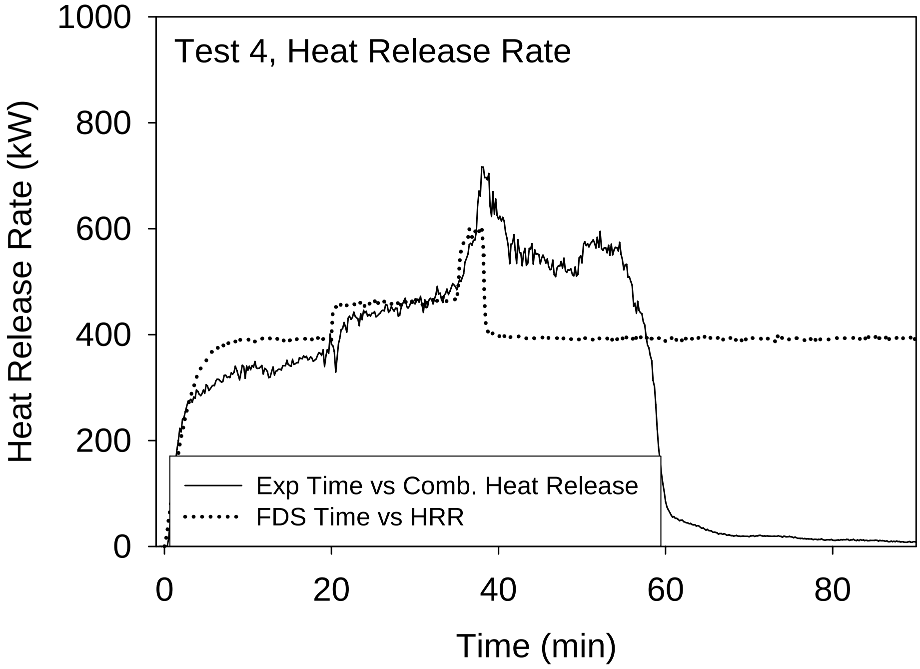


**Fig. D-5** Measured and predicted heat release rates for Test 4

## D3.2 Gas Temperatures

Gas temperatures were measured in the experiments at various locations throughout the compartment. However, given that the heat release rates were not accurately predicted, there is little point in dwelling on the gas temperature predictions. It has been shown in previous benchmark exercises that the accuracy of the temperature predictions is tied directly to the accuracy of the heat release rate. **Fig. D-6** – **Fig. D-9** shows how closely the upper layer temperature measurement and prediction mimics the measured and predicted HRR. The location of the temperature measurement was just in front of the top of the cable tray.

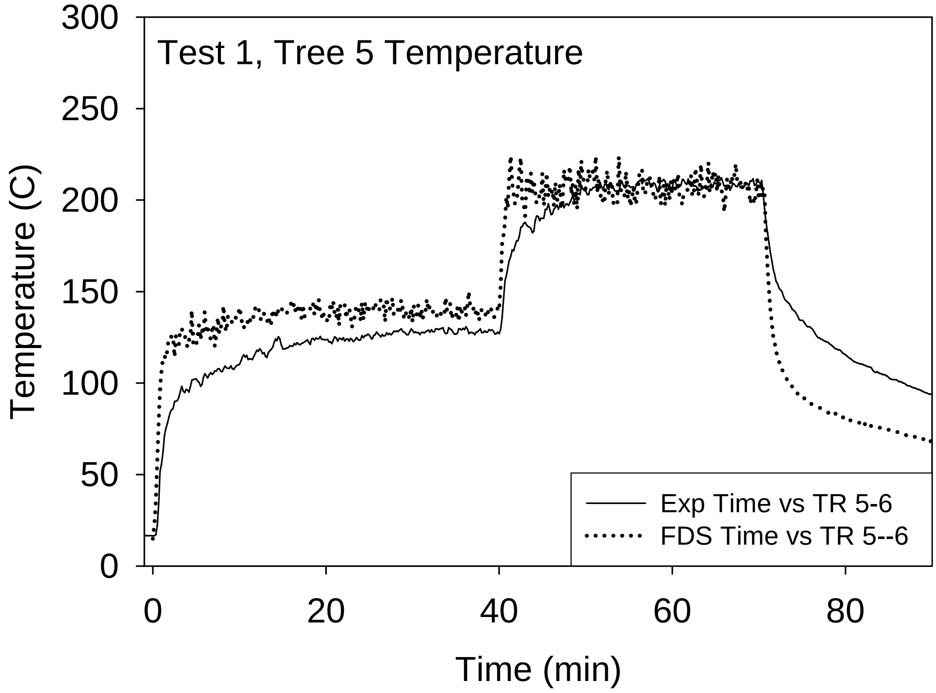


**Fig. D-6** Gas temperature comparisons for Tests 1

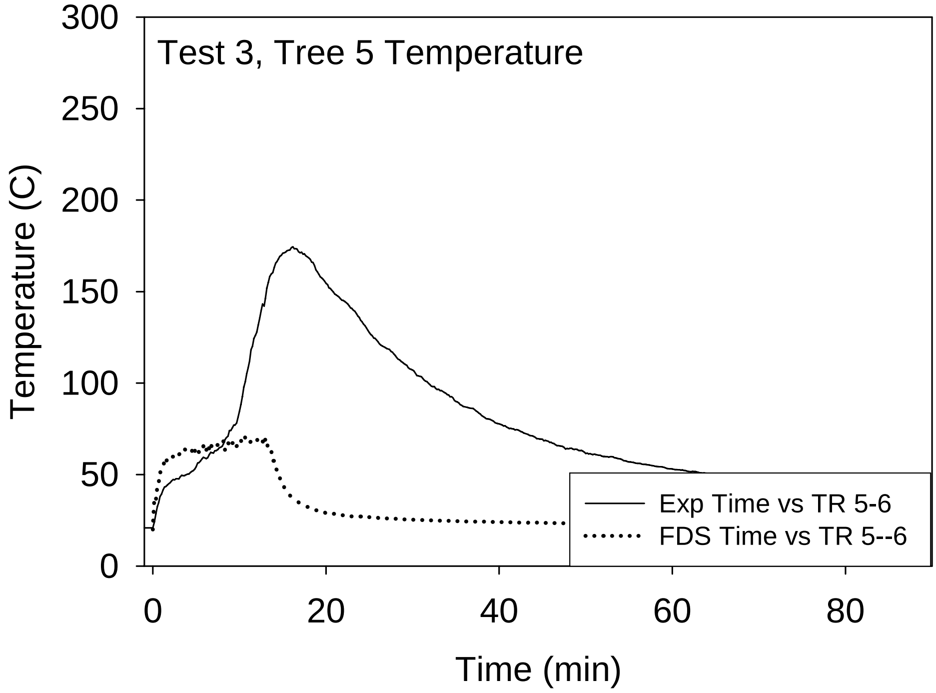


**Fig. D-7** Gas temperature comparisons for Tests 2

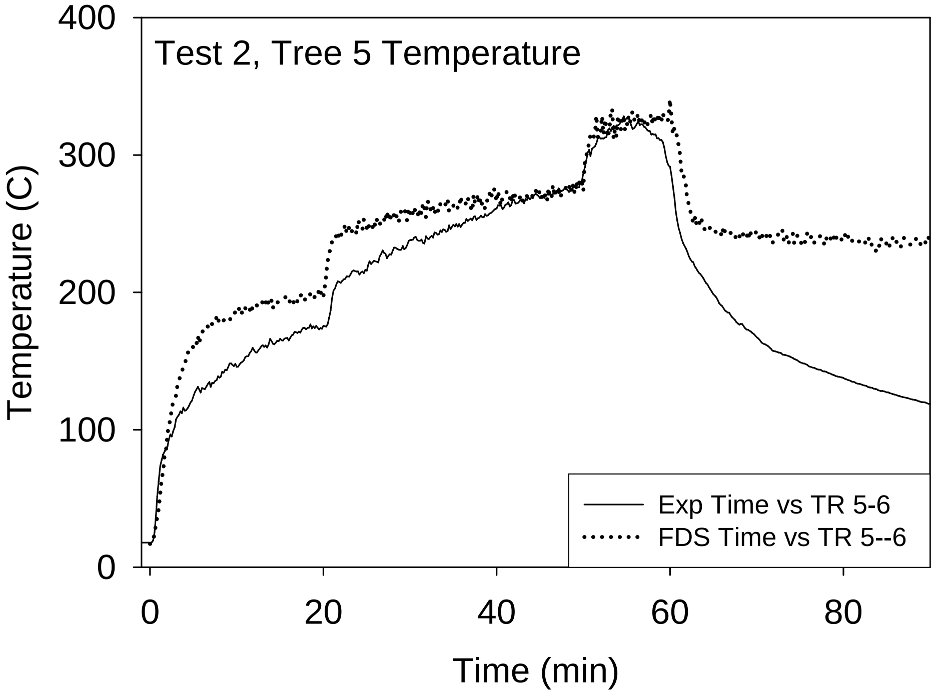


**Fig. D-8** Gas temperature comparisons for Tests 3

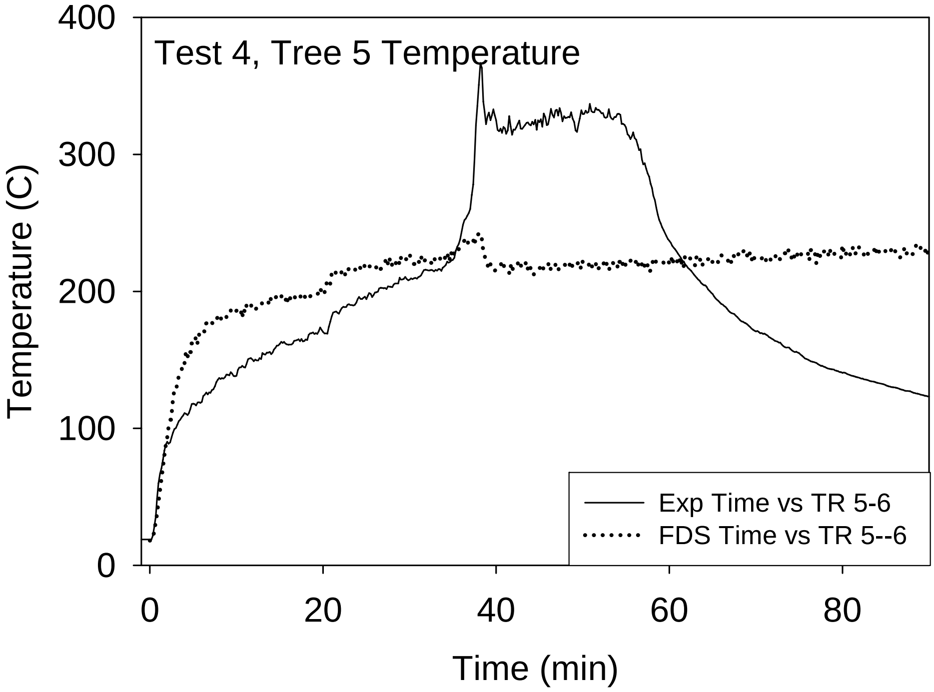


**Fig. D-9** Gas temperature comparisons for Tests 4

### D3.3 Heat Flux and Cable Temperatures

The cable tray was instrumented with 5 heat flux gauges (WS 1-5) arranged vertically between the two cable bundles. Along with the cable temperatures themselves, these gauges provided some measure of the thermal insult to the cables from the fire. Even though FDS does not have a detailed model of the bundled cables, it is still useful to look at the heat fluxes and cable temperatures to at least assess the model's ability to characterize the thermal environment near the cable tray.

Fig. D-10 and Fig. D-11 presents the heat flux measurements and predictions at the three lowest gauge locations (WS 1-3) for the experiments with no pre-heating (Tests 1 and 3). The predicted cable surface temperatures (Fig. D-12 and Fig. D-15) did not behave in the same manner as the measurements. The predicted temperatures rose steadily to the prescribed ignition temperatures, resulting in burning at a low rate, not high enough to induce spreading. The measured temperatures went through a number of significant transitions, possibly due to (1) complexities in the degradation process, (2) ignition, or (3) loss of contact with the solid. These effects were not captured by the model. To make matters worse, there was poor agreement in the heat fluxes at these locations, probably due to uncertainties inherent in near-field predictions. Regardless of the pyrolysis model, it was evident that the model, using a 5 cm grid, could not predict the heat flux accurately enough to predict flame spread if it were to occur.

For the pre-heating tests (Tests 2 and 4), the behavior in the first 20 min was more predictable, although there was still a larger discrepancy in the heat flux prediction (Figure D-16 and Figure D 17) to the upper layer flux gauges than was seen in Benchmark Exercises 3 and 4. The predicted upper layer temperatures shown in Figure D-8 – Figure D-9 were fairly accurate during the *prescribed* pre-burning stage. Such accuracy usually results in a prediction of upper layer heat flux of comparable accuracy. In Tests 2 and 4, the measured and predicted upper layer temperature was about 200 °C. At this temperature, the *radiative* heat flux within the smoke-filled upper layer would be about 2.8 $kW/m^2$. The difference between measured and predicted heat flux was probably the result of error in the predicted *convective* heat flux from the gas to the gauge, something that is difficult for FDS to predict given the complexity of the cable tray geometry. Figure D-18 – Figure D-21 shows the predicted cable surface temperatures for Test 2 and Test 4.

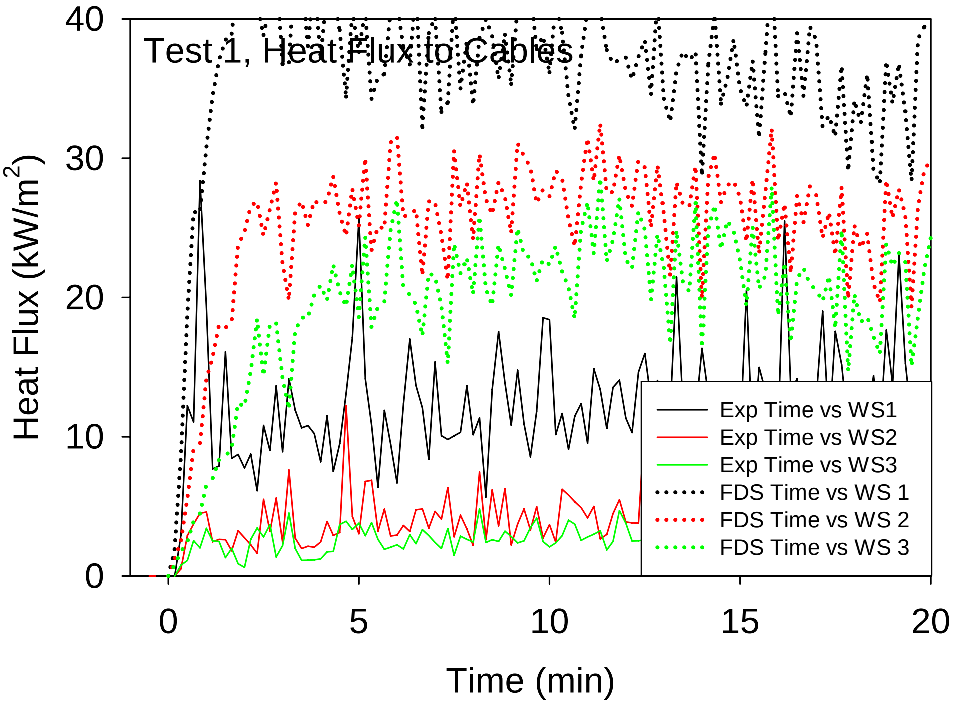


**Fig. D-10** Heat flux to cables, no pre-heating, Test 1.

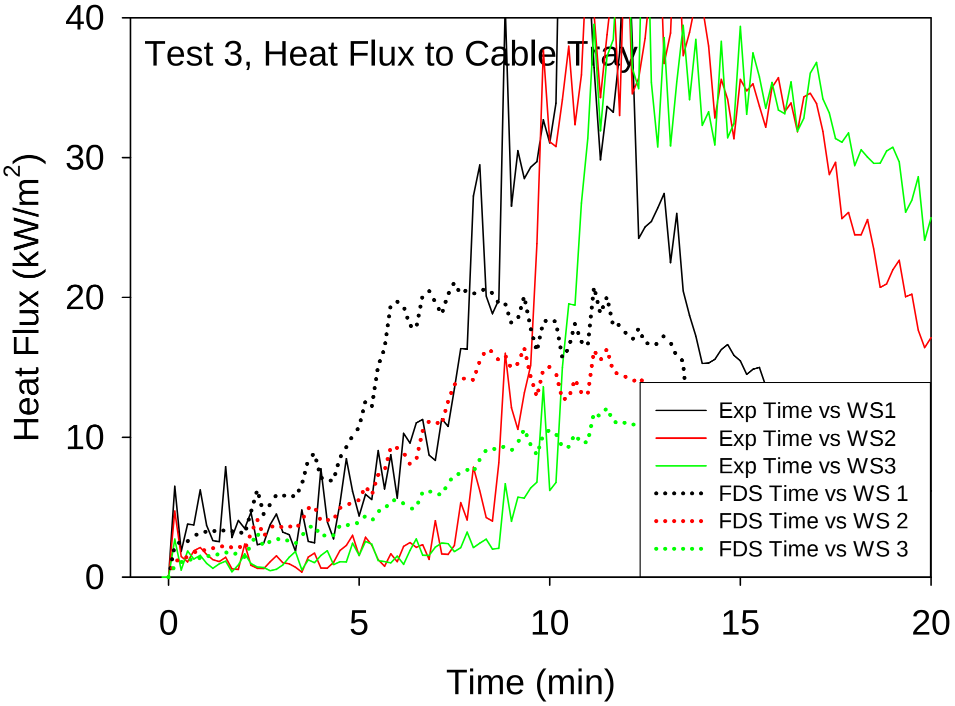


**Fig. D-11** Heat flux to cables, no pre-heating, Test 3.

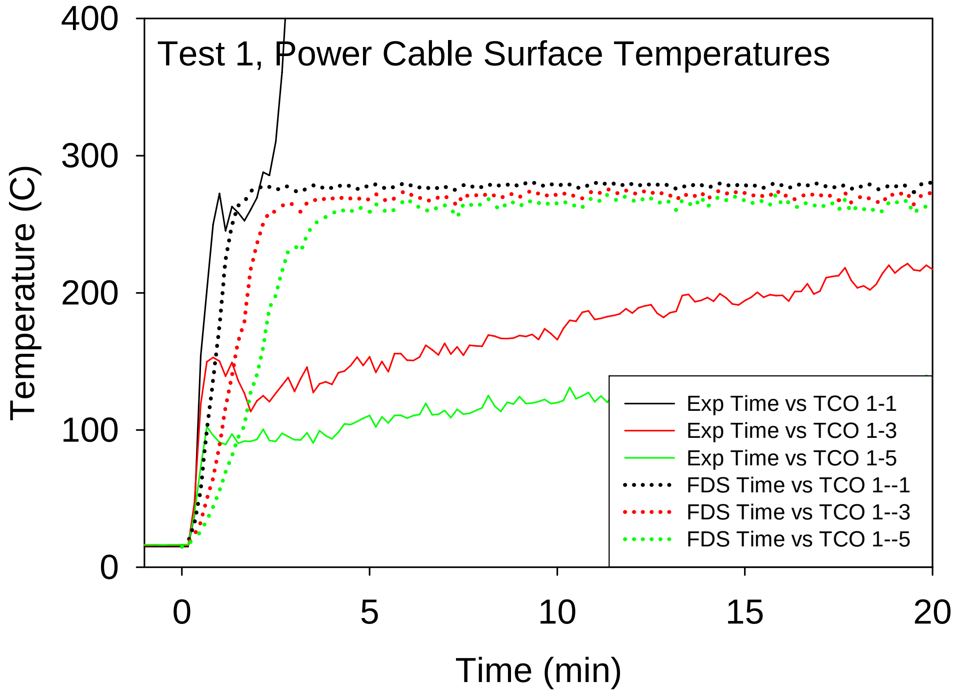


**Fig. D-12** Surface temperatures, no pre-heating, Test 1.

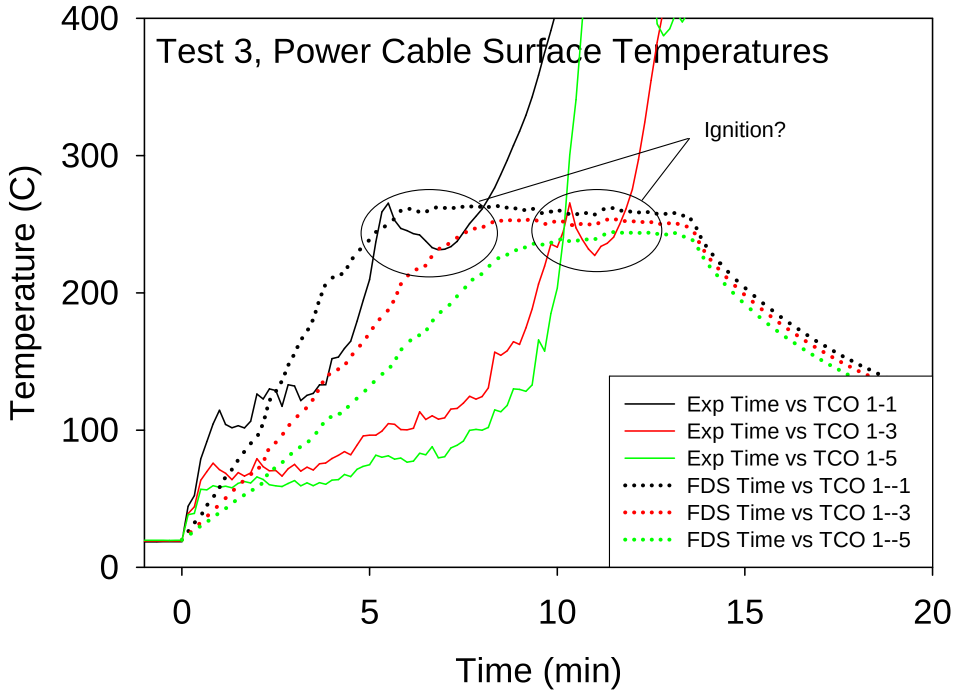


**Fig. D-13** Surface temperatures, no pre-heating, Test 3.

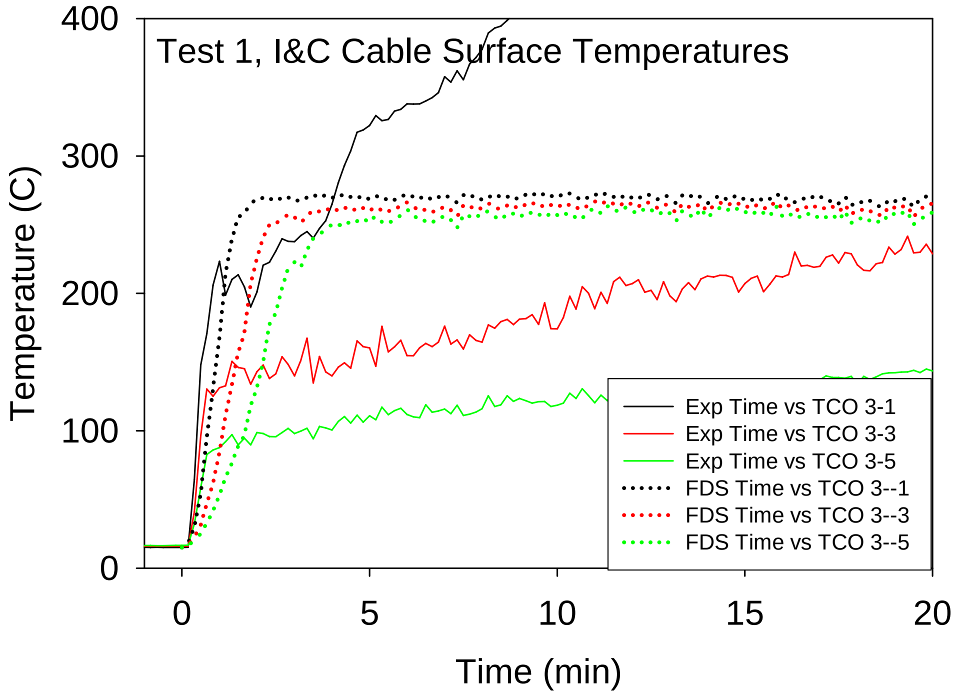


**Fig. D-14** Surface temperatures, no pre-heating, Test 1

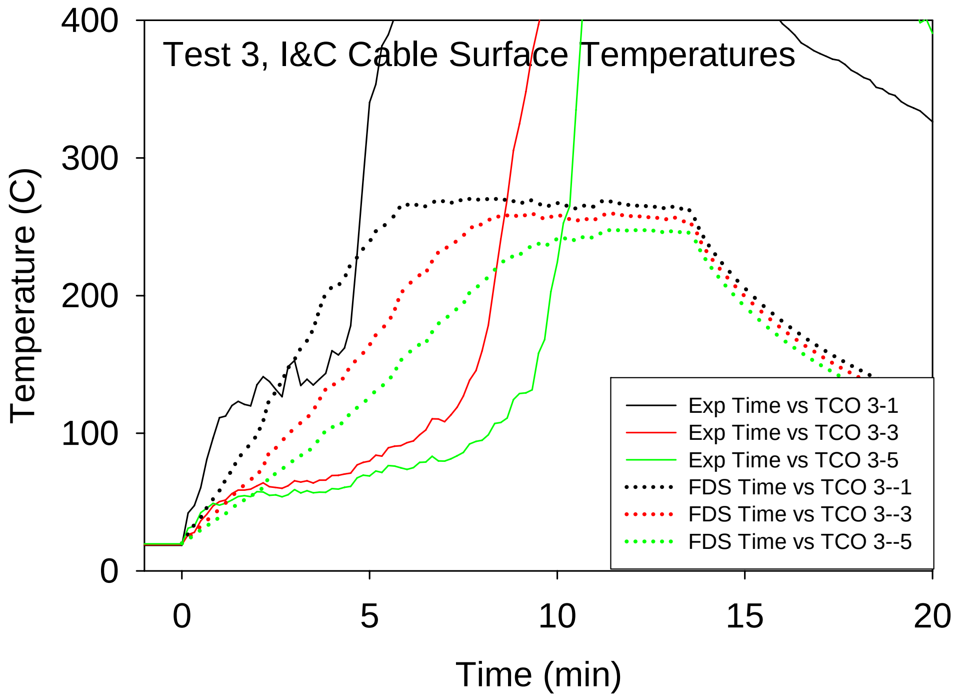


**Fig. D-15** Surface temperatures, no pre-heating, Test 3.

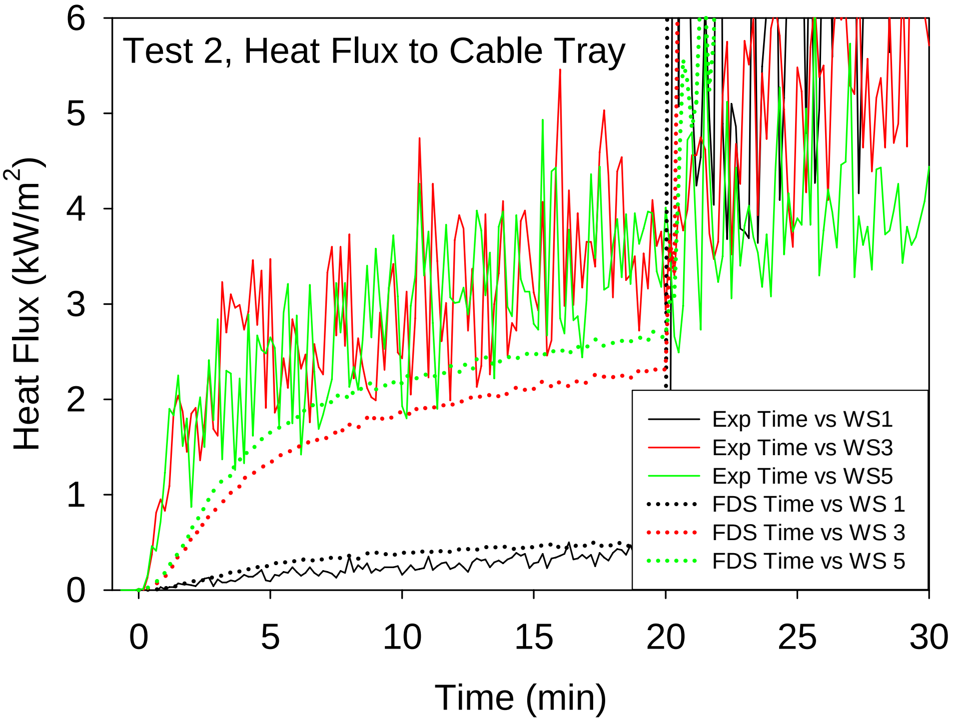


**Fig. D-16** Heat flux to cable tray, with pre-heating, Test 2.

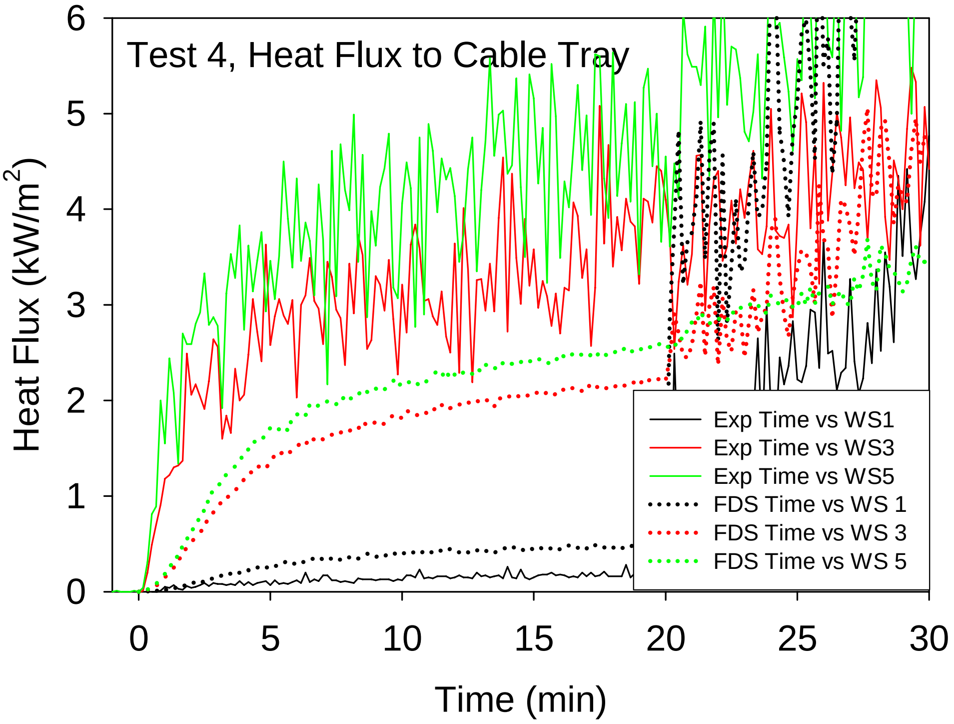


**Fig. D-17** Heat flux to cable tray, with pre-heating, Test 4.

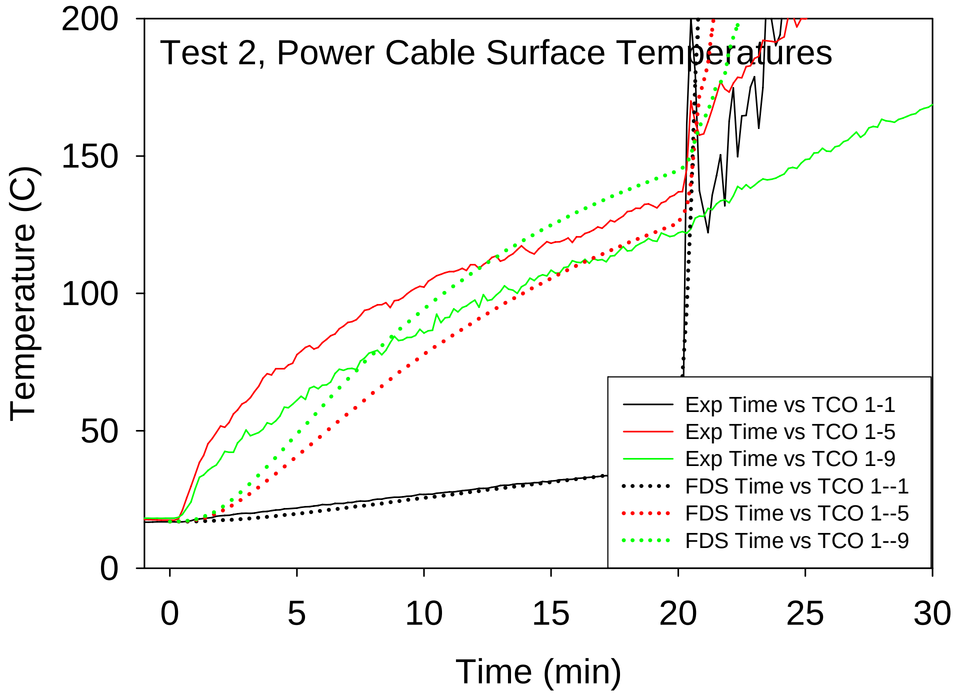


**Fig. D-18** Surface temperatures, with pre-heating, Test 2.

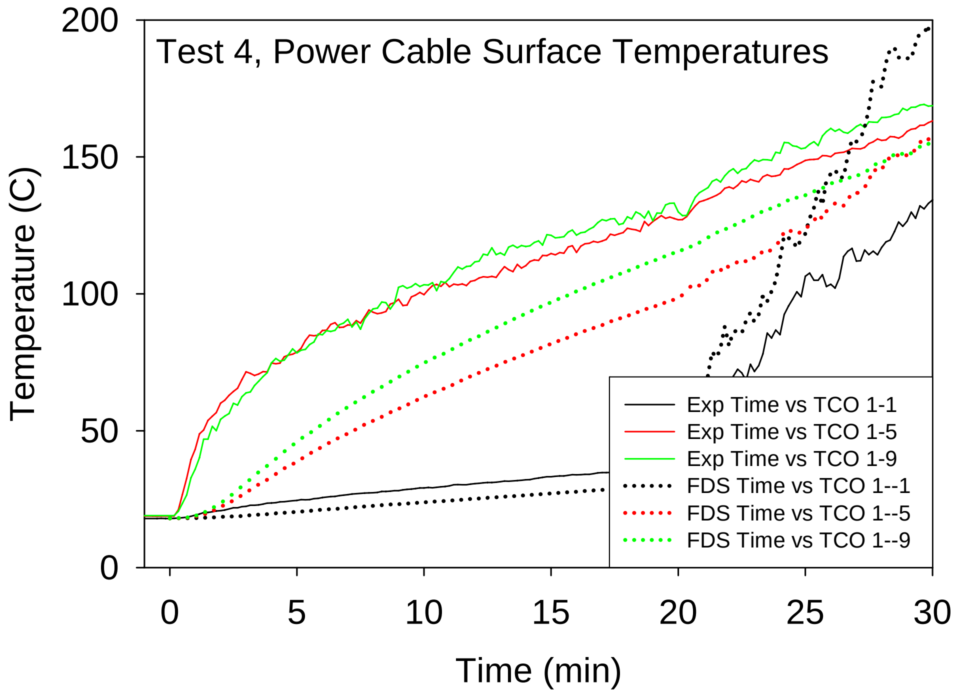


**Fig. D-19** Surface temperatures, with pre-heating, Test 4.

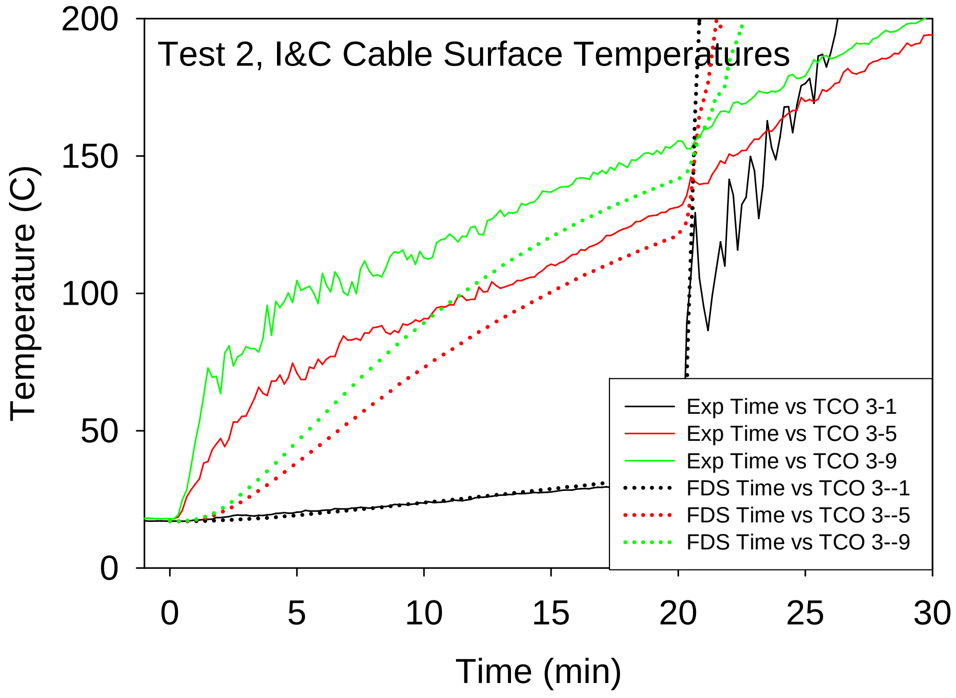


**Fig. D-20** Surface temperatures, with pre-heating, Test 2.

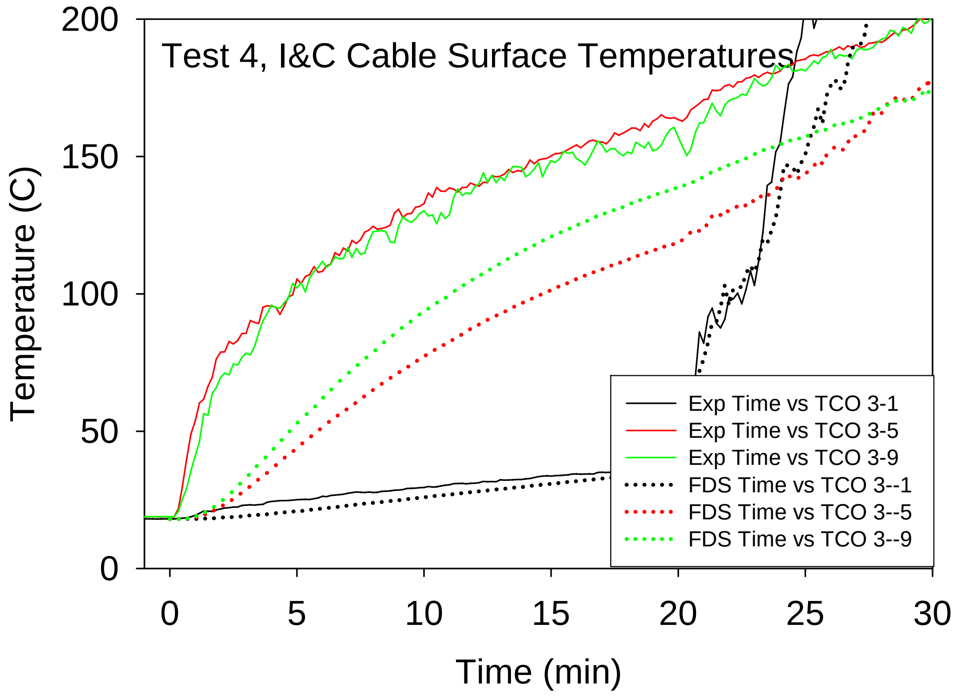


**Fig. D-21** Surface temperatures, with pre-heating, Test 4.

# D4 General Conclusions and Recommendations

Simulations of Benchmark Exercise 5 were performed with the NIST Fire Dynamics Simulator (FDS). The goal of the exercise was to predict the ignition and upward spread of fire along two sets of bundled power cables. Although the pyrolysis model within FDS was not designed for this type of simulation, it was nevertheless useful to simulate the experiments to the extent that the model could, and examine the results to gain some insight into the detailed solid phase behavior.

## D4.1 General Conclusions

The bundled cables were modeled as thin-skinned solids. In some of the tests, the cable surface temperature predictions followed the measurements to some extent, but could not simulate the behavior beyond ignition. The qualitative trends in the measured cable temperatures were not captured by the model.

Clearly, FDS in its current form is not suited for this type of prediction. Engineers using FDS to study actual fires have often 'tuned' the solid phase parameters to match a given experiment, but this should be considered *calibration*, not *validation*. No attempt was made in this exercise to 'tune" the parameters. Rather, the model was run using as many of the given material properties as possible.

## D4.2 Recommendations

It is not possible to say now how well any CFD fire model could predict the burning behavior of a complicated fuel. From the engineer's perspective, it will always be more difficult to predict the burning rate than to calculate the transport of the heat and combustion products because the number of input parameters required for the burning rate prediction is far greater than the transport. Given the difficulty and the increased uncertainty associated with a burning rate prediction, it is debatable whether or not large-scale CFD fire models ought to develop pyrolysis models at this level of complexity.

Assuming for the sake of argument that there is a desire to predict cable tray burning rates, consider two general approaches: empirical and deterministic. An empirical model would use data from experiments to characterize the burning and flame spread rates as global functions of the cable's material properties and geometry. Such a model would avoid directly computing the complex chemical and heat transfer phenomena. A deterministic model would attempt to predict the burning and spread directly from a calculation of the thermal environment surrounding the cables. Only the physical and geometrical properties of the cables would be required as input. Such a model would have to directly account for the complex heat transfer between the cables in the bundle.

At present, FDS cannot resolve the air gap between the cables. It assumes the bundle to be a solid slab (like a log), rather than a collection of thin cylinders (like kindling). For the same reason that one cannot start a fire in a fireplace with only a single log, FDS cannot predict sustained flame spread over a solid slab of plastic. The model lacks the heat trapping provided by the air gap between the cables. Using finer and finer grid cells to accomplish this is impractical, thus a purely deterministic model seems out of the question. It is possible that the entire cable bundle assembly could be divorced from the gas phase grid, allowing the cables to be represented by something other than a solid slab. Some researchers model a complex object as a collection of small 'particles", each having properties similar to the solid material, which act collectively like the object itself. Cable bundles, for example, might be modeled as a collection of small cylinders whose interaction with each other would be almost completely separate from the gas phase calculation.

Regardless of the specific form, detailed solid phase pyrolysis models should evolve over time. Validation experiments should start with objects that are simpler in form and composition than bundles of cables. Such experiments should focus solely on the burning rate prediction. There is no need for extensive compartment instrumentation. There should be enough measurements of the near-field thermal environment to allow for an assessment of each phase of the burning process: heat flux, surface temperature, ignition source, *etc*. The thermal properties of the materials should be comprehensive and from a single source. The various properties of the cables given in BE #5 were not consistent, nor from a single source. There are no set rules on how to measure the heat of gasification, ignition temperature, or heat of combustion. These values need to be clarified. In fact, the models should be used to simulate the experiments performed to obtain the properties (like the Cone Calorimeter tests) even before being used to simulate the desired experiment. This would indicate immediately if the model has the necessary physical algorithms to simulate the observed behavior.

## D5 References

/MCG 04/ McGrattan, K.B. (ed.) 2004:
Fire Dynamics Simulator (Version 4), Technical Reference Guide. NIST Special Publication 1018, National Institute of Standards and Technology, Gaithersburg, Maryland, USA, 2004

# Appendix E: COCOSYS Calculations for Benchmark Exercise No. 5

**Presented by**

**Walter Klein-Hessling**

Gesellschaft für Anlagen- und Reaktorsicherheit (GRS) mbH

Schwertnergasse 1, 50667 Köln, Germany

## E1 Introduction

Within the framework of the ‘International Collaborative Project to Evaluate Fire Models for Nuclear Power Plant Applications” a fifth benchmark exercise has been performed. The main objective of this benchmark has been the evaluation of temperatures loads and fire propagation on vertical cable trays with different material (PVC and FRNC) and different pre-heating conditions. This technical note presents the results of the COCOSYS calculations.

COCOSYS is a so-called lumped-parameter code. To simulate the local conditions (natural convection, temperature stratification) the fire compartment has been divided into a large number of control volumes. The main idea is to have for each temperature measurement or temperature point for comparison a separate control volume and to have separate control volumes around the fire plume, the ventilation system and the doors and openings, respectively.

For the simulation a 3D grid has been created using the grid generator GRIDGEN. With a specific interface routine a COCOSYS input file has been created. This interface routine calculates the view factors between different walls and from the control volumes to the walls using a Monte-Carlo-Simulation method. By this it is possible to simulate the heat release by radiation to the different targets in a realistic way.

In total 4 tests have been performed. Due to troubles with stability blind calculations have been performed only for the tests without pre-heating (Test 1 and Test 3). To overcome the problems for heating of the cables by the gas burner and to handle the remaining cable mass fractions the models in COCOSYS have been somewhat improved. Open calculations have been performed for all tests.

## E2 Nodalization and Models Used

COCOSYS is a so-called lumped-parameter code /ALL 05/, dividing the compartments into several control volumes, where the mass and energy balance is solved. The main difference between COCOSYS and CFD codes (like CFX or FDS) is that the momentum balance is not considered. The fire compartment has been subdivided into 11 levels of zones with in total 478 zones. Close to the vertical cable trays and gas burner and ethanol pool the size of the zones is smaller (Fig. E-3 and Fig. E-4). The gas burner and the ethanol pool are simulated by the fuel fire pyrolysis model in COCOSYS with a user defined pyrolysis rate. The radiation fraction of the gas flame is assumed to be 40 %. For the ethanol fire a value of 20 % has been used. In the open calculation the combustion model parameters have been adjusted to get a more realistic height of the fire and more complete combustion of the propane. In Tab. E-2 a list of the modified parameters is given.

The cable trays are simulated with the so-called simplified cable burning model. This model assumes a constant specific pyrolysis rate R [$kgs^{-1}m^{-2}$] and a propagation velocity $v_{\pm}$ [m/s] in the positive and negative direction. The resulting pyrolysis rate is assumed as:

$$r = Rb\,(d_o + vt) \tag{1}$$

with the reaction rate r [$kg\ s^{-1}$], the initial burning length $d_0$ and the width b [m] of the cable tray (**Fig. E-1**). The flame propagation depends on the direction of the tray. Therefore, the model distinguishes between horizontal and vertical cable trays. The propagation velocity may depend on the surrounding zone temperature. For the connection of different cable trays or tray segments the relative position of the connection are given by the user (**Fig. E-2**). It is possible to connect the tray segments at each end point (segmentation of cable trays according to the control volumes), or to define a crossing of tray segments, or to define parallel tray segments. The user defined distance $\Delta$ defines the time needed to propagate from one to the other tray segment

$$t_{prop} = \frac{\Delta}{v_{\pm}}\,. \tag{2}$$

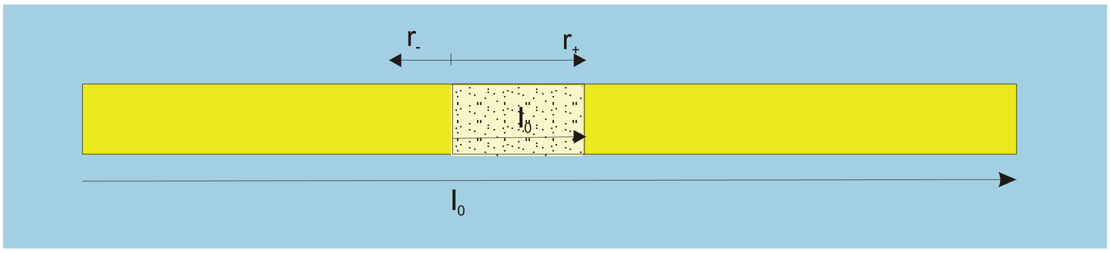


**Fig. E-1** Concept of the simple cable pyrolysis model

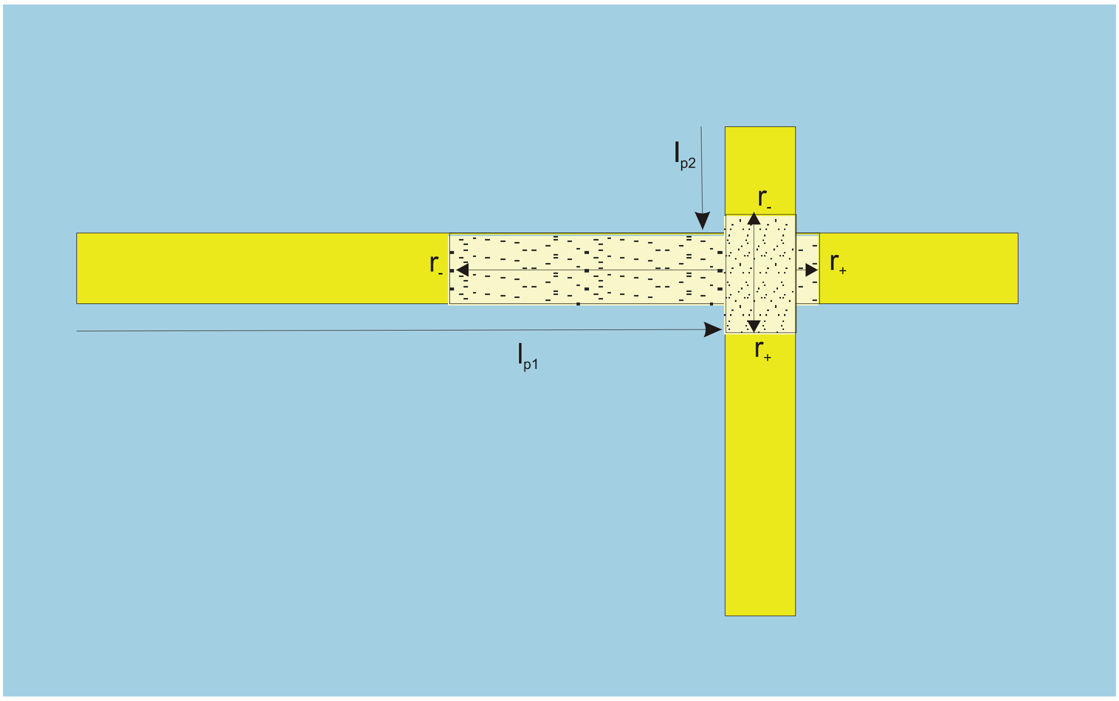


**Fig. E-2** Fire propagation along connected cable trays

For a cable tray several conditions for ignition or termination of pyrolysis (see Tab. E-1) exist.

The simplified cable burning model considers somewhat the thermal hydraulic boundary conditions, but the real temperatures on the cable surface needed for a deterministic calculation of the pyrolysis are not calculated. Especially under low oxygen conditions this model may lead to some deficiencies. Therefore, an additional criterion has been introduced for low oxygen conditions to reduce the pyrolysis rate. The considered species in the cable burning model are $H_2$, HCl, CO and $CH_X$ fractions. As already used in the oil burning model these fractions may combust in the atmosphere or be transported to other regions under low oxygen conditions.

**Tab. E-1** Criteria for ignition of a cable tray or stop of burning

| Reason | Criteria | Time delay |
|---|---|---|
| Ignition via signal (user input) | $l_0$, $d_0$ | - |
| High zone temperature | $T_{ign}$ | $t_{delay}$ |
| Ignition via another cable tray | $l_0$, $d_0$ (calculated by connection data) | $\frac{\Delta}{v_{\pm}}$ |
| Finish due to low zone temperature | $T_{out}$ | $t_{out}$ |
| Complete burn out | $t \geq t_{e_{\pm}}$ | |

The vertical cable trays are simulated as rectangular plates. Heat flow is assumed only on the plate surface only. Side effects are not considered. Especially close to the gas burner this may lead to an underestimation of the cable heating. In the blind calculations, the cables are heated from one side only. Introducing some additional junctions in the plume region the plume diverging is somewhat considered and the cables may be heated from the opposite side also (Fig. E-5).

To simulate cable tray bundles with rectangular slabs the following calculations have been used:

– The density of the slab is calculated by the average density of combustible and non-combustible material

– For the specific heat a value of 1676 J/kgK has been used. The heat conductivity has been estimated to yield the given factor of cp.

– The width of the slab can be calculated by the number of cables and the given diameter.

– The thickness of the slab has been calculated by the combustible volume of one cable and the number of cables divided by the width of the slab. The non-combustible volume is not considered here.

– For the simple cable burning model the density (kg/m²) of combustible material is needed. This could be calculated by the number of cables, the density and the volume of one cable divided by the width of the slab.

The hood is simulated with a fan system using the specified volume flow rate.

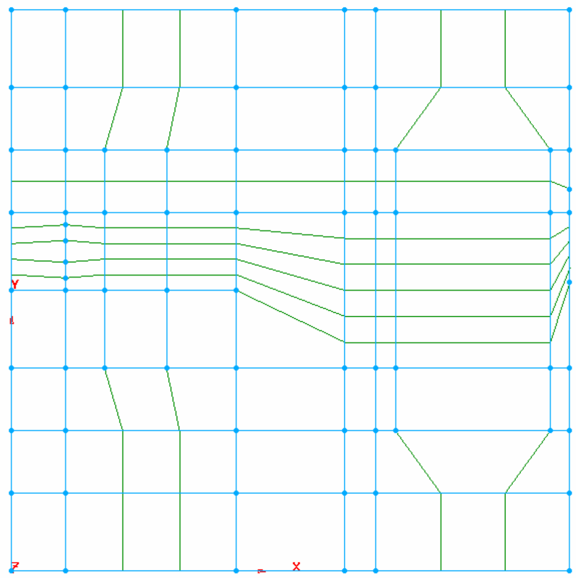

**Fig. E-3** Top view of the nodalization

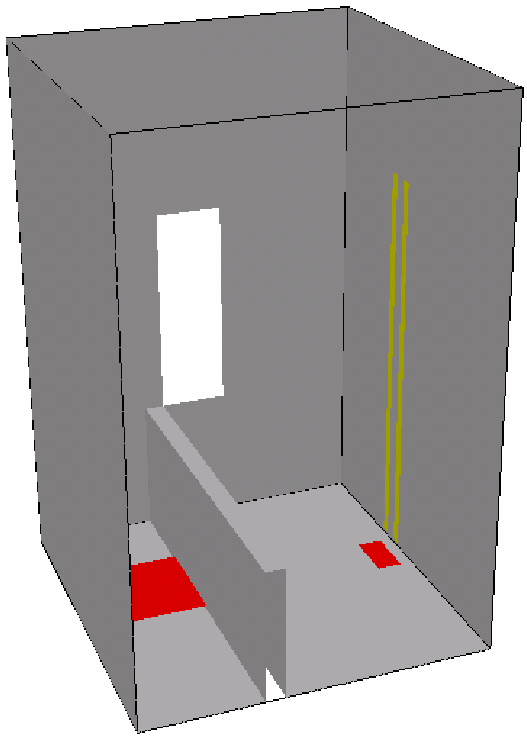

**Fig. E-4** 3D view of the experimental set-up

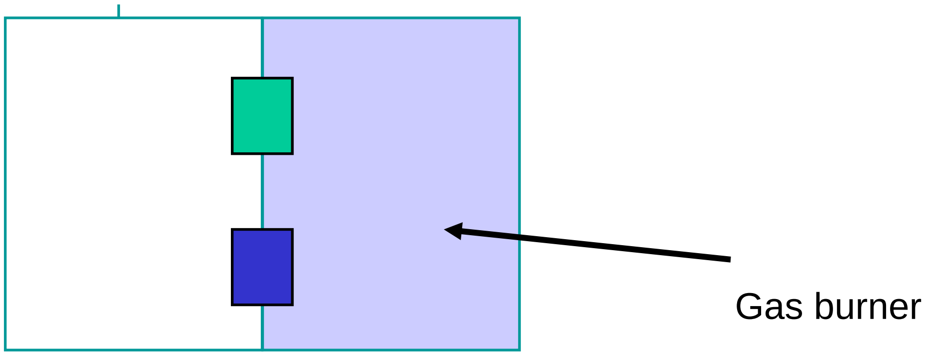


**Fig. E-5** Nodalization around the gas burner and vertical cable tray

**Tab. E-2** Modified parameters in blind and open calculations

| Parameter | Blind calculation | Open calculation |
|---|---|---|
| Radiation fraction HFRAD | 0.35 | 0.40 |
| Mixing factor PYRMIX | 0.5 | 0.75 |
| $CH_X$ reaction limit | 0.24 Vol% | 0.01 Vol% |
| Efficiency FEFF | 0.95 | 1.0 |
| Flame temperature | - | 773 K |
| Ignition temperature inside control volumes | 300 °C | 150 °C |

## E3 Results

In the following, the results of the blind and open calculations are described. As mentioned in the introduction blind calculations have been performed for the Tests 1 and 3 only. In Test 1 and 2 the FRNC cables are more or less not burning. This makes the situation somewhat easier. Therefore this experiment and the COCOSYS results are discussed first. In these calculations the developer version of COCOSYS has been used. The results of the blind calculations are shown in red curves and from the open calculation in blue curves. The experimental data is presented in dashed black lines always.

### E3.1 Test 1: FRNC Cable without Pre-heating

In this experiment the initial power of the gas burner was about 150 kW. This was increased at about 2500 s to more than 300 kW. **Fig. E-6** shows the comparison between experiment and open calculation for the energy release due to combustion. Far away from the burning process the comparison between measured and calculated temperature is quite good. The temperature range between TP2 and TP6 was simulated quite well, although the degree of the temperature stratification is underestimated. The results of the blind calculation are somewhat better compared to the open calculation in the initial phase (Fig. E-7). In the following the temperatures at the tree position TR1 (between burner and door) and TR5 (close to burner) will be discussed. The temperatures at the uppermost position 7 are overestimated by about 40 K, especially after the increase of the burning power. The main reason will be the underestimation of the air entrainment and divergence of the fire plume. Introducing some additional junctions in the plume area, leading to a spreading of hot gases improves the situation. Further the stability problems in the blind calculations are somewhat solved (see **Fig. E-8** and Fig. E-9). **Fig. E-10** and Fig. E-11 show the surface temperatures at the backside wall TW1 and the left wall TW2 close to the gas burner. The maximum temperatures at the backside wall are underestimated by about 20 K. But opposite to this the temperatures at the location TW2 are over estimated by 50 K. Between the cable tray and the wall there is one control volume per level only. This may lead to overprediction of the convective heat transfer. Particularly the temperatures in the lower regions are overpredicted. **Fig. E-12** shows the temperatures measured at the door opening. The results of COCOSYS are quite reasonable. The maximum temperature is underestimated by 25 K only. Also the distribution of inflow and outflow area is simulated quite well.

In the following, the temperatures at the cable trays will be discussed. In the blind calculations these temperatures were strongly underestimated. The following reasons are possible for the underestimation:

– The calculated zone temperatures are in some way an average temperature and lower than a realistic flame temperature. The heat release by radiation is distributed in the total control volume. The fraction released into the cables may be too low.

– The flow pattern inside the fire close to the cable trays is strongly turbulent. This may be underestimated by the usual heat transfer coefficients for natural convection.

– The heat transfer area is assumed to be a plate and will be lower than the combination of a set of cable bundles.

For the open calculation the COCOSYS program has been extended with a new heat transfer model ‘FLA’. This heat transfer uses a user-defined flame temperature instead of the local zone temperature. Additional the characteristic length has been further reduced increasing the heat transfer to the cables. For the comparison between experiment and measurement one has to consider, that the positions TCO2 and TCO4 are located much more inside the cable package. For the comparison the first layer temperature has been used always (calculated results TCO1 and TCO2 are the same). Examination of the experimental results for the power cable (Fig. E-13 and Fig. E-14) indicate that the differences in the temperature are sometimes more than 200 K, especially at the beginning of the experiment. This shows the influence of the location of temperature measurement. Further only the lower two positions show a larger temperature increase higher then 400 °C. These details cannot be simulated with COCOSYS which handle the cables as a rectangular block. The situation for the control cables is quite similar (Fig. E-15 and Fig. E-16) except that position 4 shows a temperature increase also at the end of the experiment. On the one side it looks like flame propagation, but on the other side there is practically no mass loss (about 5 kg only). The calculated temperatures of the open simulation are now much better compared to that of the blind calculation, although the deviations are still about 200 K for the maximum temperatures. The temperature increase in the upper region is simulated quite well. The situation for the inner cable temperatures is quite similar (Fig. E-17 to Fig. E-20). Here the slabs 9 and 2 have been used for TCI1 and TCI2, respectively. The measured inner temperatures give some indication for an ignition in the control cables, which was not simulated with COCOSYS.

Fig. E-21 shows the gas concentration at location GA2 inside the fire compartment. The oxygen consumption is somewhat overestimated, but the quality of the results is still quite well. The calculated range of velocity at the door opening is simulated quite well. This is necessary to get the right mass and energy balance inside the fire compartment.

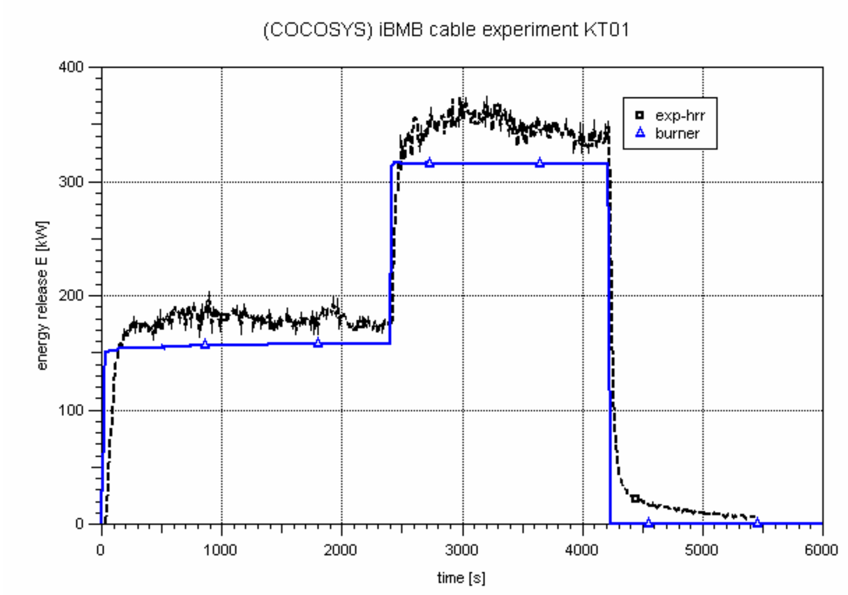


**Fig. E-6** Test 1: Energy release due to combustion

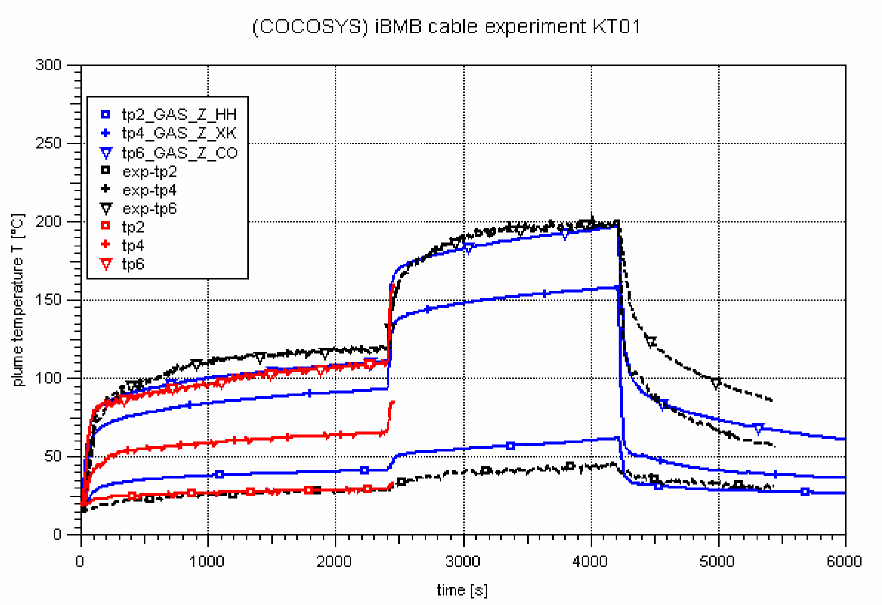


**Fig. E-7** Test 1: Temperatures at tree TP far away from gas burner

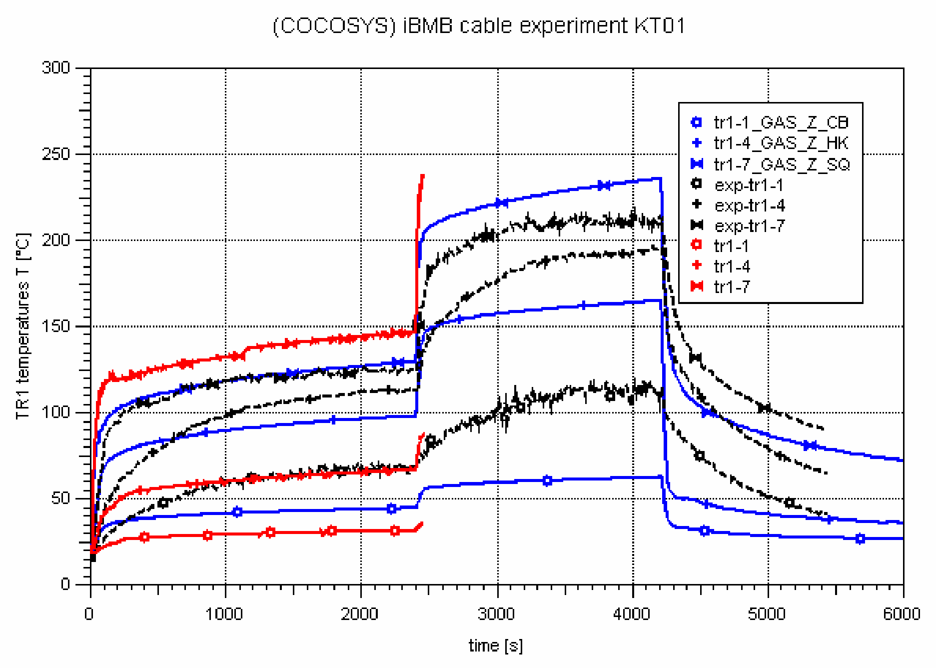


**Fig. E-8** Test 1: Temperatures at tree TR1

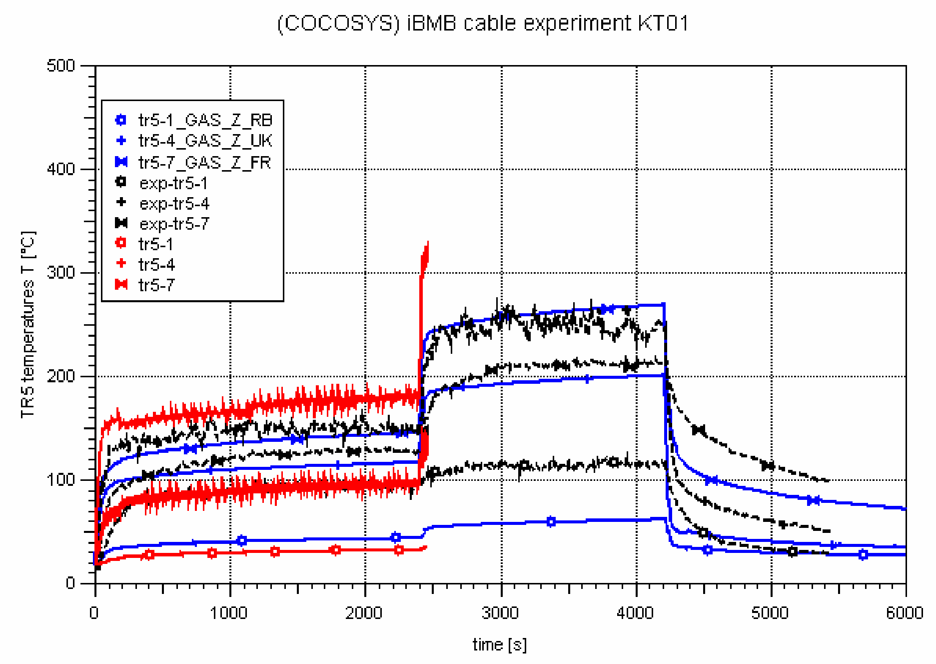


**Fig. E-9** Test 1: Temperatures at tree TR5 close to gas burner

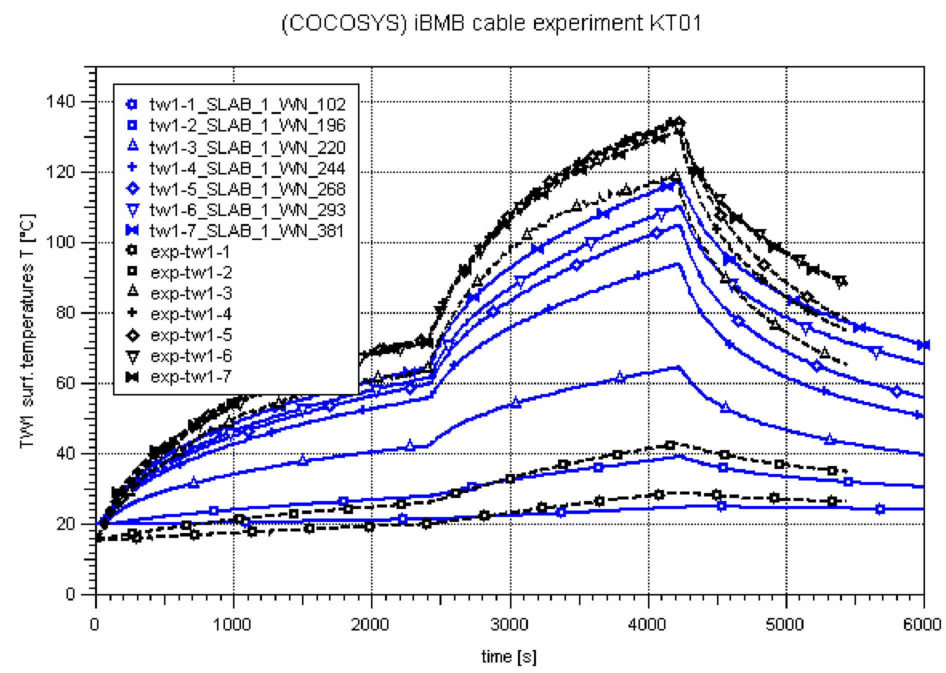


**Fig. E-10** Test 1: Surface temperature at backside wall TW1

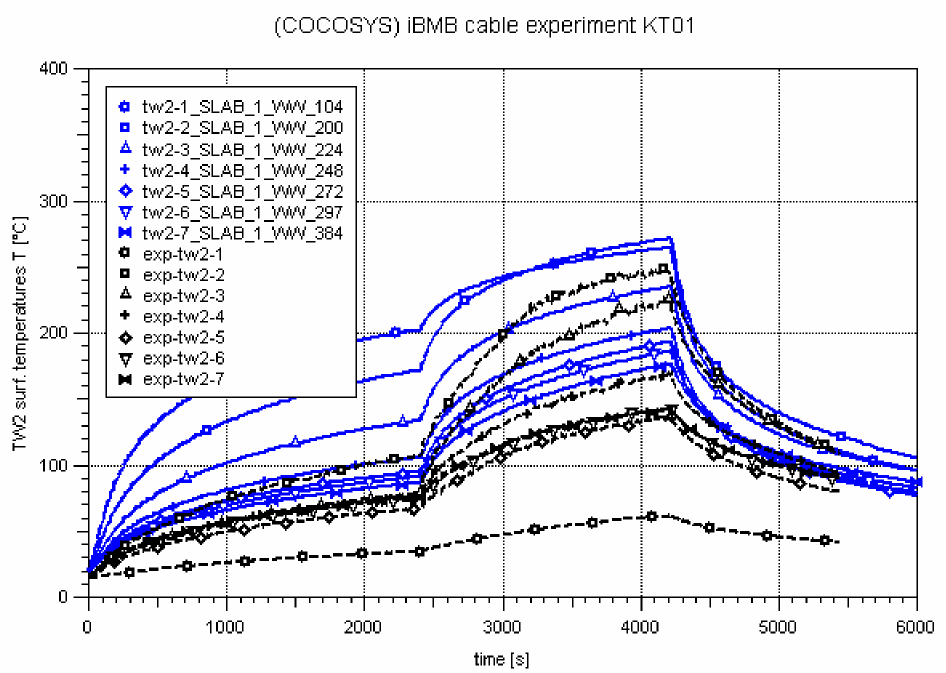


**Fig. E-11** Test 1: Surface temperature at left side wall TW2 close to gas burner

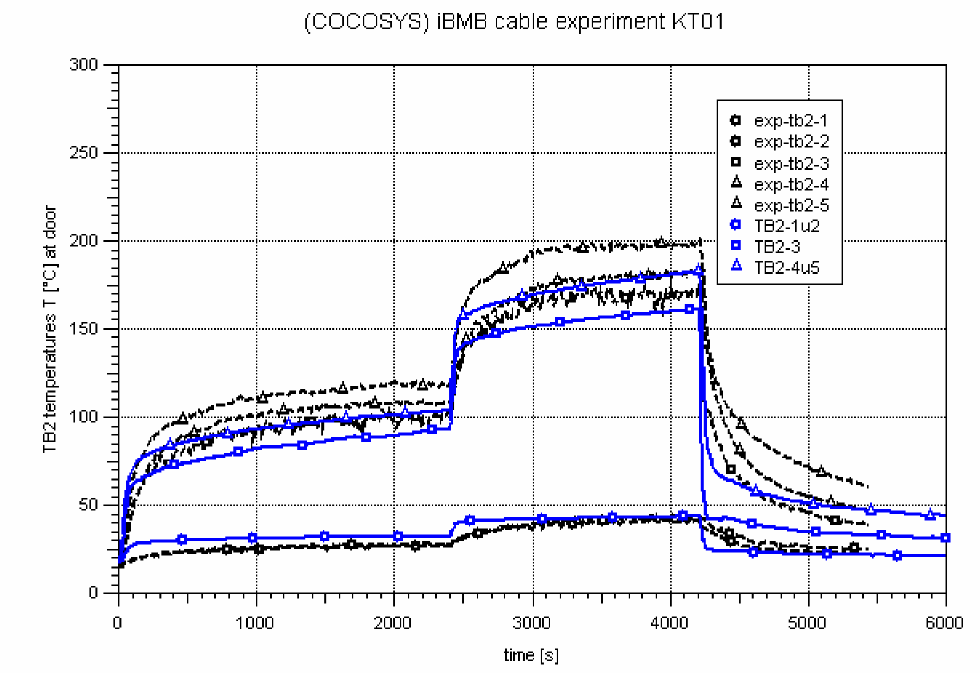


**Fig. E-12** Test 1: Temperature at door location TB2

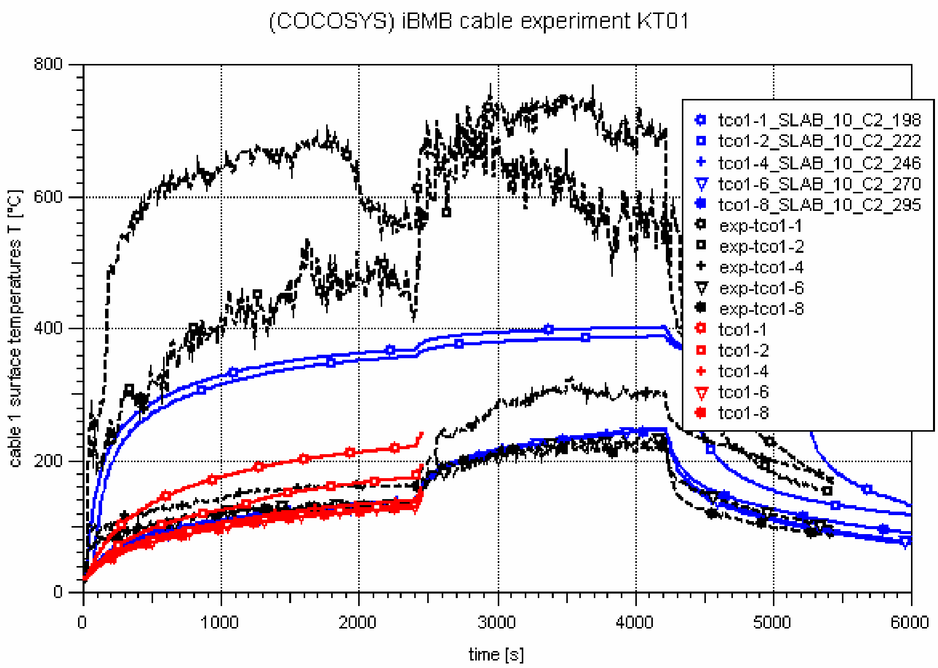


**Fig. E-13** Test 1: Cable surface temperature at TCO1 location (outside, power cable)

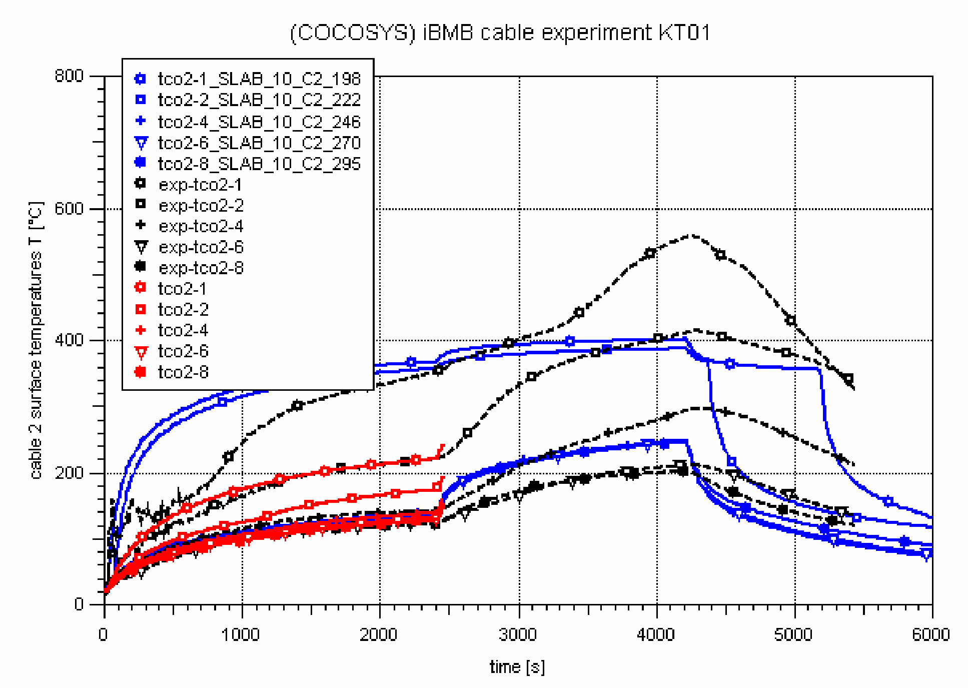


**Fig. E-14** Test 1: Cable surface temperature at TCO2 (inside, power cable)

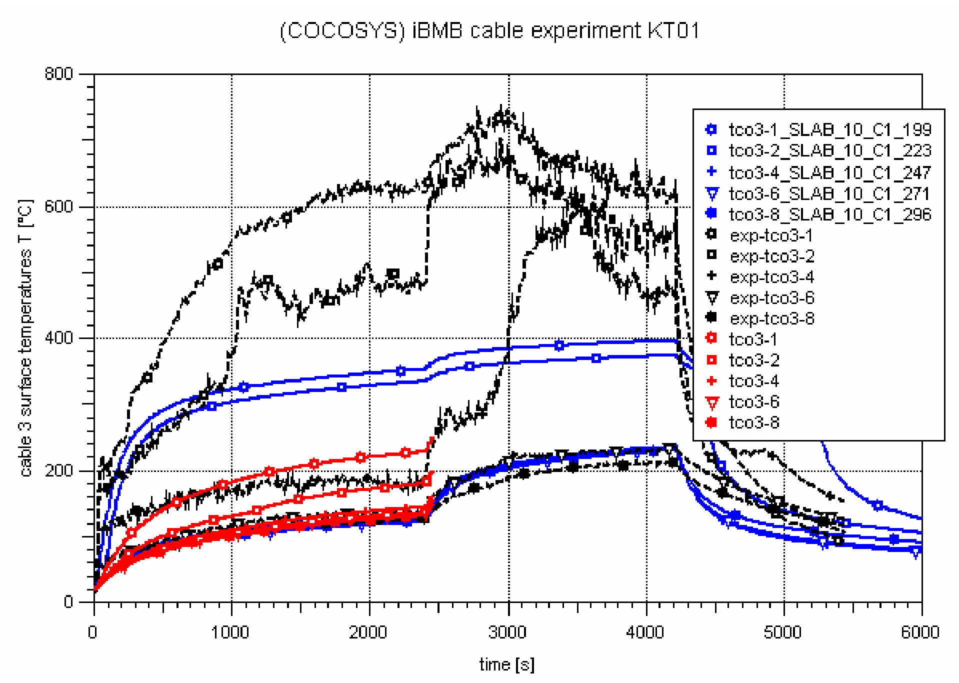


**Fig. E-15** Test 1: Cable surface temperature at TCO3 (outside, I&C cable)

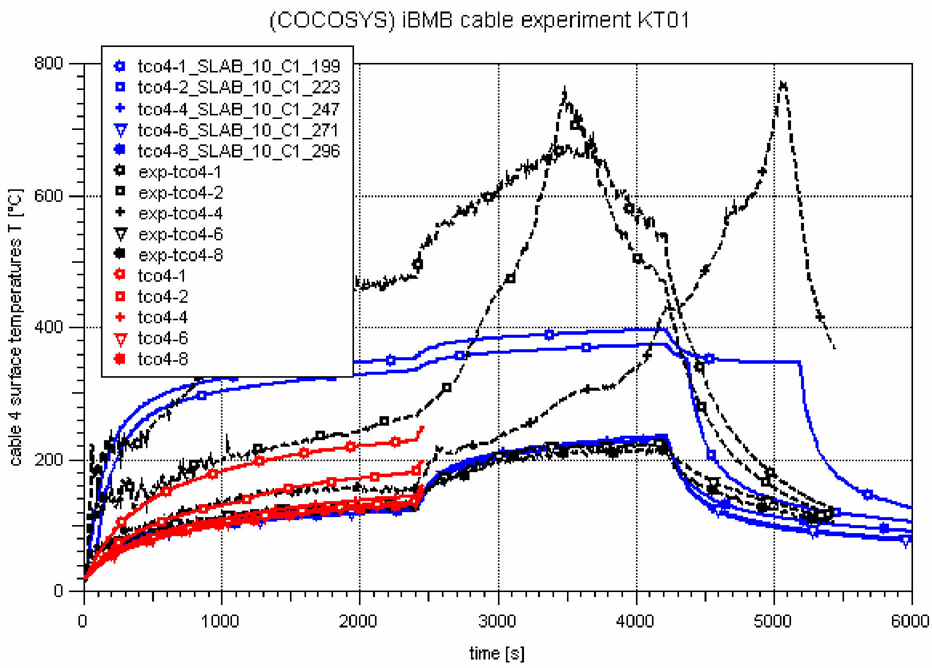


**Fig. E-16** Test 1: Cable surface temperature (inside, I&C cable)

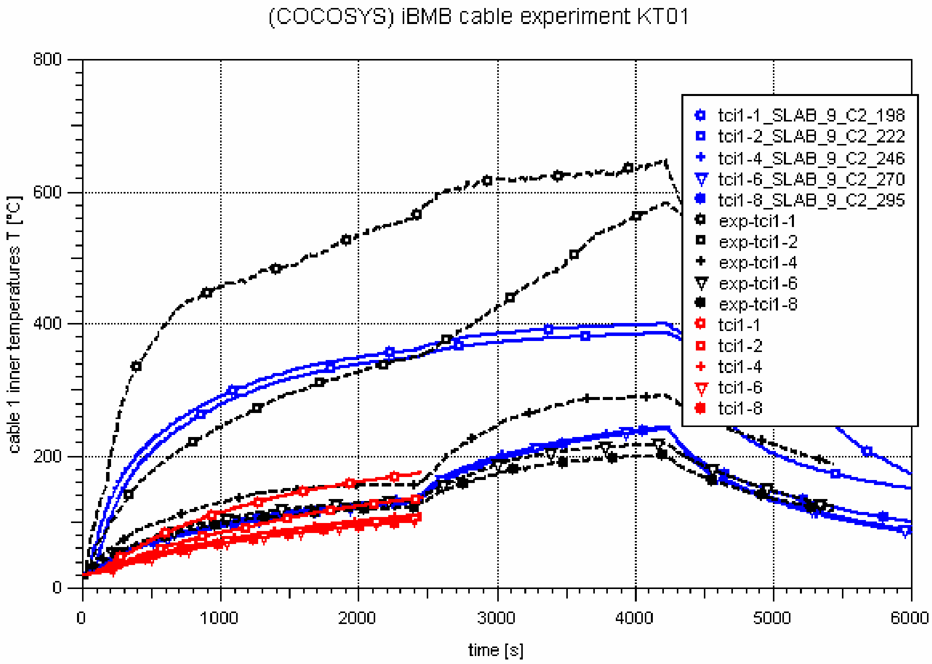


**Fig. E-17** Test 1: Cable center temperatures at TCI1

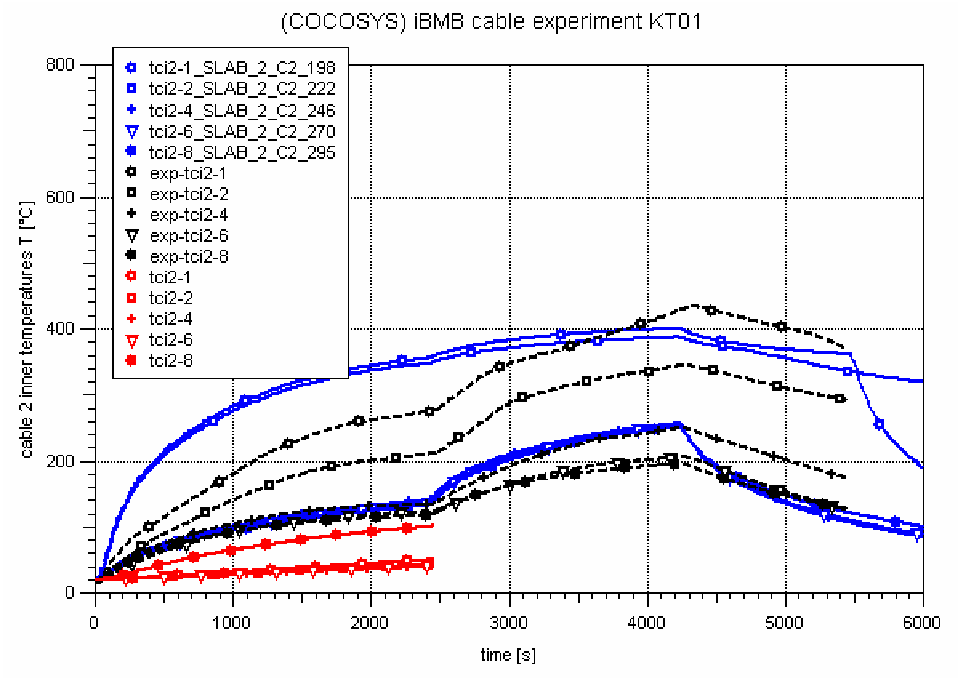


**Fig. E-18** Test 1: Cable center temperature at TCI2

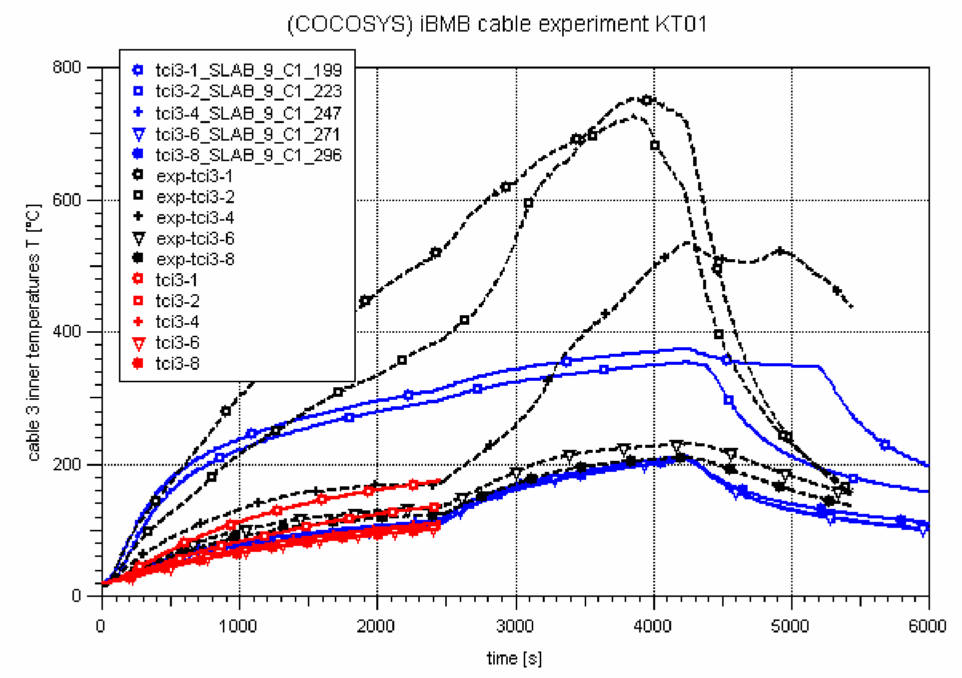


**Fig. E-19** Test 1: Cable center temperature at TCI3

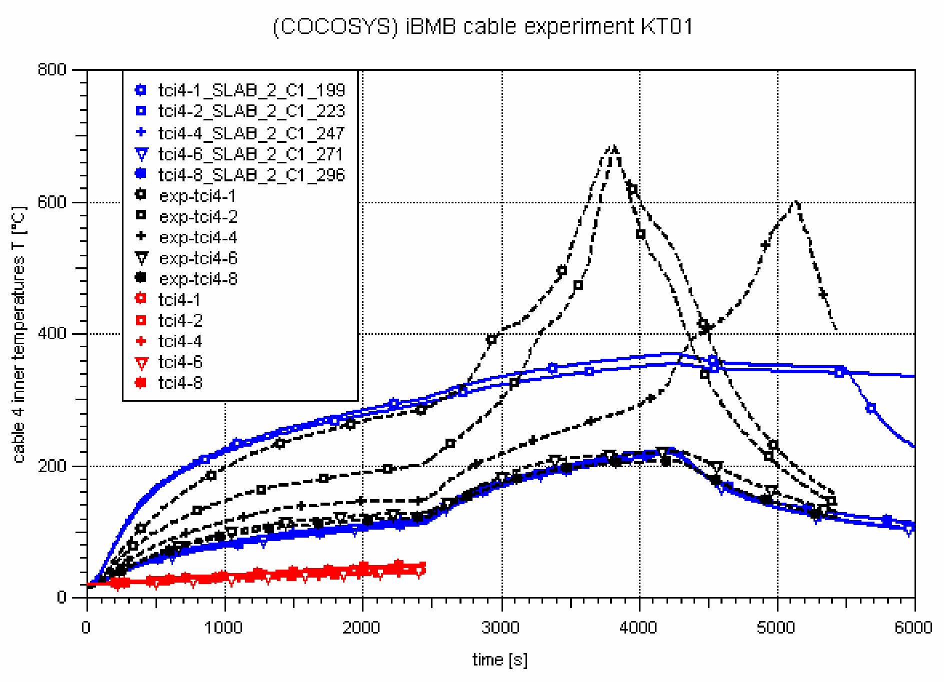


**Fig. E-20** Test 1: Cable center temperature at TCI4

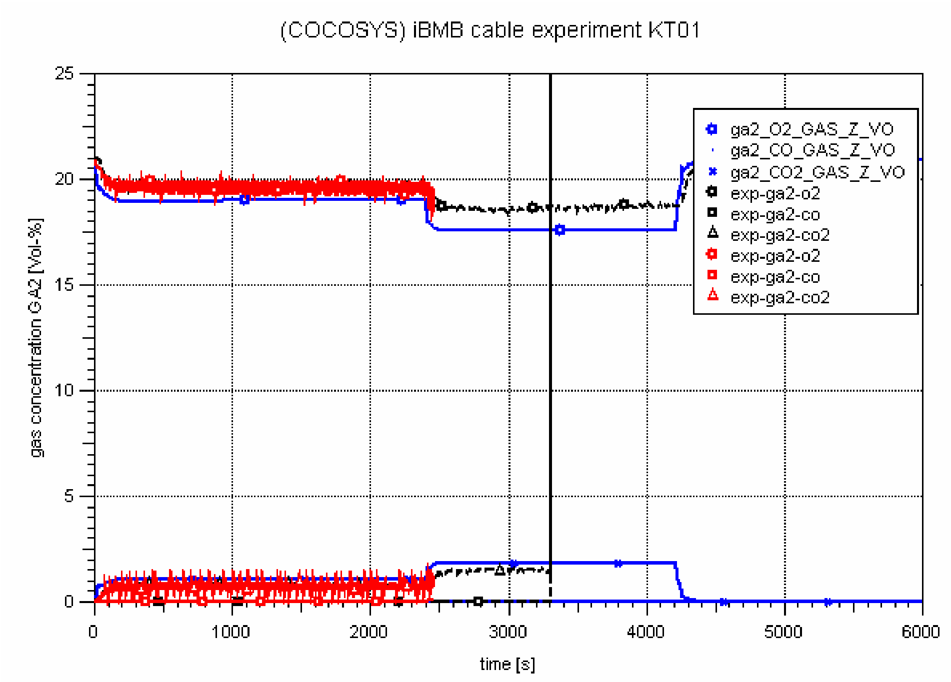


**Fig. E-21** Test 1: Gas concentration at GA2

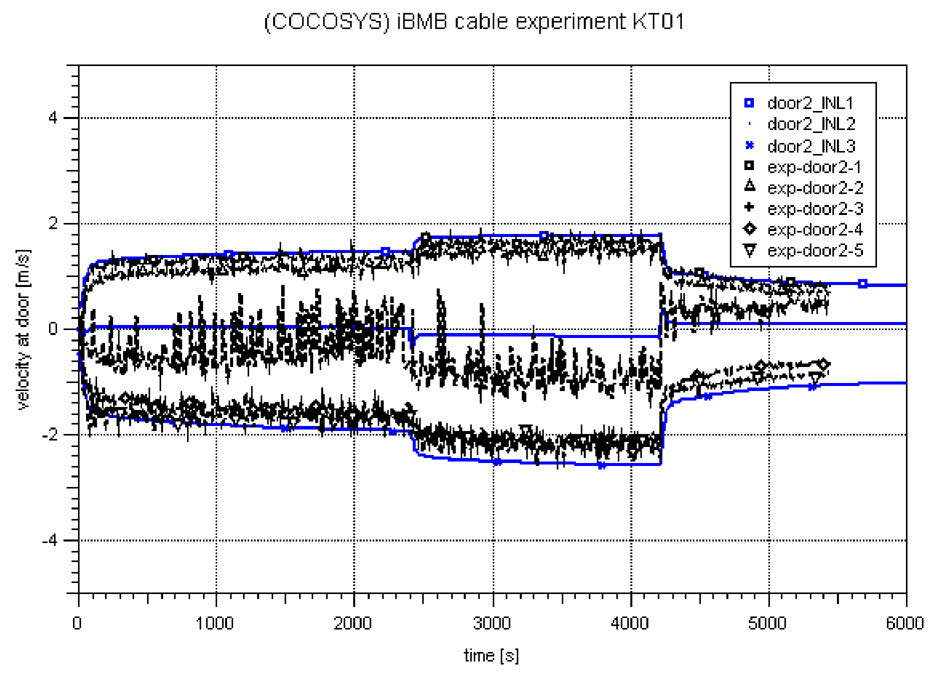


**Fig. E-22** Test 1: Velocity at door opening

### E3.2 Test 2: FRNC Cable with Pre-heating

The second experiment is quite similar to the first one. The differenc is the pre-heating with an ethanol pool fire. The start and increase of the gas burner fire could be seen in the energy release rate. COCOSYS showed quite comparable results (Fig. E-23). The temperature characteristic above the ethanol pool looks a bit different between COCOSYS results and measured values (Fig. E-24). The temperature TP2 is underestimated by COCOSYS possible due to the averaging in the control volume above the pool. The floor area of this control volume is higher than the pool surface. The temperature gradient of TP6 is calculated higher than measured.

The temperature profiles at the trees TR1 and TR5 are calculated quite well. Only the uppermost temperature is overestimated by about 100 K (Fig. E-25 und Fig. E-26). Similar good results have been obtained for the wall surface temperatures TW1 and TW2 (Fig. E-27 and Fig. E-28). Only the lowest temperature point TW2-1 has been overestimated strongly. It is interesting, to note that the result for TW2 is much better for Test 2 compared to Test 1.

In the following, the surface temperatures of the power cables (TCO1, TCO2) and the I&C cables (TCO3, TCO4) will be compared. Comparing the experimental results the results for TCO1 and TCO2 are quite different, when the gas burner has been activated (Fig. E-29, Fig. E-30). The time characteristic is quite different also. For example the temperatures of TCO2 are still rising, although the gas burner has been switched off. It is clear, that these effects cannot be reproduced by COCOSYS. Considering the local effect the COCOSYS results are quite good. The results for the I&C cables are quite similar. The differences for the experimental results are much larger between power and I&C cables then simulated by COCOSYS. This shows that the simulation of thermal load is somewhat insensitive to the detailed structure of cable material.

The quality of the results for the center temperature is quite similar to that of the surface temperature. The measured temperatures of up to 600 °C indicate some burning at the I&C cables (Fig. E-36). This was not simulated by COCOSYS.

Fig. E-37 presents the comparison for the gas concentration GA2. The oxygen concentration is somewhat underestimated. The comparison of $CO_2$ concentration is quite good.

Fig. E-38 presents the comparison of velocities through the door. In this nodalization the door area is divided into 3 areas. Anyway the simulation of the velocities in COCOSYS is quite good, underlining that the energy distribution is simulated correctly.

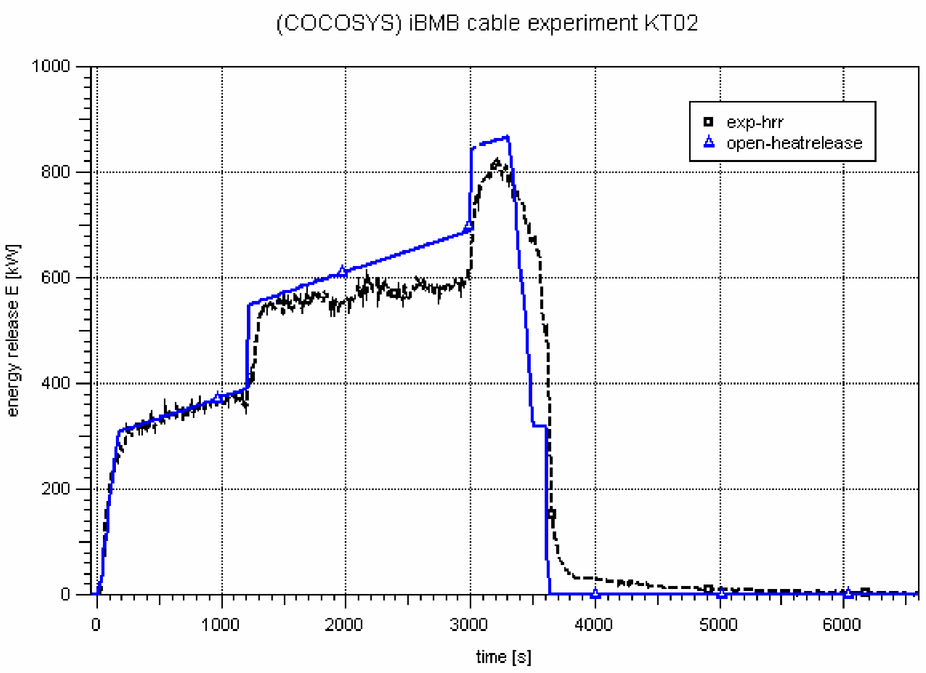


**Fig. E-23** Test 2: Energy release due to combustion

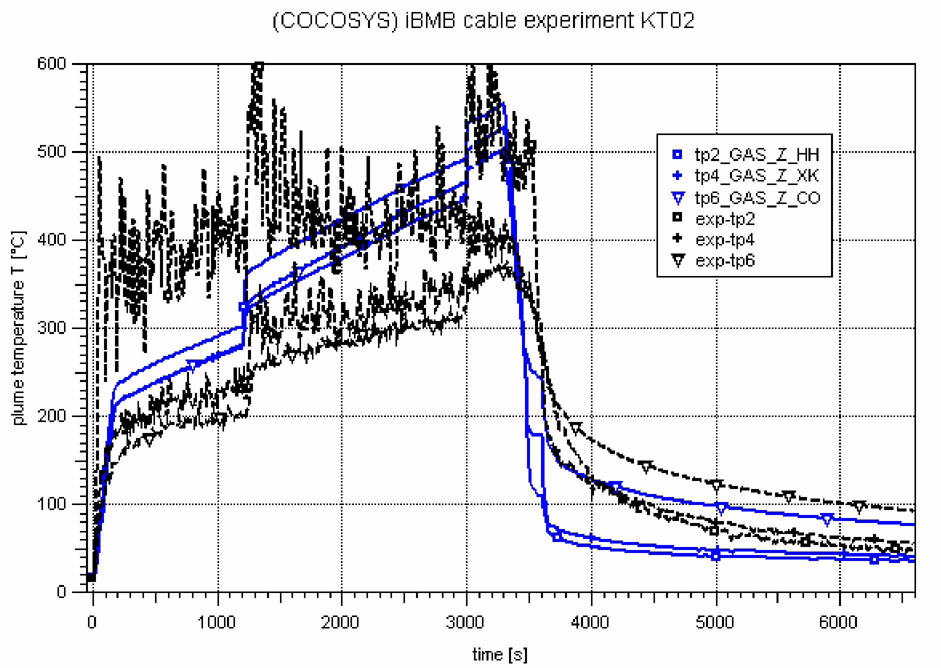


**Fig. E-24** Test 2: Temperatures at tree TP above pool

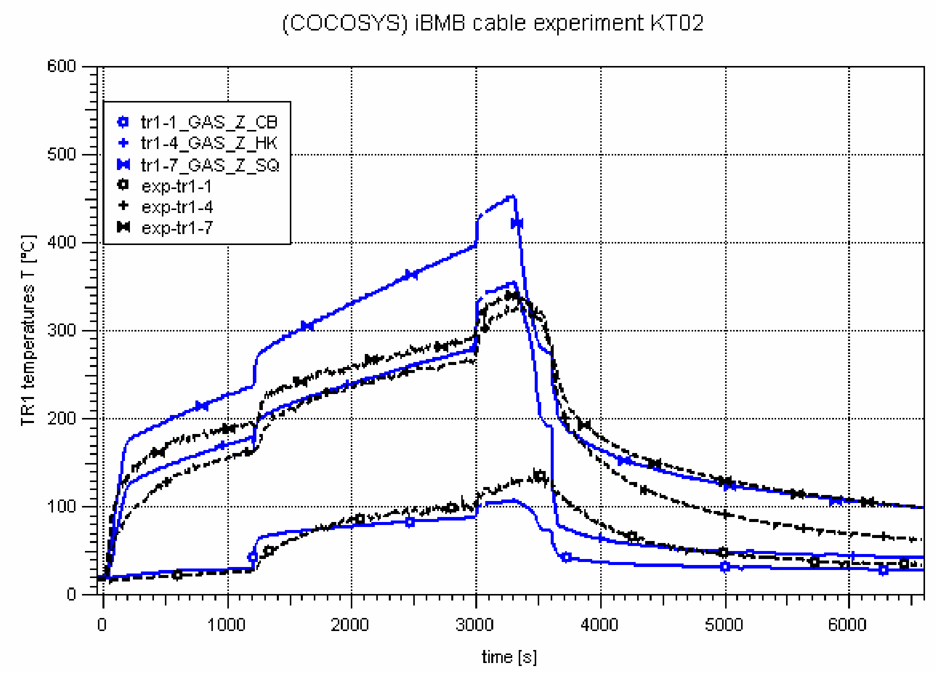


**Fig. E-25** Test 2: Temperatures at tree TR1

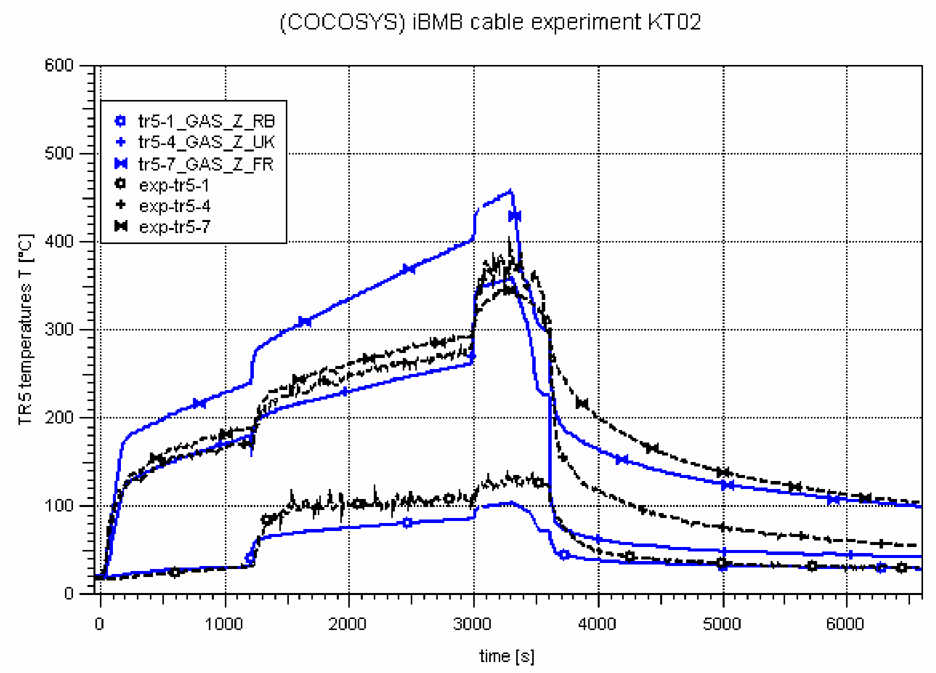


**Fig. E-26** Test 2: Temperatures at tree TR5 close to gas burner

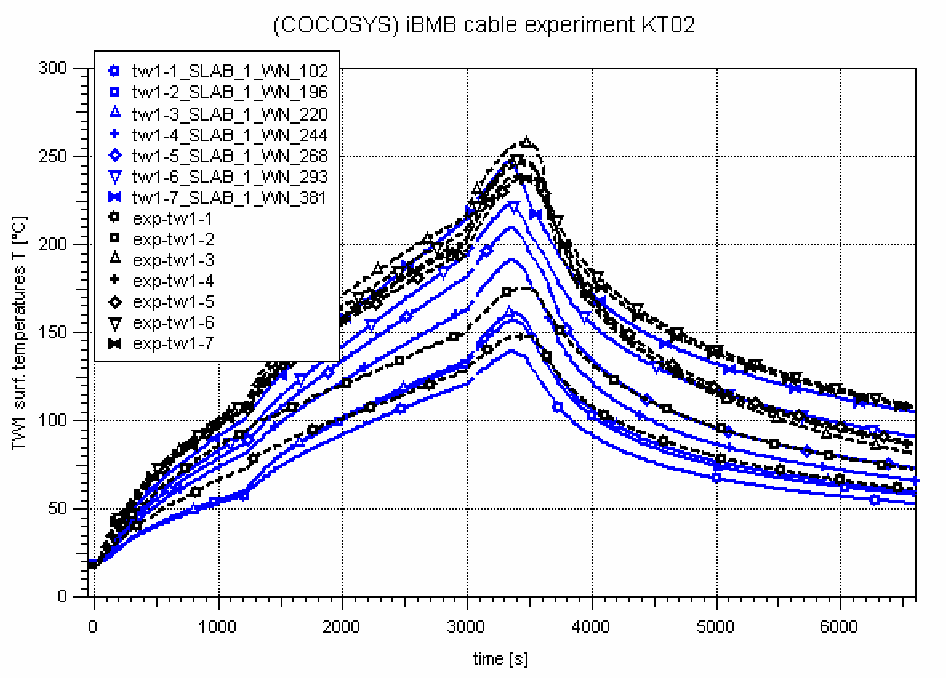


**Fig. E-27** Test 2: Surface temperature at backside wall TW1

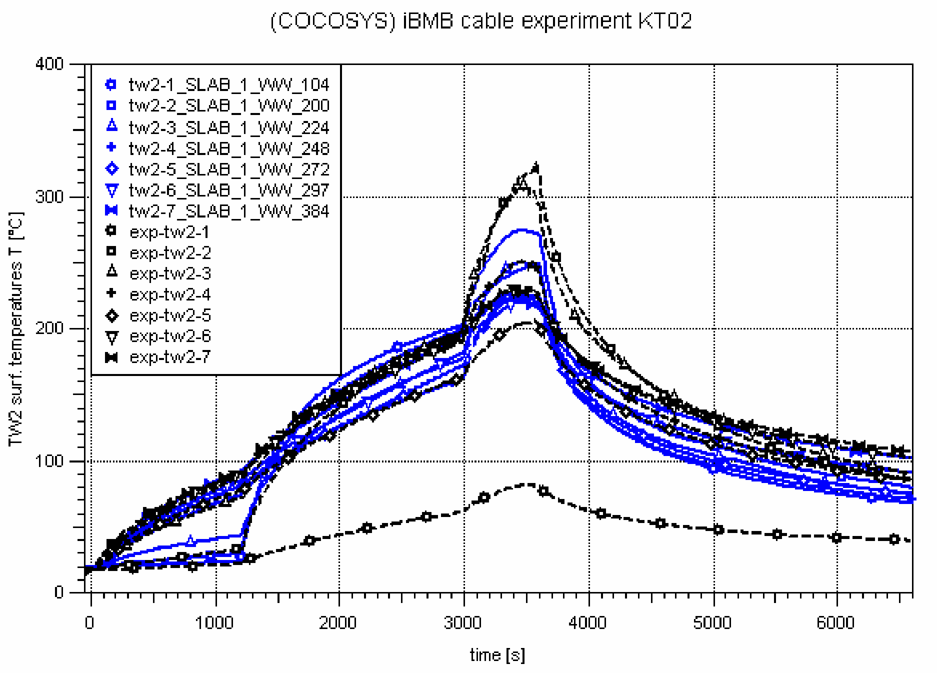


**Fig. E-28** Test 2: Surface temperature at left side wall TW2 close to gas burner

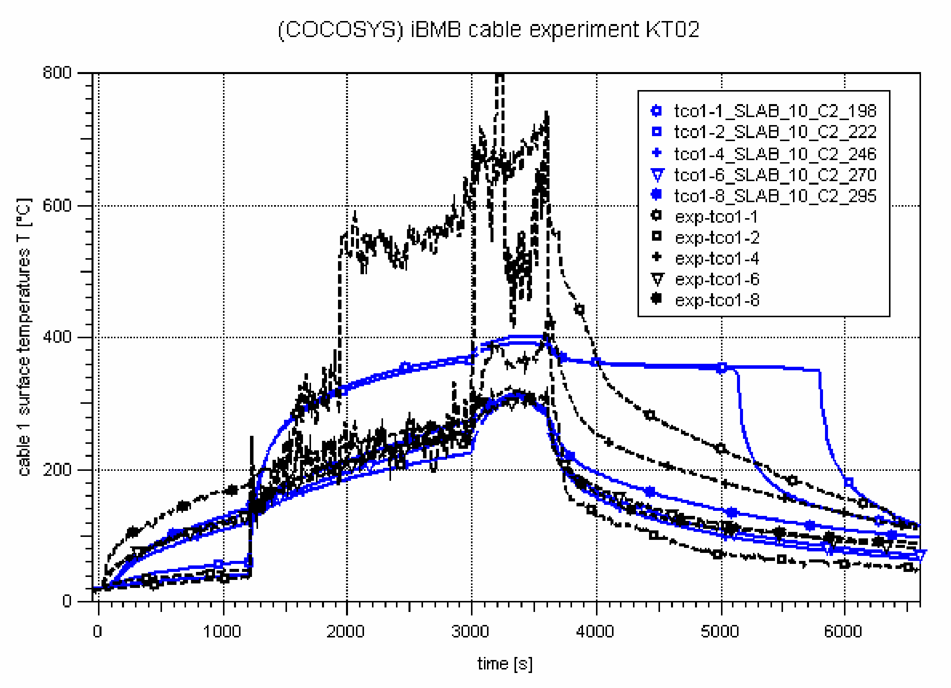


**Fig. E-29** Test 2: Cable surface temperature at TCO1 location (outside, power cable)

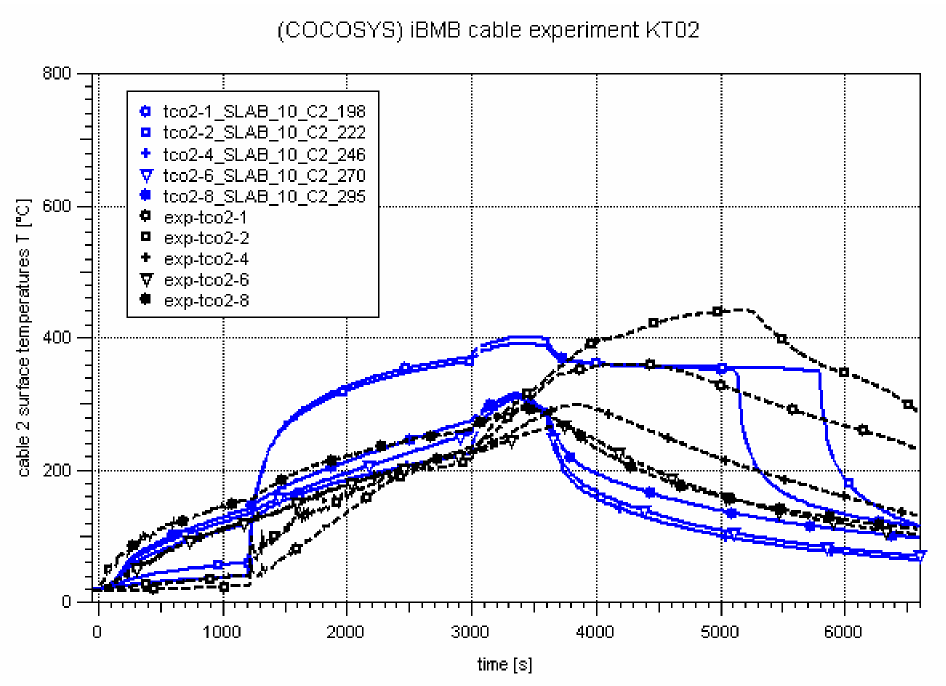


**Fig. E-30** Test 2: Cable surface temperature at TCO2 (inside, power cable)

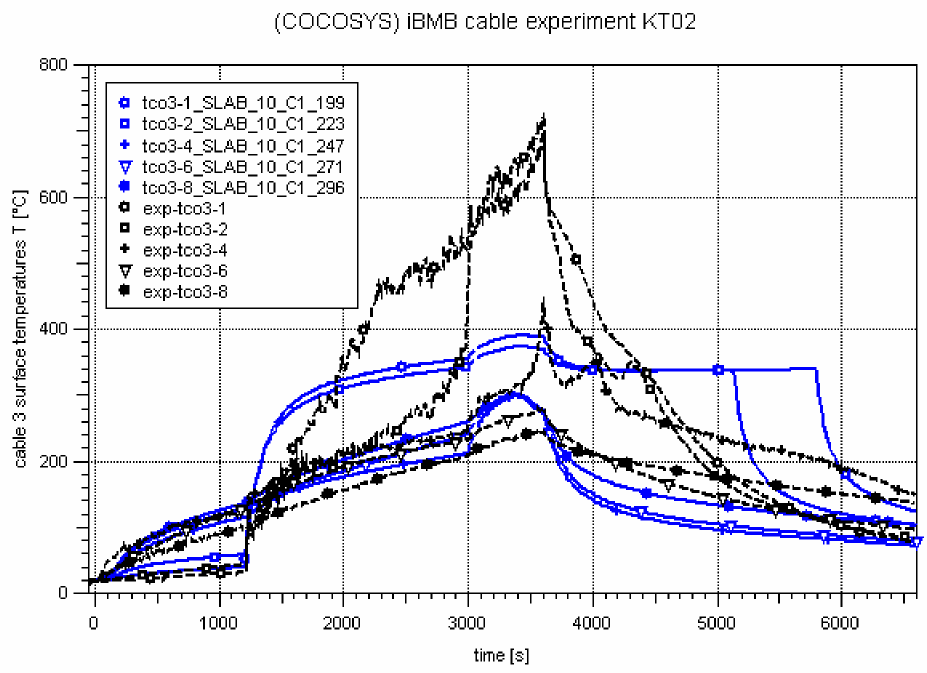


**Fig. E-31** Test 2: Cable surface temperature at TCO3 (outside, I&C cable)

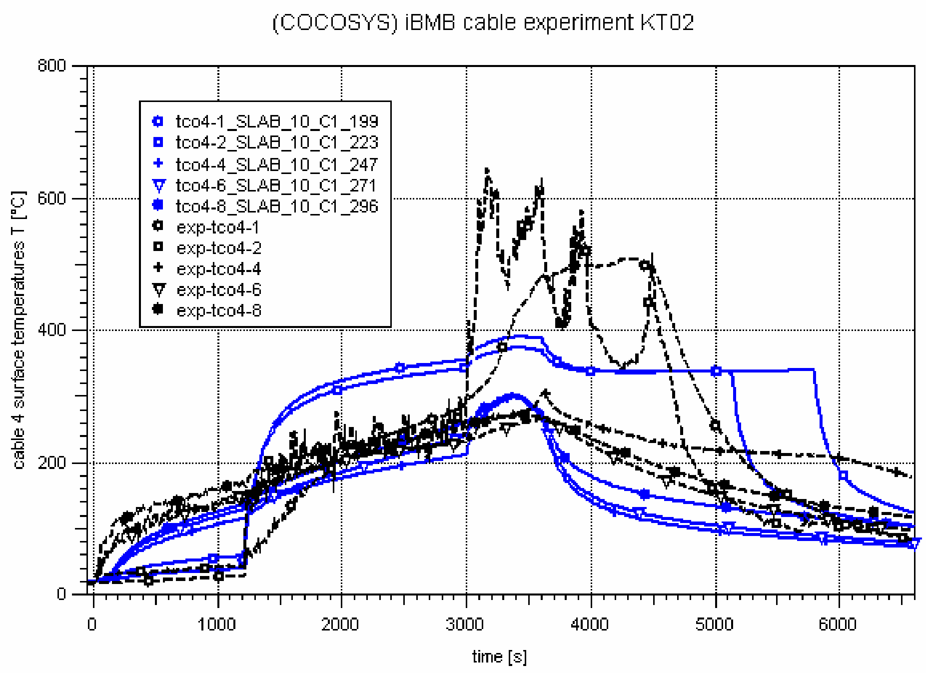


**Fig. E-32** Test 2: Cable surface temperature (inside, I&C cable)

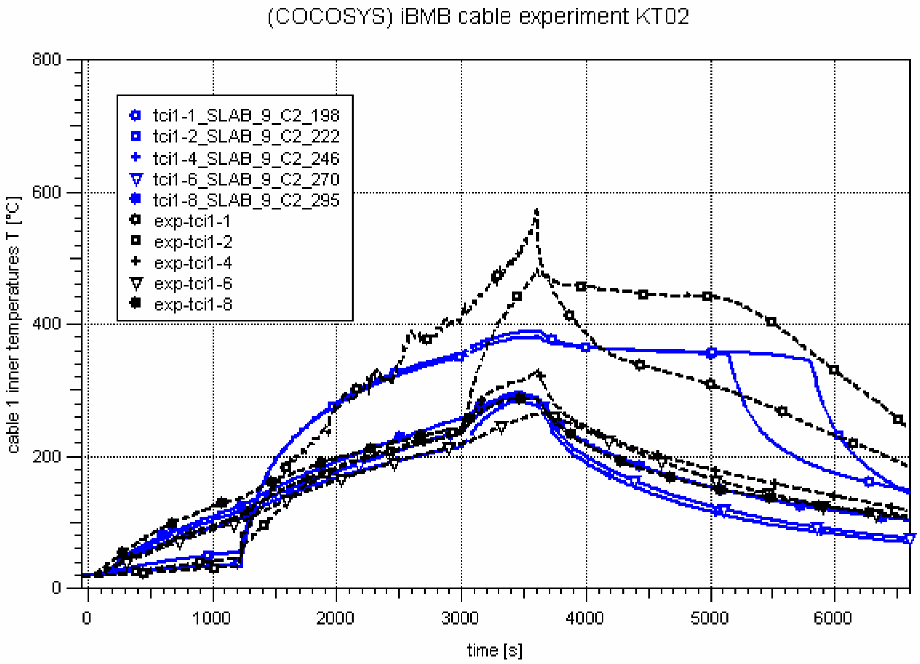


**Fig. E-33** Test 2: Cable center temperatures at TCI1

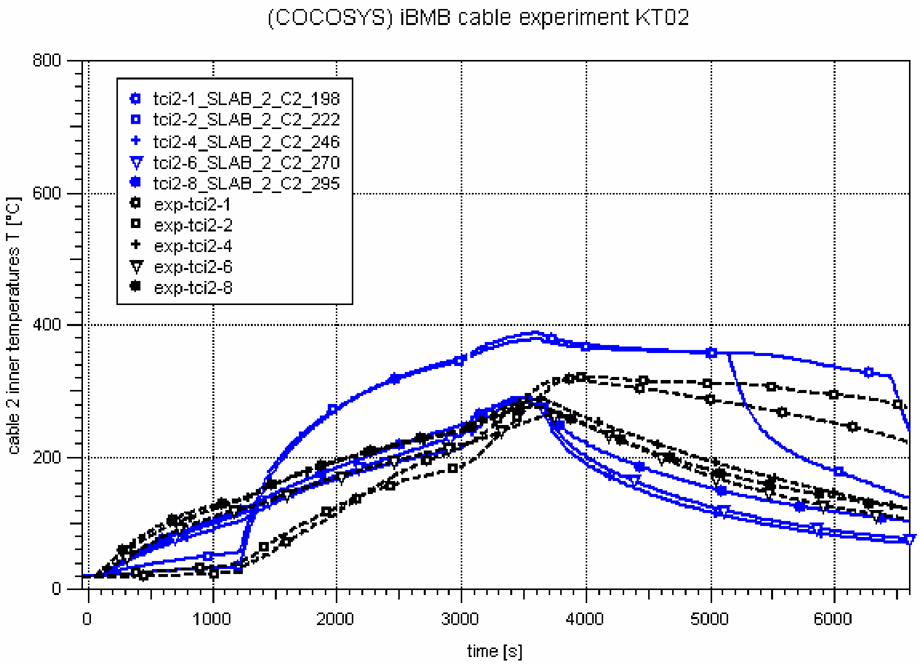


**Fig. E-34** Test 2: Cable center temperature at TCI2

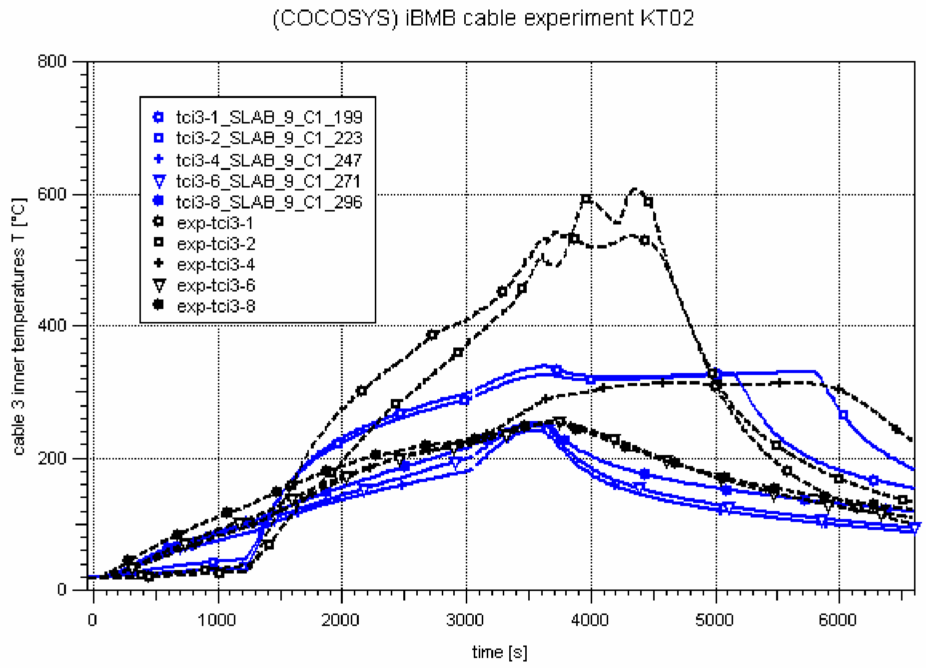


**Fig. E-35** Test 2: Cable center temperature at TCI3

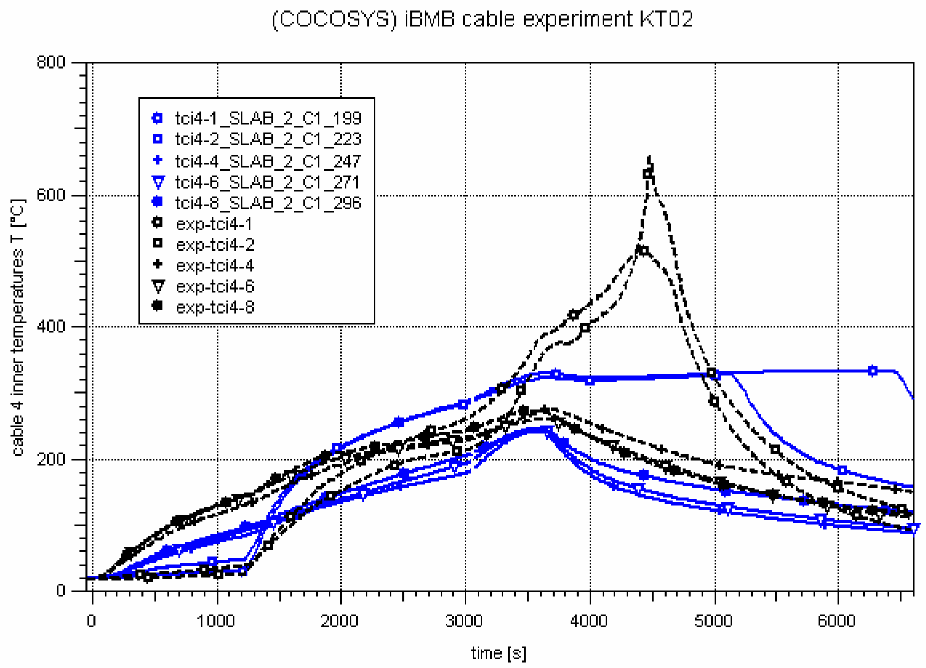


**Fig. E-36** Test 2: Cable center temperature at TCI4

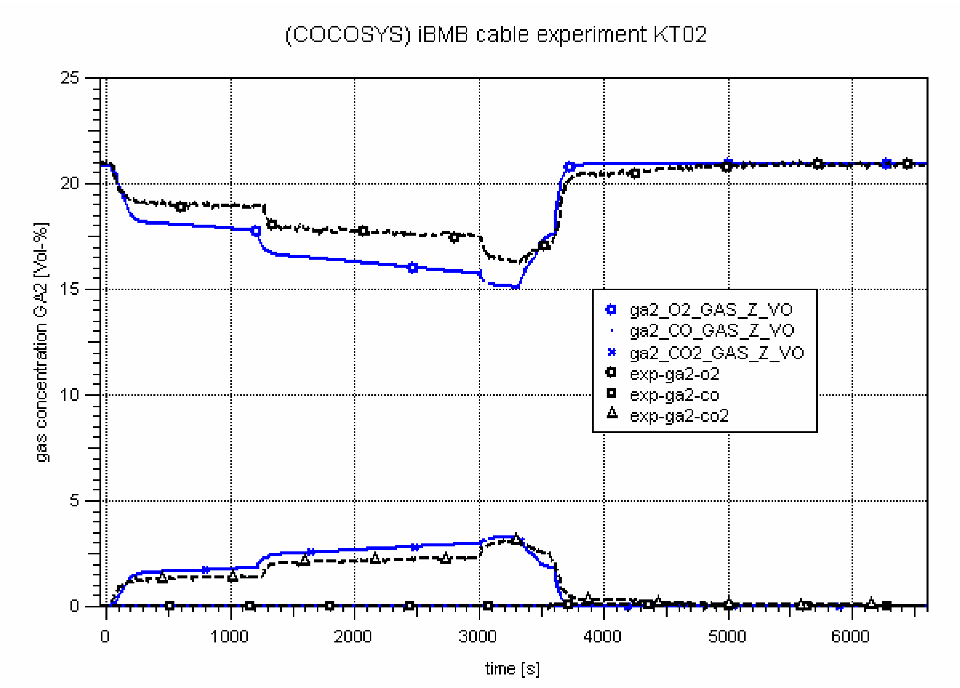


**Fig. E-37** Test 2: Gas concentration at GA2

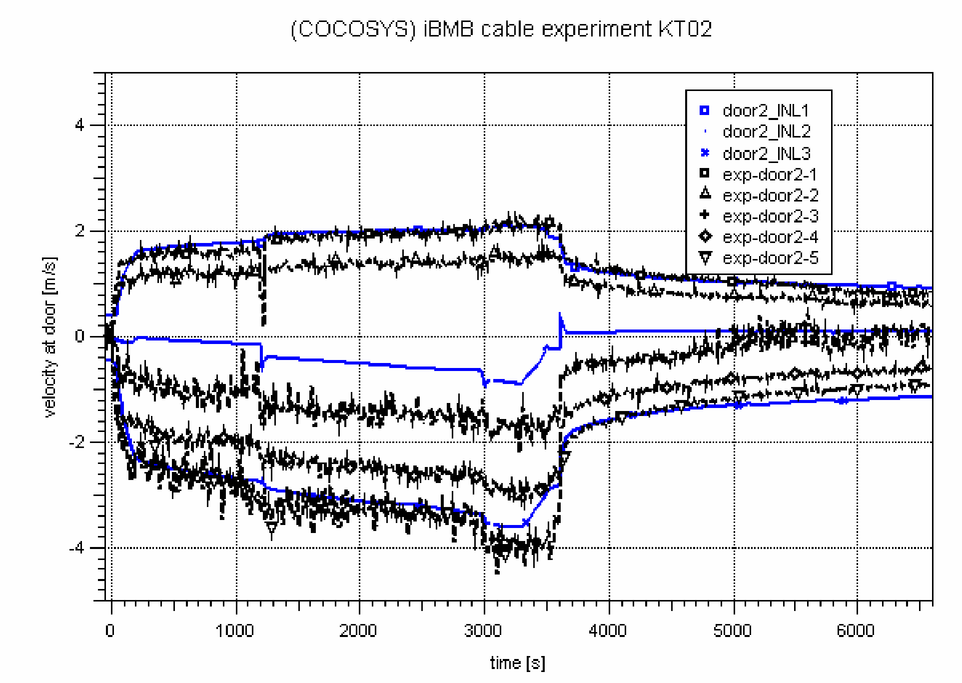


**Fig. E-38** Test 2: Velocity at door opening

## E3.3 Test 3: PVC Cable without Pre-heating

In the following the COCOSYS results of Test 3 will be discussed. The experimental procedure is quite similar to Test 1. The gas burner heat release is about 50 kW. At about 800 s the gas burner is stopped. At this point the measured heat release is decreasing all the time. In the blind calculation the ignition was somewhat too late. Also the increase of pyrolysis rate is underestimated. One main problem of the simplified cable fire model was that if the burning process was started for a cable segment it would burned down completely. But several experiments show, that in case of relative low temperatures the burning process is not complete. Therefore the model has been extended. Now a temperature dependent function of a remaining cable mass fraction can be defined. According to this experiment the remaining cable mass fraction was set to 60 %, without regarding the temperature dependence. With this concept the decrease of energy release could be simulated. The characteristic of experiment and calculation for the energy release now looks quite similar (Fig. E-39).

Fig. E-40 shows the comparison for the temperatures at tree TP (far away from the gas burner). The quality of the results are quite good. The time delay in the temperature decrease results from the longer duration of the burning process. The temperature at the upper most measurement point is overestimated by about 40 K.

The maximum temperatures at the tree positions TR1 and TR5 are overestimated by about 100 K to 180 K (Fig. E-41 and Fig. E-42). The main reason is the incorrect prediction of air entrainment and plume size close to the fire. The quality of the calculated wall temperatures is similar to that of Test 1. The stratification at TW1 is calculated as less steep than measured. Larger deviations occur at TW2 especially in the lower region.

Fig. E-45 to Fig. E-48 show the surface temperature on the PVC cables at the locations TCO1 to TCO4. The temperature increase for the power cable is now calculated much better in the open calculations. The time delay of temperature increase is an indication of the flame propagation. The temperature increase is calculated somewhat too early, but the time interval is quite similar, indicating that the flame propagation is calculated correctly. The differences between TCO1 and TCO2 in the measurements could of course not be reproduced with COCOSYS. The temperature decrease in TCO2 is much slower compared to that of TCO1. The simulation of I&C cable surface temperatures is now quite good.

Fig. E-49 and Fig. E-50 show the inner cable temperatures at the power cables. The maximum temperature at TC1 is quite similar between experiment and simulation. But the time characteristic is much slower in the experiment. Although the energy release is decreasing the measured temperatures continue to stay at a rather high level. The calculated temperatures of the blind calculation are much too low. The temperatures at the backside at TCI2 are underestimated in the simulation. The main reason is that there is no fire calculation at the backside of the cable tray. Therefore the two lowest positions show some temperature increase only. The question is how the burning surface could be estimated more realistically.

The simulated time characteristic of TCI3 is much better for the I&C cables compared to that of the power cables. But the maximum temperature is underestimated by about 200 K. The calculated of TCI4 are too low for the same reason as for TCI2 (Fig. E-51 and Fig. E-52).

Fig. E-53 presents the comparison for the pressure differences inside the fire compartment. The calculated results are quite similar to the experimental values.

Fig. E-54 and Fig. E-55 show the comparison for the gas concentrations at GA1. The oxygen concentration is underestimated by about 0.5 Vol%. The results of the blind calculation are somewhat better. The maximum $CO_2$ concentration is simulated quite well in the open calculation. At the end of the experiment there is still some $CO_2$ measured. This is not the case in the open calculation because the combustion is stopped.

The calculated range of velocity at the door opening was simulated quite well. It is clear that the velocity distribution could be simulated in a rough way the three junctions only. (Fig. E-56).

Fig. E-57 and Fig. E-58 show the pyrolysis rate (weight loss of cables) and the integral weight loss. At about 300 s the experimental value increases strongly, but decreases after the gas burner is switched of. In the blind calculation the ignition of the cables was simulated somewhat delayed. Also the increase of the pyrolysis rate was underestimated. Reaching the maximum value the cables are still burning and consume the complete cable mass. In the open calculation the ignition of cables was performed by a signal at 300 s and not calculated by the model itself. The increase of pyrolysis rate was larger, but not reaching the maximum value of about 0.02 kg/s. Using the remaining mass fraction option the rate decreases at about 1300 s. The reason for the calculated mass loss rate being to low may be a too low specific reaction rate r. The times for temperature increase look quite good so that the flame propagation should adequately predicted.

Fig. E-59 shows the mass flow rate into the fire compartment, which is somewhat overestimated in the COCOSYS calculation. But the difference is not so large, so that one can assume that the overall energy and mass distribution is simulated quite well. Large deviation was found for the heat loss into the walls, which seems to be wrong in the experimental data (Fig. E-60). The heat loss through the door opening is simulated quite well (Fig. E-61).

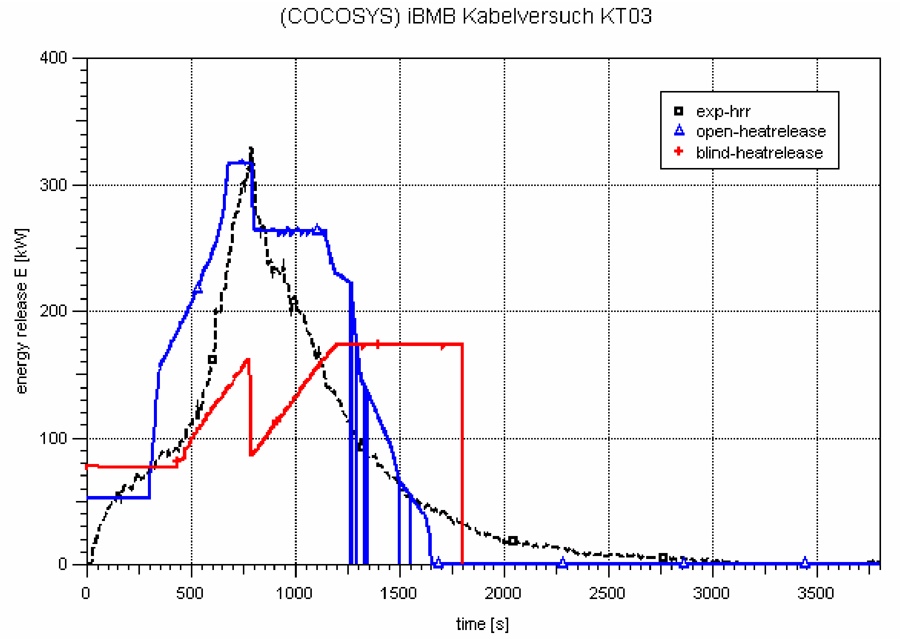


**Fig. E-39** Test 3: Energy release due to combustion

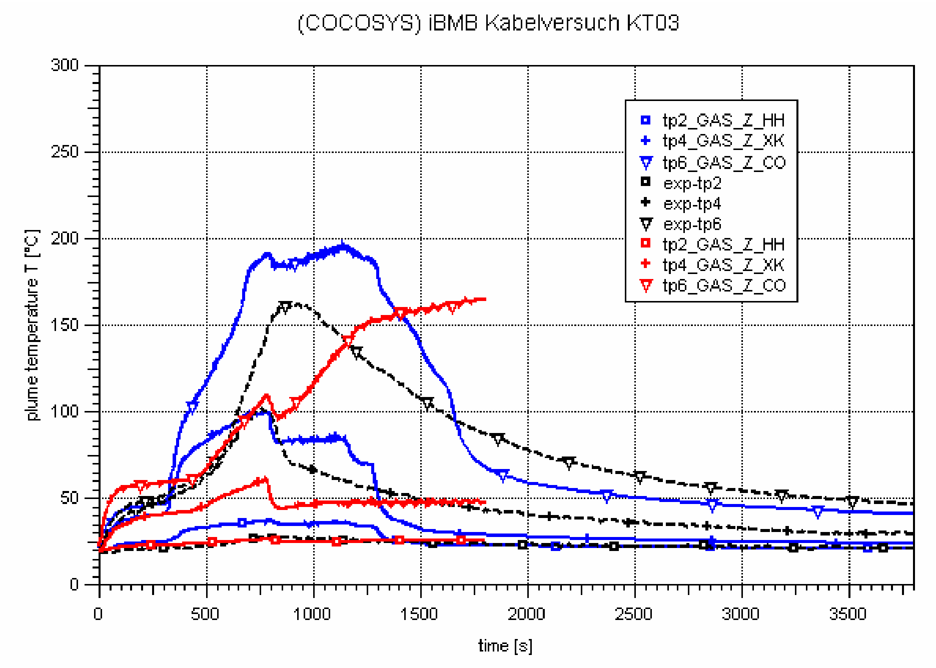


**Fig. E-40** Test 3: Temperatures at tree TP (far away from gas burner)

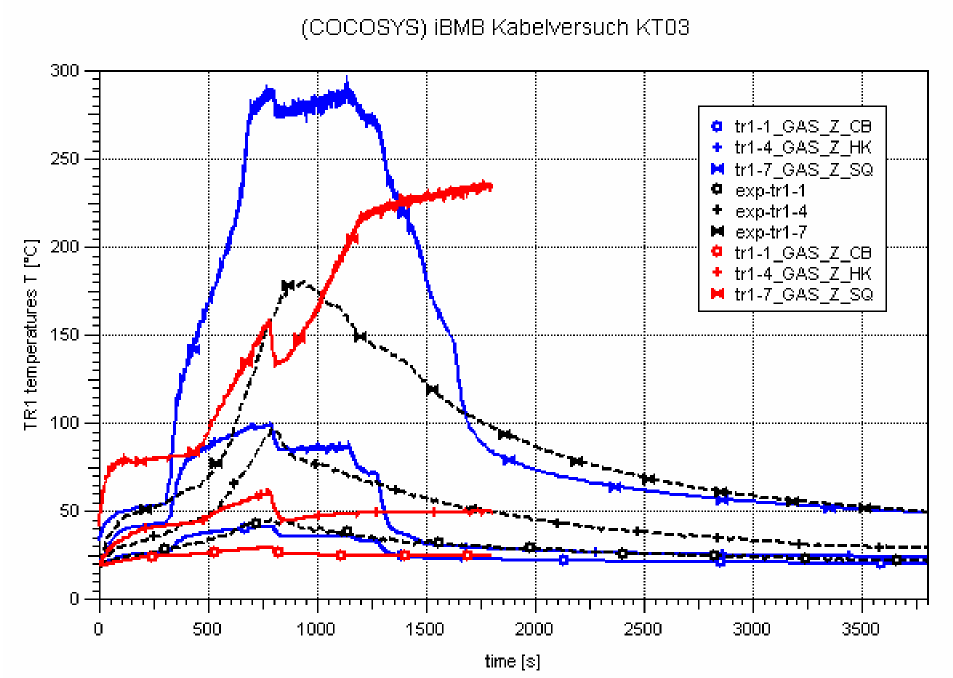


**Fig. E-41** Test 3: Temperature at tree TR1

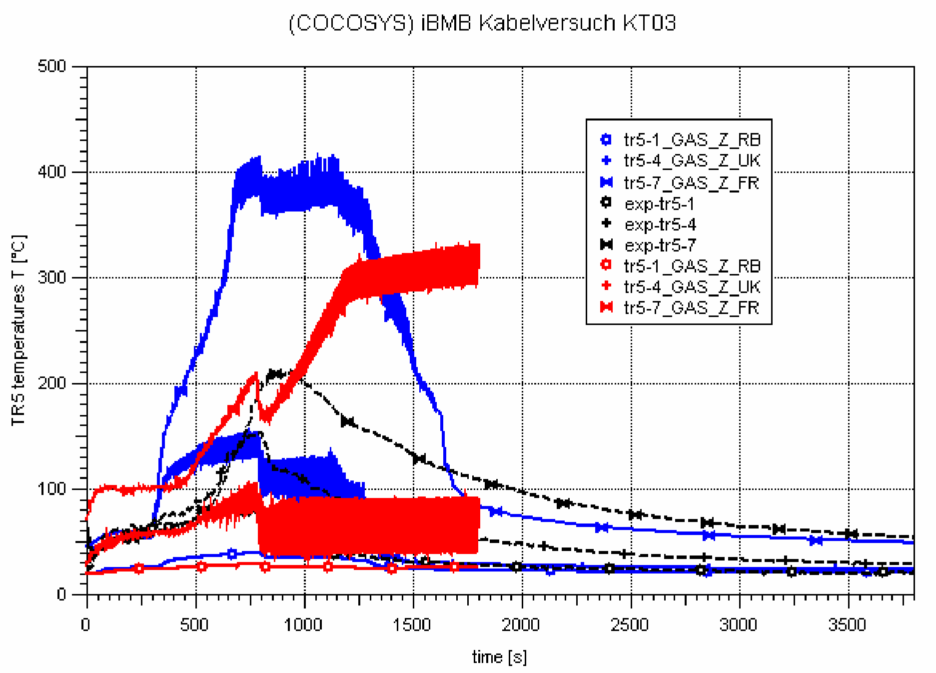


**Fig. E-42** Test 3: Temperature at tree TR5 close to gas burner

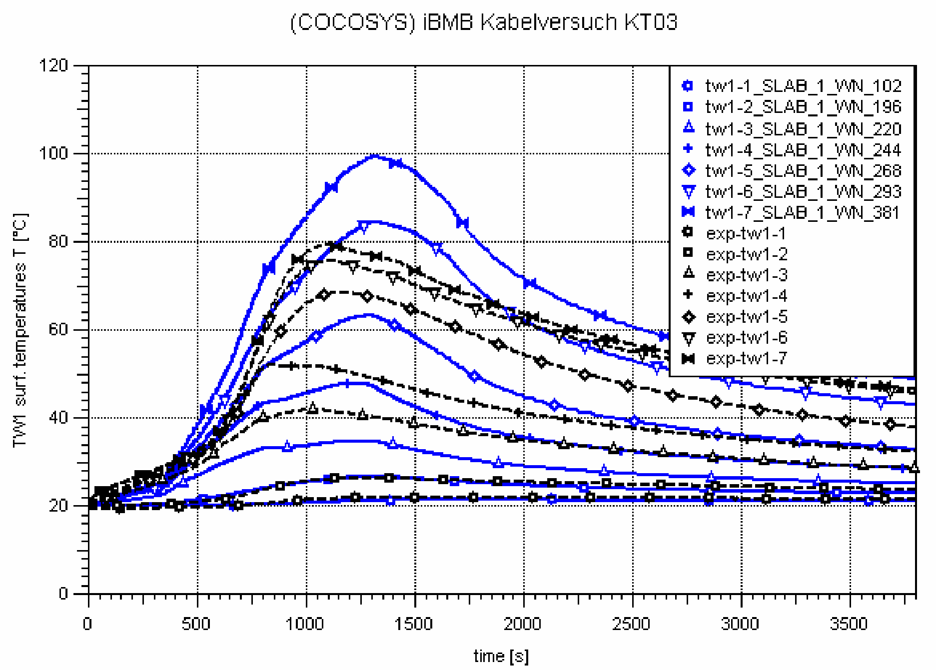


**Fig. E-43** Test 3: Wall surface temperature at TW1 (backside)

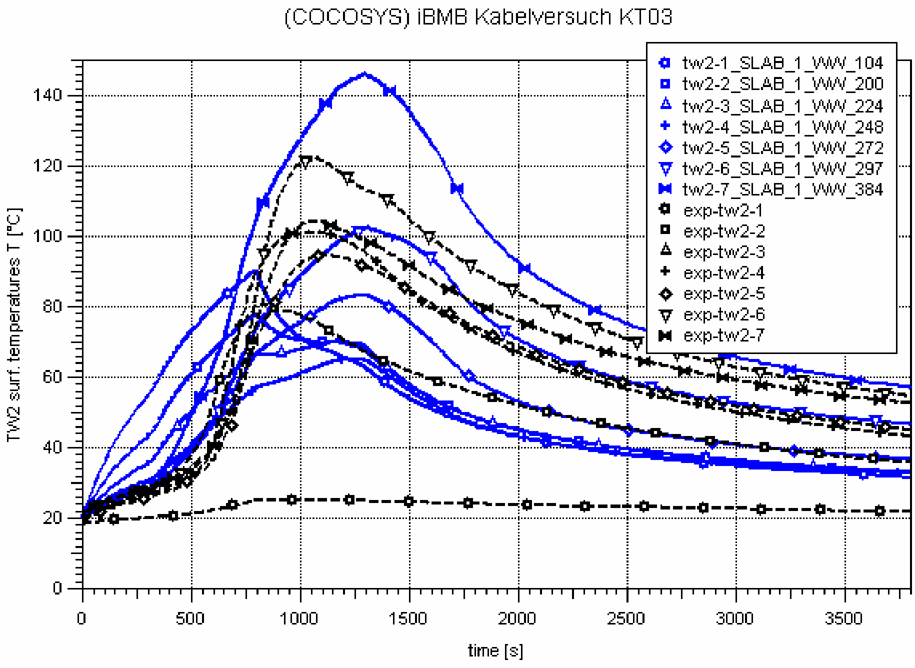


**Fig. E-44** Test 3: Wall surface temperature at TW2 (close to gas burner)

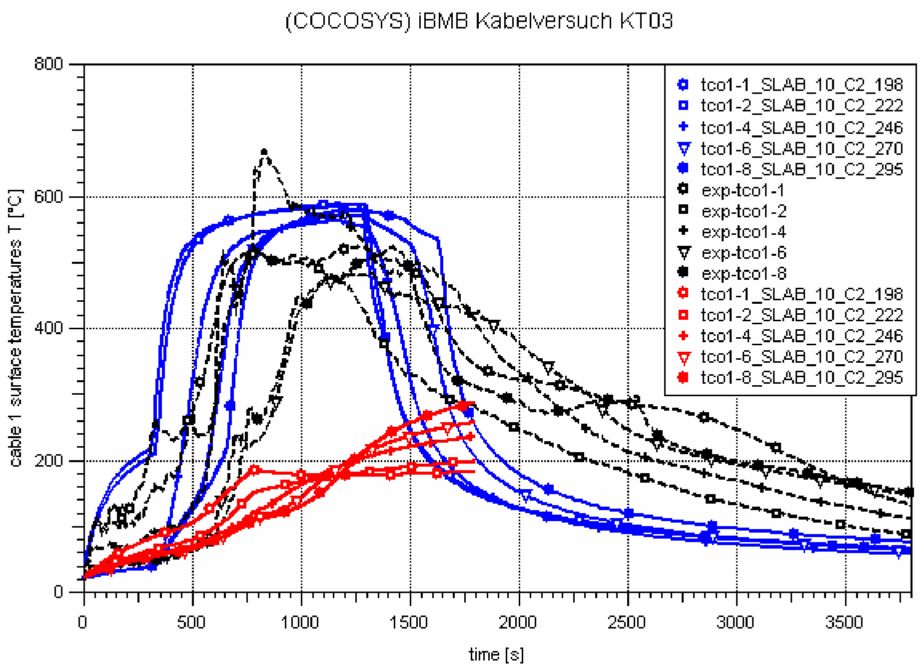


**Fig. E-45** Test 3: Cable surface temperature at TCO1

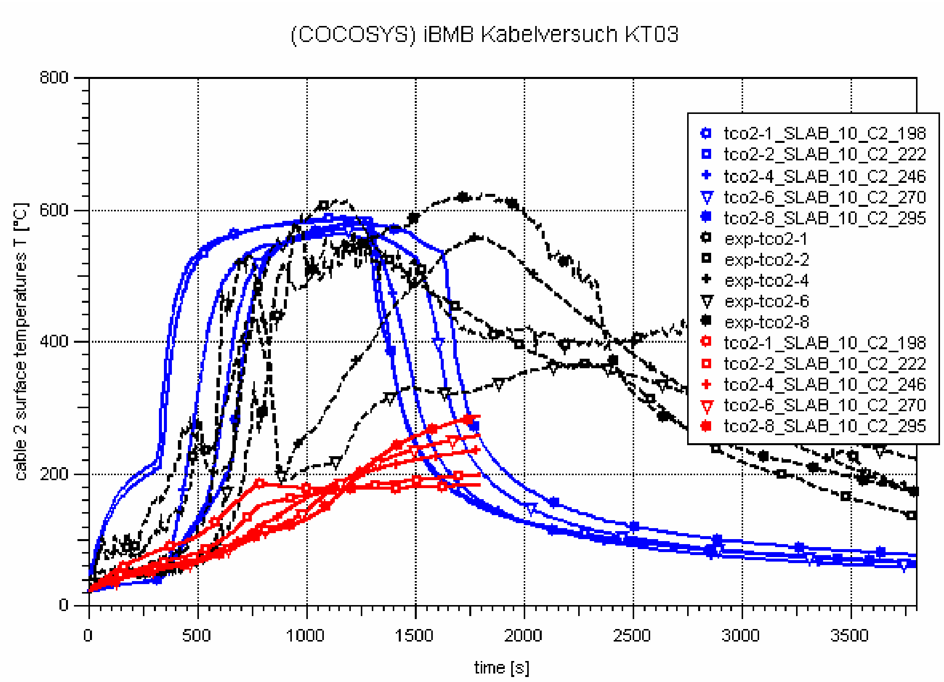


**Fig. E-46** Test 3: Cable surface temperature at TCO2

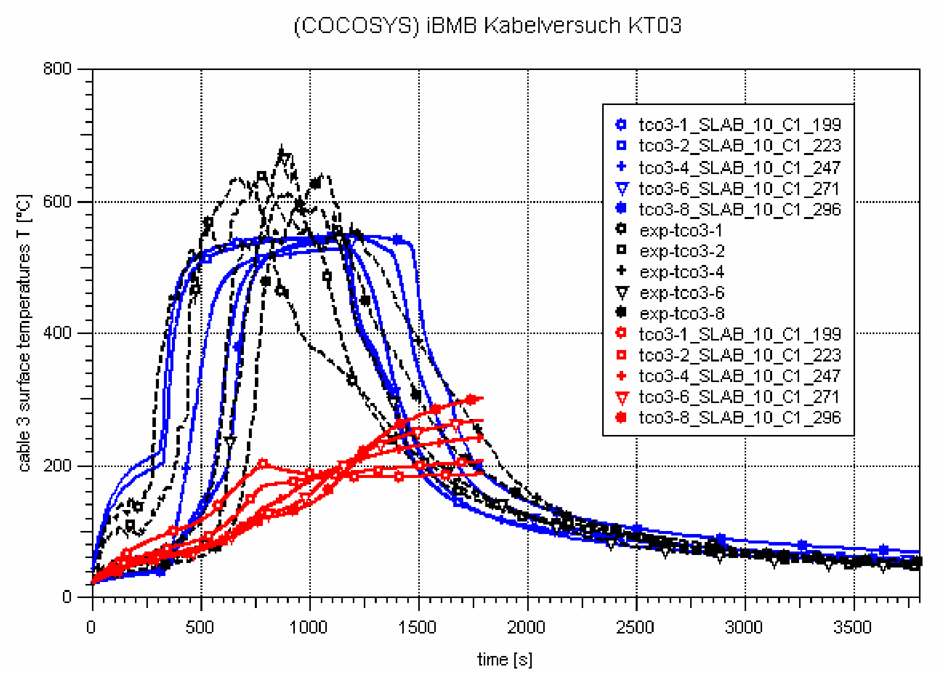


**Fig. E-47** Test 3: Cable surface temperature at TCO3

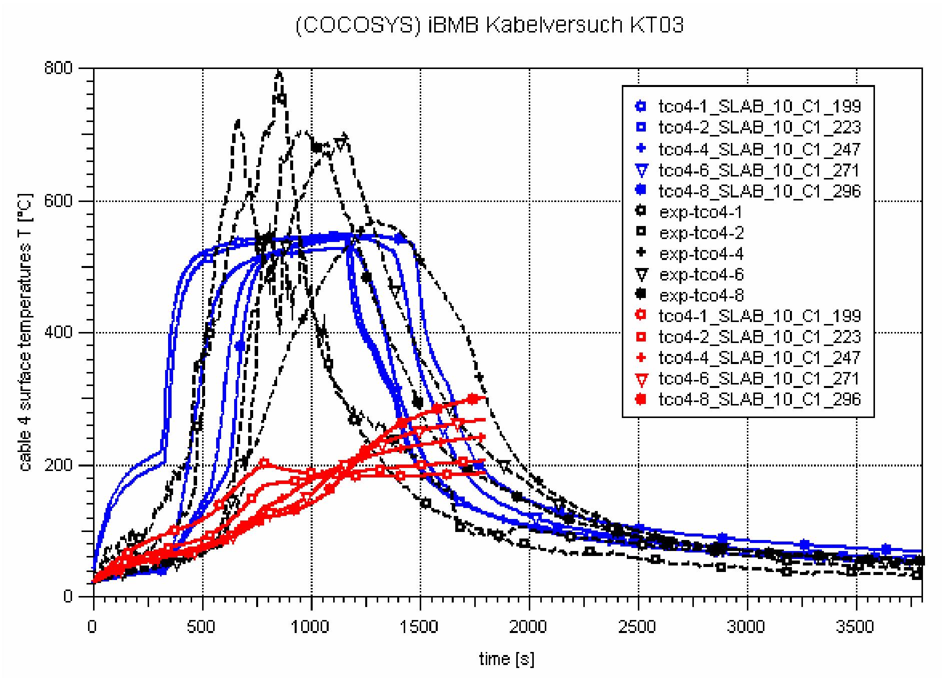


**Fig. E-48** Test 3: Cable surface temperature at TCO4

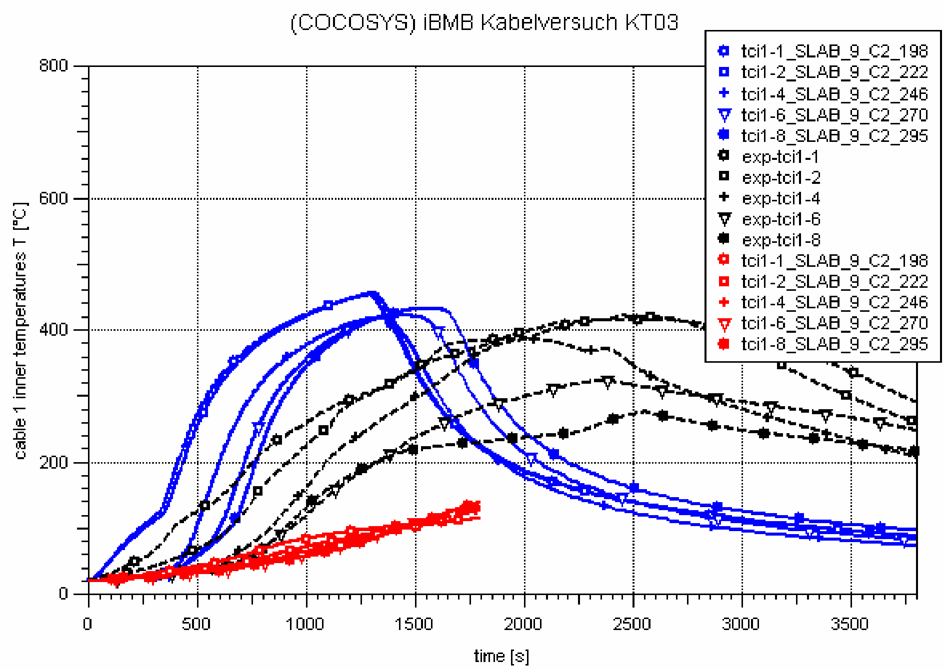


**Fig. E-49** Test 3: Inner cable temperature at TCI1

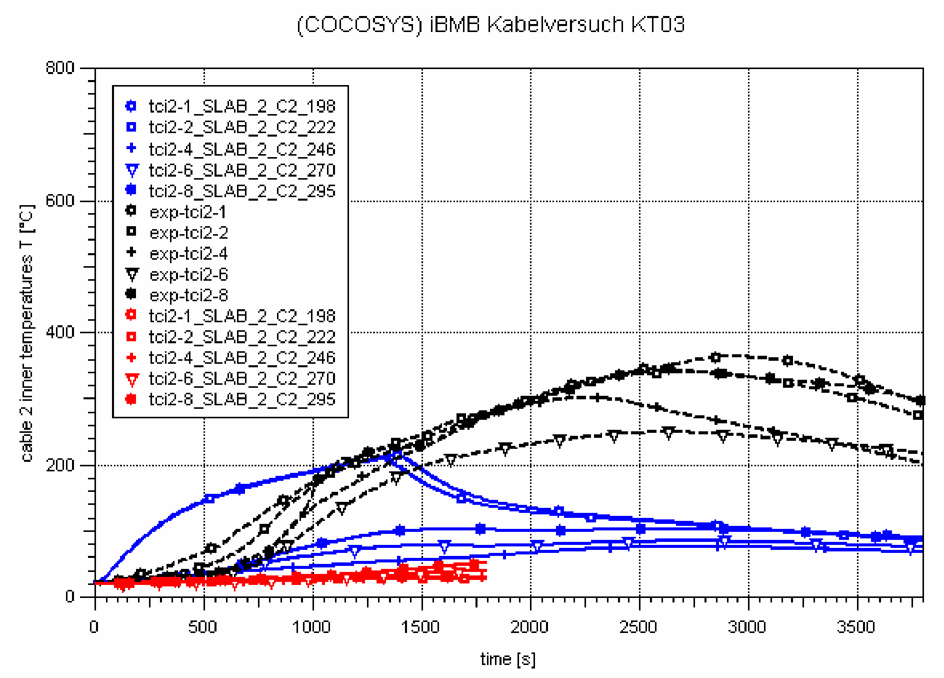


**Fig. E-50** Test 3: Inner cable temperature at TCI2

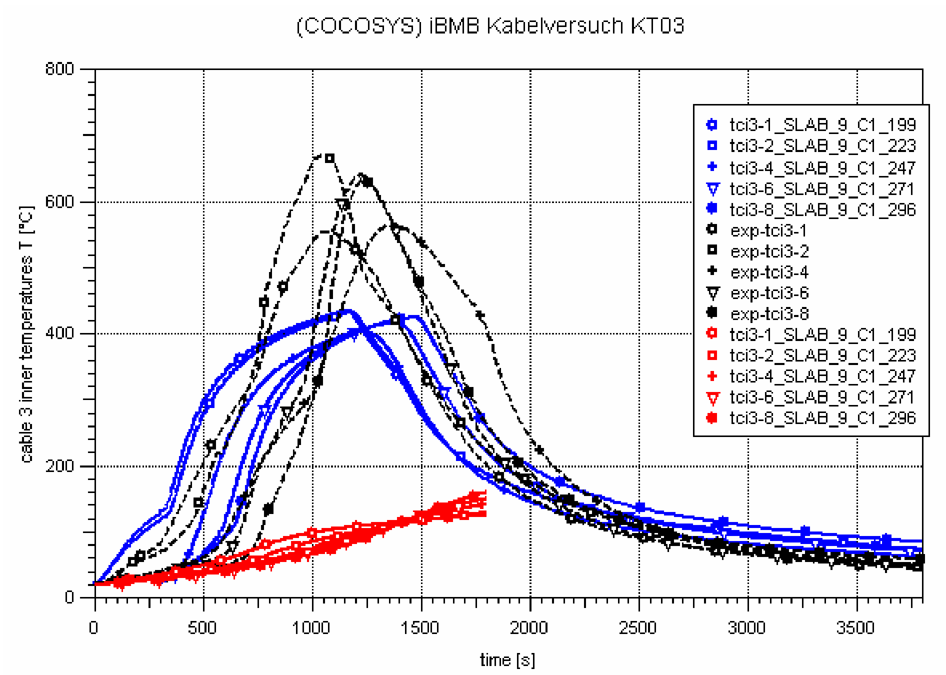


**Fig. E-51** Test 3: Inner cable temperature at TCI3

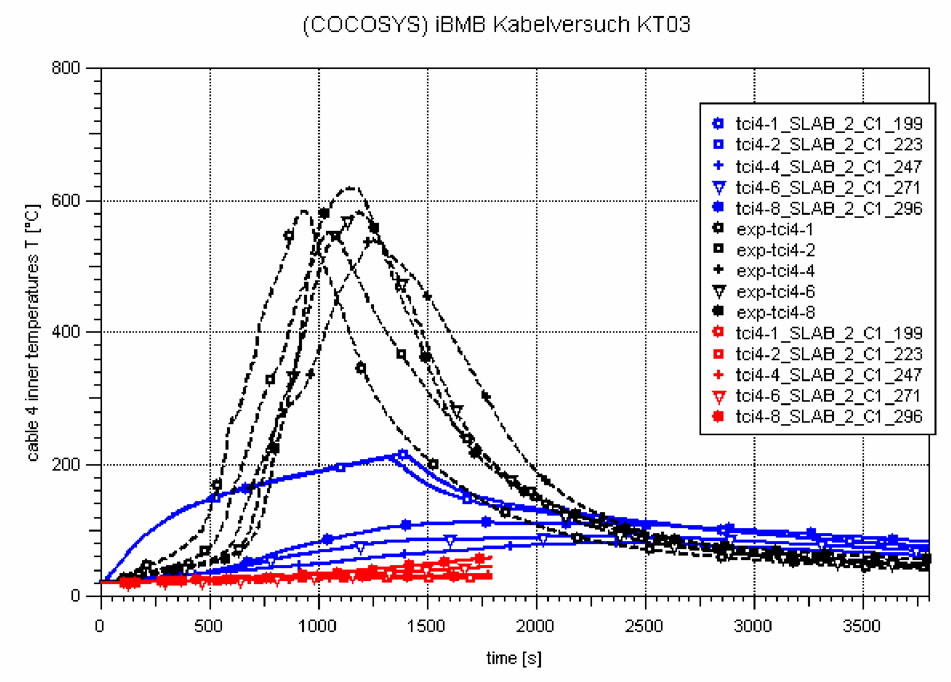


**Fig. E-52** Test 3: Inner cable temperature at TCI4

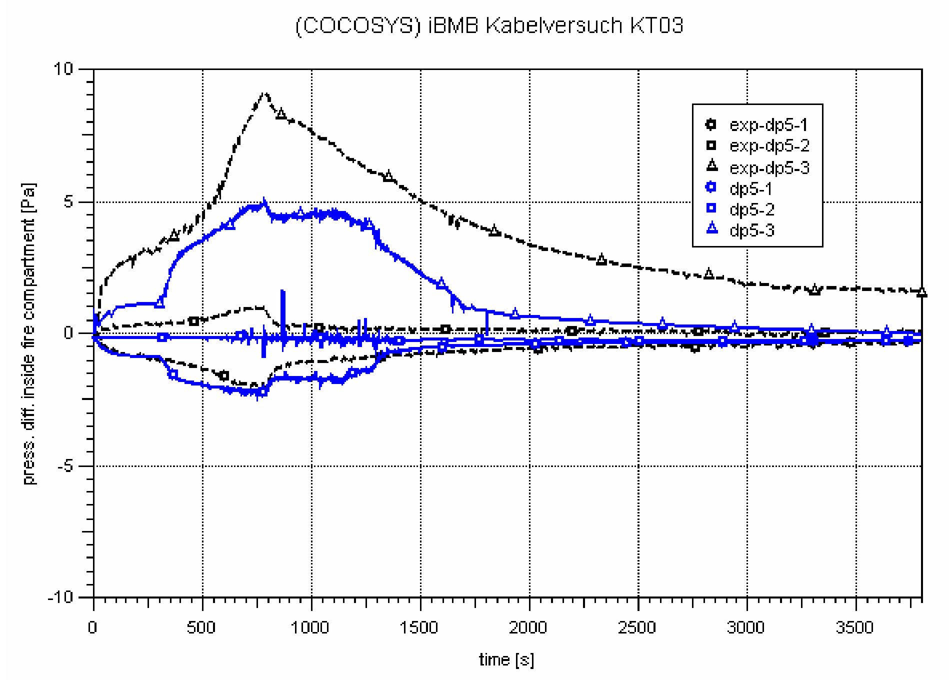


**Fig. E-53** Test 3: Pressure difference inside the fire compartment

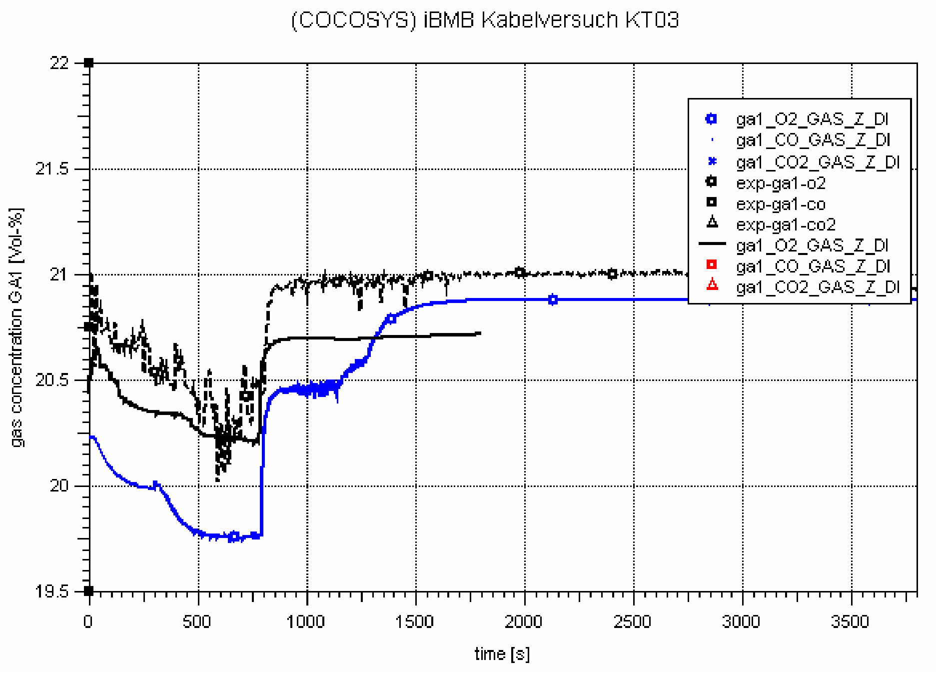


**Fig. E-54** Test 3: Oxygen concentration at location GA1

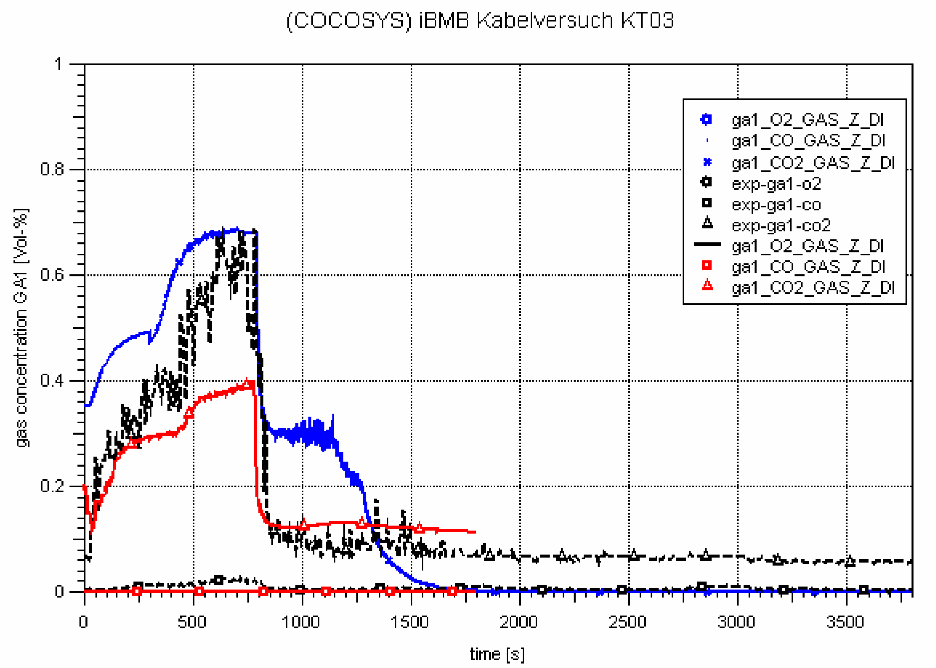


**Fig. E-55** Test 3: CO & CO2 concentration at location GA1

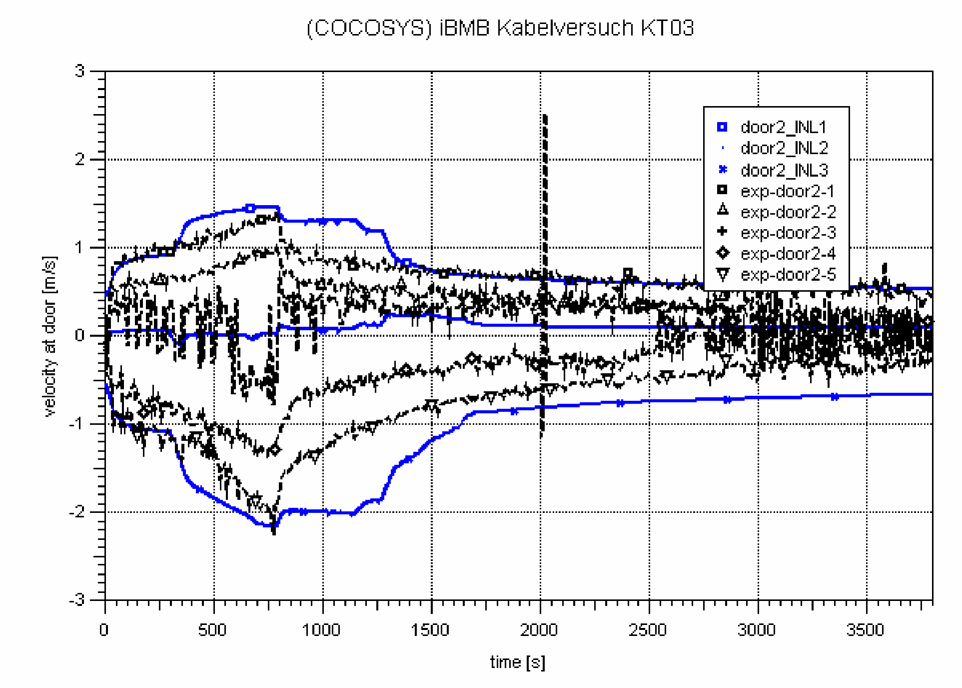


**Fig. E-56** Test 3: Velocity at door opening

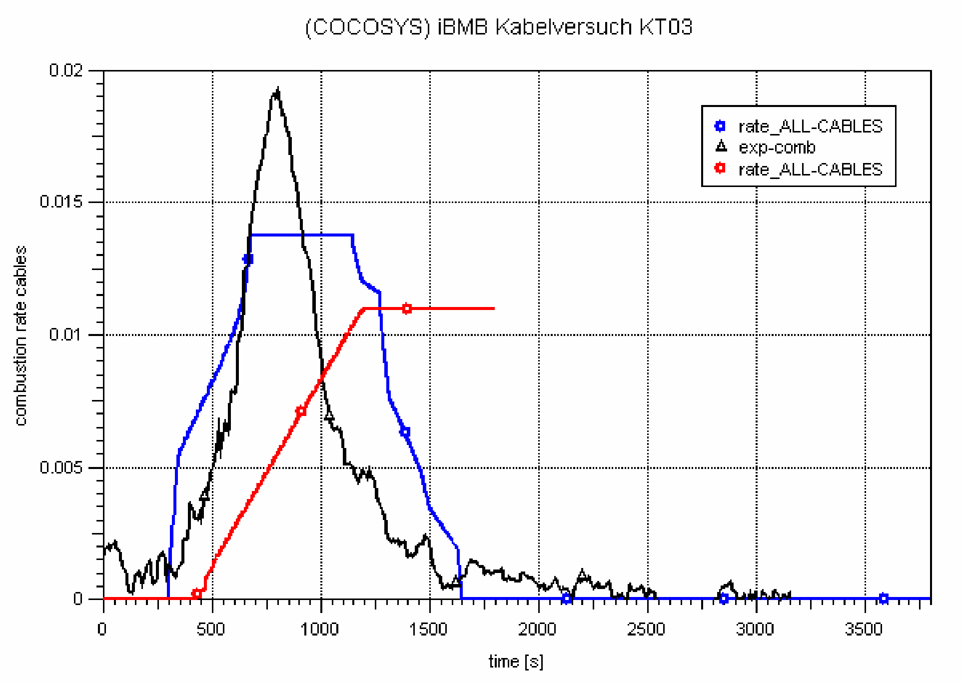


**Fig. E-57** Test 3: Pyrolysis rate (weight loss rate)

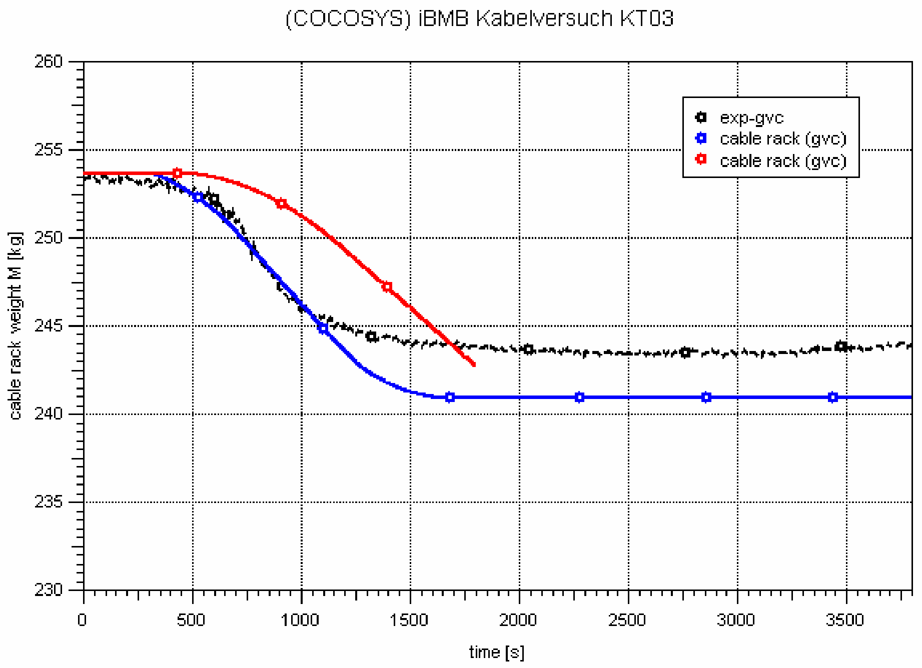


**Fig. E-58** Test 3: Weight of cable trays

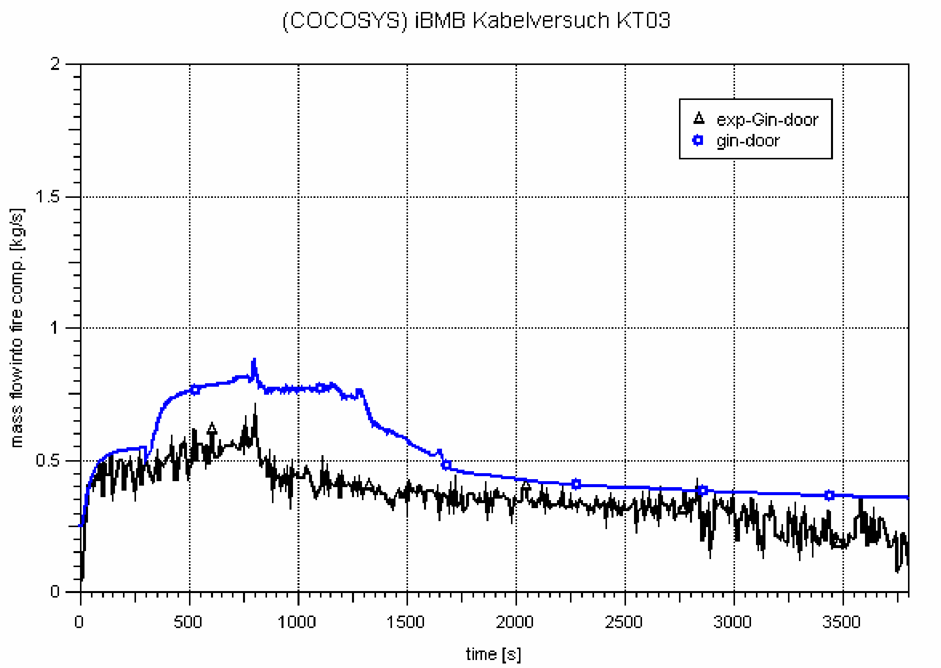


**Fig. E-59** Test 3: Mass flow rate into the fire compartment

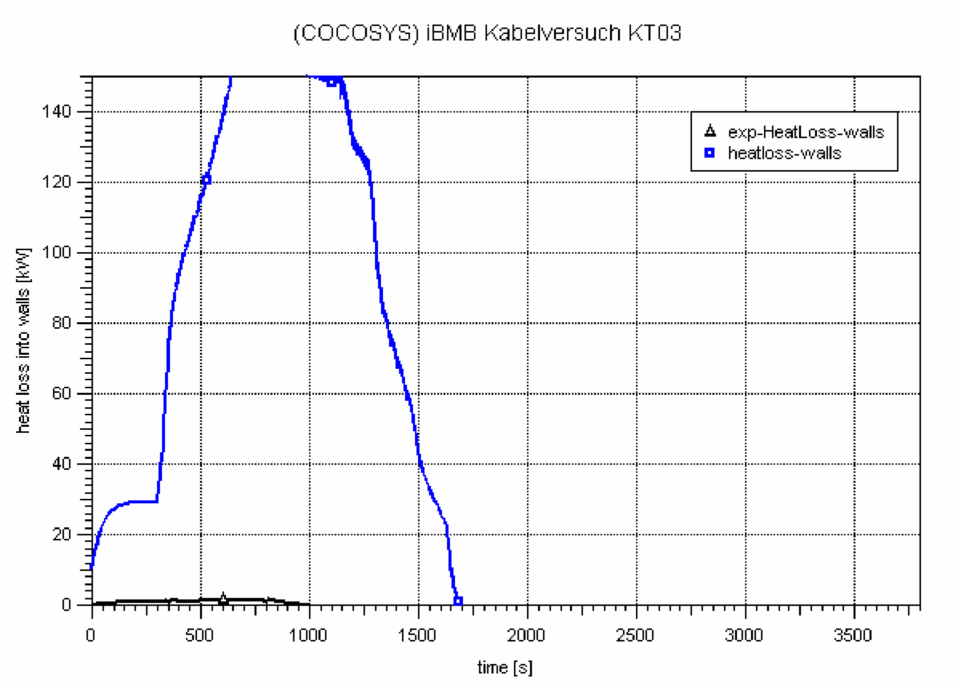


**Fig. E-60** Test 3: Heat loss into walls

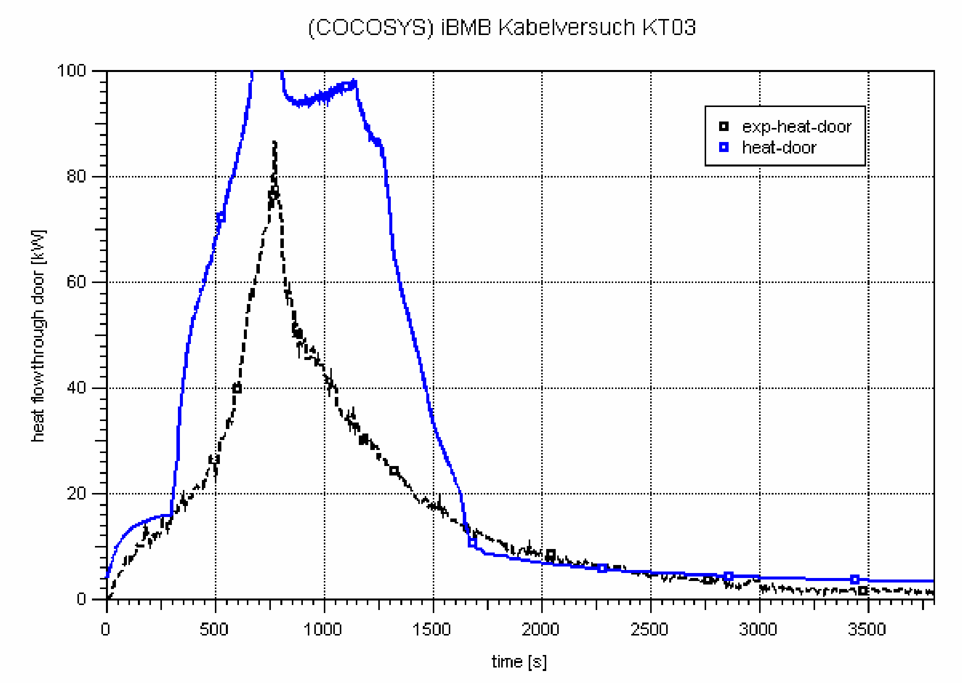


**Fig. E-61** Test 3: Heat flow through door opening

### E3.4 Test 4: PVC Cable with Pre-heating

In Test 4 the atmosphere has been pre-heated by an ethanol pool. The gas burner has been started at 1130 s with 50 kW. At 2130 s the heat release has been increased to 100 kW. Fig. E-62 shows the comparison between calculation and experiment for the heat release. The heat release rate has been overestimated at about 1500 s, at which point COCOSYS the cables start to burn. This is about 600 s too early.

The quality of the calculated plume temperature is similar to that of Test 2. The lowest value TP2 is simulated too low. Due to the missing plume model for simulation of air entrainment the temperatures at the higher positions are simulated too high (Fig. E-63).

The temperatures at trees TR1 and TR5 are simulated quite well. Only the uppermost position is overestimated by about 150 to 200 K. The temperature increase is too early due to ignition of cables at 1500 s.

The simulation of the wall surface temperatures is quite good (Fig. E-66, Fig. E-67). Only the uppermost temperature at TW2 is a little bit overestimated. Similar good results have been obtained for the temperature at the door and inside the exhaust. All these temperature show a somewhat earlier increase in the calculation.

The Fig. E-70 to Fig. E-77 show the surface and center temperatures of the power and I&C cables. The generic behavior is similar to that in the previous cases. The duration of the heating process is longer for the calculation of the power cables. In COCOSYS the differences between power and I&C cable is much less, leading to the conclusion that the material composition is not considered detailed enough. The ignition time of power cables is later than I&C cables. In COCOSYS the ignition of I&C cables was simulated quite well. Because the burning process is simulated on one side only the center temperatures TCI2 and TCI4 are simulated to be too low.

Fig. E-78 and Fig. E-79 compare the results for the gas concentrations at GA1 and GA2. The $O_2$ concentration at GA2 is a little bit underestimated corresponding to the too large calculated temperatures.

The pyrolysis rate is shown in Fig. E-80 and Fig. E-81. The peak rate is underestimated in COCOSYS. The weight measurement show some initial evaporation during the pre-heating phase. This was not simulated in COCOSYS. Anyway the calculated results are quite reasonable.

A correct simulation of energy and mass exchange could be estimated by comparing the heat losses and mass flow rate through the door (Fig. E-82 to Fig. E-85). All these results presented are quite good. Most of the deviations are related to the prediction of early ignition of the power cables.

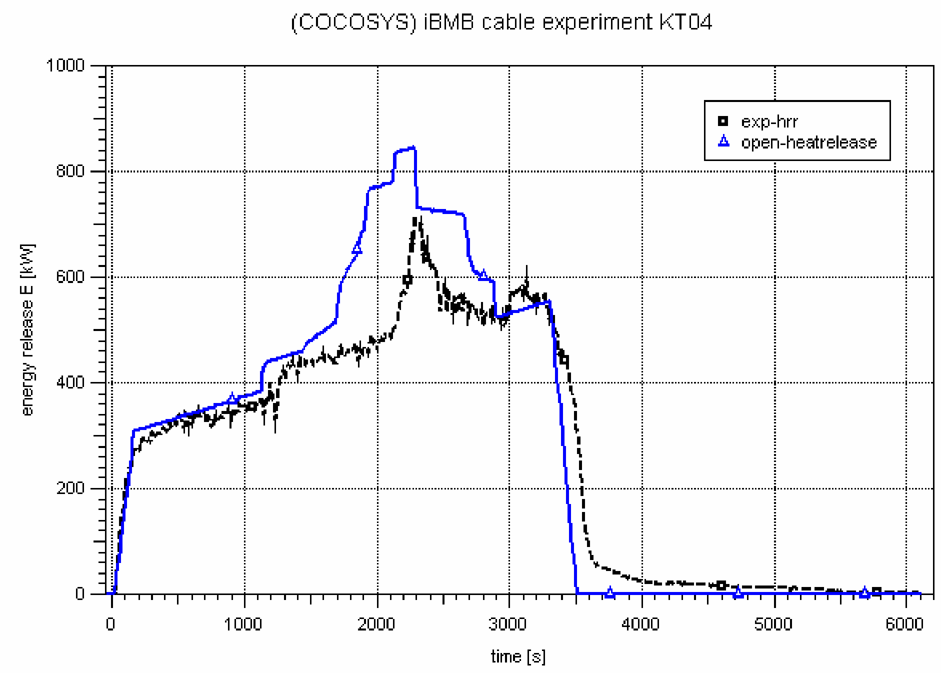


**Fig. E-62** Test 4: Energy release due to combustion

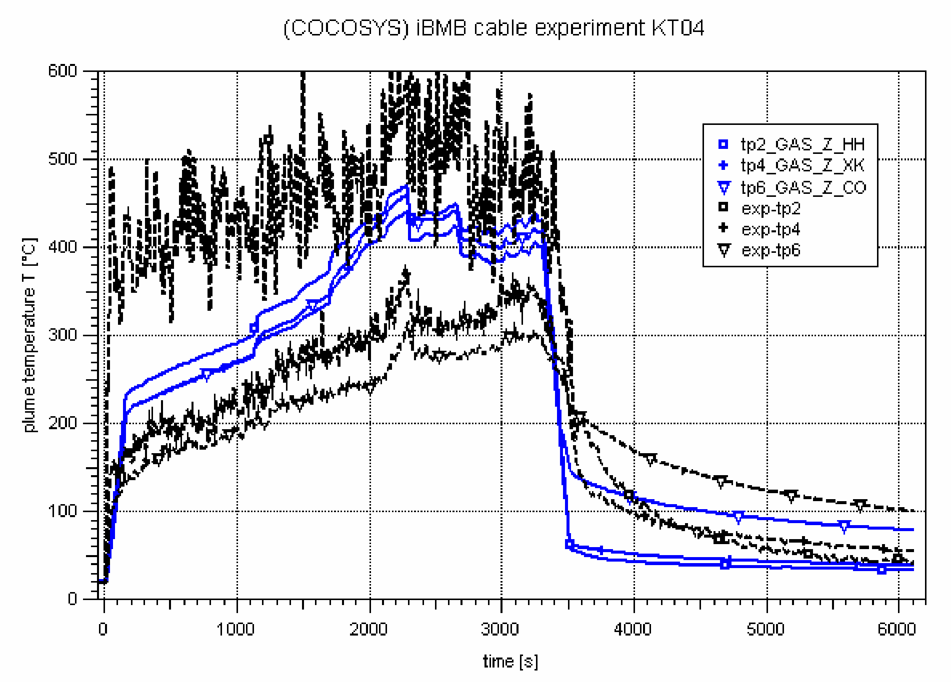


**Fig. E-63** Test 4: Temperatures above the pool

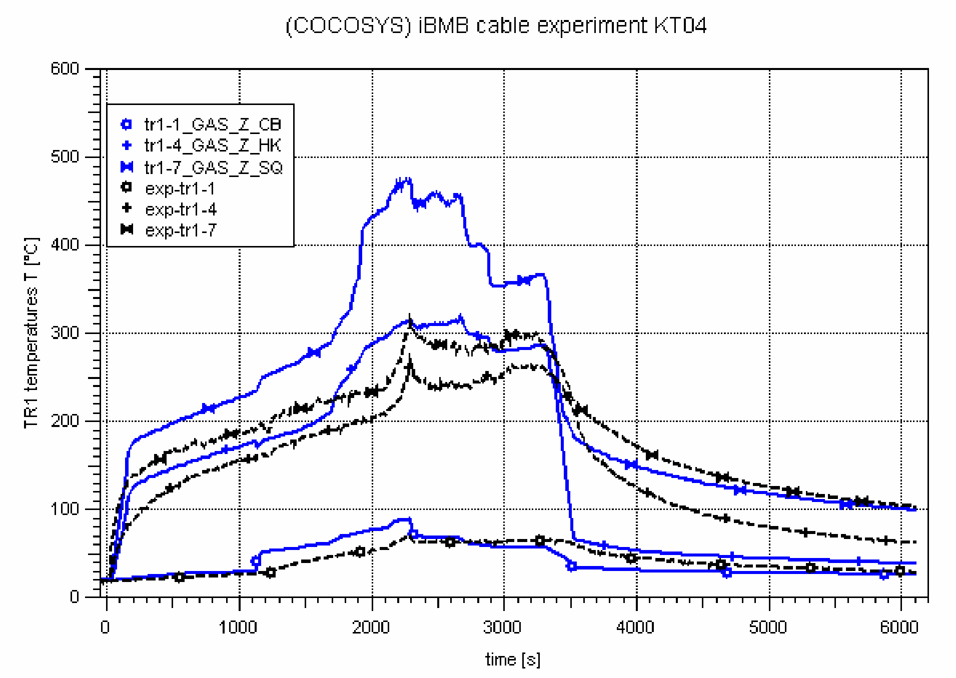


**Fig. E-64** Test 4: Temperatures at tree TR1

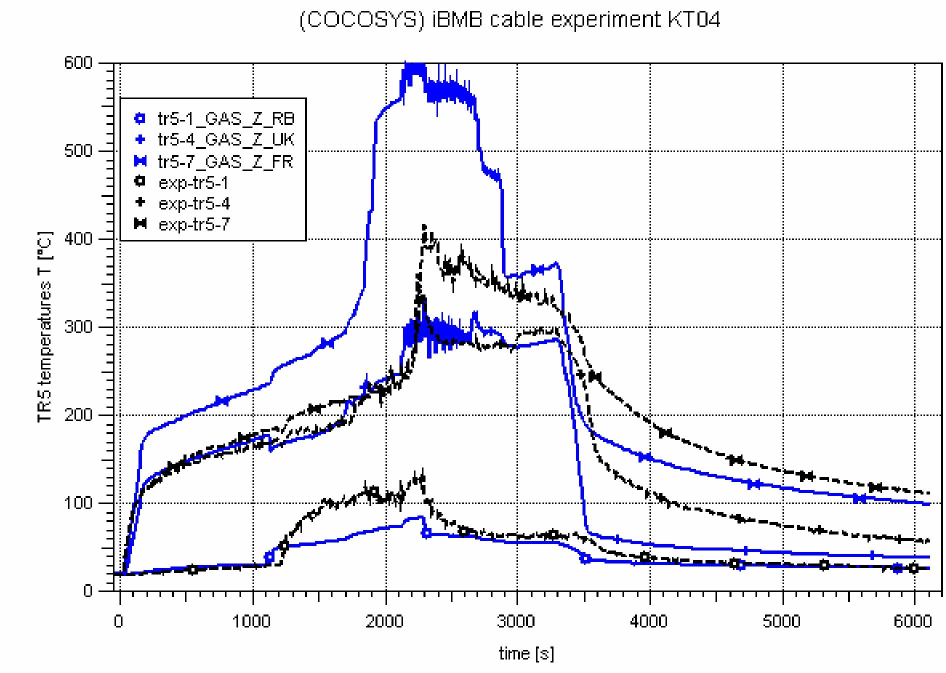


**Fig. E-65** Test 4: Temperatures at tree TR5 close to gas burner

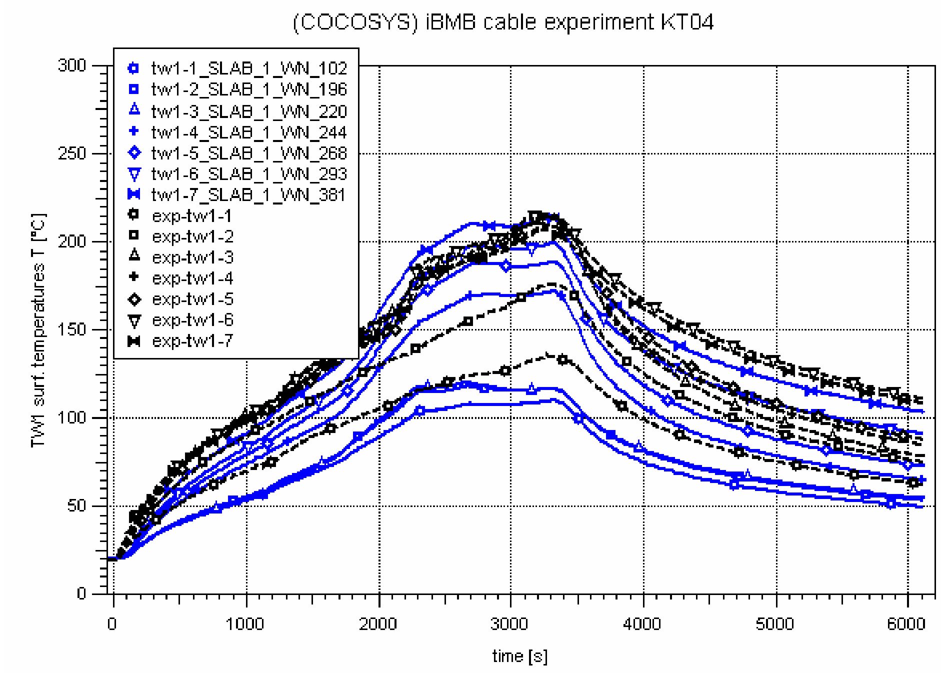


**Fig. E-66** Test 4: Surface temperature at backside wall TW1

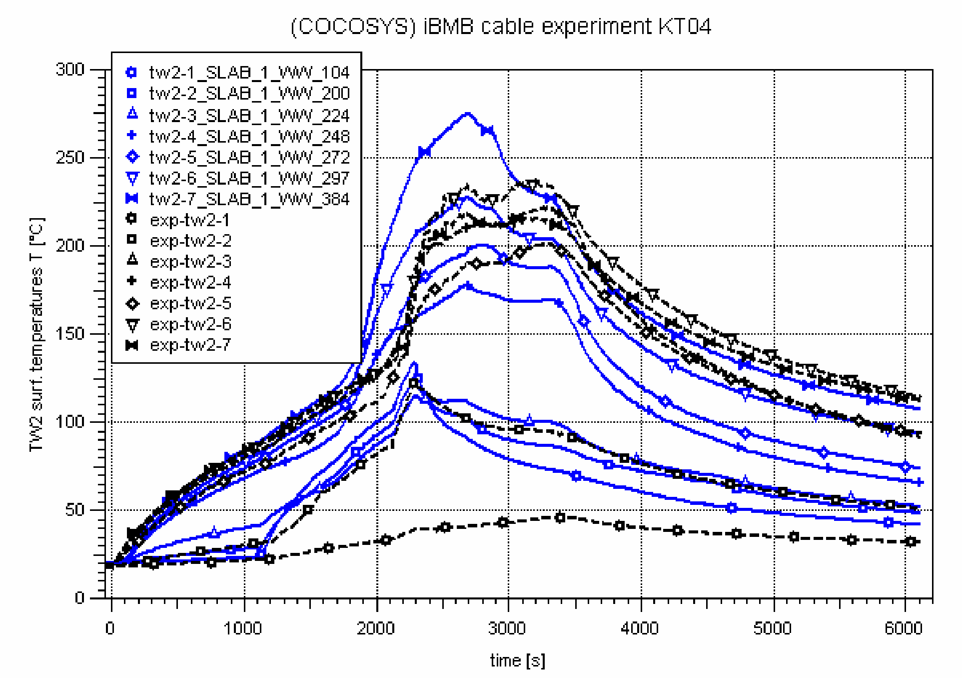


**Fig. E-67** Test 4: Surface temperature at left side wall TW2 close to gas burner

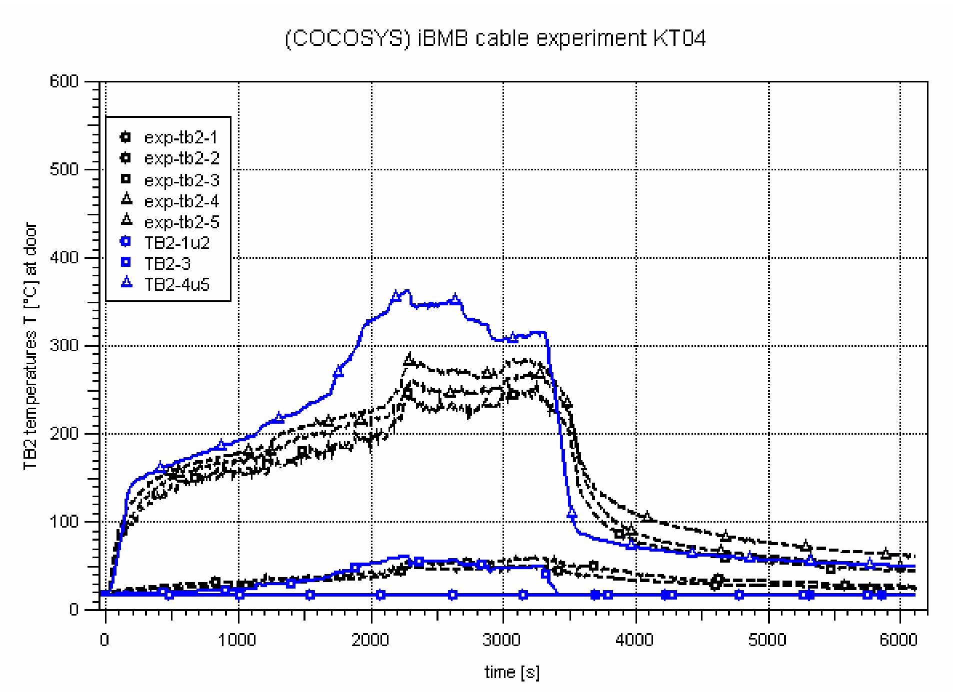


**Fig. E-68** Test 4: Temperature at door location TB2

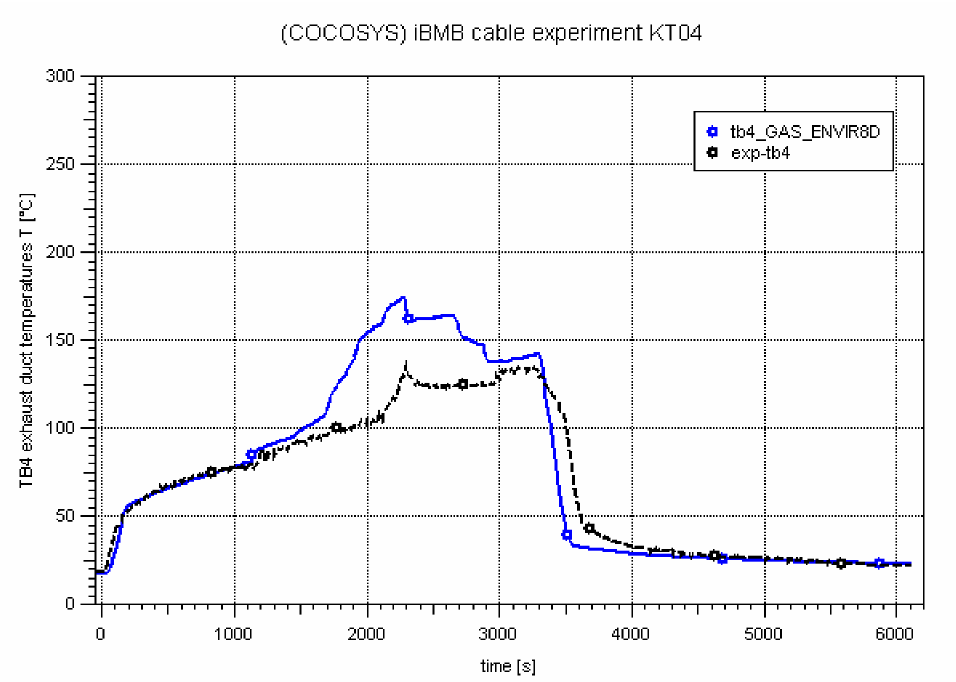


**Fig. E-69** Test 4: Temperature inside the exhaust duct

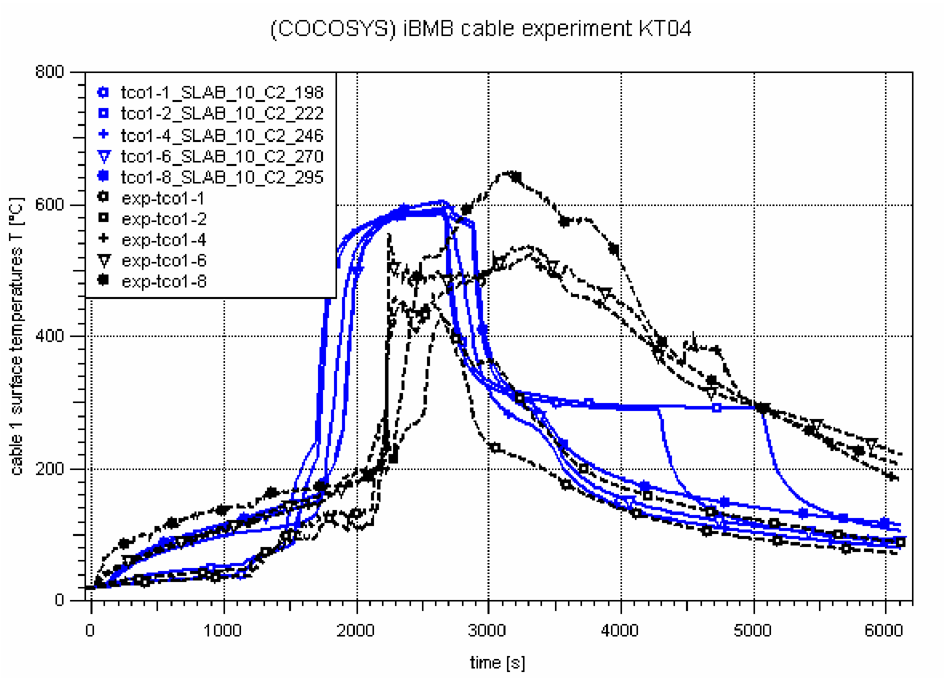


**Fig. E-70** Test 4: Cable surface temperature at TCO1 location (outside, power cable)

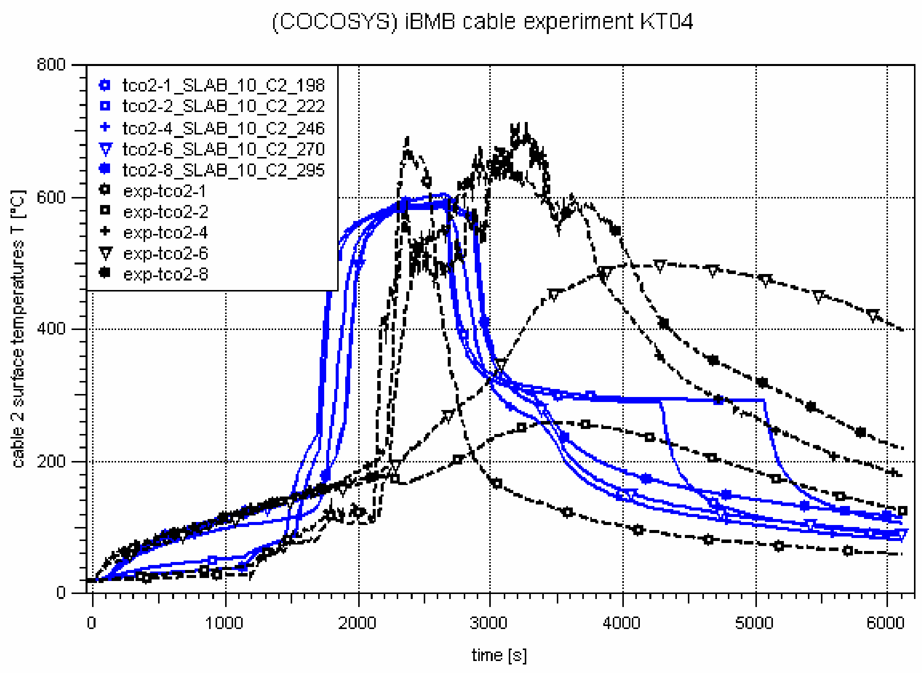


**Fig. E-71** Test 4: Cable surface temperature at TCO2 (inside, power cable)

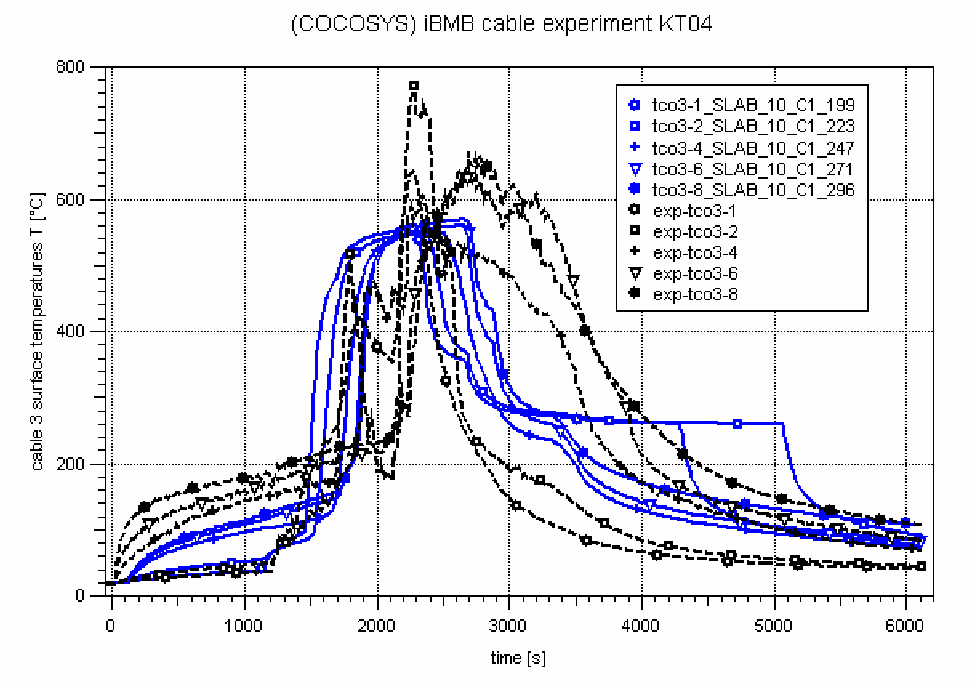


**Fig. E-72** Test 4: Cable surface temperature at TCO3 (outside, I&C cable)

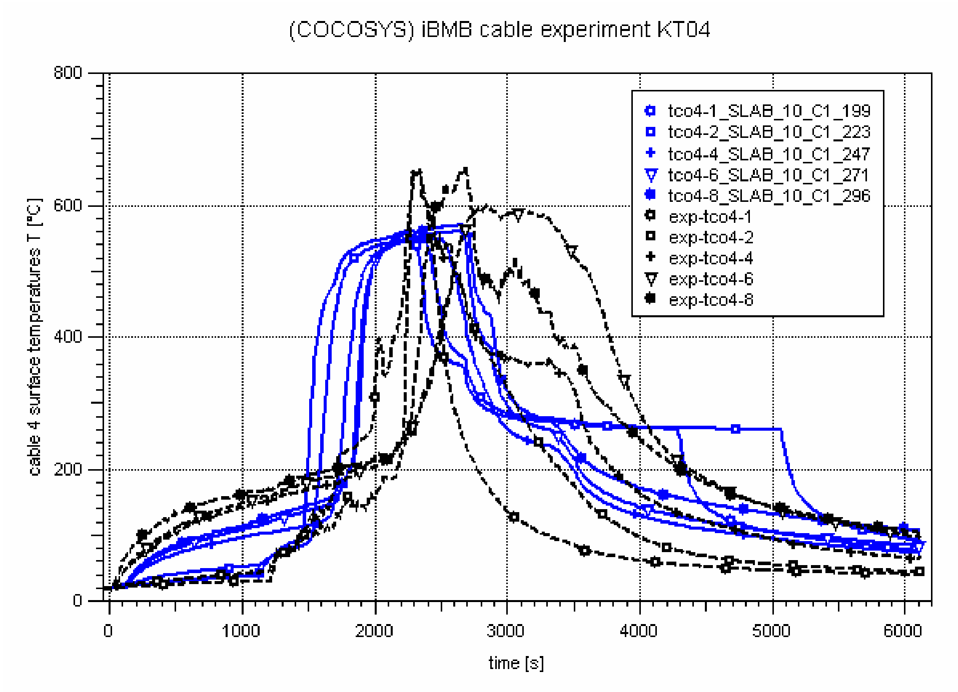


**Fig. E-73** Test 4: Cable surface temperature (inside, I&C cable)

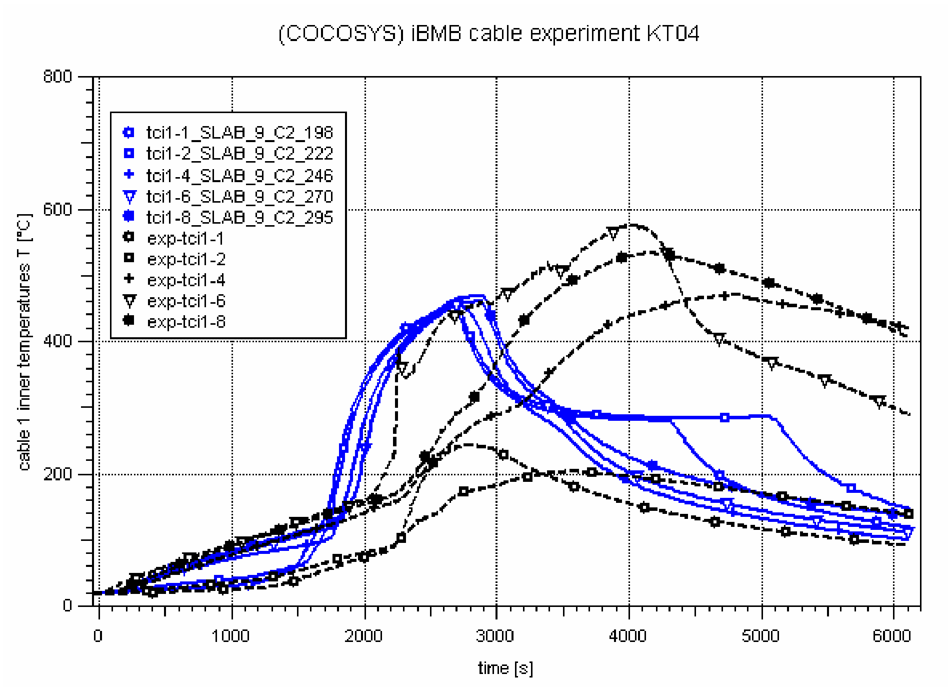


**Fig. E-74** Test 4: Cable center temperatures at TCI1

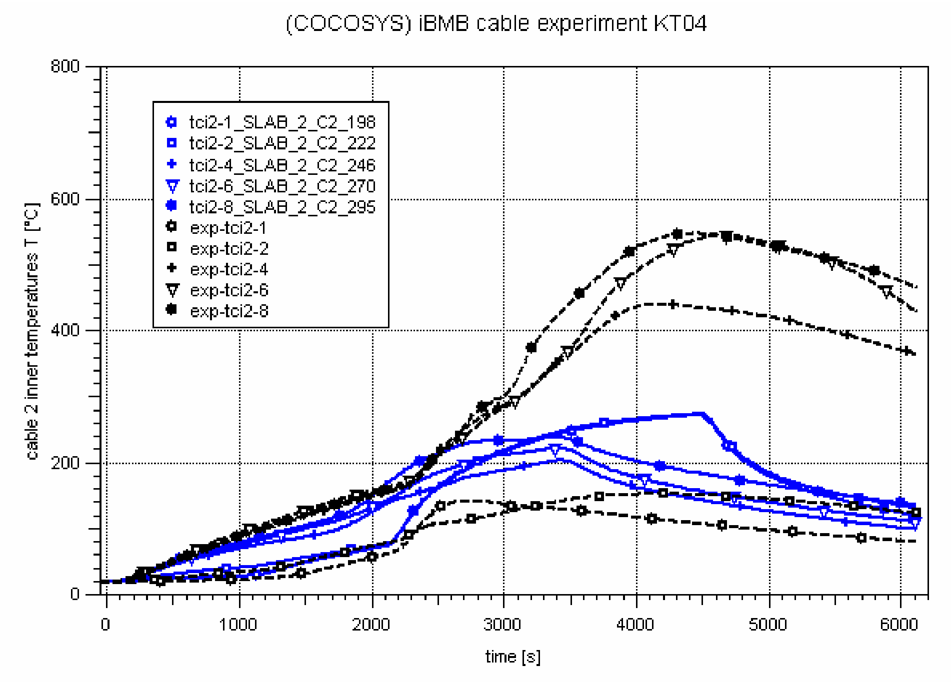


**Fig. E-75** Test 4: Cable center temperature at TCI2

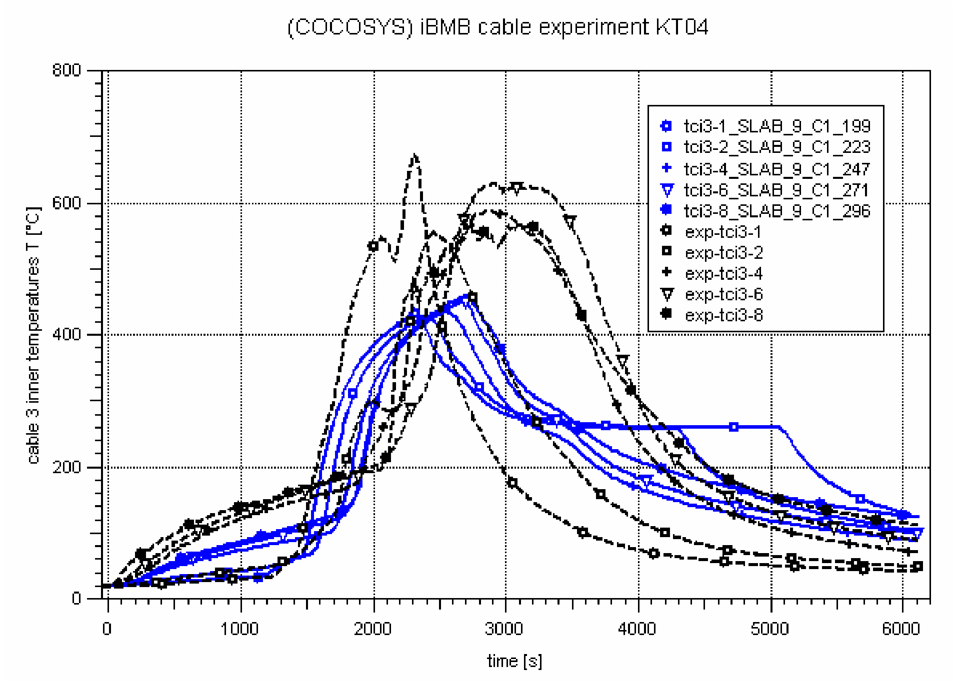


**Fig. E-76** Test 4: Cable center temperature at TCI3

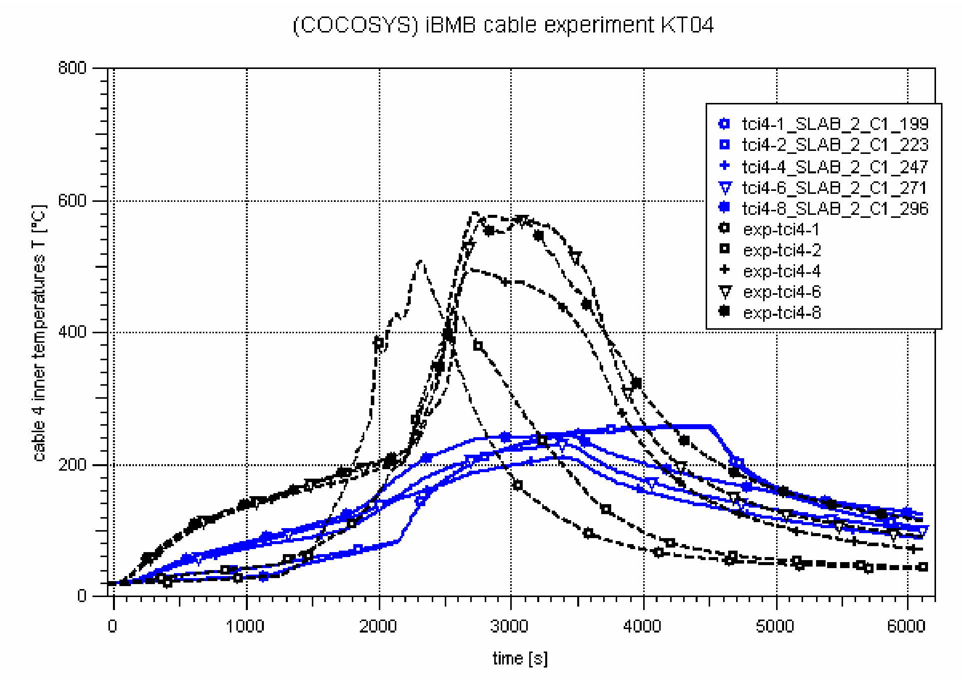


**Fig. E-77** Test 4: Cable center temperature at TCI4

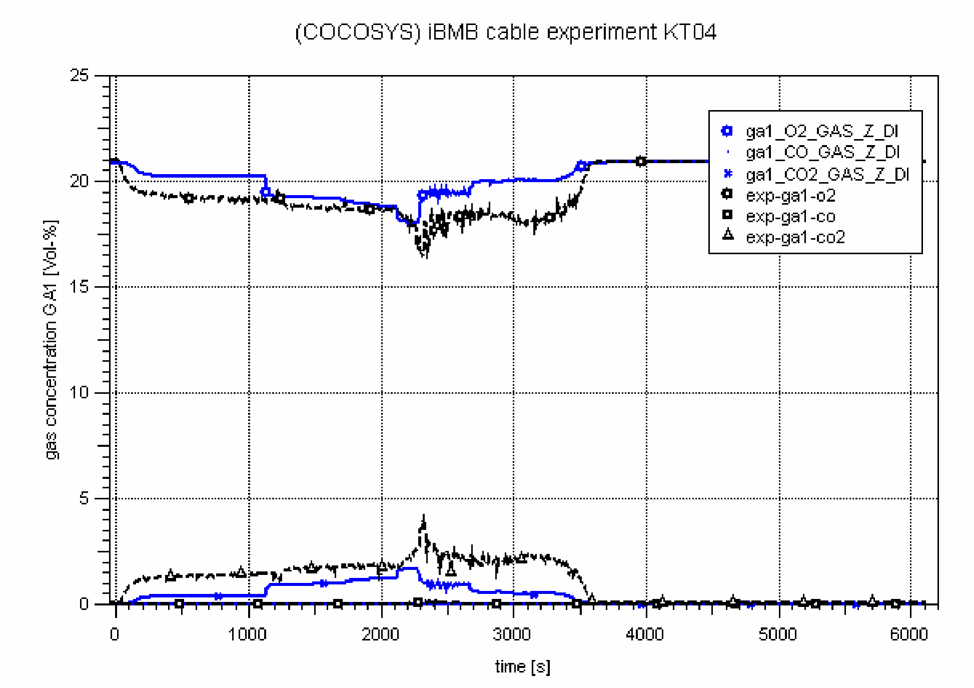


**Fig. E-78** Test 4: Gas concentration at GA1

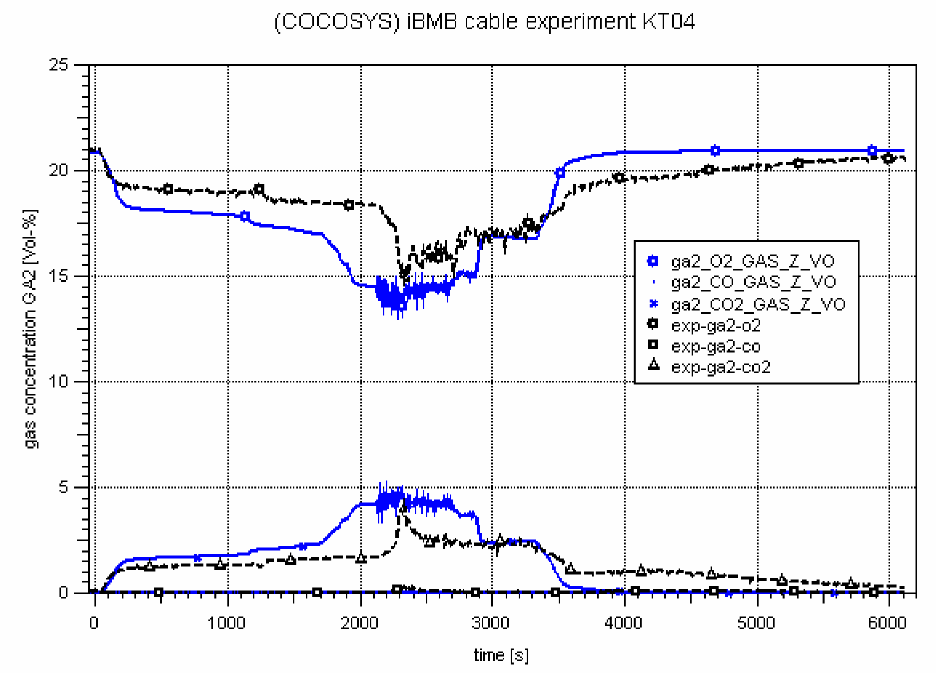


**Fig. E-79** Test 4: Gas concentration at GA2

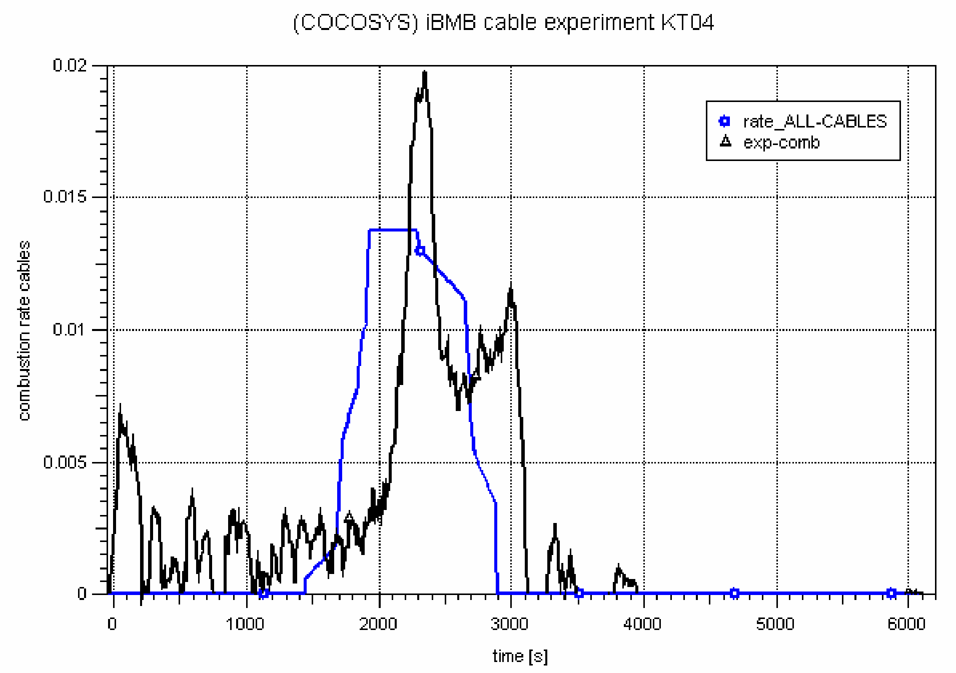


**Fig. E-80** Test 4: Cable pyrolysis rate (weight loss)

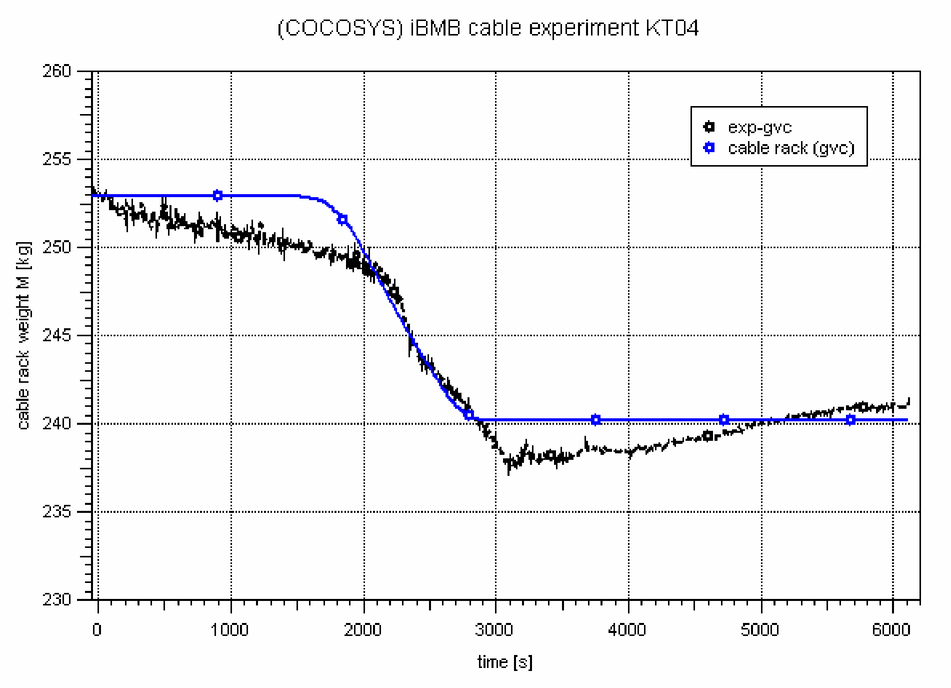


**Fig. E-81** Test 4: Weight loss of cable trays

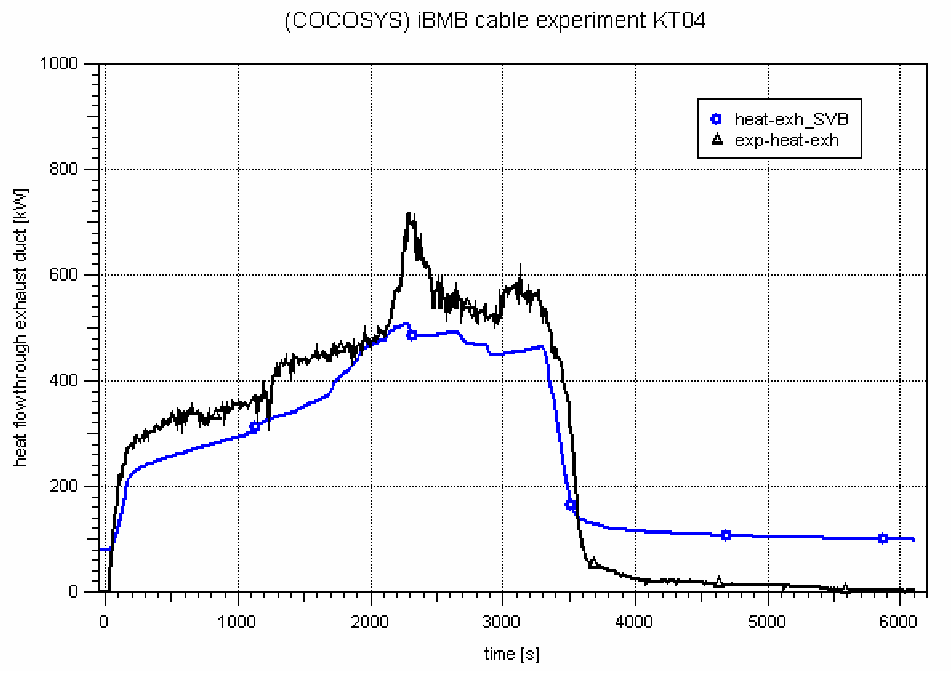


**Fig. E-82** Test 4: Heat flow the exhaust duct

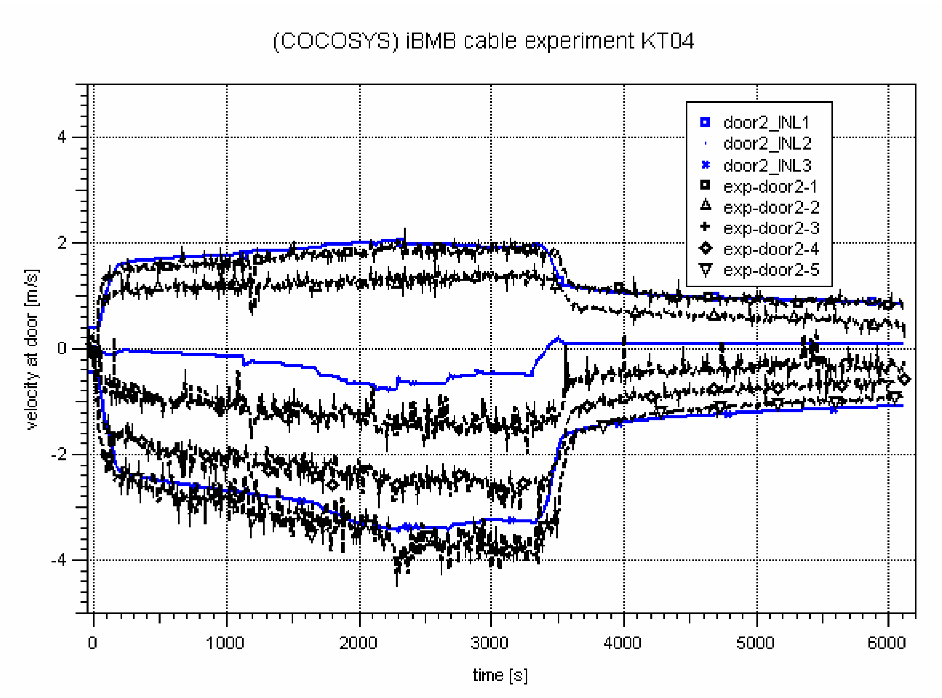


**Fig. E-83** Test 4: Velocity at door

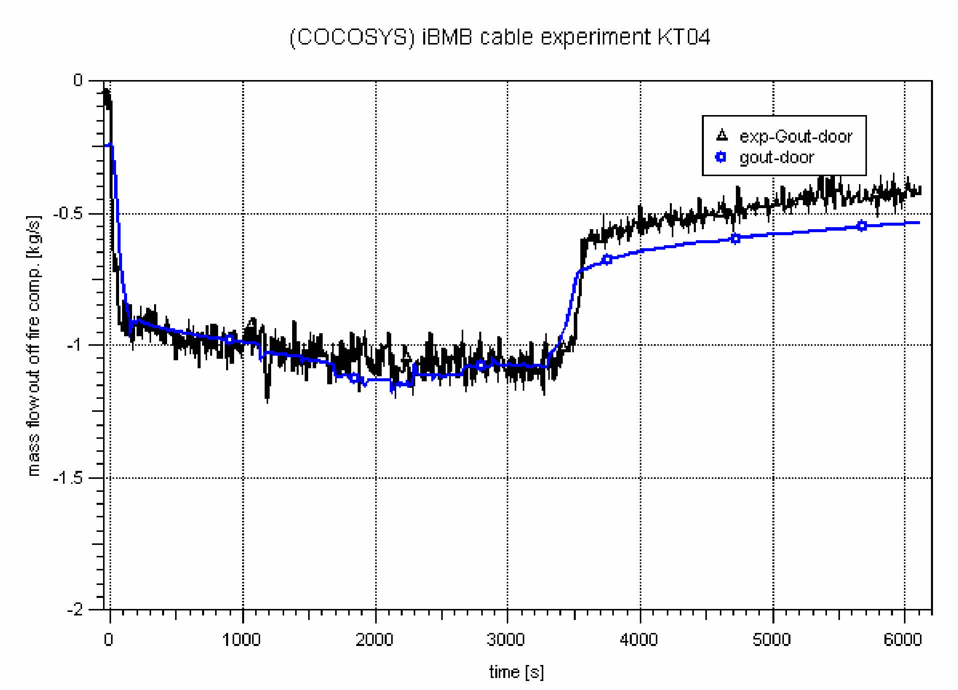


**Fig. E-84** Test 4: Mass flow out of fire compartment through the door

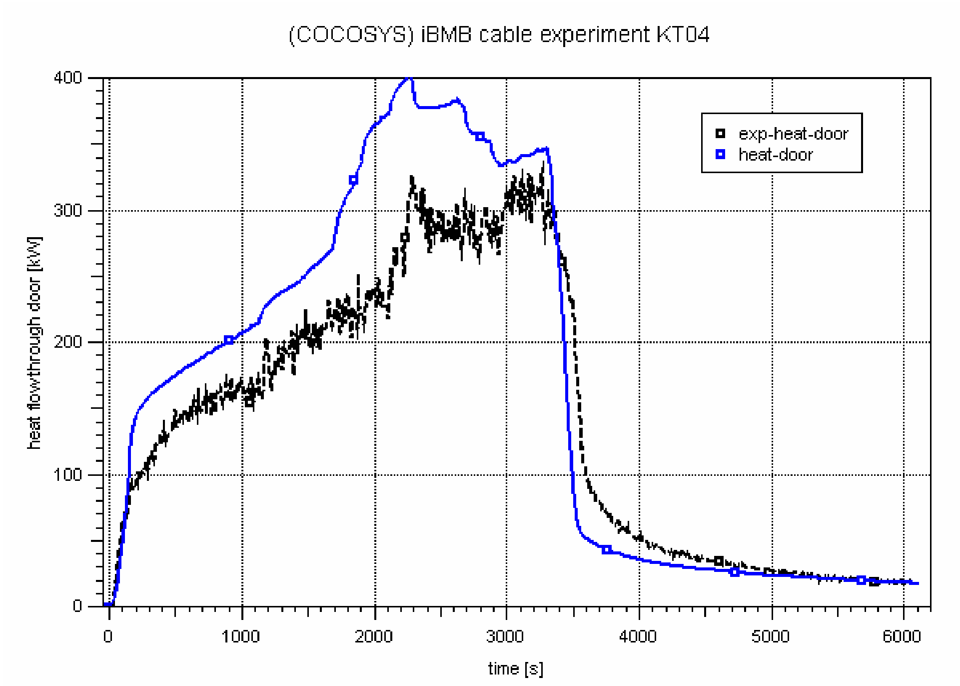


**Fig. E-85** Test 4: Heat loss through door

## E4 Conclusions

Within the frame of ICFMP calculations with COCOSYS have been carried out for Benchmark Exercise No. 5. In this experiment vertical cable fire with different materials (PVC and FRNC) and under different pre-heating conditions has been investigated. Due to larger problems with the stability of the calculation blind calculations have been performed for Test 1 and Test 3 only. After the release of experimental data large deviations have been found for the cable heat-up and pyrolysis rate. The overall energy and mass balance have been simulated quite well. Some problems results from the missing plume model in COCOSYS, leading to incorrect air entrainment and plume size. Therefore, as usual, the deviations of results close to the fire are larger.

For the open calculations the COCOSYS program has been extended at two points:

– Improve the heat transfer into the cables close to the gas burner fire

– Introduce a remaining mass fraction for incomplete burn-down of cables

This was a first test of these new options. The quality has to be validated further. Some problems still exist concerning the stability in the zones close to the vertical trays.

It is planned to implement a plume model within the frame of the next COCOYS developing project.

The cable trays are simulated as rectangular slabs. The real situation is much more complex. This could be estimated in differences between TCI2 and TCI4. For power cables some delayed heating could be observed. All these effects could not be simulated with COCOSYS. Further the differences between power and I&C cables are much larger in the experiment than predicted with COCOSYS.

The ignition of PVC cables was not modeled realistically. Some improvements are still necessary.

Looking at experimental data, the FRNC cables are practically not burning. The simulation of such a cable material is therefore very difficult because it will start to burn at certain higher temperatures. Local effects like blistering of cable material and small local fires can not be simulated with such a simple model approximation.

The gasification observed during the pre-heating of PVC cables could not be simulated with COCOSYS using the simple cable burning model. A more detailed model considering the evaporation of different fractions of material is still planned, but not in the near future.

Considering the difficult boundary conditions (but which are much simpler compared to real plant conditions) the results of COCOSYS are quite encouraging.

## E5 References


/ALL 05/ Allelein, H.-J. et al.:
Weiterentwicklung der Rechenprogramme COCOSYS und ASTEC, Abschlussbericht, GRS-A-3266, Gesellschaft für Anlagen- und Reaktorsicherheit, April 2005

# Appendix F: CFX Calculations for Benchmark Exercise No. 5

**Presented by**

**Matthias Heitsch**

Gesellschaft für Anlagen- und Reaktorsicherheit (GRS) mbH

Schwertnergasse 1, 50667 Köln, Germany

# F1 Introduction

This report describes the calculations carried out for Benchmark Exercise No. 5 with the code CFX 10 /ANS 05/ within the frame of the International Collaborative Project for the Evaluation of Fire Models (ICFMP). The code version 10 of the CFX family offers the ability to use a mixture of structured (hexahedral) and unstructured (tetras, pyramids) cells to represent a given geometry. This provides the flexibility to model any kind of arrangement and is important if complex flow patterns are expected.

Benchmark Exercise No. 5 is focused on the pyrolysis from sufficiently heated cable trays. This complex process is not available as a kind of model in CFX. However, the basic elements for inclusion of arbitrary models are provided in the code concept. Therefore first steps were made to implement a pyrolysis model in CFX. Taking into account the large effort which has been made with other codes to implement and validate such a model, only Test 1 from the available tests was analyzed.

## F2 Computer Model of the Test Facility

The test facility in this Benchmark Exercise was also used in Benchmark Exercise No. 4. This time the computational grid was built differently. Basic structures such as cable bundles, separating wall, gas burner and preheating pool are composed of structured cells; the rest is then filled by unstructured cells. This procedure is quite fast and more flexible than using exclusively hexahedral cells but results with more cells in the computational domain.

Fig. F-1 shows an overview of the mesh. A horizontal cut is depicted in Fig. F-2. It shows the finer mesh close to the cable bundles. Care was taken to resolve the inside of the cable bundles with small enough cells close to the surface. This can be seen in Fig. F-3. In the vertical direction a corresponding number of subdivisions was chosen (70) to restrict aspect ratios of cells to about 25. Individual cables within the bundles are not represented in the mesh (although it is possible to do). Instead the density of the bundles is assumed to be represented only by insulator. This approach is acceptable as long as heat does not propagate into the copper wires of cables. Some uncertainty arises from the selection of heat conductivity and heat capacity of the cable materials (FRNC). Only the product is provided in the test specification, but CFX needs to input both values separately. It was decided to use the heat conductivity of PVC and calculate the heat capacity to fit into the given product equal to $\lambda * \rho * c_P$.

The mesh sums up to a total of 162520 elements. The majority is tetrahedral cells (129530) followed by 27890 hexahedral cells, which are mainly found in the cable bundles. In the computational domain we find gas space and solids which represent the cable bundles. For CFX three different domains were consequently defined. These domains interact through domain interfaces. These interfaces can also be used to establish sources of mass and energy to model pyrolysis.

The external hood is not included in the computational grid.

### F2.1 Pyrolysis Model

CFX offers the possibility of specifying sources of mass and energy in volumes and at boundaries. Boundaries can also be interfaces between fluid and solid domains. In the general case each cell close to the boundary between gas and the combustible solid can be checked if a given ignition temperature is exceeded. If this is the case then the pyrolysis of the solid body depending on a given (probably temperature dependent) reaction rate can be invoked. Oxygen from the surrounding atmosphere is consumed as well as carbon from the solid. The total amount of carbon in the solid is the upper limit which can be consumed. Co and $CO_2$ are released to the gas space. According to the solid composition additional gas releases possible. **Fig. F-4** illustrates the current approach.

A problem is how to distribute the carbon consumption inside the solid. The total consumption across the interface can be determined by summarizing along all cell faces. Currently this sum is then equally distributed as a sink term to all cells inside the combusting solid. This method needs improvement because pyrolysis is a local phenomen.

In the given context the basic idea of passing each individual cell along the interface of the cable bundles and employing local pyrolysis rates could not be implemented because of practical reasons. The limitation is that such a model can only be implemented by extra Fortran routines which need a certain 64-Bit compiler. This compiler is not yet available. Consequently a simpler approach was chosen, which does not need extra routines. Only the maximum temperature of the cable bundle is checked as a set-on switch of pyrolysis and a constant combustion rate (not varying from cell to cell) of 0.002 kg/s (derived from the experiment) is used as basis for releases of energy, CO and $CO_2$.

## F3 Physical Description of the Tests by CFX

In the experiments a propane burner was used to heat up the cable bundles. For some tests an additional ethanol pool fire for preheating was used. Because only Test 1 is considered here, ethanol is not included in the species list of CFX. The gas mixture of air and the fuel propane is modeled by the individual species, which are propane, oxygen, nitrogen, carbon-monoxide, carbon-dioxide and steam. Soot is also created according to the Magnusson soot model implemented in CFX. In this model a number of constants are used, which were not further investigated in the given context. Nitrogen represents a background fluid, not participating in any reaction. The chemical reaction itself is represented by a two-step mixing controlled reaction within the Eddy Dissipation model. The summarizing reaction modeled reads

$$C_3H_8 + 5O_2 \rightarrow 3CO_2 + 4H_2O \tag{E-1}$$

A predefined share of the reaction heat (30 %) is emitted from the surface of the gas burner surface as radiation flux and distributed by the P1 radiation model in CFX. This radiation model solves an extra transport equation and assumes direction independent radiation transport. It allows heating of the fluid due to radiation from a boundary (here the fuel pan). The fuel flow from the gas burner is prescribed according to the measured heat release recalculated as fuel mass consumption. The chemical reaction happens according to the mixing intensity in the fluid domain and according to the local availability of fuel and oxygen. Flows through the door happen according to density differences by pressure, temperature and composition.

A simplification was made concerning the heat flow into the surrounding walls. These walls are not included in the mesh and hence the heat flow is calculated at constant wall temperature. This overestimates the removal of energy from the fluid. Alternatively a one-dimensional heat conduction model as a boundary condition to CFX without including the walls directly in the mesh is available, but was not applied.

# F4 Simulation Results and Comparison to Test Data

The specification of all tests is found in /HOS 05/. Test 1 was carried out without pre-heating pool.

## F4.1 Test 1

The fuel release rate from the gas burner which is used by CFX is shown in **Fig. F-6**. The curve shown is recalculated from a heat release curve (**Fig. F-5**) provided in the specification report. The blue curve in this figure is supplied to CFX. The difference between the blue curve and the red curve which represents the total heat release is constituted by the extra heat production by pyrolysis. The current simulation by CFX however does not include pyrolysis in the first test phase before the gas burner power is doubled.

Selected gas temperatures along three probe lines (TP, TR1 and TR3) are depicted in Fig. F-7, Fig. F-8 and Fig. F-9. They all show a similar tendency. The calculated histories follow quite strictly the changes in the heat release curve whereas the measured data follow the heat release curve much slowly. Temperatures close to the floor are overestimated for probe lines TP and TR3, which are above or close to the pool. Temperatures along the line close to the door (TR1) are slightly lower than the measured values. This may be due to the flow incoming through the door (see also Fig. F-12). A distribution of flow velocities over the height of the door is presented in **Fig. F-10**. Measured velocities are matched quite well. The correspondence to measured data is improved after the power increase of the gas burner at about 2400 s. In the test data inflow and outflow through the door are separated. This is not available for CFX. Instead the total flow is provided. In Fig. F-11 these flows are compared. The calculated flow is close to zero, the measured is slightly negative. The difference is probably compensated by higher heat fluxes to walls in the simulation. Fig. F-12 and Fig. F-13 illustrate the typical flow distribution across the door opening. The boundary between inwards and outwards directed flow contributions is moving over time and is typically inclined over the cross section of the door (Fig. F-13).

The gas analysis is described by oxygen and $CO_2$ histories. These are compared to measured data in Fig. F-14 and Fig. F-15. It reveals that more oxygen than measured is consumed in the simulation. Accordingly the built-up of $CO_2$ is over-predicted. It is not clear whether the released amount of propane (recalculated, see Fig. F-6) is incorrect or whether the ventilation of fresh air through the door influenced the gas composition at the analysis locations more strong than calculated.

No data are available for the heat fluxes to the individual walls. Calculated values are shown in Fig. F-16. The sum of heat fluxes to all walls can be compared to the measured total heat flux as presented in Fig. F-17. In the beginning there is some over estimation in the simulation because the wall temperatures are kept constant (simplification).

The pyrolysis model applied is based on the maximum surface temperatures on the cable bundles. The calculated maximum temperatures together with corresponding ignition temperatures are shown in Fig. F-18. Bundle C denotes the smaller bundle with cable material C and D denotes the bundle with material D. The bundles are not heated equally. The non-uniform heat-up of the bundles is characterized in Fig. F-18 and illustrated in Fig. F-19. In bundle C the ignition temperature is not reached. The simulation consequently predicts no pyrolysis in bundle C and in bundle D only in the second phase of the test. The energy release is shown in **Fig. F-20**. This behavior is also reflected in the incident radiative flows at the surface of the two bundles **Fig. F-21**. The flows are positive as long as the net energy flow is directed towards the bundles. In the late phase of the experiment bundle D is at higher temperature than the environment. Consequently it loses energy by radiation.

## F5 Conclusions

Test 1 of the pyrolysis experiments was simulated in open mode. For this purpose, a simple extension for CFX was implemented to include the principal behavior.

Heat release in Test 1 involves only a small contribution from pyrolysis. It is therefore possible that other approximations made in describing the experiment are responsible for the overall unsatisfactory comparison with test data.

The nominal heat release curve provided by the specification report was directly used to recalculate the mass flow of gas consumed by the gas burner.

Improvements are necessary in the representation of the outer walls. For these walls a simplified one dimensional heat conduction model is sufficient but could not be used because of lack of the special compiler needed for CFX. On the other hand the use of a 64 Bit AMD cluster machine reduced computing times considerably. When the upgraded 64 Bit compiler becomes available at GRS, the pyrolysis model can be further developed and the available user heat conduction model may be applied.

An issue is the resolution of the cable bundles. In view of preparing the same strategy for experiments and for nuclear applications it was decided to model the cable bundles entirely by their insulator and neglect the wires inside. This approach is only realistic as long as heat does not penetrate through the whole cable bundle. More experience is needed how the complex structure of bundles of modern cables can be modeled realistically.

## F6 Acknowledgement

The presented work was funded by the German Federal Ministry for the Environment, Nature Conservation and Nuclear Safety (BMU), which is gratefully acknowledged.

## F7 References


/ANS 05/ ANSYS Inc.;
CFX-10, User Documentation, ANSYS Inc., USA, 2005

/HOS 05/ Hosser, D., Riese, O., Klingenberg, M.:
Durchführung von weiterführenden Kabelbrandversuchen einschließlich der Präsentation der Ergebnisse im Rahmen des internationalen Projektes ICFMP, Vorhaben SR 2449, Unterauftrag UA-2298, Schriftenreihe Reaktorsicherheit und Strahlenschutz, BMU-2005-663, 2005

## F8 Figures

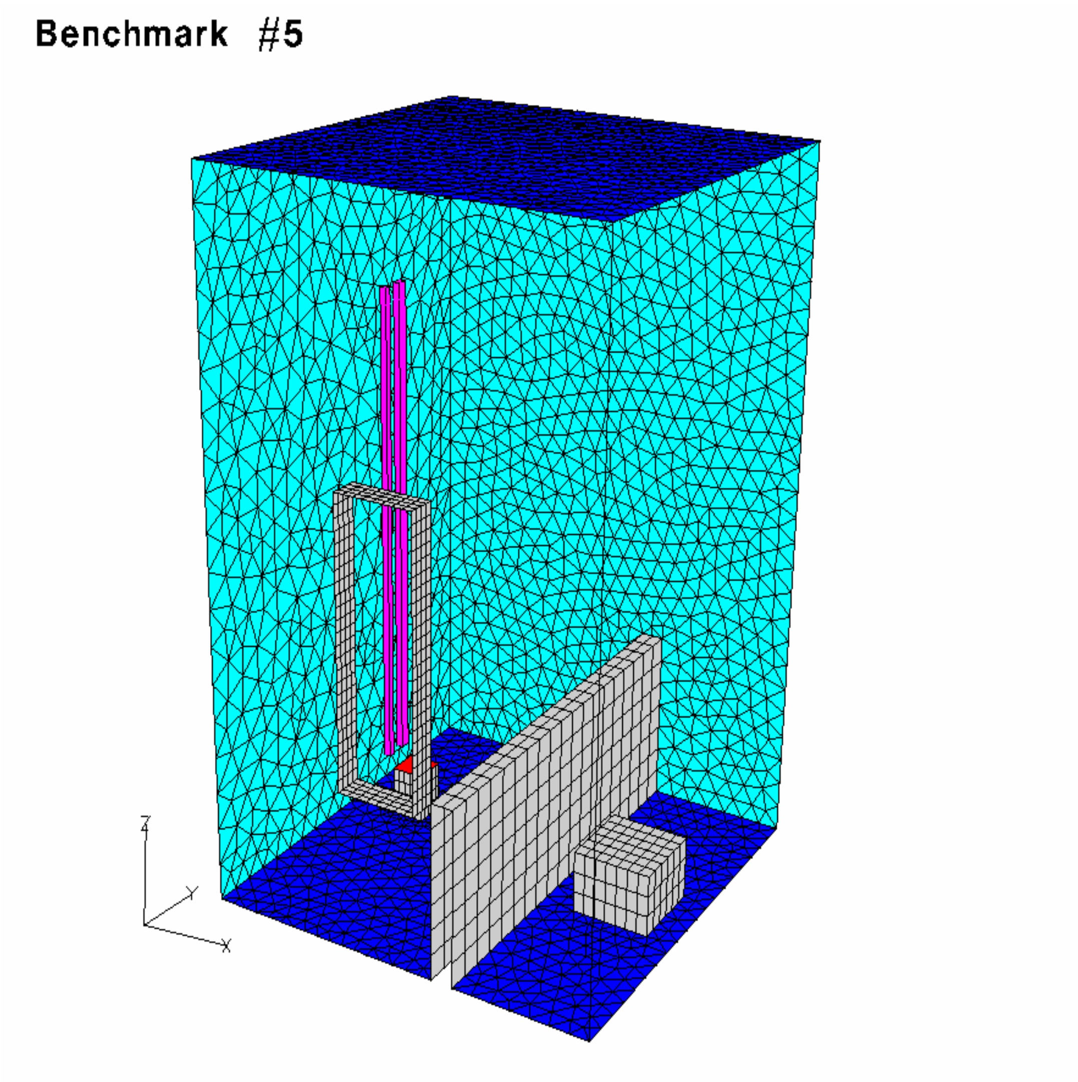


**Fig. F-1** Cut through the CFX model of the test facility in configuration for Benchmark Exercise No. 5

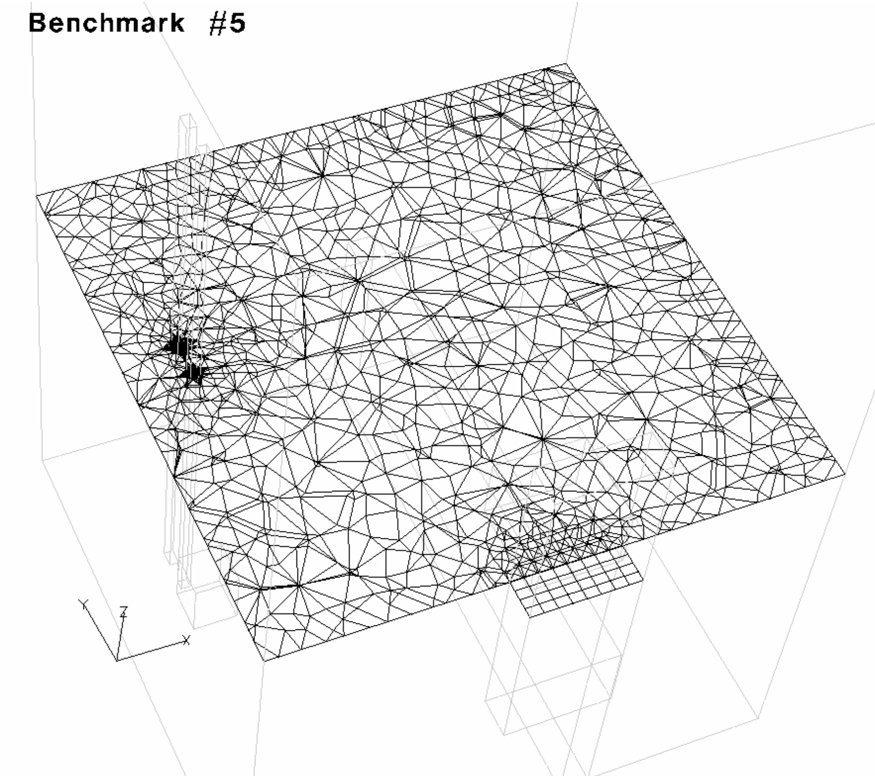


**Fig. F-2** Details of the mesh in a horizontal cut through the test facility

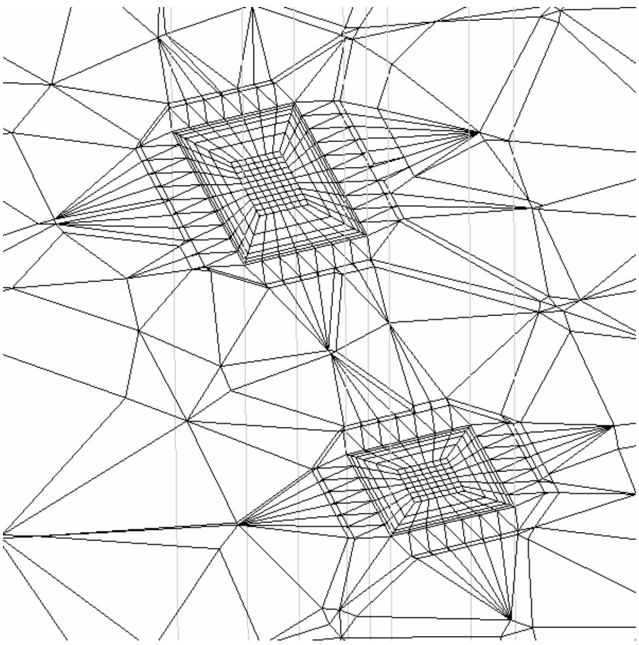

**Fig. F-3** Structured mesh to represent cable bundles

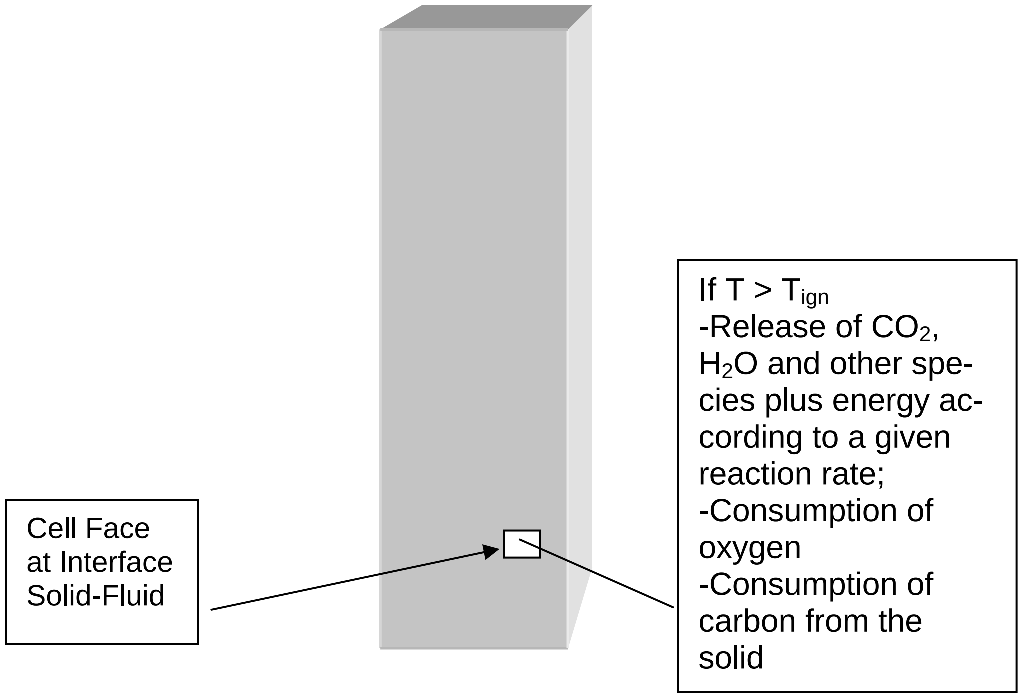


**Fig. F-4** Principle model to include effects of pyrolysis

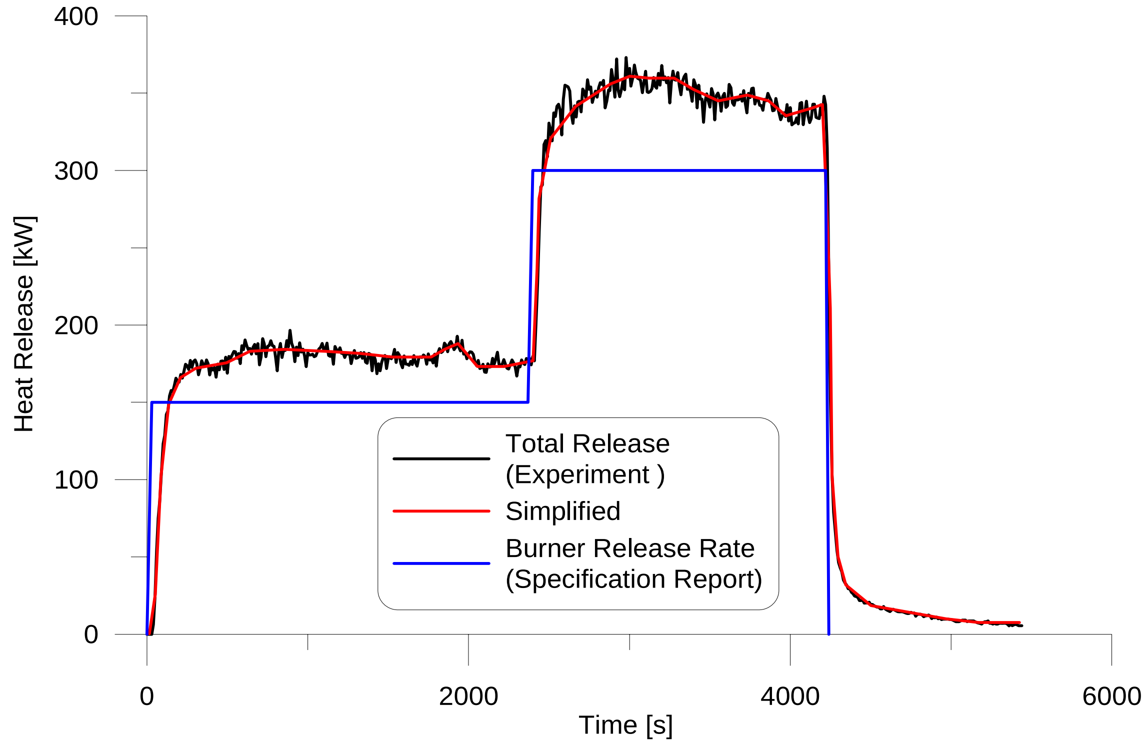


**Fig. F-5** Given heat release from the gas burner in Test

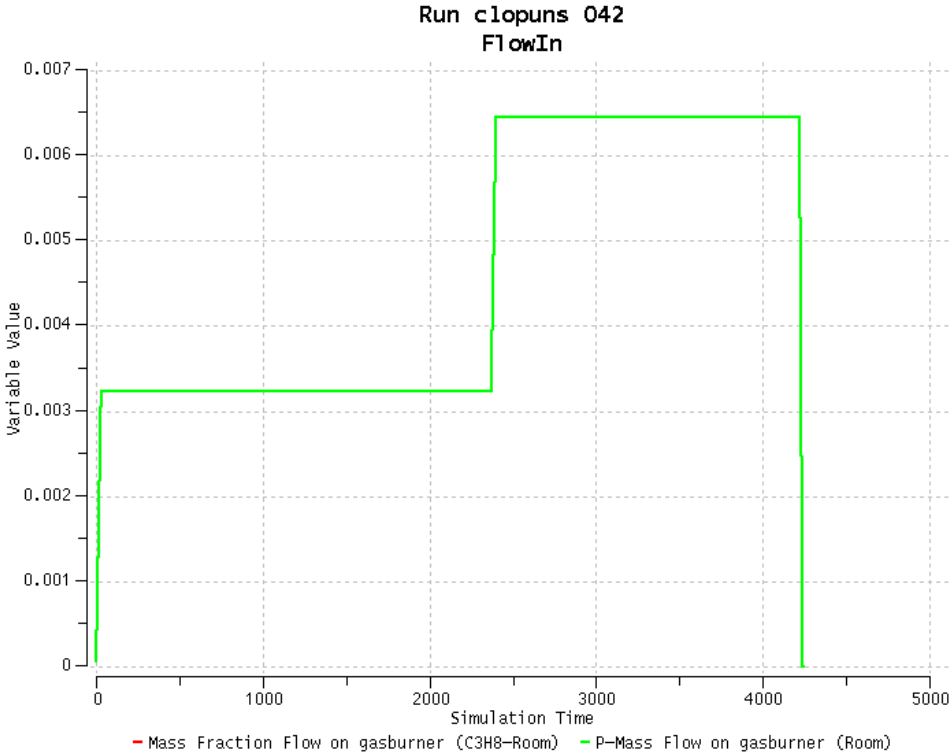


**Fig. F-6** Recalculated propane consumption [kg/s] in Test 1

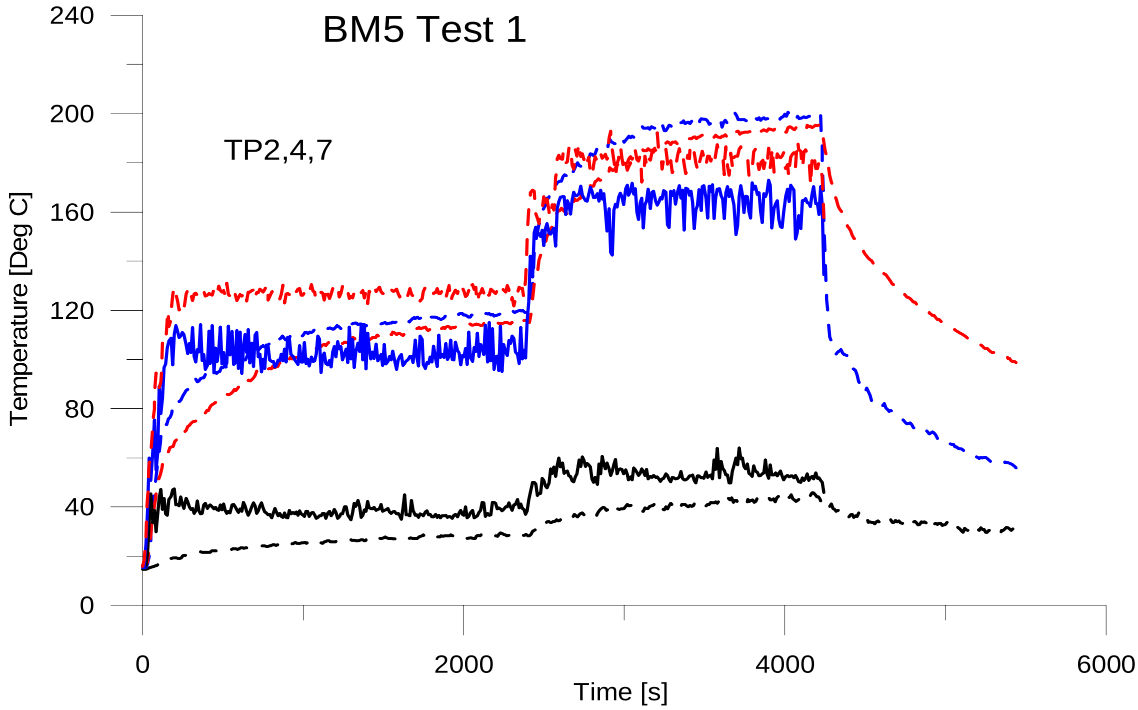


**Fig. F-7** Gas temperatures in plume

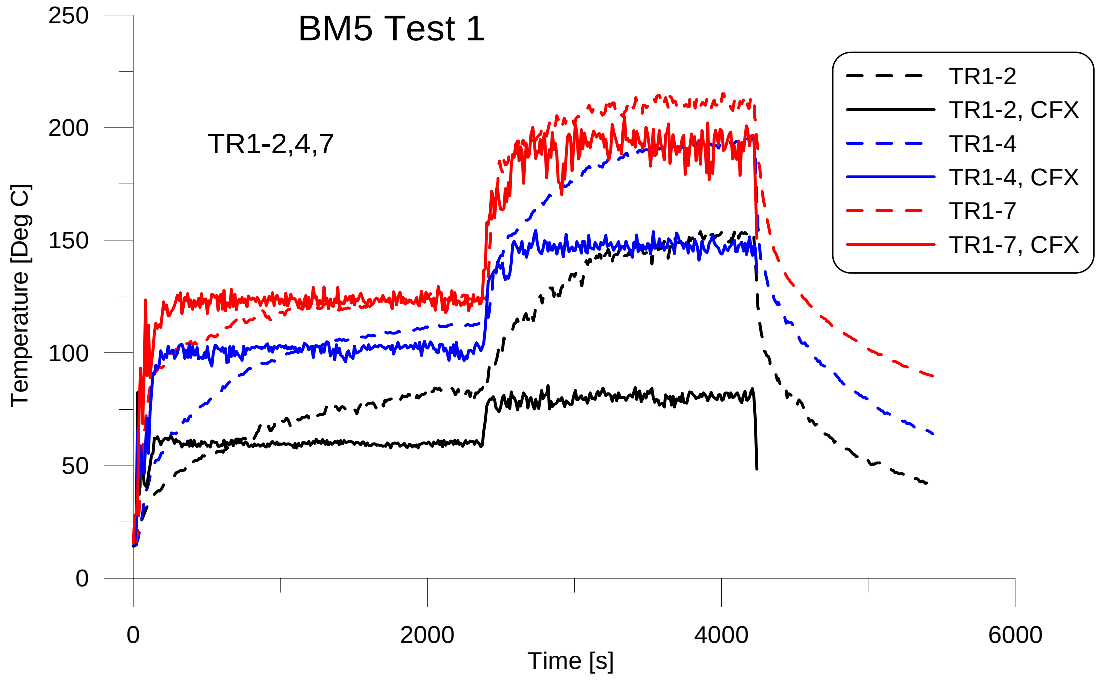


**Fig. F-8** Gas temperatures along line TR1

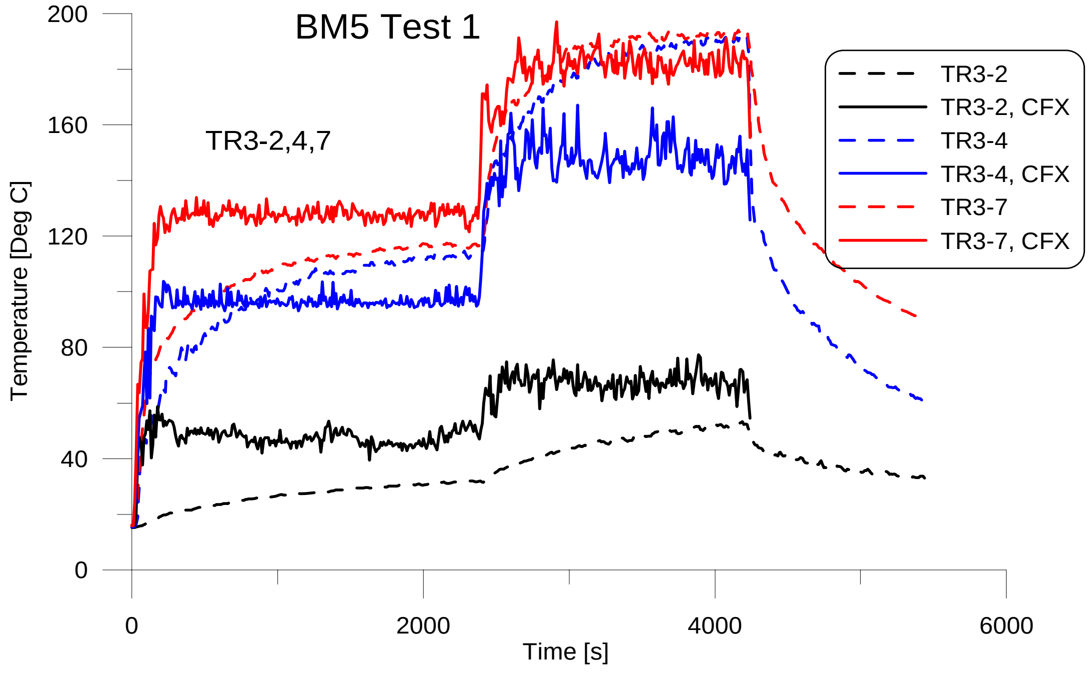


**Fig. F-9** Gas temperatures along line TR3

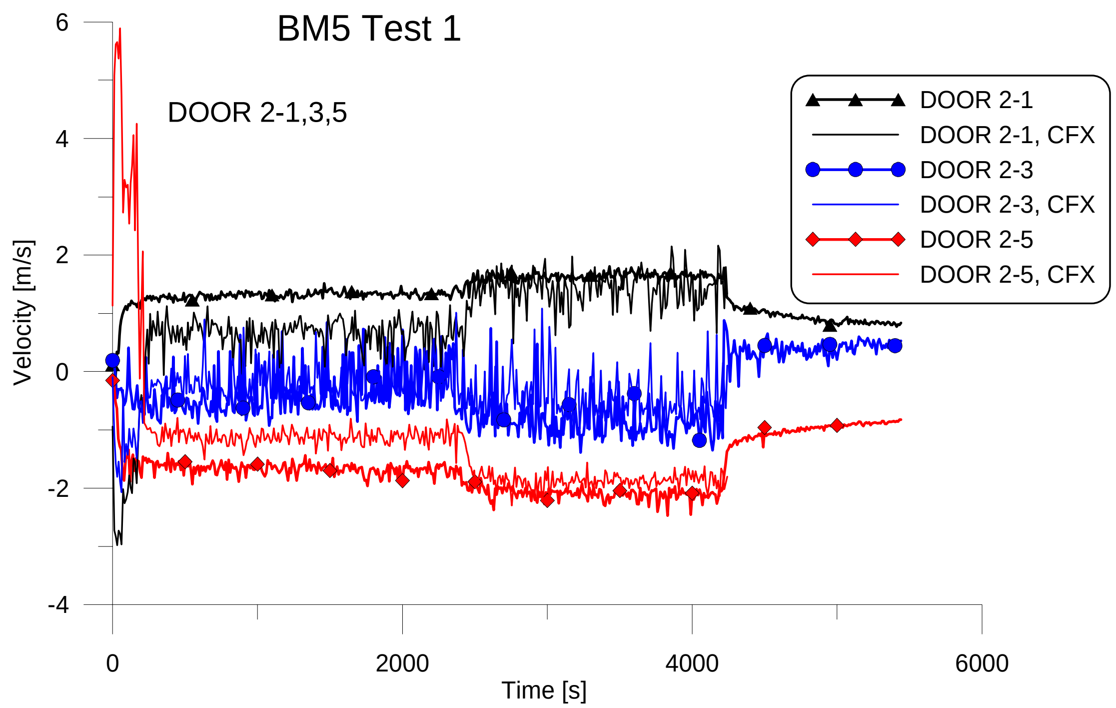


**Fig. F-10** Selected door velocities

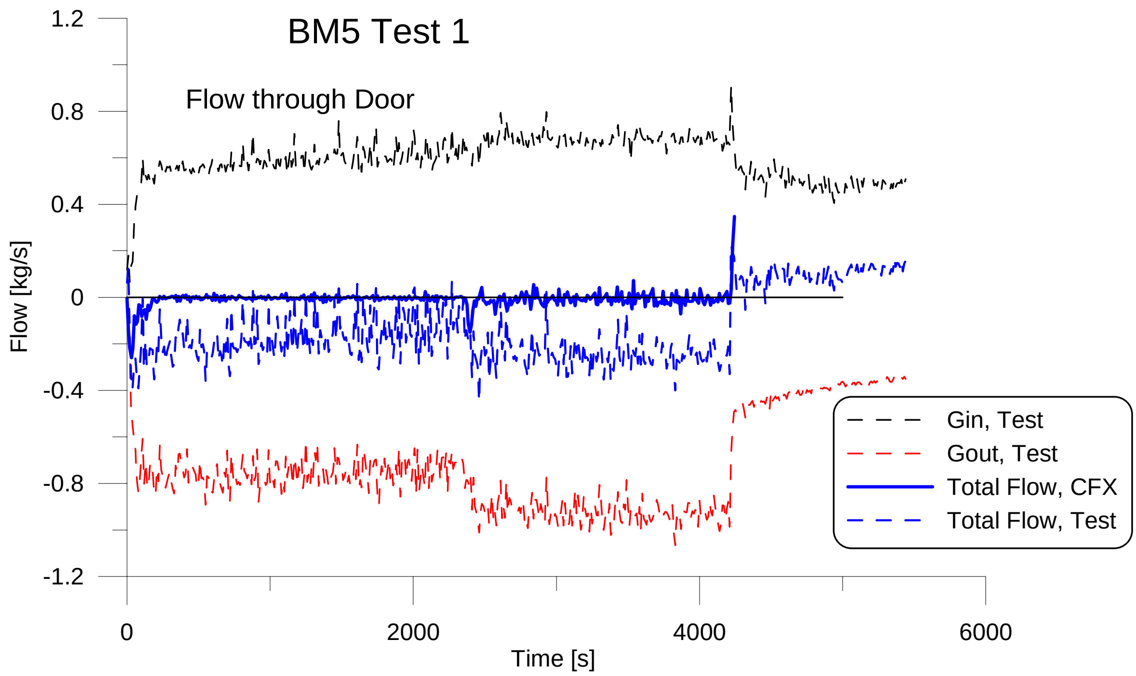


**Fig. F-11** Comparison of mass flow through door

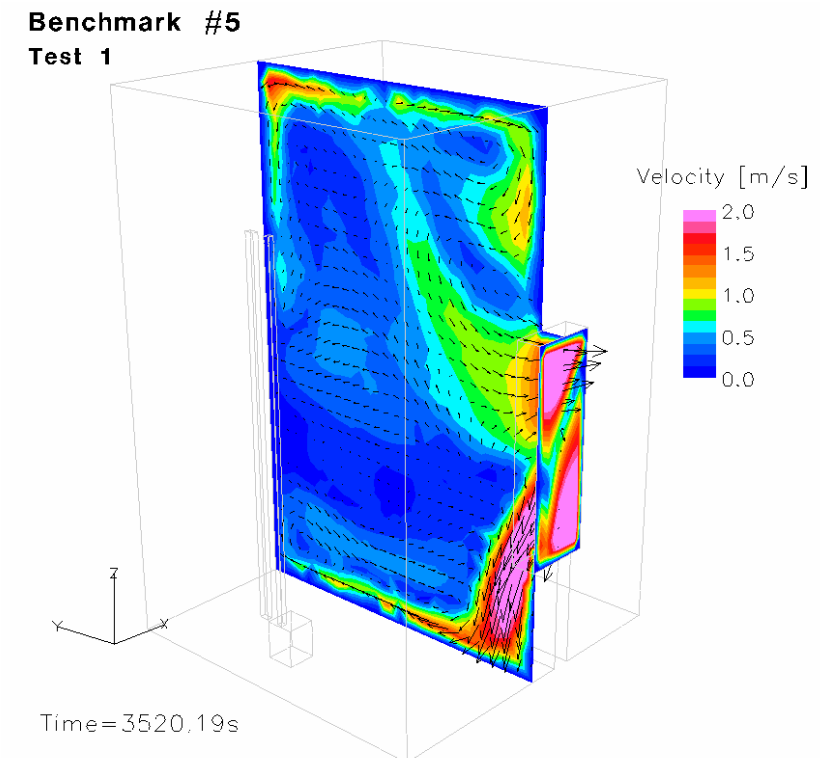


**Fig. F-12** Inflow of cold air through the door at about 3520 s

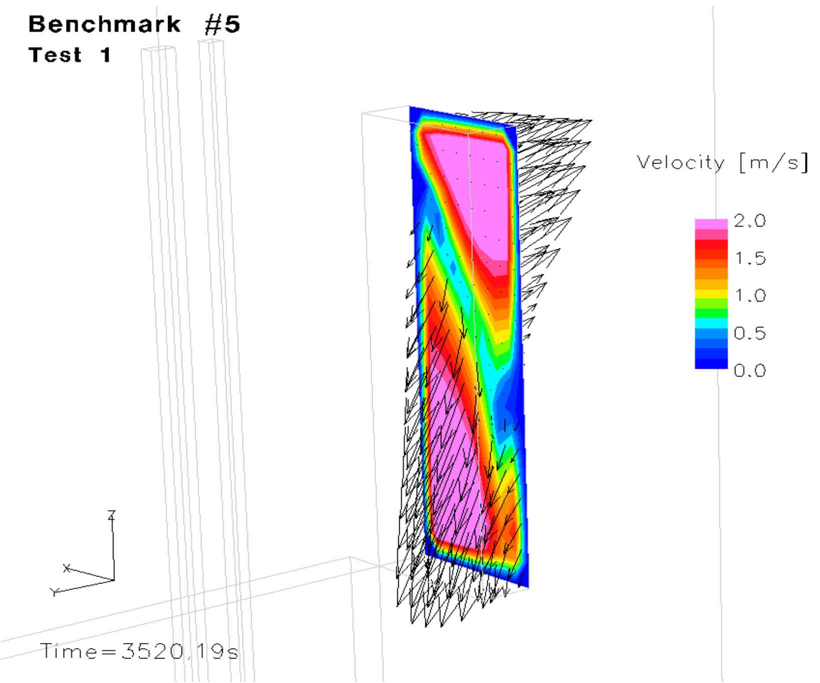


**Fig. F-13** Distribution of in and outflow in the door (view from inside the facility)

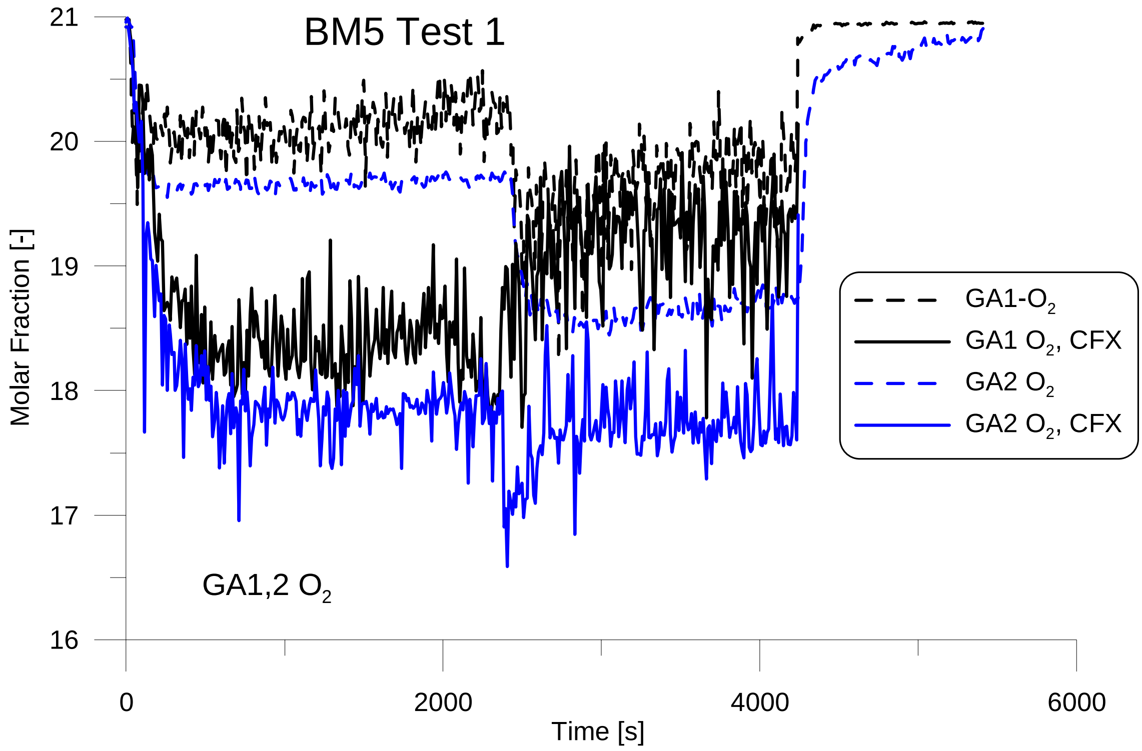


**Fig. F-14** Oxygen consumption at probe locations GA1 and GA2

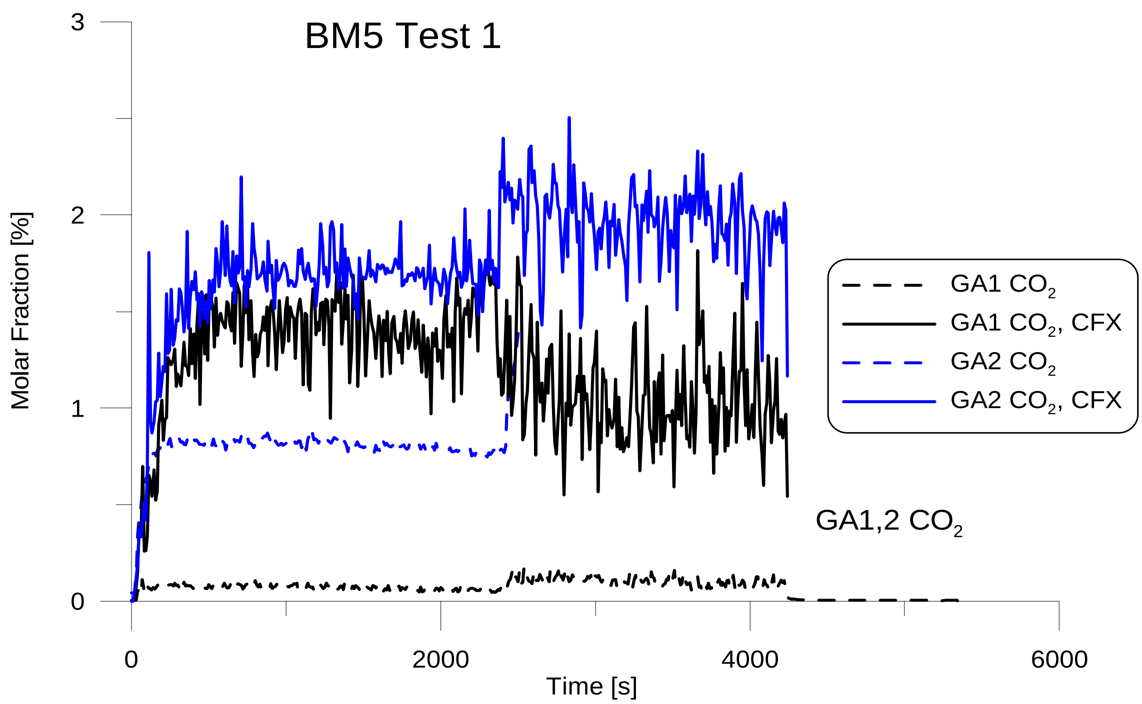


**Fig. F-15** $CO_2$ formation at probe locations GA1 and GA2

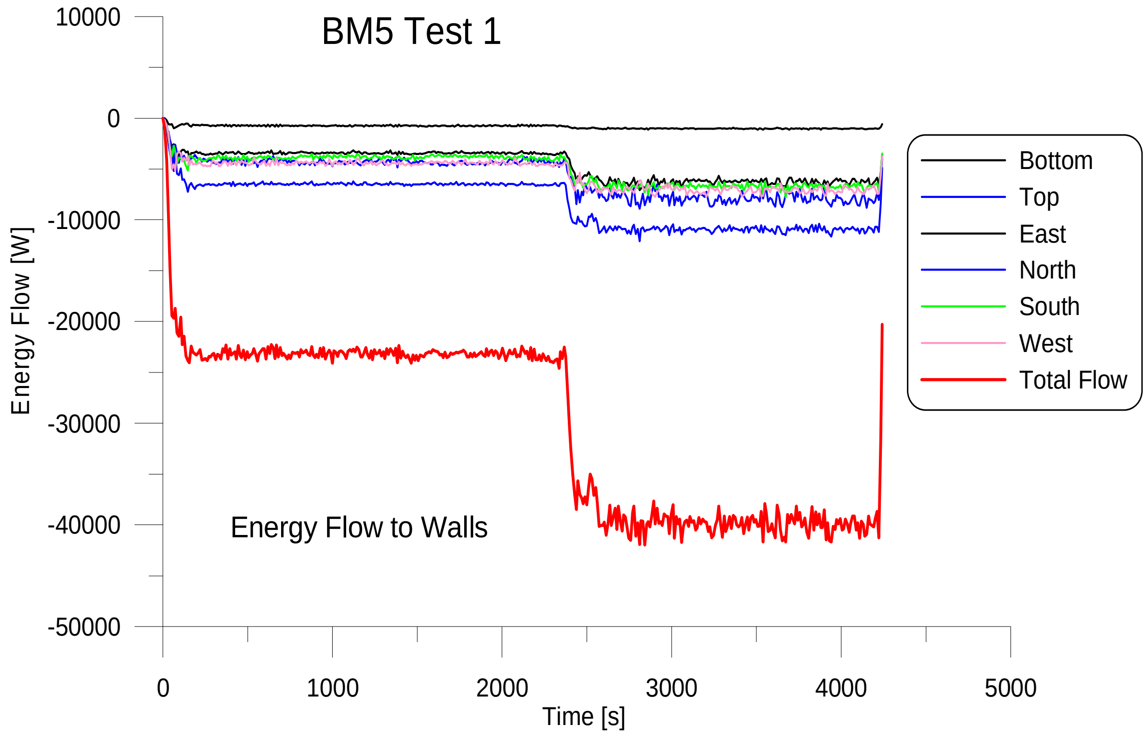


**Fig. F-16** Convective energy flow to walls

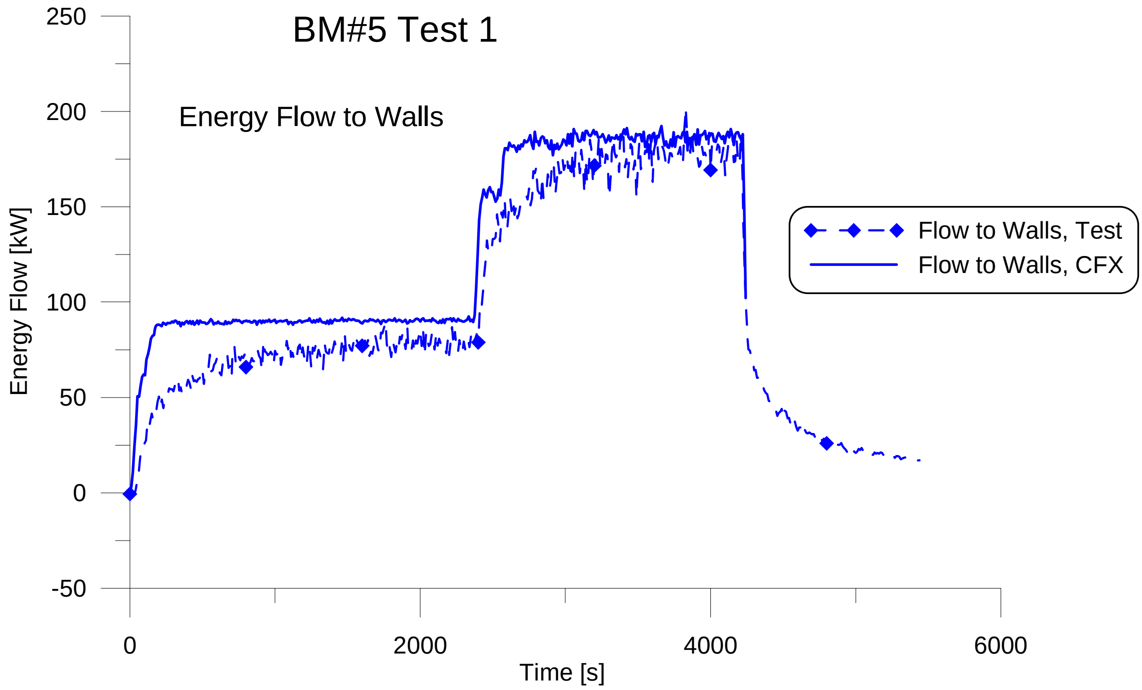


**Fig. F-17** Total energy flow to the walls

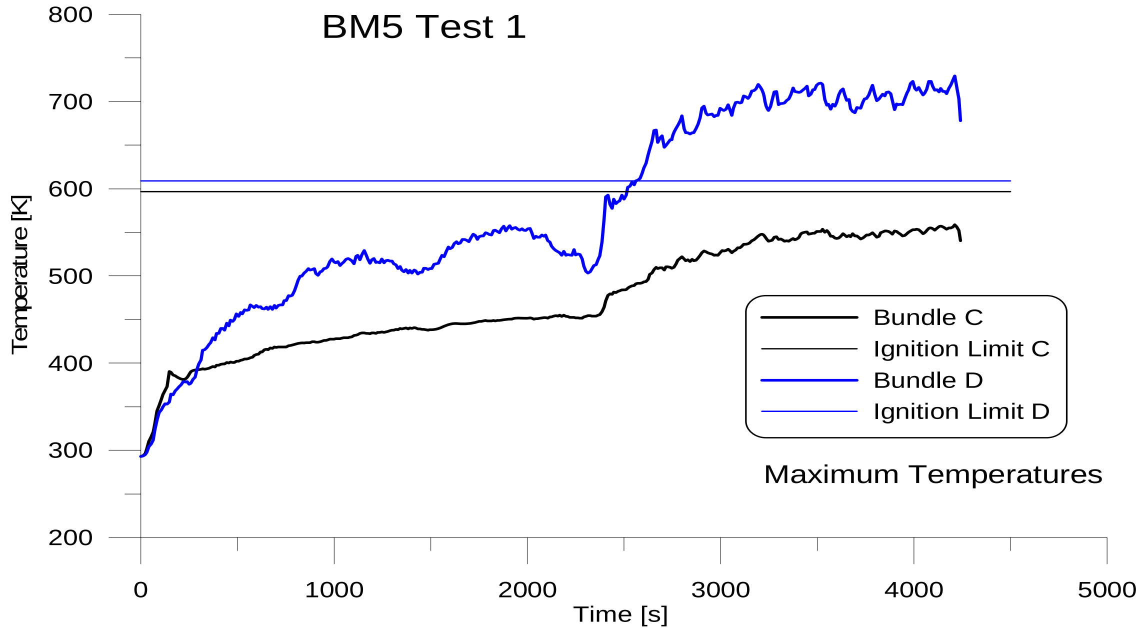


**Fig. F-18** Maximum temperatures of cable bundles

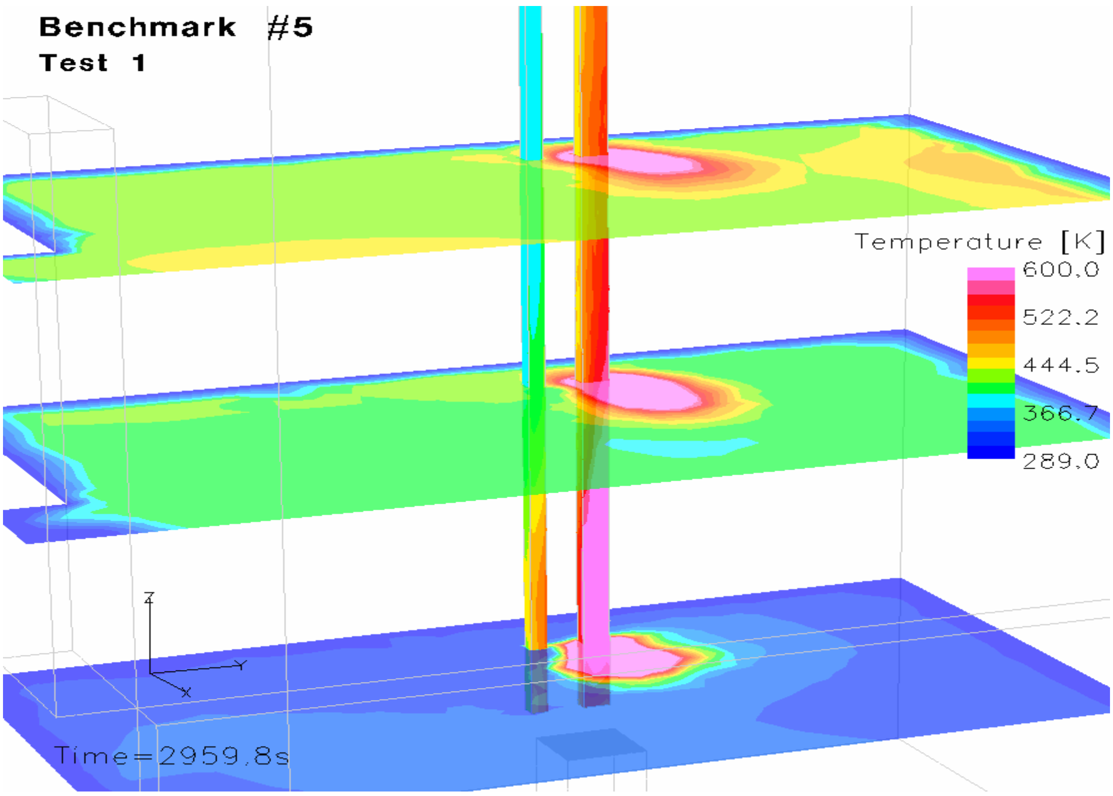


**Fig. F-19** Example of higher heat-up of bundle D due to inclination of the flame away from the door

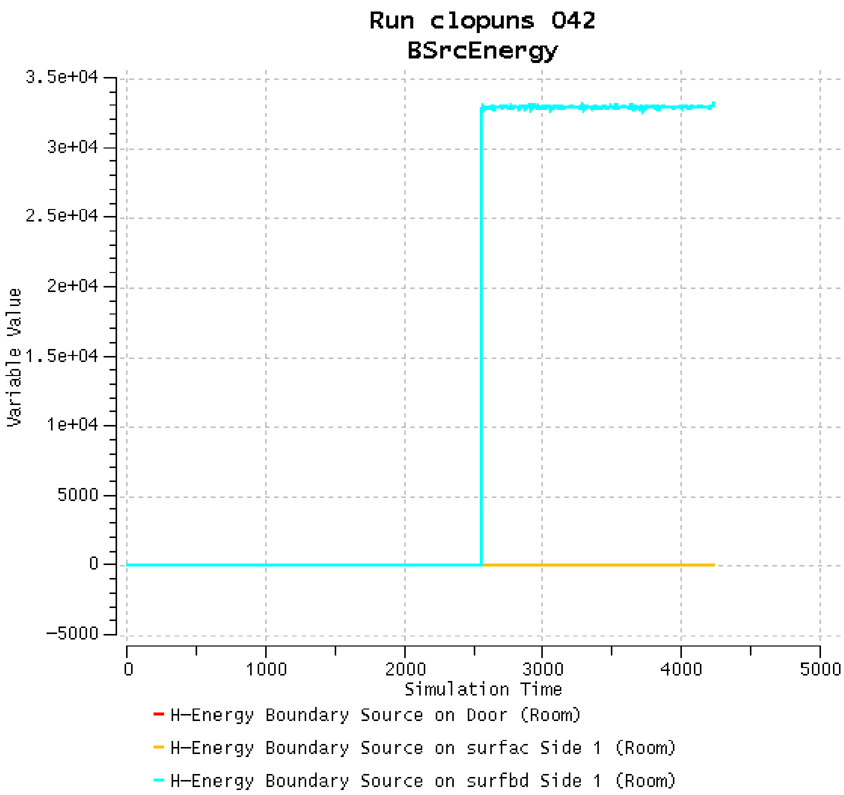


**Fig. F-20** Energy release by pyrolysis

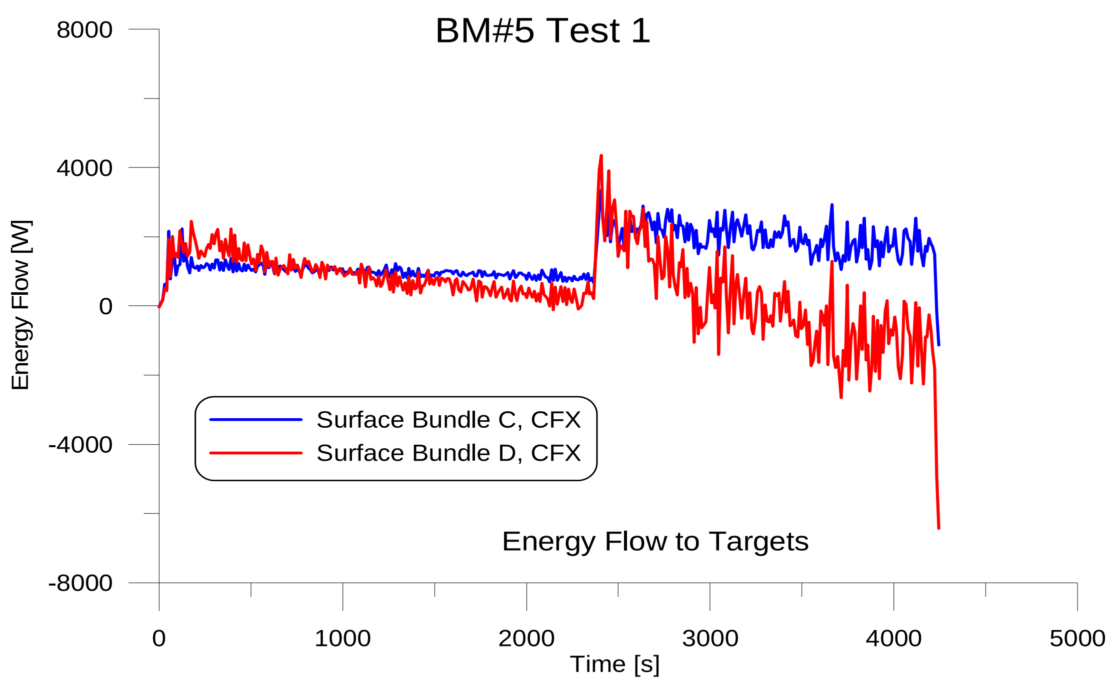


**Fig. F-21** Cumulative radiative flow to cable bundles

**Gesellschaft für Anlagen- und Reaktorsicherheit (GRS) mbH**

Schwertnergasse 1
**50667 Köln**
Telefon +49 221 2068-0
Telefax +49 221 2068-888

Forschungsinstitute
**85748 Garching** b. München
Telefon +49 89 32004-0
Telefax +49 89 32004-300

Kurfürstendamm 200
**10719 Berlin**
Telefon +49 30 88589-0
Telefax +49 30 88589-111

Theodor-Heuss-Straße 4
**38122 Braunschweig**
Telefon +49 531 8012-0
Telefax +49 531 8012-200

**www.grs.de**

**ISBN 978-3-931995-81-2**